A processing strategy for the application of the GPS in networks

P.J. de Jonge

NCG Nederlandse Commissie voor Geodesie Netherlands Geodetic Commission

Delft, August 1998

Colophon
A processing strategy for the application of the GPS in networks
P.J. de Jonge
Publications on Geodesy 46
ISBN 90 6132 266 9
ISSN 0165 1706

Publications on Geodesy is the continuation of Publications on Geodesy New Series

Published by: NCG Nederlandse Commissie voor Geodesie Netherlands Geodetic Commission, Delft, The Netherlands
Printed by: Meinema Drukkerij, Delft, The Netherlands
Cover: Polyhedron consisting of the between-receiver single differences formed at one epoch between 14 receivers. The WGS-84 ellipsoid is visualized by depicting some of its meridians and parallels.

NCG Nederlandse Commissie voor Geodesie
P.O. Box 5030, 2600 GA Delft, The Netherlands
Tel.: 31 (0)15-278 28 19
Fax: 31 (0)15-278 17 75
E-mail: ncg@geo.tudelft.nl
WWW: www.knaw.nl

The NCG Nederlandse Commissie voor Geodesie Netherlands Geodetic Commission is an institute of the Royal Netherlands Academy of Arts and Sciences (KNAW).

Contents

Preface

This thesis is the result of my Ph.D. studies conducted in the group Mathematical Geodesy and Positioning of the Faculty of Civil Engineering and Geosciences of the Delft University of Technology.

The Netherlands Organization for Scientific Research (NWO) and the Faculty of Civil Engineering and Geosciences are gratefully acknowledged for their financial support that enabled me to conduct these studies.

A number of persons have directly or indirectly contributed to this work. In particular I want to mention here my Ph.D. advisor Peter Teunissen and my colleague Christian Tiberius. Since 1993 we have cooperated closely in the development of the integer estimation method LAMBDA (Least-squares AMBiguity Decorrelation Adjustment).

Furthermore I want to mention Yehuda Bock who gave me the opportunity to visit his group in 1996 to gain experience with the ambiguity resolution in regional networks, and in whose group I am currently working.

Hans van der Marel kindly provided the software used to construct the pictures of the sparse matrices in Chapter 4, and Martin Jutte reproduced Figure 2.10.

Paul de Jonge
La Jolla, August 1998

Summary

A processing strategy for the application of the GPS in networks

The objective of this thesis is the development of a geodetic data reduction model for the use of the GPS for high precision relative positioning, with an emphasis on static network applications. The following aspects can be distinguished: optimum use of available data, estimability of parameters, the use of an efficient estimation method for the estimation of both the continuous and integer parameters, and the development of an efficient testing procedure to detect gross errors in the data.

To enable the optimum use of the collected data we use the original observables instead of the more common use of (double) differenced observables. This also enables the estimation of parameters (receiver and satellite clocks) eliminated in the differencing approach. Instead of the common use of linear combinations of the GPS observable types, we use the original observable types. Again this enables the estimation of parameters otherwise eliminated (ionospheric slant delays) and guarantees that the full information contained in the observables is preserved. Since, when using the original observables, the models for GPS relative positioning are not of full rank, the rank defect is analyzed and resolved, and resulting estimable functions are given. In particular, an algorithm for resolving the rank defect due to the GPS carrier phase ambiguities is described.

The use of the original observables asks for an efficient data reduction model. The data reduction is therefore carried out in two steps. In the first step the local parameters, viz. clocks and ionospheric slant delays are eliminated and only the global parameters (coordinates, tropospheric zenith delays, ambiguities) are estimated using Cholesky factorization of the sparse, reduced normal matrix. For the ordering of the global parameters during the factorization an a priori ordering is given which to a large extent preserves sparsity. In the second step the local parameters are computed, and the (sometimes tens of thousands) observations are efficiently tested for gross errors (outliers and cycle slips). The testing of observations lacks in the existing GPS data processing softwares for networks. The data reduction for the original observations does in general not cost more time than the reduction for the double differenced observations, and besides enables the quality analysis of single observations instead of functions thereof.

For high precision relative positioning the integer estimation of the GPS phase ambiguities and subsequent constraining of the ambiguities at their integer values (fixed solution) is needed. The integer estimation is carried out using the LAMBDA (Least-squares AMBiguity Decorrelation Adjustment) method. It consists of a general decorrelation of the ambiguities materialized in a so-called Z-matrix, followed by a depth-first search in the hyper-ellipsoid formed by the variance-covariance matrix of the ambiguities. The construction of the Z-matrix (explicitly and implicitly) and the search are derived, and described in detail.

Results of the integer estimation are given for baselines up to 56 km, and for a small network with three of the four stations allowed to be moving. The integer estimation method was also applied to a regional network in California, set up for monitoring of crustal movements. The results show the applicability of the method to both short baselines (up to 10-20 km) with an observation time span of the order of seconds, and regional networks with station separation of up to hundreds of kilometers and an observation time span of the order of one day.

Samenvatting (in Dutch)

Een verwerkingsstrategie voor de toepassing van het GPS in netwerken

De doelstelling van dit proefschrift is de ontwikkeling van een gegevensverwerkingsmodel voor het gebruik van het GPS voor zeer precieze relatieve plaatsbepaling, met een nadruk op de statische netwerk toepassing. In het onderzoek kunnen de volgende aspecten worden onderscheiden: optimaal gebruik van de data, schatbaarheid van de parameters, het gebruik van een efficiënte schattingsmethode voor zowel de reëelwaardige als de geheeltallige parameters, en de ontwikkeling van een efficiënte procedure om grove fouten in de waarnemingen te ontdekken.

Om optimaal gebruik van het waarnemingsmateriaal te waarborgen worden de originele waarnemingen in plaats van de vaak toegepaste dubbele verschillen van de waarnemingen gebruikt. Dit stelt ons tevens in staat om parameters te schatten die anders geëlimineerd worden (ontvanger- en satellietklokken). In plaats van de vaak toegepaste lineaire combinaties van GPS waarnemingstypen, gebruiken we de originele waarnemingstypen. Dit maakt het weer mogelijk om parameters die anders geëlimineerd worden te schatten (ionosferische vertragingen), en garandeert het behoud van de volledige informatie aanwezig in de waarnemingen. Omdat voor de originele waarnemingen de modellen voor relatieve plaatsbepaling met GPS niet van volle rang zijn, wordt het rangdefect geanalyseerd, en worden resulterende schatbare functies gegeven. In het bijzonder wordt een algoritme voor de oplossing van het rangdefect veroorzaakt door de GPS fase meerduidigheden beschreven.

De gegevensverwerking wordt uitgevoerd in twee stappen. In de eerste stap worden de lokale parameters (klokken en ionosferische vertragingen) geëlimineerd waarna de overige parameters (coördinaten, troposferische zenit vertragingen, meerduidigheden) geschat worden met behulp van Cholesky factorisatie van de ijle, gereduceerde normaalmatrix. Voor de ordening van de parameters gedurende de factorisatie, wordt een a priori methode gegeven, die de ijlheid grotendeels behoudt. In de tweede stap worden de lokale parameters berekend en worden de (soms tientallen duizenden) waarnemingen op efficiënte wijze getoetst op grove fouten. De toetsing van waarnemingen ontbreekt in bestaande GPS verwerkingssoftware voor netwerken. De gegevensverwerking kost in het algemeen niet meer tijd dan die voor de dubbele verschilmetingen, en maakt een kwaliteitsanalyse van enkele waarnemingen in plaats van functies van waarnemingen mogelijk.

Voor zeer precieze relatieve plaatsbepaling, is geheeltallige schatting van de GPS fase meerduidigheden, en een daarop volgend vasthouden van de meerduidigheden op hun geheeltallige waarden, noodzakelijk. De geheeltallige schatting wordt uitgevoerd met de LAMBDA methode. Deze bestaat uit een decorrelatie van de meerduidigheden gevolgd door een zoekprocedure in de hyper-ellipsoïde gevormd door de variantie-covariantie matrix van de meerduidigheden. De constructie van de decorrelerende matrix (zowel expliciet als impliciet) en de zoekprocedure worden afgeleid en in detail beschreven.

Resultaten van de geheeltallige schatting worden gegeven voor basislijnen tot 56 km, en voor een klein netwerk met drie van de vier stations bewegend. De geheeltallige schattingsmethode is ook toegepast op een regionaal netwerk in Californië, opgezet om aardkorstbewegingen te bepalen. De resultaten laten zien dat de methode zowel toegepast kan worden voor korte basislijnen (tot 10-20 km) en een waarnemingstijdsspan van enkele seconden, als voor regionale netwerken met afstanden tussen stations van honderden kilometers en een tijdsspan van een dag.

List of symbols

$_i$	Receiver identification
r	Number of receivers, or position vector [m]
^{j}	Satellite identification
m	Number of satellites
$_{,k}$ or ^{,k}	Epoch number
k_{df}	Critical value
df	Degrees of freedom
α	Level of significance
γ	Power of test
γ	Proportion factor between ionospheric delay on L1 and L2
$^{(-)}$	Previous iteration
δt	Clock error [s]
N	Real valued ambiguity, or normal matrix
$\bar{N}$	Integer part of real valued ambiguity
$\mathcal{I}$	Ionospheric delay of the L1 observable [m]
I	Unit matrix
η	Observable dependent multiplication factor for ionospheric delay
T, T_h, T_w	Tropospheric zenith delay [m]
T_{df}	Test statistic
μ	Mapping function of tropospheric zenith delay
ρ	Topocentric distance [m]
τ	Travel time of signal [s]
u	Unit direction vector from receiver to satellite
ν	Unit direction vector from satellite to receiver
f_1, f_2	Frequency [Hz]
λ_1, λ_2	Wavelength [m]
λ, λ_0	Non-centrality parameter
c	Speed of light [m/s]
$c_{p,k}$	Vector specifying alternative hypothesis
Φ_i^j	Carrier phase observable times c [m]
P_i^j	Pseudo range observable [m]
$P_A^\perp$	Projector matrix
P	Probability
P1,P2	Pseudorange observable types
ε	Observation noise and unmodeled effects [m]
Σ	A priori modeled error sources [m]

t	GPS time [s]
t^*	Receiver time [s]
∇t	Difference between common time of epoch and time tag [s]
∇	Minimal detectable bias
$\hat{\nabla}$	Estimated error
x	Vector of parameters to be estimated [m]
y	Vector of observations [m]
Δ	Increments to a priori values [m]
$\dot{\Omega}_e$	Earth's rotation rate [m/s]
A	Design matrix
d	Rank defect design matrix for the clocks
$\bar{d}$	Design matrix for the clocks (of full rank)
0_q	Null-vector of length q
$0_{p,q}$	$p \times q$ matrix with all entries equal to 0
e_q	Vector of length q with all entries equal to 1
e	Unit vector of local system
$E_{p,q}$	$p \times q$ matrix with all entries equal to 1
E_q	$q \times q$ matrix with all entries equal to 1
E	Elevation angle
z	Zenith angle
E	Set of edges of a graph
$E\{\}$	Expectation operator
$D\{\}$	Dispersion operator
h	Right-hand side of the normal equation system
Q	Variance-covariance matrix of observables (m^2)
C	Cholesky factor (lower triangular matrix)
L	Unit lower triangular matrix
L1,L2	Carrier phase observable types
D	Diagonal matrix
σ	Standard deviation of observable
w	Weight of observable
$w_{p,k}$	w-test statistic
$\tilde{}$	Satellite average
V	Basis for null space
V	Set of nodes (vertices) of a graph
G	Graph $G = G(V, E)$
$\mathcal{N}(A)$	Null space of A

$\mathcal{R}(A)$	Range space of A
$\mathbf{R}^q$	Vector space of all q-tuples with real coordinates
$\mathbf{Z}^q$	Vector space of all q-tuples with integer coordinates
$\|.\|$	Absolute value of scalar, length of a vector

List of abbreviations

A-S	Anti-Spoofing
C/A	Coarse/Acquisition(-code)
CS	Control Segment
DD	Double Difference(d)
DLR	Deutsches Zentrum für Luft- und Raumfahrt (German Aerospace Center)
DUT	Delft University of Technology
ECEF	Earth-Centered Earth-Fixed
ECI	Earth-Centered Inertial
GAMIT	GPS At MIT
GD	Group Delay
GPS	Global Positioning System
IERS	International Earth Rotation Service
IGS	International GPS Service for Geodynamics
ITRF	IERS Terrestrial Reference Frame
LAMBDA	Least-squares AMBiguity Decorrelation Adjustment
MDB	Minimal Detectable Bias
MGP	Mathematical Geodesy and Positioning
MIT	Massachusetts Institute of Technology
MST	Minimum Spanning Tree
MW	Melbourne-Wübbena(-combination)
OMT	Overall Model Test
P	Precision(-code)
PRN	Pseudo Random Noise
SA	Selective Availability
SD	Single Difference(d)
VLBI	Very Long Baseline Interferometry
WGS-84	World Geodetic Survey 1984

Chapter 1

Introduction

1.1 The Global Positioning System

In this section we will give a short introduction into the Global Positioning System, for more information we refer to (Leick 1995), (National Research Council 1995), (Parkinson and Spilker Jr. 1996a), (Parkinson and Spilker Jr. 1996b), (Kleusberg and Teunissen 1996), (Hofmann-Wellenhof et al. 1997), (Strang and Borre 1997).

The Global Positioning System, or GPS, is a development of the US military to provide real-time, world wide absolute positioning with a high accuracy. The system as it was developed is based on the principle of the measurement of ranges between the unknown user position to the (known) positions of 24 satellites orbiting the Earth in six orbit planes (A to F) at a distance of approximately 26,000 km from its center. Currently the third generation (Block IIR) of GPS satellites is being deployed (see Figure 1.1).

The position of the satellites can be computed using ephemerides that are contained in a so-called navigation message which is part of the signal transmitted by the satellites. These ephemerides are computed by the Control Segment (CS), consisting of five tracking stations

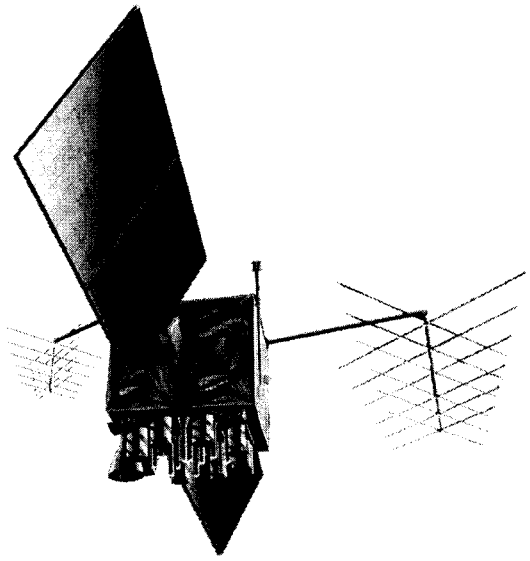

Figure 1.1: Block IIR GPS satellite.

more or less equally distributed around the equator, and a master control center. The extrapolated ephemerides (broadcast ephemerides) are regularly uploaded to the satellites from the tracking stations.

The ranges are determined by comparing the time tag of transmission of the signal at the satellite with the time tag of reception of the signal at the receiver. If the clocks of the receiver and of the transmitter would be perfectly synchronized, and if the signal would travel through vacuum, multiplication of the time difference with the speed of light would give the range between the antenna phase center of the receiver and that of the satellite.

If these perfect, unbiased ranges would be available, the ranges between the unknown user position and three satellites would be sufficient to obtain an estimate for that position[1].

As in general neither the clocks of the satellites, nor those of the receivers are synchronized with the official time of the GPS system (GPS time which equals UTC (Universal Coordinated Time) at the start of the test phase of GPS, at January 6, 1980), the ranges become biased by these unknown offsets. This basic GPS observable is called pseudorange.

Using pseudoranges instead of ranges, besides the position of the user, extra unknown parameters have to be solved for (the offsets of the receiver and satellite clocks with respect to GPS time). The offsets of the satellite clocks are however also computed by the CS and uploaded to the satellites, thus only the offset of the clock of the receiver needs to be estimated.

The GPS satellites transmit their signals at two frequencies (L1=1575.42 MHz, and L2=1227.6 MHz) in the L-band. These carriers are modulated by so-called PRN (Pseudo Random Noise) codes, which are unique for each satellite. In this thesis the GPS satellites will be referred to by their PRN code. There are two types of codes, viz. a Precision (P) and a Coarse/Acquisition (C/A) code. The P-code has a 10 times higher resolution than the C/A code and thereby the determination of the pseudoranges can be done more precisely. The L1 carrier is modulated by the P (P1) and C/A code, the L2 carrier only by the P (P2) code. The P-code was available to civilian users only in the test phase of the GPS system. It now is encrypted to the so-called Y-code, to make spoofing of the code impossible (implementation of Anti-Spoofing or A-S). The key is available only to the US military and their allies for military use. The C/A code is available to all users.

Since the implementation of A-S several techniques have been developed to determine P-code like pseudoranges, but the precision of these pseudoranges is still lower than the original P-code pseudoranges, albeit higher than the C/A pseudoranges.

The time of transmission of the signal at the satellite is broadcast at an interval of six seconds. Within this interval, time of transmission is determined by comparing the code on the GPS signal with a copy of that code generated by the receiver. In this thesis pseudorange observables will be denoted as pseudorange or code observables. The pseudorange at L1 will be denoted as P1 irrespective if it is a C/A pseudorange, a genuine P1 pseudorange or a P1 like pseudorange. The pseudorange at L2 will accordingly denoted as P2.

Selective Availability or SA, is another measure taken to deprive civilian users from the highest possible accuracy. In principle it consists of two parts, viz. a dithering of the satellite clocks and degradation of the broadcast ephemerides. Currently the latter does not seem to be implemented. Authorized users again can undo the effect of SA. As a result of A-S and

[1]Under the assumption that neither the positions of the three satellites, nor the user position and the positions of two satellites lie at one line (low precision), and that a sufficient accurate approximate position of the user position is available (since in general there are two possible solutions, i.e. for a user on Earth, one solution is on Earth, and one outside).

SA, a civilian user can determine absolute position with a horizontal precision of some tens of meters, whereas an authorized user can determine position with a precision of several meters.

Positioning using carrier phase
From the start of the test phase of the GPS system, it was observed that instead of using the pseudoranges one could use the carrier phase instead, in a similar fashion to the already existing VLBI technique.

By measuring the incoming phase of the carrier and keeping track of the number of whole cycles from one epoch to the next, an *ambiguous* or biased pseudorange is obtained. It is ambiguous since it gives only the change of distance between receiver and satellite between epochs. The unknown number of cycles that has to be added to make it a genuine pseudorange is called the (GPS carrier phase) ambiguity. The carrier phase observable will be denoted in this thesis as carrier phase or phase. The carrier phase observable on the L1 frequency will be denoted as L1, and the one on the L2 frequency, as L2.

Using the model for the satellite clock error contained in the broadcast ephemerides, carrier phase observations can be used for absolute positioning (Bock et al. 1984), but the accuracy of the coordinates will be governed by the SA effect, and is therefore comparable to the results obtained using pseudorange observations.

In a relative positioning setup, where two or more receivers simultaneously track a common set of satellites, corrections to both receiver and satellite clock errors may be estimated, and very precise and accurate coordinate differences with respect to a known position are obtained. Relative positioning has found successful application in fields like geodynamics, surveying and navigation.

Since 1994 precise ephemerides (which are an order more precise than the broadcast ephemerides) are estimated by a consortium of geodetic and geophysical institutes (International GPS Service for Geodynamics or IGS), to enhance the precision of crustal deformation studies. In California and Japan, arrays of several hundreds of stations have been established with the purpose of continuously monitoring plate movements on a daily basis.

For surveying and navigation purposes the precision requirements are less than for the geodynamics case, but one would like to have a position in (near) real time.

1.2 Objective and outline of the thesis

The objective of this thesis is the development of a geodetic data reduction model for the use of GPS for high precision relative positioning, with an emphasis on static network applications. The following aspects can be distinguished: optimum use of available data, estimability of parameters, the use of an efficient estimation method for the estimation of both the continuous and integer parameters, and the development of an efficient testing procedure to detect gross errors in the data.

The processing strategy is in principle applicable to any network of receivers, irrespective of the distance between the receivers. For longer distances however, the functional model will have to contain more terms (e.g. orbital parameters, correction for solid Earth tides) than for shorter distances.

As said before, the main focus is at the application in static networks, i.e. two or more[2], non-moving receivers, but most of the procedures described have also been applied to moving

[2]The two receiver or single baseline case is the limiting case of a network.

receivers.

In Chapter 2 the functional model for both the pseudorange and carrier phase observable types is given. The error sources affecting the observables are described, and ways to model them are given. Emphasis lies on description of error sources that are not well covered in existing literature. Nothing will be said about the GPS orbits; we presume to have available broadcast or precise ephemerides.

Using the functional model of Chapter 2, in Chapter 3 an efficient procedure for the estimation of the unknown parameters of interest, and a testing procedure for the detection of outliers and cycle slips for the observations involved, will be presented for the case when only one GPS observable type (pseudorange or carrier phase) is used.

To enable the optimum use of the collected data we use the original observables instead of the more common use of (double) differenced observables. Using the original observables is equivalent to applying the double difference technique when the same data is used in both approaches. The undifferenced approach however, sometimes enables to use data that in the double difference approach has to be discarded. Only for baselines it does not matter which of the approaches is used. Furthermore the undifferenced approach enables the estimation of parameters (receiver and satellite clocks) that are eliminated with the double difference approach.

It will be shown that when using undifferenced observables, the system of observation equations exhibits a rank defect that can be resolved by choosing an appropriate S-basis. The resulting estimable functions of parameters will be given. In particular, an algorithm for resolving the rank defect due to the GPS carrier phase ambiguities is described.

The use of the original observations asks for an efficient data reduction model. The data reduction is therefore carried out in two steps. In the first step the local parameters, (receiver and satellite clocks) are eliminated and only the global parameters (coordinates, tropospheric zenith delays, ambiguities) are estimated using Cholesky factorization of the reduced normal matrix. In the second step the local parameters are computed, and the observations are tested for gross errors (outliers and for the phase observations also cycle slips). The data reduction model proposed, does in general not cost more time than the data reduction for the double differenced observations, and besides enables the testing of single observations, instead of functions thereof.

Chapter 4 treats the case when more than one GPS observable type is used. Instead of the common use of linear combinations of the GPS observable types, we have chosen to use the original observable types. Again this enables the estimation of parameters otherwise eliminated (ionospheric slant delays) and guarantees that the full information contained in the observables is preserved.

Four different models are shown, and for these, the rank defect, a possible S-basis and resulting estimable functions will be given. Again an efficient procedure for estimating the parameters and testing the observations will be shown. As the normal matrices arising from the processing of large time spans may be sparse, the influence of the ordering of the parameters on preserving the sparsity in the subsequent Cholesky factorization will be shown.

In Chapter 5 integer estimation of the GPS double difference ambiguities will be treated. For high precision relative positioning the integer estimation of the GPS phase ambiguities and subsequent constraining of the ambiguities at their integer values (fixed solution) is needed. The integer estimation is carried out using the LAMBDA (Least-squares AMBiguity Decorrelation Adjustment). The method consists of a general decorrelation of the ambiguities materialized in a so-called Z-matrix, followed by a depth-first search in the hyper-ellipsoid

formed by the variance-covariance matrix of the ambiguities. Depending on the application at hand, it may be more efficient to compute the Z-matrix implicitly. The construction of the Z-matrix (explicitly and implicitly) and the search are derived, and described in detail.

In Chapter 6 ambiguity resolution for medium distances (10^1–10^3 km) will be treated. The ionospheric delays play a key role here. Two ways to constrain these delays, and results obtained by them will be given. The LAMBDA method was applied to resolve the ambiguities of a regional network in California. For this analysis the method was implemented in the GAMIT software of MIT/Scripps Institution of Oceanography.

Most of the ideas of this thesis have been implemented in the GPS processing program GPSVEQ developed by the author, and most of the examples have been computed using it. A short description of the program can be found in Appendix A.

References

Bock, Y., R. I. Abbot, C. C. Counselman III, S. A. Gourevitch, R. W. King, and A. R. Paradis (1984). Geodetic accuracy of the Macrometer^{tm} model V-1000. *Bulletin Géodésique 58*, 211–221.

Hofmann-Wellenhof, B., H. Lichtenegger, and J. Collins (1997). *GPS theory and practice* (Fourth ed.). Springer Verlag.

Kleusberg, A. and P. J. G. Teunissen (Eds.) (1996). *GPS for Geodesy*, Volume 60 of *Lecture Notes in Earth Sciences*. Springer Verlag.

Leick, A. (1995). *GPS Satellite Surveying* (Second ed.). John Wiley & Sons, Inc.

National Research Council (1995). *The Global Positioning System, A Shared National Asset.* National Academy Press.

Parkinson, B. W. and J. J. Spilker Jr. (Eds.) (1996a). *Global Positioning System: Theory and Applications Volume I*, Volume 163 of *Progress in Astronautics and Aeronautics*. American Institute of Aeronautics and Astronautics, Inc.

Parkinson, B. W. and J. J. Spilker Jr. (Eds.) (1996b). *Global Positioning System: Theory and Applications Volume II*, Volume 163 of *Progress in Astronautics and Aeronautics*. American Institute of Aeronautics and Astronautics, Inc.

Strang, G. and K. Borre (1997). *Linear Algebra, Geodesy, and GPS*. Wellesley-Cambridge Press.

Chapter 2

Functional model for the GPS observables

In this chapter we will develop the functional model for the GPS code and phase observables in precise relative positioning. The observables are to be related to the unknown parameters of interest (usually the receiver's coordinates) and the bias parameters (e.g. clocks and phase ambiguities). The structure of this chapter is the following. We will start with the non-linear observation equations followed by the linearized ones needed for the (iterated) least-squares adjustment. The underlying simplifications and assumptions will be described. For the computation of the non-linear as well as the linearized equations we need the satellite position and some quantities derived from it such as the topocentric distance and its derivatives. A method for the computation of these quantities will be derived.

Some error sources affecting the GPS observables may be corrected for a priori. A number of these error sources, viz. the satellite clock, phase center variation and offset, delays due to the troposphere and ionosphere, solid Earth tides and phase wind-up, will (shortly) be described. Emphasis lies on aspects that are not well covered in existing literature. Nothing will be said about the GPS orbits; we presume to have available broadcast or precise ephemerides. It will however not affect the applicability of processing methods proposed in this thesis.

For reasons of legibility the stochastic character of the observables and estimated parameters is not denoted by any particular symbol.

2.1 The GPS observation equations

The non-linear observation equations for the carrier phase observables on L1 and L2 and the pseudorange observables on L1 and L2 read respectively (in meters)

$$\begin{aligned}\Phi^j_{i,\mathrm{L1}}(t_i) - \Sigma_{\Phi^j_{i,\mathrm{L1}}}(t_i) =& \rho^j_i(t_i - \tau^j_i, t_i) + c\delta t_{i,\mathrm{L1}}(t_i) - c\delta t^{j,\mathrm{L1}}(t_i - \tau^j_i) + \mu^j_i(t_i - \tau^j_i, t_i)T_i(t_i) \\ & - \mathcal{I}^j_i(t_i) + \lambda_1 N^j_{i,\mathrm{L1}} + \varepsilon_{\Phi^j_{i,\mathrm{L1}}}(t_i) \qquad (2.1)\\ \Phi^j_{i,\mathrm{L2}}(t_i) - \Sigma_{\Phi^j_{i,\mathrm{L2}}}(t_i) =& \rho^j_i(t_i - \tau^j_i, t_i) + c\delta t_{i,\mathrm{L2}}(t_i) - c\delta t^{j,\mathrm{L2}}(t_i - \tau^j_i) + \mu^j_i(t_i - \tau^j_i, t_i)T_i(t_i) \\ & - \gamma\mathcal{I}^j_i(t_i) + \lambda_2 N^j_{i,\mathrm{L2}} + \varepsilon_{\Phi^j_{i,\mathrm{L2}}}(t_i) \qquad (2.2)\\ P^j_{i,\mathrm{P1}}(t_i) - \Sigma_{P^j_{i,\mathrm{P1}}}(t_i) =& \rho^j_i(t_i - \tau^j_i, t_i) + c\delta t_{i,\mathrm{P1}}(t_i) - c\delta t^{j,\mathrm{P1}}(t_i - \tau^j_i) + \mu^j_i(t_i - \tau^j_i, t_i)T_i(t_i) \\ & + \mathcal{I}^j_i(t_i) + \varepsilon_{P^j_{i,\mathrm{P1}}}(t_i) \qquad (2.3)\\ P^j_{i,\mathrm{P2}}(t_i) - \Sigma_{P^j_{i,\mathrm{P2}}}(t_i) =& \rho^j_i(t_i - \tau^j_i, t_i) + c\delta t_{i,\mathrm{P2}}(t_i) - c\delta t^{j,\mathrm{P2}}(t_i - \tau^j_i) + \mu^j_i(t_i - \tau^j_i, t_i)T_i(t_i) \\ & + \gamma\mathcal{I}^j_i(t_i) + \varepsilon_{P^j_{i,\mathrm{P2}}}(t_i) \qquad (2.4)\end{aligned}$$

where

$_i, ^j$	Receiver, respectively satellite identification.
t_i	Time of reception of the signal at receiver i in GPS time; $t_i = t_i^* - \delta t_i(t_i)$, with t_i^* the time of reception in receiver time (the time tag), and $\delta t_i(t_i)$ the receiver clock error [s].
$\rho_i^j(t_i - \tau_i^j, t_i)$	Topocentric distance between receiver i at time t and satellite j at time $t_i - \tau_i^j$: $\rho_i^j(t_i - \tau_i^j, t_i) = \|r^j(t_i - \tau_i^j) - r_i(t_i)\|$, where r^j and r_i are defined in an Earth-Centered Inertial (ECI) system [m].
$r_i(t_i)$	Position vector of receiver i at time of reception t_i of the signal [m].
$r^j(t_i - \tau_i^j)$	Position vector of satellite j at time of transmission $t_i - \tau_i^j$ [m].
τ_i^j	Travel time of the signal, i.e. time needed for the signal to travel from the satellite to the receiver [s].
$\delta t_i(t_i)$	Receiver clock error at time of reception t_i [s].
$\delta t^j(t_i - \tau_i^j)$	Satellite clock error at time $t_i - \tau_i^j$ of transmission of the signal [s].
c	The speed of light in vacuum (299,792,458.0 m/s).
$T_i(t_i)$	Delay due to the troposphere in the direction of the zenith [m].
$\mu_i^j(t_i - \tau_i^j, t_i)$	Function which maps the zenith delay into the receiver-satellite direction: $\mu_i^j(t_i - \tau_i^j, t_i) = \mu_i^j\left(r^j(t_i - \tau_i^j), r_i(t_i)\right)$. A different mapping function for the hydrostatic ('dry') and the water vapor ('wet') zenith delay may be defined.
$\mathcal{I}_i^j(t_i)$	Delay due to the ionosphere on L1 [m].
γ	Factor relating the ionospheric delay experienced by the L1 and P2 observable types to the delay experienced by the L1 and P1 observable types; $\gamma = {f_1}^2/{f_2}^2$
f_1	Frequency of L1 = 1575.42 = 77 × 20.46 MHz.
f_2	Frequency of L2 = 1227.60 = 66 × 20.46 MHz.
λ_1	Wavelength of the L1-carrier: $\frac{c}{f_1} \approx 0.19$ m.
λ_2	Wavelength of the L2-carrier: $\frac{c}{f_2} \approx 0.24$ m.
N_i^j	Real valued ambiguity term for the carrier phase observable; $N_i^j = \bar{N}_i^j + \phi_i - \phi^j$ [cycles].
ϕ_i, ϕ^j	Initial phase at receiver, and satellite, respectively [cycles].
$\varepsilon(t_i)$	Observation noise and unmodeled effects [m].
$\Sigma(t_i)$	A priori corrections for satellite clock, phase center variation, tropospheric and ionospheric delays, solid Earth tides, and phase wind-up, (see Sections 2.3–2.8) [m].

In the observation equations quantities occur that are defined at the time of reception of the signal t, at the time of transmission $t - \tau$, and at a combination of the two. The ambiguity term that occurs in the equations for the carrier phase does not change with time. Note that each receiver has its own time of reception (in GPS time); the difference between the time of reception of two receivers is for a modern geodetic receiver at most 1 ms (see Section 2.1.2). The time of transmission of the signals varies through the difference of the time it needs to travel to two receivers that are not equidistant to the satellite. For each observable a receiver and satellite clock error is defined, hence the term 'pseudorange'. The phase observables are also biased by an unknown number of cycles and are thus ambiguous pseudoranges.

Although in principle the clock errors are equal for all observable types for a particular receiver-satellite combination, the lumping of unmodeled observable type-specific error sources into the clock errors makes it necessary to introduce *distinct clock errors for each observable type* for each epoch. So, strictly speaking, the term clock error is somewhat misleading. Depending on the application at hand, some parameters may be omitted from the observation equations.

2.1.1 Linearization of the observation equations

Since the equations for the GPS observables are non-linear it is necessary to linearize them, e.g. for the L1 phase observable we have (hereafter we leave out the subscript $_i$ for the time of reception of the signal at receiver i):

$$\Delta\Phi^j_{i,\mathrm{L1}}(t) = \sum \left.\frac{\partial \Phi^j_{i,\mathrm{L1}}}{\partial x}\right|_{x=x^0} \Delta x + \mathcal{O}(\Delta x^2), \tag{2.5}$$

with x the unknowns we want to estimate, and the 'observed' minus 'computed' observation as

$$\Delta\Phi^j_{i,\mathrm{L1}}(t) = \Phi^j_{i,\mathrm{L1}}(t) - \Phi^j_{i,\mathrm{L1}}(t)^0 \tag{2.6}$$

The computed observation $\Phi^j_{i,\mathrm{L1}}(t)^0$ reads

$$\begin{aligned}\Phi^j_{i,\mathrm{L1}}(t)^0 = {} & \rho^j_i\big|_{r^j(t-\tau^j_i),r_i(t)^0} + c\delta t_{i,\mathrm{L1}}(t)^0 - c\delta t^{j,\mathrm{L1}}(t-\tau^j_i)^0 \\ & + \mu^j_i\big|_{r^j(t-\tau^j_i),r_i(t)^0} T^j_i(t)^0 - \mathcal{I}^j_i(t)^0 + \lambda_1 N^j_{i,\mathrm{L1}}{}^0\end{aligned} \tag{2.7}$$

We regard the position of the satellite $r^j(t)$ as a known function of time, i.e. we do not estimate (corrections to) orbital parameters. The parameters to be estimated are then the position vector of the receiver, the receiver clock error, the satellite clock error, the tropospheric zenith delay, the ionospheric slant delay and the real valued ambiguity.

The receiver clock error appears two times in the observation equation. It is part of the expression for the topocentric range to compute the position of the satellite at the time of transmission:

$$\rho^j_i(t-\tau^j_i, t) = \|r^j(t^* - \delta t_{i,\mathrm{L1}}(t) - \tau^j_i) - r_i(t)\|$$

and it appears as $c\delta t_{i,\mathrm{L1}}(t)$ as a correction term to the biased pseudorange $\Phi^j_{i,\mathrm{L1}}$. For the topocentric range it is sufficient that the time of reception of the signal is known with an

accuracy of a few tenths of microseconds as this corresponds to a maximum change in the topocentric range of a few tenths of mm. The maximum of the derivative of the topocentric range with respect to the travel time of the signal is approximately 800 m/s, hence the maximum error in the topocentric distance with an error in the time of reception of 1 μs is 10^{-6} s $\times$ 800 m/s = 0.8 mm.

Although each observable type is biased by a different receiver clock error, for the topocentric range we assume a common clock error for all types. This will not degrade the eventual solution since the order of accuracy required for the time of transmission exceeds the order of the differences between the clock errors by several orders (see Figure 4.3 where the maximum difference between the L1 and L2 clock error equals a few cm or 0.1 ns).

For the receiver clock error as a correction term to the biased range, we need a higher accuracy, since the eventual bias in it is multiplied by the speed of light. So for this purpose we estimate for each observable type a different clock (see Eqs. (2.1–2.4)).

If a priori approximate values for the parameters x^0 are not available or of low quality, the least-squares adjustment needs to be iterated. The linearized observation equation for the L1 observable for the current iteration step reads then (using $^{(-)}$ to indicate the previous iteration):

$$\begin{aligned}\Delta\Phi^j_{i,\mathrm{L1}}(t) = &\left(\frac{\partial\rho^j_i}{\partial {r_i}^T} + \frac{\partial\mu^j_i}{\partial {r_i}^T}\right)\Bigg|_{r^j(t-\tau^j_i),r_i(t)^{(-)}} \Delta r_i(t)\\ &+ \left(c + \left(\frac{\partial\rho^j_i}{\partial t} + \frac{\partial\mu^j_i}{\partial t}\right)\Bigg|_{r^j(t-\tau^j_i),r_i(t)^{(-)}} \frac{\partial t}{\partial \delta t_i}\right)\Delta\delta t_{i,\mathrm{L1}}(t) - c\Delta\delta t^{j,\mathrm{L1}}(t-\tau^j_i)\\ &+ \mu^j_i\big|_{r^j(t-\tau^j_i),r_i(t)^{(-)}}\,\Delta T_i(t) - \Delta\mathcal{I}^j_i(t)\\ &+ \lambda_1\Delta N^j_{i,\mathrm{L1}}\end{aligned} \tag{2.8}$$

which with $\frac{\partial t}{\partial \delta t_{i,\mathrm{L1}}} = -1$, u^j_i the unit direction vector from receiver to satellite, and $\dot\rho$ and $\dot\mu$ the time derivatives of the topocentric distance and the mapping function of the troposphere respectively, turns into

$$\begin{aligned}\Delta\Phi^j_{i,\mathrm{L1}}(t) = &\left(-{u^j_i}^T + \frac{\partial\mu^j_i}{\partial {r_i}^T}\right)\Bigg|_{r^j(t-\tau^j_i),r_i(t)^{(-)}} \Delta r_i(t)\\ &+ \left(c - (\dot\rho^j_i + \dot\mu^j_i)\big|_{r^j(t-\tau^j_i),r_i(t)^{(-)}}\right)\Delta\delta t_{i,\mathrm{L1}}(t) - c\Delta\delta t^{j,\mathrm{L1}}(t-\tau^j_i)\\ &+ \mu^j_i\big|_{r^j(t-\tau^j_i),r_i(t)^{(-)}}\,\Delta T_i(t) - \Delta\mathcal{I}^j_i(t)\\ &+ \lambda_1\Delta N^j_{i,\mathrm{L1}}\end{aligned} \tag{2.9}$$

The computed observation, and 'observed' minus 'computed' for the current iteration step read

$$\begin{aligned}\Phi^j_{i,\mathrm{L1}}(t)^{(-)} = &\,\rho^j_i\big|_{r^j(t-\tau^j_i),r_i(t)^{(-)}} + c\delta t_{i,\mathrm{L1}}(t)^{(-)} - c\delta t^{j,\mathrm{L1}}(t-\tau^j_i)^{(-)}\\ &+ \mu^j_i\big|_{r^j(t-\tau^j_i),r_i(t)^{(-)}}\,T_i(t)^{(-)} - \mathcal{I}^j_i(t)^{(-)} + \lambda_1 {N^j_{i,\mathrm{L1}}}^{(-)}\end{aligned} \tag{2.10}$$

$$\Delta\Phi^j_i(t) = \Phi^j_i(t) - \Phi^j_i(t)^{(-)} \tag{2.11}$$

The approximate values for the next iteration are computed as

$$\begin{aligned} r_i(t) &= r_i(t)^{(-)} &&+\Delta r_i(t) \\ \delta t_{i,\mathrm{L1}}(t) &= \delta t_{i,\mathrm{L1}}(t)^{(-)} &&+\Delta\delta t_{i,\mathrm{L1}}(t) \\ \delta t^{j,\mathrm{L1}}(t) &= \delta t^{j,\mathrm{L1}}(t)^{(-)} &&+\Delta\delta t^{j,\mathrm{L1}}(t) \\ T_i(t) &= T_i(t)^{(-)} &&+\Delta T_i(t) \\ \mathcal{I}_i^j(t) &= \mathcal{I}_i^j(t)^{(-)} &&+\Delta\mathcal{I}_i^j(t) \\ N_{i,\mathrm{L1}}^j &= N_{i,\mathrm{L1}}^{j\ (-)} &&+\Delta N_{i,\mathrm{L1}}^j \end{aligned} \tag{2.12}$$

The linearized observation equations and approximate observations for the other observable types can be derived analogously and are identical except for the frequency and observable type dependent coefficients for the ionosphere and ambiguity parameters.

2.1.2 Assumptions and simplifications

Mapping function for tropospheric zenith delay:
The time derivative of the mapping functions for the tropospheric zenith delay as well as the derivative with respect to the position of the receiver, are so small compared with the corresponding derivatives of the topocentric distance, that they can safely be omitted from the linearized observation equation. It reads then

$$\begin{aligned} \Delta\Phi_{i,\mathrm{L1}}^j(t) = &-u_i^{jT}\Big|_{r^j(t-\tau_i^j),r_i(t)^{(-)}} \Delta r_i(t) \\ &+ (c - \dot{\rho}_i^j\big|_{r^j(t-\tau_i^j),r_i(t)^{(-)}})\Delta\delta t_{i,\mathrm{L1}}(t) - c\Delta\delta t^{j,\mathrm{L1}}(t-\tau_i^j) \\ &+ \mu_i^j\big|_{r^j(t-\tau_i^j),r_i(t)^{(-)}} \Delta T_i(t) - \Delta\mathcal{I}_i^j(t) \\ &+ \lambda_1\Delta N_{i,\mathrm{L1}}^j \end{aligned} \tag{2.13}$$

Receiver clock error:
As mentioned before, the receiver clock error appears two times in the observation equations: firstly it is part of the expression for the time at which the topocentric distance has to be evaluated, and secondly it is one of the biases which cause the GPS observables to be pseudoranges instead of ranges.

For the evaluation of the topocentric distance, the accuracy required is of the order of some tenths of μs. Some receivers continuously adjust the receiver (quartz crystal) clock such that its deviation from GPS time is of this order. This is done within the receiver software using a single point pseudorange solution. Other possibilities to obtain a sufficiently accurate receiver clock is to use an external clock with a higher stability. Clocks used for this purpose are of the rubidium cell, cesium beam, or hydrogen maser type (see Table 2.1).

The third possibility to obtain accurate estimates for the receiver clock error is to use the estimates from a previous pseudorange solution, which can either be a single point solution or a solution from a relative positioning setup. In this solution the receiver clock error is set to zero for the evaluation of the topocentric distance.

As we will show later, the receiver and satellite clock errors are not unbiased estimable. When processing pseudoranges, each clock error is biased by some function of the rest of

Clock	Stability [s/s]		
	10 min	1 day	10 days
Quartz Crystal	$10^{-6} - 10^{-11}$	$10^{-6} - 10^{-11}$	$10^{-5} - 10^{-10}$
Rubidium Cell	10^{-13}	10^{-12}	10^{-11}
Cesium Beam	10^{-12}	10^{-13}	10^{-13}
Hydrogen Maser	10^{-15}	10^{-14}	10^{-13}

Table 2.1: Clock types and their stability (from McDonald (1991)).

the clock errors, depending on which function of clocks is constrained to resolve the rank defect (see Section 3.3). When carrier phases are processed an additional bias in the form of a function of the ambiguities is introduced.

One choice for the function of clocks to be constrained is e.g. the geometric average of the satellite clock errors. If we have corrected the observations a priori with the a priori satellite clock error model that is contained in the broadcast ephemerides, these corrections will be of the order of 50 m or a few hundred ns for the pseudorange satellite clocks. The error caused by the bias in the receiver clock error is then (with m the number of satellites)

$$\dot{\rho}_i^j \frac{1}{m} \sum_{j=1}^{m} (\delta t^j - \delta t^{j0})$$

This error will be partly absorbed by the receiver and satellite clock errors; more so when the distances between receivers are short, since then the time derivative of the topocentric distance is not too different for different receivers.

Now we have a sufficiently accurate estimate for the receiver clock error, it is regarded as a deterministic parameter in the observation equation as far as the topocentric distance is concerned, and hence no linearization with respect to this parameter is needed. The linearized observation equation reads then

$$\begin{aligned} \Delta\Phi_{i,\mathrm{L1}}^j(t) = & -u_i^{jT}\Big|_{r^j(t-\tau_i^j),r_i(t)^{(-)}} \Delta r_i(t) \\ & + c\Delta\delta t_{i,\mathrm{L1}}(t) - c\Delta\delta t^{j,\mathrm{L1}}(t-\tau_i^j) \\ & + \mu_i^j\Big|_{r^j(t-\tau_i^j),r_i(t)^{(-)}} \Delta T_i(t) - \Delta\mathcal{I}_i^j(t) \\ & + \lambda_1 \Delta N_{i,\mathrm{L1}}^j \end{aligned} \tag{2.14}$$

If we do not have an accurate estimate for the receiver clock error, the observation equation remains as it is. This form can however only be used when also at least one pseudorange observable type is included in the adjustment, and no ionospheric delays are included in the model. For the evaluation of the topocentric distance, the receiver clock error belonging to the pseudorange is used. The linearized observations equations for e.g. an adjustment with L1 and P1 read then

$$
\begin{aligned}
\Delta\Phi^j_{i,\mathrm{L1}}(t) = & -u_i^{jT}\Big|_{r^j(t-\tau_i^j),r_i(t)^{(-)}} \Delta r_i(t) \\
& + (c - \dot{\rho}_i^j\big|_{r^j(t-\tau_i^j),r_i(t)^{(-)}})\Delta\delta t_{i,\mathrm{L1}}(t) - c\Delta\delta t^{j,\mathrm{L1}}(t-\tau_i^j) \\
& + \mu_i^j\big|_{r^j(t-\tau_i^j),r_i(t)^{(-)}} \Delta T_i(t) \\
& + \lambda_1 \Delta N^j_{i,\mathrm{L1}} \\
\Delta P^j_{i,\mathrm{P1}}(t) = & -u_i^{jT}\Big|_{r^j(t-\tau_i^j),r_i(t)^{(-)}} \Delta r_i(t) \\
& + (c - \dot{\rho}_i^j\big|_{r^j(t-\tau_i^j),r_i(t)^{(-)}})\Delta\delta t_{i,\mathrm{P1}}(t) - c\Delta\delta t^{j,\mathrm{P1}}(t-\tau_i^j) \\
& + \mu_i^j\big|_{r^j(t-\tau_i^j),r_i(t)^{(-)}} \Delta T_i(t)
\end{aligned}
\tag{2.15}
$$

with

$$t = t_i^* - \delta t_{i,\mathrm{P1}}$$

In practice often one uses c instead of $c - \dot{\rho}$. Because $\dot{\rho}$ is so small compared to c, and several iterations are made, the result will be the same. The convergence will be slower, but the construction of the design matrix is more simple.

Satellite clock error:
The implicit assumption we made (assuming the signals of the satellite are simultaneously received by the receivers), is that the satellite clocks are sufficiently stable over a period of

$$\max \|\tau_{i1}^j - \tau_{i2}^j\| \tag{2.16}$$

This is necessary since we compute only one clock parameter (per observable type) per epoch, assuming that it is valid for all observables referring to that satellite. Since however in general not all ranges from the satellite to the various receivers are equal, the travel time of the signal will vary. This implies that if the signals are simultaneously received, their transmission times and thus the accompanying satellite clock errors will differ.

As generally the signals are not simultaneously received by the receivers Eq. (2.16) changes into

$$\max \|(t_{i1} - \tau_{i1}^j) - (t_{i2} - \tau_{i2}^j)\| \tag{2.17}$$

The clock errors are computed for a common time t_c, which is taken as the nominal time of reception, e.g. the whole second. With

$$\nabla t_i = t_i^* - t_c \tag{2.18}$$

and using the relation

$$t_i^* = t_i + \delta t_i \tag{2.19}$$

we have

$$t_i = t_c + \nabla t_i - \delta t_i \tag{2.20}$$

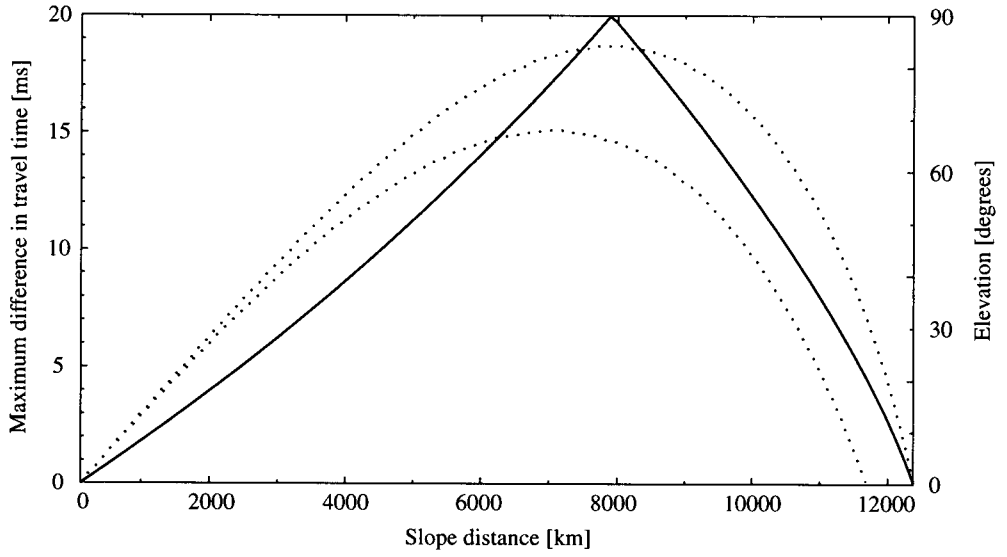

Figure 2.1: Maximum difference in travel time as function of the baseline length for a cut-off of zero degrees (upper dotted curve), and for a cut-off of 10 degrees (lower dotted curve). One receiver is observing the satellite at an elevation equal to the cut-off, the second receiver is observing it at an elevation shown by the solid curve (only shown for the cut-off of zero degrees).

Thus we have the condition that the satellite clock errors should be sufficiently stable over a period of

$$\begin{aligned} \max \|(t_c + \nabla t_{i1} - \delta t_{i1} - \tau_{i1}^j) - (t_c + \nabla t_{i2} - \delta t_{i2} - \tau_{i2}^j)\| = \\ \max \|(\nabla t_{i1} - \delta t_{i1}) - (\nabla t_{i2} - \delta t_{i2}) - (\tau_{i1}^j - \tau_{i2}^j)\| = \\ \max \|\nabla t_{i1} - \delta t_{i1}\| + \max \|\nabla t_{i2} - \delta t_{i2}\| + \max \|\tau_{i1}^j - \tau_{i2}^j\| \end{aligned} \tag{2.21}$$

for any two receiver pair $i1$ and $i2$. The term

$$\|\nabla t_i - \delta t_i\| = \|t_i - t_c\| \tag{2.22}$$

is for most geodetic receivers at most 1 ms (Ashtech Z-XII3 and Trimble 4000 SSI: in principle less than 1 ms, Turbo Rogue SNR-8000 and Leica SR399: in principle less than 0.3 μs). The maximum difference in travel time for one satellite to a pair of receivers on Earth depends on the minimum elevation for which observations are made (cut-off angle). For a spherical approximation of the Earth with a radius of 6,378 km, and a circular approximation of the GPS satellite orbits with radius of 26,562 km, the maximum difference in travel time as function of the baseline length is depicted in Figure 2.1. The two receivers and satellite are in the same plane together with the geocenter, as this gives the maximum difference. The difference is plotted for two cut-off angles; the upper dotted curve is for a cut-off of zero degrees, the lower dotted curve for a cut-off of 10 degrees. One receiver observes at an elevation equal to the cut-off angle; the solid line gives the elevation of the second receiver for the cut-off of zero degrees. For slope distances until approximately 8,000 km, the maximum

difference is obtained when the projection of the satellite on the line through the two receivers is outside the interval formed by the receivers; for larger distances, the projection lies inside the interval. Hence the sharp angle in the curve for the elevation for the second receiver. Due to the actual satellite configuration, the computed scenarios are a little bit too pessimistic, but give a fair idea of the size of the phenomenon.

The maximum (one receiver observes the satellite in the zenith, the other observes it under an elevation angle of zero degrees) is approximately 19 ms. The satellite clock rate due to the effect of Selective Availability is given in Rocken and Meertens (1991) as 2 Hz/nominal frequency of the carrier, so for L1 we have $\approx 1.27\ 10^{-9}$ s/s. Translating this to a range rate we have to multiply it by c, yielding ≈ 0.4 m/s. This value was confirmed by computations we made. In Figure 2.2 delays due to the satellite clock error are plotted. They are biased by the geometric average of all clocks; this bias is different at each epoch, but it is approximately zero. In Figure 2.3 the first divided differences of the satellite clocks are plotted; with an exception of one outlier, the computed clock rates are comparable to the values found by (ibid.). The outlier is caused by the transition of one set of broadcast ephemerides to another. This transition can also be observed in Figure 2.2. The size of the discontinuity is a few meters, corresponding with approximately 0.01 μs, which is in agreement with the values found by Zumberge and Bertiger (1996).

Assuming a maximum difference between the time of reception of the signal by two receivers of 2×1 ms, and adding the maximum difference in travel time of the signal to it, SA will cause a bias in the range of approximately 8 mm ($(19 + 2)$ms $\times$ 0.4 m/s). When the satellite clock error is evaluated at the geometric average of $t_i - \tau_i^j$, the actual maximum range error may be smaller. Feigl et al. (1991) and Wu et al. (1992) give methods to minimize the effect of Selective Availability.

2.2 Computation of the satellite position

In the linearized observation equation and the computed observations, quantities occur that are a function of the position of the satellite at the time of transmission of the signal $t - \tau$; viz. the topocentric distance ρ and the unit direction vector u. (Hereafter we leave out the subscript and superscript indicating the receiver and the satellite.)

When using the broadcast ephemerides, the position of the satellite is computed from information contained in the so called 'navigation message' which is part of the signal transmitted by the satellites. When using precise ephemerides, the position is computed by a Lagrange interpolation of positions which are given at an interval of 15 minutes. The broadcast ephemerides are given in WGS-84, the precise ephemerides in ITRFXX, where XX depends on the reference system adopted at the date when the ephemerides were computed (now, in 1998, we have ITRF96).

For the computation a common time t_c (GPS time) is introduced for every epoch. The advantage of this approach is that we need to evaluate the ephemerides of the satellite only once per epoch.

The material in Teunissen and van der Marel (1992) has been the inspiration of the procedures that will be described below.

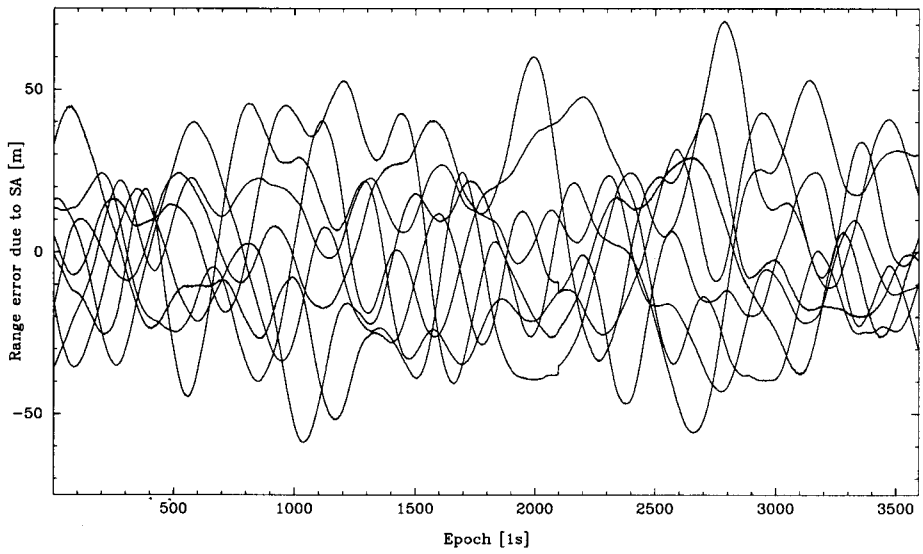

Figure 2.2: Range errors due to Selective Availability.

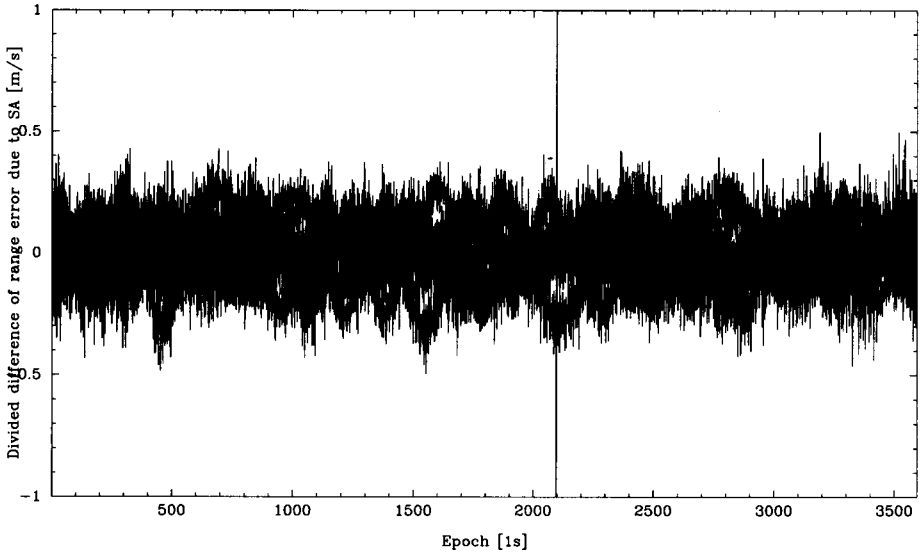

Figure 2.3: Divided difference of range errors due to Selective Availability.

Topocentric distance.
We need the position of the satellite at time $t_c - \tau$ with $\tau = \rho(t_c - \tau, t_c)/c$ (for a receiver on Earth τ is on the order of 0.1 s). The topocentric distance $\rho(t - \tau, t)$ was defined as

$$\rho(t - \tau, t) = \|r^j(t - \tau) - r_i(t)\| \tag{2.23}$$

with $r^j(t - \tau)$ and $r_i(t)$ defined in an arbitrary Earth-Centered Inertial (ECI) system. We want however, to use $r^j(t - \tau)$ and $r_i(t)$ defined in WGS-84 or in the system of the ITRF, which both are Earth-Centered Earth-Fixed (ECEF) systems.

Coordinates from an ECEF system with the Z-axis along the nominal Earth's spin axis, positive in the northern hemisphere, coinciding with the Z-axis of an ECI system, and of equal scale, are transformed to the ECI system as

$$r(t)_{\text{ECI}} = R(t)r(t)_{\text{ECEF}} \tag{2.24}$$

with

$$R(t) = \begin{bmatrix} \cos(\dot{\Omega}_e t + \Psi) & -\sin(\dot{\Omega}_e t + \Psi) & 0 \\ \sin(\dot{\Omega}_e t + \Psi) & \cos(\dot{\Omega}_e t + \Psi) & 0 \\ 0 & 0 & 1 \end{bmatrix} \tag{2.25}$$

with $\dot{\Omega}_e$ the Earth's rotation rate, and Ψ free to choose, giving an infinite number of ECI systems. So we have

$$\rho(t - \tau, t) = \|r^j(t - \tau)_{\text{ECI}} - r_i(t)_{\text{ECI}}\| \tag{2.26}$$

$$= \|R(t - \tau)r^j(t - \tau)_{\text{ECEF}} - R(t)r_i(t)_{\text{ECEF}}\| \tag{2.27}$$

For the common time t_c, with $\Psi = -\dot{\Omega}_e t_c$ we have

$$\rho(t_c - \tau, t_c) = \|R(-\tau)r^j(t_c - \tau)_{\text{ECEF}} - r_i(t_c)_{\text{ECEF}}\| \tag{2.28}$$

As a first approximation for τ we compute

$$\tau = \|r^j(t_c)_{\text{ECEF}} - r_i(t_c)_{\text{ECEF}}\|/c \tag{2.29}$$

With this approximated value we compute the first term of (2.28) as

$$R(-\tau)r^j(t_c - \tau) = R(-\tau)[r^j(t_c)_{\text{ECEF}} - \tau\,\dot{r}^j(t_c)_{\text{ECEF}} + \tfrac{1}{2}\tau^2\,\ddot{r}^j(t_c)_{\text{ECEF}}] \tag{2.30}$$

The satellite position and its first and second time derivative are thus evaluated only once, namely at t_c; its position at $t - \tau = t_c - (\nabla t - \delta t) - \tau$ (see Eq. (2.20)) is found by a Taylor series. For the computation of the satellite position and its time derivatives see Appendix B. The value of $(\nabla t - \delta t)$ is at maximum 1 ms (see Section 2.1.2). Using the new position we compute again a topocentric distance. If the difference between this and the previous distance is larger than a user defined threshold, a new travel time is computed from it, and with it a new position of the satellite is computed. Usually three iterations are sufficient to get differences between the topocentric distances of the last two iterations of the order of 10^{-8} m.

$\rho_{\text{old}} = \|r^j(t_c)_{\text{ECEF}} - r_i(t_c)_{\text{ECEF}}\|$
$\tau = \rho_{\text{old}}/c$
$d = \rho_{\text{old}}$
while $d > \varepsilon$
$\kappa = (\nabla t - \delta t) + \tau$
$\rho(t-\tau,t) = \|R(-\tau)[r^j(t_c)_{\text{ECEF}} - \kappa\,\dot{r}^j(t_c)_{\text{ECEF}} + \frac{1}{2}\kappa^2\,\ddot{r}^j(t_c)_{\text{ECEF}}] - r_i(t)_{\text{ECEF}}\|$
$\tau = \rho(t-\tau,t)/c$
$d = \|\rho(t-\tau,t) - \rho_{\text{old}}\|$
$\rho_{\text{old}} = \rho(t-\tau,t)$
end

Note that the increment for the Taylor series equals $-\kappa = -(\nabla t - \delta t) - \tau$, but the argument for the rotation equals $-\tau$.

Derivative of topocentric distance with respect to time.
Besides the topocentric distance sometimes also its time derivative is needed (viz. if we do not regard the receiver clock error as a deterministic parameter, see Section 2.1.2). With the time derivative of the inner product $\langle x, x\rangle$ as

$$\frac{\partial}{\partial t}\langle x, x\rangle = 2\langle \dot{x}, x\rangle$$

it reads, in an ECI system

$$\dot{\rho}(t-\tau,t) = \frac{1}{\rho(t-\tau,t)}\langle \frac{\partial(r^j(t-\tau) - r_i(t))}{\partial t}, r^j(t-\tau) - r_i(t)\rangle \tag{2.31}$$

In an ECI system, the time derivative of $r_i(t)$ is non-zero, so we have

$$\dot{\rho}(t-\tau,t) = \frac{1}{\rho(t-\tau,t)}\langle \dot{r}^j(t-\tau)_{\text{ECI}} - \dot{r}_i(t)_{\text{ECI}}, r^j(t-\tau)_{\text{ECI}} - r_i(t)_{\text{ECI}}\rangle \tag{2.32}$$

With the satellite's respectively the receiver's velocity parameterized in ECEF coordinates as

$$\dot{r}^j(t-\tau)_{\text{ECI}} = R(t-\tau)\dot{r}^j(t-\tau)_{\text{ECEF}} + \dot{R}(t-\tau)r^j(t-\tau)_{\text{ECEF}} \tag{2.33}$$

and

$$\dot{r}_i(t)_{\text{ECI}} = R(t)\dot{r}_i(t)_{\text{ECEF}} + \dot{R}(t)r_i(t)_{\text{ECEF}} \tag{2.34}$$

where

$$\dot{R}(t) = \dot{\Omega}_e \begin{bmatrix} -\sin(\dot{\Omega}_e t + \Psi) & -\cos(\dot{\Omega}_e t + \Psi) & 0 \\ \cos(\dot{\Omega}_e t + \Psi) & -\sin(\dot{\Omega}_e t + \Psi) & 0 \\ 0 & 0 & 0 \end{bmatrix}, \tag{2.35}$$

we eventually get for the time derivative of the topocentric distance

$$\dot{\rho}(t-\tau,t) = \frac{1}{\rho(t-\tau,t)} \langle R(t-\tau)\dot{r}^j(t-\tau)_{\text{ECEF}} + \dot{R}(t-\tau)r^j(t-\tau)_{\text{ECEF}} - R(t)\dot{r}_i(t)_{\text{ECEF}} - \dot{R}(t)r_i(t)_{\text{ECEF}}, R(t-\tau)r^j(t-\tau)_{\text{ECEF}} - r_i(t)_{\text{ECEF}}\rangle \tag{2.36}$$

Assuming that the receiver is stationary in the ECEF system, thus $\dot{r}_i(t)_{\text{ECEF}} = 0$, and again taking $\Psi = -\dot{\Omega}_e t_c$, the time derivative of the topocentric distance for t_c becomes

$$\dot{\rho}(t_c - \tau, t_c) = \frac{1}{\rho(t_c - \tau, t_c)} \langle R(-\tau)\dot{r}^j(t_c - \tau)_{\text{ECEF}} + \dot{R}(-\tau)r^j(t_c - \tau)_{\text{ECEF}} - \omega \times r_{i_{\text{ECEF}}}, R(-\tau)r^j(t_c - \tau)_{\text{ECEF}} - r_{i_{\text{ECEF}}} \rangle \tag{2.37}$$

with

$$\omega = \begin{bmatrix} 0 \\ 0 \\ \dot{\Omega}_e \end{bmatrix} \tag{2.38}$$

2.3 Satellite clock

In the broadcast ephemerides a polynomial model for the satellite clock error is included. This clock error which is used as the approximated value for the estimated clock error, and hence will be denoted by $\delta t^{j^0}(t)$, is computed as

$$\delta t^{j^0}(t) = a_0^j + a_1^j(t - t_{oc}^j) + a_2^j(t - t_{oc}^j)^2 + \Delta t_R^j(t) - \begin{cases} T_{\text{GD}}^j & \text{for P1} \\ \gamma T_{\text{GD}}^j & \text{for P2} \end{cases} \tag{2.39}$$

where a_0, a_1 and a_2 are the coefficients of the polynomial, representing the offset, drift and aging of the clock. Currently it seems that a_2 is always set to zero. The clock error is evaluated a t in GPS time, and $t - t_{oc}$ is the difference between the time of evaluation and the reference time for the polynomial in seconds.

Since the satellite clock is moving with respect to the observing receiver, a relativistic correction has to be added. The large part of this correction is taken care of by a small change in the nominal frequency standard of the satellite clocks. This corrects the effect for a nominal circular satellite orbit. A small correction has to be added to take care for the actual velocity in the actual satellite orbit. A first order approximation for an ECEF observer and a GPS satellite in a Keplerian orbit reads (Spilker Jr. 1996).

$$\Delta t_R^j(t) = -2\frac{\sqrt{GM}}{c^2} e\sqrt{A}\sin E(t) \tag{2.40}$$

$$= -2\frac{\langle r^j(t), \dot{r}^j(t) \rangle}{c^2} \tag{2.41}$$

where

GM	Gravitational constant of the Earth.
c	Speed of light in vacuum.
e	Eccentricity of the satellite orbit.
$E(t)$	Eccentric anomaly of the satellite orbit.
A	Semi-major axis of the satellite orbit.

and where $r^j(t)$ and $\dot{r}^j(t)$ are expressed in the ECI system.

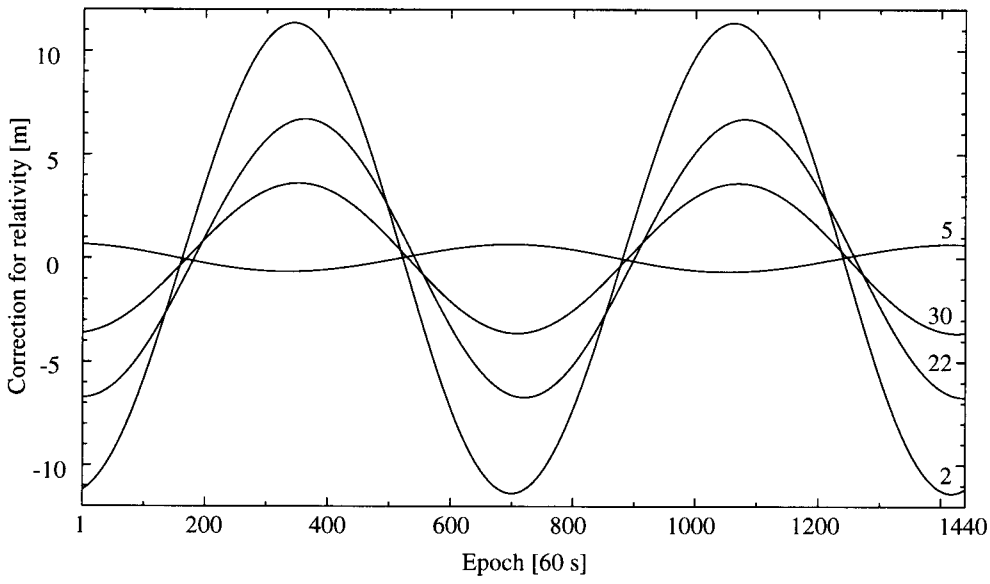

Figure 2.4: Correction for relativity for PRN's 02, 05, 22, and 30.

The difference between expression (2.40) and (2.41) is so small that both may be used, but for the perturbed Keplerian GPS satellite orbit (2.40) is an approximation. Note that in Spilker Jr. (1996) the sign for (2.41) is misprinted. In Figure 2.4 the relativity correction (in meters) for PRN's 02, 05, 22, and 30 (all from orbit plane B) is plotted. The maximum value for the correction is approximately 10 m or 35 ns.

The last term in Eq. (2.39) is a correction for the group delay difference in the satellite transmission between P1 and P2 (also called differential instrumental delay bias, or differential equipment delay). It is based on a calibration prior to the launch of the satellite, and hence in principle constant. Values for it were changed however, somewhere between September 1995 and December 1996. The coefficient a_0 of the clock polynomial is determined on the basis of an observable made of a P1 and P2 observable in which the first order ionospheric delay has been eliminated (ionosphere-free observable). This is equivalent to employing a model for the P1 and P2 observables where for each epoch, for each receiver-satellite combination, an ionospheric delay is included.

Although in Eqs. (2.3) and (2.4) no group delays are included since they are not estimated in our processing setup, they are in principle present:

$$P^j_{i,\mathrm{P1}} = \rho^j_i + c\delta t_{i,\mathrm{P1}} - c\delta t^{j,\mathrm{P1}} + \mathcal{I}^j_i + \mathrm{d}_{i,\mathrm{P1}} - \mathrm{d}^{j,\mathrm{P1}} \tag{2.42}$$

$$P^j_{i,\mathrm{P2}} = \rho^j_i + c\delta t_{i,\mathrm{P2}} - c\delta t^{j,\mathrm{P2}} + \gamma\mathcal{I}^j_i + \mathrm{d}_{i,\mathrm{P2}} - \mathrm{d}^{j,\mathrm{P2}} \tag{2.43}$$

In Section 4.2.5 we will show that if these group delays are present, though not estimated, the estimated receiver clock errors are biased.

If one uses a model in which ionospheric delays are not included, (and where for each observable type a distinct clock is modeled), one has to correct the clock error for all code observables types using the T_{GD} parameter according to Eq. (2.39) to get unbiased estimates

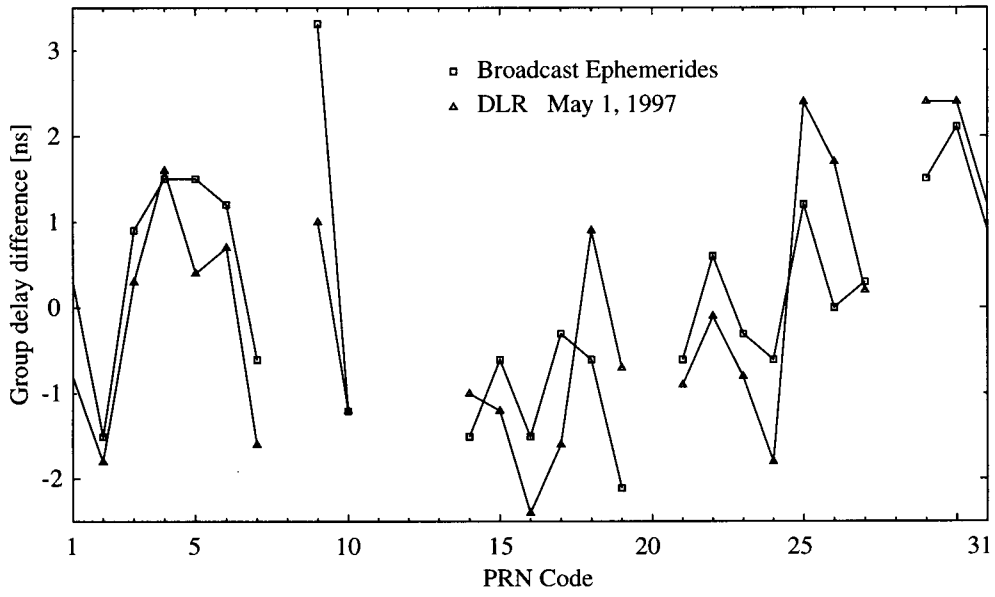

Figure 2.5: Values for differential group delay from DLR and from the broadcast ephemerides.

for the receiver clock errors. The T_{GD} parameter in the broadcast ephemerides is defined as (Spilker Jr. 1996)

$$T_{GD}^{j} = \frac{1}{1-\gamma}(d^{j,P1} - d^{j,P2}) \tag{2.44}$$

Spilker Jr. (1996) states that if ionospheric delays are estimated, i.e. the same model is used as at the CS, the clocks may be corrected, but do not need to. The estimates for the ionospheric delays are biased however. So for the unbiased estimation of these delays, the correction should still be applied.

Unbiased estimates for the receiver clock errors are needed to correct the time tag of the observations (see Section 2.1.2). Unbiased estimates of satellite clock errors are useful to monitor the SA effect (see e.g. Figure 2.2), and can be used in DGPS (Differential GPS) systems. Unbiased estimates for ionospheric delays may be used for monitor purposes and also in DGPS.

Independent estimates for the differential group delay have been published by several authors (Wanninger and Sardon 1993), (Wanninger and Sardon 1994), (Georgiadiou 1994). At the DLR (Deutsches Zentrum für Luft- und Raumfahrt) Fernkundungsstation in Neustrelitz, Germany, group delays for all satellites and a number of receivers at (mainly European) permanent stations are estimated on a daily basis. Each group delay is biased by some function of other group delays; e.g. the group delays for the satellites are biased by the average of the group delay of all satellites. In Figure 2.5 the values for a particular day as computed by DLR and the values from a set of broadcast ephemerides of 1997 are depicted. The values of DLR are defined as $d^{j,P2} - d^{j,P1}$ and are therefore converted to the definition of T_{GD} as in Eq. (2.44).

This a priori correction for the satellite clock error is for a relative positioning setup not really necessary, since the satellite clock error can be estimated (in contrast to the single

	North	East	Height
L1	1.5	-1.2	75.1
L2	-1.1	1.7	69.2

Table 2.2: Offsets for Trimble Geodetic L1/L2 compact antenna with ground plane [mm] in a local level system.

receiver setup). It may still be applied to speed up convergence for the iterated least-squares solution and to observe the effect of Selective Availability, since this is the only effect not included in the clock model.

Clock errors are optionally present in the precise ephemerides; they are given at an interval of 15 minutes. Clock errors for a desired epoch are computed by a Lagrange interpolation.

2.4 Phase center variation and offset

An ideal antenna has dimensions that are small compared to the wavelength of the transmitted or received wave. The surface of equal phase, the so-called wave front is then perfectly spherical, with the phase center in its center. Unfortunately, such a perfect antenna is equally sensitive to all waves irrespective of the direction to, or from which the wave is transmitted respectively received. For the GPS, antennas are used that are more sensitive in certain directions. The transmitting antenna is designed such that most of the signal is transmitted towards the Earth, the receiving antenna is designed such that almost no signal is received from an elevation less than zero degrees. In order to design such type of antenna, the dimension of the antenna has to be of the order of the wavelength. This causes the outgoing or incoming wave front to divert from the desired spherical form; every direction has its local spherical wave front, and consequently its own phase center. This direction dependence is mostly due to variations in elevation of the received signal because of the rotation symmetry of the antenna with respect to its Z-axis. Small variations due to azimuthal asymmetries are calibrated during the production process, and are assumed equal for all antennas of a certain make, provided that they are equally oriented with respect to a mark put on the antenna during production. Hence the well known operational requirement to orient the antenna with the mark pointing northward.

One of the most frequently correction tables in use nowadays is the one that is accepted as the standard for the IGS community, where almost all antennas in use in the geodetic community are calibrated with respect to the Dorne Margolin antenna (Rothacher and Mader 1996). Besides the elevation dependent phase center variation, also the fixed offsets of the mean phase center of both frequencies from the so-called 'Antenna Reference Point', (ARP) an easily identified and well documented mark at the receiver antenna, can be found in these lists. An example of the offsets and elevation dependent corrections for the Trimble Geodetic L1/L2 compact antenna with ground plane can be found in Table 2.2 and Figure 2.6. The correction for the offsets has to be added to the height and horizontal offsets of the antenna. The correction for the phase center variation has to be subtracted from the observations (ibid.).

For the antennas of the satellites no elevation dependent corrections are available. As far

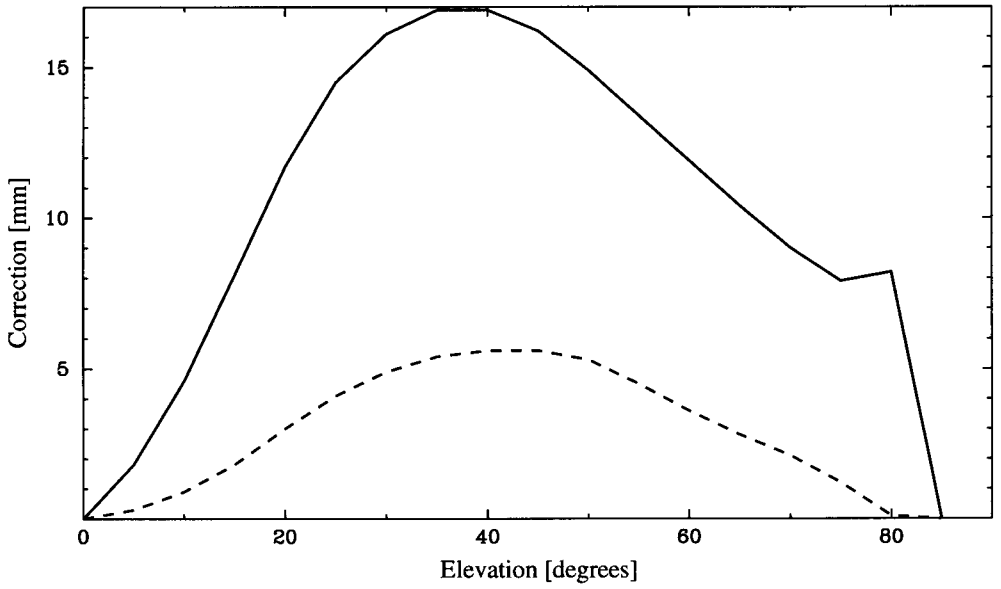

Figure 2.6: Antenna phase center variation: elevation (E) dependent correction terms for the Trimble Geodetic L1/L2 compact antenna with ground plane (mm).

	e_1	e_2	e_3
Block I	0.2100	0.0000	0.8540
Block II/IIA	0.2794	0.0000	1.0259

Table 2.3: Offsets between mass center of satellite and phase center of antenna [m], in the local satellite-fixed system (see Section 2.8).

as the offsets are concerned, it depends if one uses the broadcast ephemerides or the precise ephemerides. The broadcast ephemerides are defined for the nominal phase center of the antenna, whereas the precise ephemerides are defined for the mass center of the satellite. In the latter case, the position of the phase center depends on the position of the mass center, the offsets of the antenna phase center with respect to the center of mass, and the orientation of the satellite. The offsets are different for different generations of the GPS satellites; they can be found in Table 2.3.

2.5 Tropospheric delay

The troposphere is the lower part of the Earth's atmosphere, which extends to a height of between 9 km at the poles and 16 km at the equator. The presence of neutral atoms and molecules in it, delays the GPS signals traveling through it; this is called refraction.

The tropospheric delay T at zenith is usually divided in a dry or hydrostatic part T_h and

a wet or water vapor part T_w:

$$T = T_h + T_w \tag{2.45}$$

It is mapped into a slant delay for a signal received at elevation E, using different mapping functions for the hydrostatic (μ_h) and the water vapor part (μ_w)

$$T(E) = \mu_h(E)T_h + \mu_w(E)T_w \tag{2.46}$$

The hydrostatic part can be computed a priori as (Saastamoinen 1973), (Davis et al. 1985)

$$T_h = 0.0022768\frac{P}{g_m} \tag{2.47}$$

with

$$g_m = 9.784(1 - 0.00266\cos 2\phi - 0.00028H) \tag{2.48}$$

where P is the pressure at the station in mbar, ϕ its geocentric latitude, and H its orthometric height.

There exist several models for the water vapor part too, using temperature, pressure and relative humidity at the station, but they are far less accurate (Hopfield 1969), (Saastamoinen 1973). Therefore often zenith delays are estimated. If one has sufficiently accurate meteo date available, the hydrostatic part can be computed a priori and corrected for, and the water vapor part can be estimated. If this is not the case, only the hydrostatic part is estimated. Since the mapping functions for the hydrostatic and water vapor part are quite similar, part of the water vapor part will be absorbed by the estimate for the hydrostatic part (Davis et al. 1985). Estimating both, results in estimates of low precision that are highly correlated.

The estimate for the zenith delay is also highly correlated with the estimate for the height of the station. It is therefore necessary to include data of low elevation angle, and the time span should be of the order of one hour. If the total time span is longer, more than one delay may be estimated. When the separation between stations is small, the zenith delays are almost parallel to each other and this will again result in poor estimability. In that case, one of the zenith delays should be kept fixed to a known value, using one of the a priori models for the water vapor or the total zenith delay.

The most elementary mapping function for the zenith delay reads

$$\mu(E) = \frac{1}{\sin E} \tag{2.49}$$

Better results, especially for data of low elevation, are obtained using mapping functions consisting of a continued fraction:

$$\mu(E) = \cfrac{1}{\sin E + \cfrac{\alpha_1}{\sin E + \cfrac{\alpha_2}{\sin E + \cfrac{\alpha_3}{\sin E + \cdots}}}} \tag{2.50}$$

See e.g. Marini (1972), Herring (1992) and Niell (1996). For an overview of the performance of several mapping functions see Mendes and Langley (1994).

2.6 Ionospheric delay

The signals of the GPS satellites experience a delay when passing through the ionospheric layer. This layer reaches from approximately 70 to 1000 kilometers above the Earth's surface. The carrier phase experiences an advance or negative delay, while the code on the carrier experiences a positive delay of the same size. In a first order approximation, the size of the delay in meters depends reciprocally on the squared frequency of the signal (and thus is a dispersive effect), and linearly on the number of free electrons passed when traveling through the ionospheric layer.

The number of free electrons depends among other things on the local time of the day, the location on Earth, and where we are in the sun spot cycle. At daytime the Sun's radiation increases the number of free electrons. The maximum occurs at around 14.00 local time, the minimum at around 2.00. When the sun spot number increases, so does the amount of free electrons. The sun spot number passes through an eleven-year cycle, of which the next maximum is to be expected around the year 2002. In general, there is a fair amount of correlation both in time and in place for the ionospheric delay. At a lower elevation the length of the path from satellite to receiver increases, and thus also the ionospheric delay increases.

Besides the refraction part there is also diffraction, i.e. the path diverts from the straight line from satellite to antenna. This effect is on the millimeter level, and largely cancels in the relative positioning setup.

There are roughly three ways to handle the ionospheric delays. For short baselines the delay experienced at both ends of the baseline is almost equal, since signals pass the ionospheric layer at paths close in distance, and also elevation angles at both end points of the baseline are almost equal. Hence it will be absorbed by the satellite clock, and does not need to be modeled.

For larger distances the delay can be modeled for each receiver-satellite combination as a slant delay. Use is made of the fact that the ionospheric delay is dispersive. Commonly instead of modeling the delay, it is eliminated: from two observable types, one at each frequency, a so-called ionosphere-free observable is formed. When it is formed using the carrier phases it is called LC or L3. As we will show in Chapter 4 this is equivalent to modeling ionospheric slant delays

Another option is to model the ionospheric delay by a series in the local hour angle of the Sun at the so-called ionospheric point and the geocentric latitude of this ionospheric point. For the model the ionospheric layer is supposed to be concentrated in an infinitesimal thin layer at an height of approximately 300–400 km above the Earth's surface. The ionospheric point is the point where the line receiver-satellite intersects the ionospheric layer. In Figure 2.7 the ionospheric layer is depicted together with a schematic receiver-satellite combination. Instead of a slant delay $\mathcal{I}_i^j$ at the receiver position, a vertical delay $\mathcal{I}_v$ at the ionospheric point is then modeled. The relation between the two is

$$\mathcal{I}_i^j = \frac{1}{\cos z'} \mathcal{I}_v \tag{2.51}$$

with

$$\sin z' = \frac{R}{R+h} \sin z \tag{2.52}$$

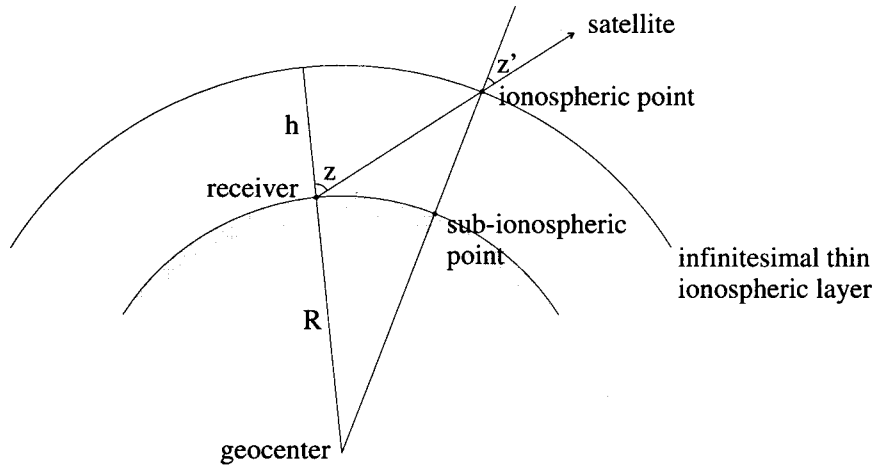

Figure 2.7: Geometry for modeling the ionospheric delay using an infinitesimal thin ionospheric layer.

where R is the Earth's radius, h the height of the ionospheric layer, and z the zenith angle at the receiver position.

Usually a Taylor series or a series in spherical base functions is used; it has a fairly low resolution but only a limited set of parameters is introduced. The thus estimated model is defined in an Earth-Centered Sun-Fixed system, i.e. the Earth rotates underneath it. The temporal variation and spatial variation in latitude is modeled by it.

The modeling by slant delays inhibits a much higher resolution both in time and space, but to the expense of the introduction of a large number of extra parameters. The latter can be alleviated by constraining these parameters. Since the modeling by a series can capture the long term effects, the slant delays only have to model the short term residual effects, and can thus be tightly constrained. Instead of constraining the ionospheric delays in an absolute sense, they can also be constrained in a between station sense, see Chapter 6.

Sometimes first a model is estimated using an independent data set, and consequently applied to the data at hand, where the short term ionospheric delay is then modeled by (constrained) slant delays. In this thesis the ionospheric delays are only modeled as slant delays.

In Figure 2.8 a projection of the ionospheric points on the Earth's surface (sub-ionospheric points) is depicted for two stations and four satellites, for a time span of one day. It shows that the space over which an antenna senses the ionosphere is quite large, and that for long baselines the points are too far apart to benefit from the spatial correlation.

For an overview of the treatment of the effects caused by the ionosphere on GPS precise positioning see Odijk (1997).

2.7 Solid Earth tides

The gravitational attraction of the Sun and the Moon, and the fact that the Earth is an elastic body, impose periodic displacements to stations on the Earth. This phenomenon is called solid Earth tides. Without going into great detail, the size and direction of the

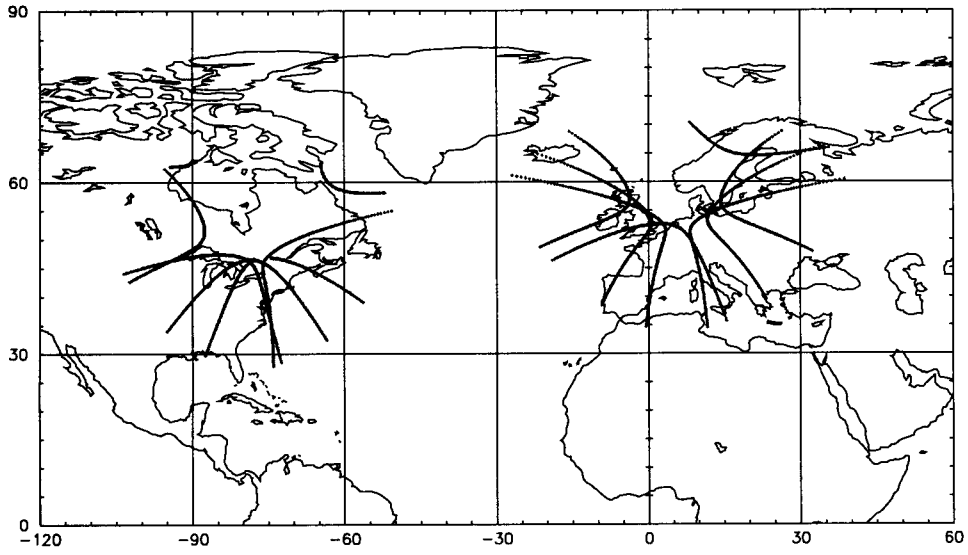

Figure 2.8: Ionospheric points for Algonquin and Kootwijk for PRN 1,2,3 and 4 for an elevation cut-off of zero degrees, and a time span of one day.

displacement depends on the position of the station with respect to the Sun and the Moon, the accelerating forces of the Sun and the Moon, and the rheology of the Earth.

The tidal potential W for a point i on the Earth due to a celestial body b is given by (Vaníček and Krakiwsky 1986)

$$W^b = \frac{GM_b}{\|r_b\|} \sum_{n=2}^{\infty} \left(\frac{\|r_i\|}{\|r_b\|} \right)^n P_n(\cos z_b) \tag{2.53}$$

where

$P_n(x)$	The Legendre polynomials ($n = 2, 3, \ldots$).
GM_b	Gravitational constant of the celestial body.
r_i	Unit vector from the geocenter to station i.
r_b	Unit vector from the geocenter to the center of celestial body b.
z_b	Angle between the geocentric position vectors of station i and the center of celestial body b.

(The celestial bodies involved are the Sun and the Moon.)

The largest contribution comes from the second-order harmonic term:

$$W_2^b = GM_b \frac{\|r_i\|^2}{\|r_b\|^3}\left(\tfrac{3}{2}\cos^2 z_b - \tfrac{1}{2}\right) \tag{2.54}$$

To an accuracy of a few percent for the combined effect of the Sun and the Moon, it suffices to include only the second-order terms; inclusion of the third order term for the Moon improves the accuracy to about 0.03 % (ibid.). In geocentric coordinates ϕ, λ and R (latitude, longitude, radius), the tidal displacements read (ibid.)

$$d\phi = \frac{l_2}{g}\frac{\partial W_2^b}{\partial \phi} \quad ; \quad d\lambda = \frac{l_2}{g\cos\phi}\frac{\partial W_2^b}{\partial \lambda} \quad ; \quad dR = h_2\frac{W_2^b}{g} \tag{2.55}$$

where h_2 and l_2 are the Love and Shida number of second degree. With

$$\begin{bmatrix} \frac{\partial W}{\partial \phi} \\ \frac{1}{\cos\phi}\frac{\partial W}{\partial \lambda} \end{bmatrix} = \begin{bmatrix} 1 & \\ & \frac{1}{\cos\phi} \end{bmatrix} \begin{bmatrix} \frac{\partial X}{\partial \phi} & \frac{\partial Y}{\partial \phi} & \frac{\partial Z}{\partial \phi} \\ \frac{\partial X}{\partial \lambda} & \frac{\partial Y}{\partial \lambda} & \frac{\partial Z}{\partial \lambda} \end{bmatrix} \begin{bmatrix} \frac{\partial W}{\partial X} \\ \frac{\partial W}{\partial Y} \\ \frac{\partial W}{\partial Z} \end{bmatrix} \tag{2.56}$$

and

$$\begin{bmatrix} dX \\ dY \\ dZ \end{bmatrix} = \begin{bmatrix} \frac{\partial X}{\partial \phi} & \frac{\partial X}{\partial \lambda} & \frac{\partial X}{\partial R} \\ \frac{\partial Y}{\partial \phi} & \frac{\partial Y}{\partial \lambda} & \frac{\partial Y}{\partial R} \\ \frac{\partial Z}{\partial \phi} & \frac{\partial Z}{\partial \lambda} & \frac{\partial Z}{\partial R} \end{bmatrix} \begin{bmatrix} d\phi \\ d\lambda \\ dR \end{bmatrix} \tag{2.57}$$

where

$$\begin{bmatrix} \frac{\partial X}{\partial \phi} & \frac{\partial X}{\partial \lambda} & \frac{\partial X}{\partial R} \\ \frac{\partial Y}{\partial \phi} & \frac{\partial Y}{\partial \lambda} & \frac{\partial Y}{\partial R} \\ \frac{\partial Z}{\partial \phi} & \frac{\partial Z}{\partial \lambda} & \frac{\partial Z}{\partial R} \end{bmatrix} = \begin{bmatrix} -\sin\phi\cos\lambda & -\cos\phi\sin\lambda & \cos\phi\cos\lambda \\ -\sin\phi\sin\lambda & \cos\phi\cos\lambda & \cos\phi\sin\lambda \\ \cos\phi & 0 & \sin\phi \end{bmatrix} \tag{2.58}$$

and g is approximated as $GM/\|r_i\|^2$, where GM is the gravitational constant of the Earth, one gets for the tidal displacement vector in the Cartesian system

$$[\ dX \quad dY \quad dZ\ ]^T = \frac{GM_b}{GM}\frac{\|r_i\|^4}{\|r_b\|^3}\{h_2\tfrac{1}{2}\left(3\cos^2 z_b - 1\right) r_i + 3l_2\cos z_b(r_b - r_i\cos z_b)\} \tag{2.59}$$

Substitution of $\cos z_b = \langle r_i, r_b\rangle$ in Eq. (2.59) gives the equation as given in McCarty (1992).

In Figure 2.9 the movement of Delft (the Netherlands), and Alonquin (Canada) with respect to Kootwijk (the Netherlands) due to the solid Earth tides is depicted, for a time span of one day. The distance between Delft and Kootwijk is approximately 100 km, the distance between Alonquin and Kootwijk is approximately 5,620 km.

2.8 Phase wind-up

In contrast to ordinary radio links on Earth that use linearly polarized electro magnetic waves, links between (high orbiting) satellites and the Earth use a circular polarization for the wave. The reason lies in the fact that the waves have to cross the ionospheric layer,

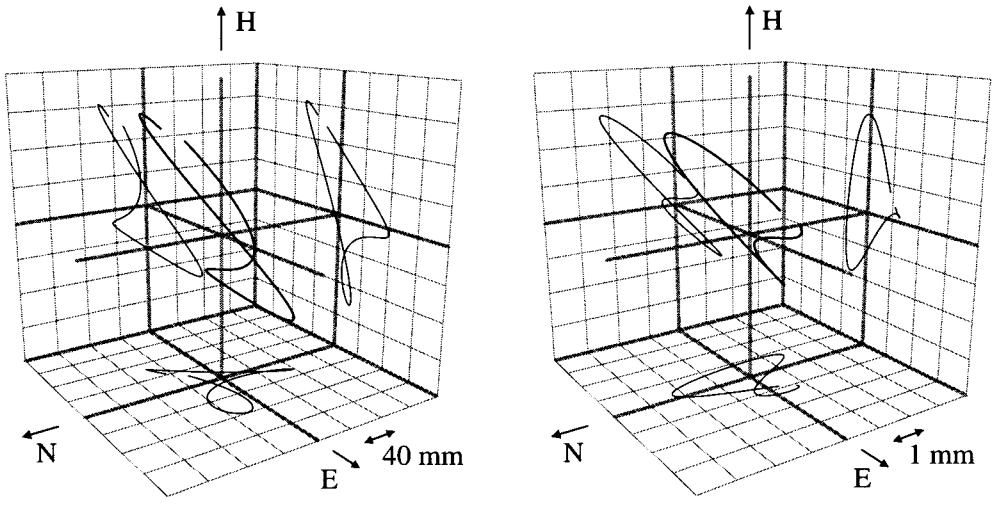

Figure 2.9: Movement of station due to solid Earth tides during one day. Alonquin with respect to Kootwijk (left), and Delft with respect to Kootwijk (right).

where its polarization through an interaction with the free electrons starts to rotate. This phenomenon is called Faraday rotation.

The intensity of the rotation depends on the total electron concentration, which is highly variable. For a linearly polarized wave received by a fixed dipole this would result in a highly fluctuating signal.

When using a circular polarization, the electric field makes a spiral movement from the transmitter to the receiver (see Figure 2.10). If the field, looking into the direction of the propagation of the wave, rotates clockwise, it is called a right-hand circular polarization. The GPS uses this type of polarization; the Faraday rotation does not effect the intensity of the received signal, but when using only one dipole, only half of the signal strength is received.

For the determination of the signal strength of a circularly polarized wave received by one dipole, we can decompose the circularly polarized wave into two linear polarized waves; one with an electric field in a plane parallel to the dipole, and one with an electric field perpendicular to that plane. The phase difference between the two electric fields is 90^0, and the energy of the wave is equally divided over the two linear polarized waves. As a consequence, the signal strength received with one dipole is half of the total signal strength. To receive the total signal strength, an extra dipole has to be added, perpendicular to the first dipole (crossed dipole). The signal of the extra dipole is combined with the first dipole after the phase difference of 90^0 is removed by the electronics in the antenna (de Jong 1989).

Since the electric field is permanently rotating, the carrier phase observation made by the receiver at two subsequent epochs is not only a function of the change in distance between receiver and satellite, but it is also a function of the rotation of the receiver and satellite antenna. In kinematic applications this phenomenon can clearly be observed, see e.g. Tiberius et al. (1997). Due to the rotation of the Earth and the changing attitude of the satellite needed to keep the antenna pointed towards the geocenter, and the solar panel support beam perpendicular to the satellite-Sun direction, also phase observations made in static applications exhibit a small bias.

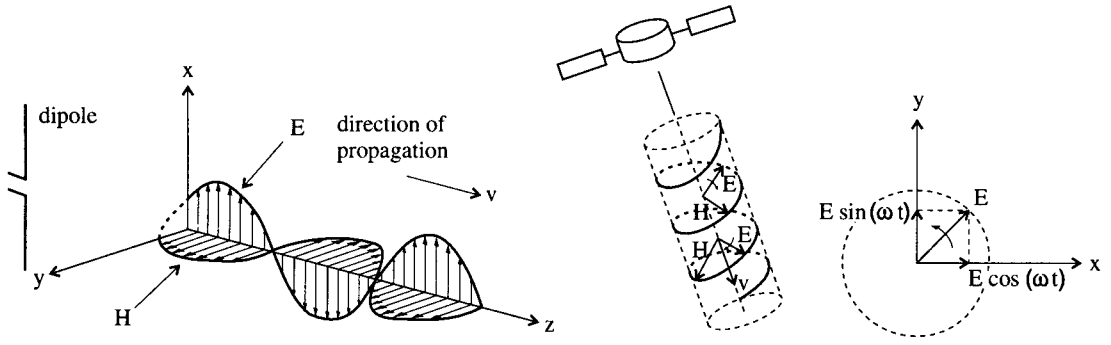

Figure 2.10: Linearly polarized wave (left), and circularly polarized wave (right) (from de Jong (1989)).

The effect is called phase wind-up, and it is different for observations made at one receiver to two different satellites, and for observations made at two different receivers to one satellite.

Consequently the effect is only partly absorbed by the estimates for the satellite and receiver clock error; the constant part is absorbed by the estimate for the phase ambiguity.

In Wu et al. (1993), the effects of the phase wind-up are evaluated and a method to correct it are given. The effect is negligible for short baselines, but for a 4,300 km baseline the peak to peak effect may be as large as 4 cm at the L1 frequency for an elevation cut-off of 10 degrees.

The correction is based on the change of the angle between two so-called effective dipoles, one at the receiver, and one at the satellite. For the receiver the dipole is defined in a local North, West, Up system, whose axes are denoted by e_i'. The dipole for the satellite is defined in a satellite-centered coordinate system, denoted by e_i. The choice for the axes of this system is driven by the fact that the antenna of the satellite is kept pointed towards the geocenter, and that the solar panel support beam is designed to be perpendicular to the satellite-Sun direction. The system is defined (Lichten and Border 1987) in such a way that the third axis is positive along the antenna direction towards the geocenter:

$$e_3 = \frac{-r^j}{\|r^j\|} \tag{2.60}$$

The second axis is taken along the solar panel beam, normal to the satellite-Sun direction $(r^S - r^j)$ and the third axis; i.e. normal to the plane containing satellite, Earth and Sun:

$$e_2 = \frac{e_3 \times (r^S - r^j)}{\|e_3 \times (r^S - r^j)\|} \tag{2.61}$$

And the first axis completes the right-hand system (see Figure 2.11).

$$e_1 = \frac{e_2 \times e_3}{\|e_2 \times e_3\|} \tag{2.62}$$

The effective dipoles which represent the resultants of the crossed dipole antennas are defined as:

$$\vec{D} = \underbrace{e_1 - \nu\langle \nu, e_1 \rangle}_{\text{(i)}} + \underbrace{\nu \times e_2}_{\text{(ii)}} \tag{2.63}$$

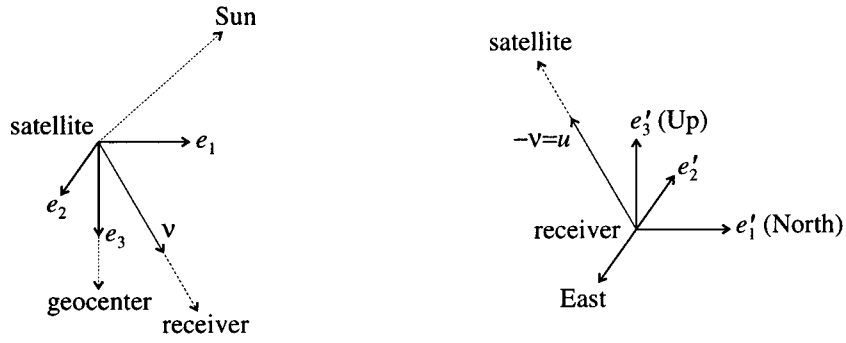

Figure 2.11: Satellite fixed coordinate system (left), and receiver fixed coordinate system (right) for the computation of phase wind-up correction.

at the satellite, and

$$\vec{D}' = \underbrace{e_1' - \nu\langle \nu, e_1' \rangle}_{\text{(i')}} - \underbrace{\nu \times e_2'}_{\text{(ii')}} \tag{2.64}$$

at the receiver, with e_i and e_i' the unit vectors defining the local system at the satellite, respectively the receiver, and $\nu = -u$ the unit vector in the direction satellite-receiver. The two dipoles constituting the crossed dipole are defined to be coinciding with the e_1 and e_2 axis, but can be chosen to be any pair of unit vectors in the e_1-e_2 plane, obtained by rotating the pair e_1, e_2. In this way the signal of the second dipole is delayed by 90^0 with respect to the signal of the first dipole. In Eqs. (2.63) and (2.64), (i) and (i') are the projections of the first dipole onto a plane normal to ν, whereas (ii) and (ii') are the projections of the second dipole onto the same plane rotated by 90^0.

The phase wind-up correction is defined as the angle between the two effective dipoles, while it is taken care of that the transitions from $-\pi$ to π radians are taken into account by adding 2π radians to the correction for each transition.

With the effective dipole of the satellite denoted by $\vec{D}$ and that of the receiver by $\vec{D}'$, the fractional part of the phase wind-up correction is then defined by

$$\vartheta_f(t_k) = sign(\xi) \arccos\langle \vec{D}', \vec{D} \rangle \tag{2.65}$$

where

$$\xi = \langle \nu, (\vec{D}' \times \vec{D}) \rangle \tag{2.66}$$

and *sign*() is the function that gives the sign of a number. The integer part is defined as

$$\vartheta_i(t_k) = nint(\frac{\vartheta_f(t_k) - \vartheta_f(t_{k-1})}{2\pi})2\pi \tag{2.67}$$

where *nint*() is the nearest integer function. The total phase wind-up correction is then $\vartheta(t) = \vartheta_i(t) + \vartheta_f(t)$ where implicitly it is assumed that the difference of the total correction

for two subsequent epochs is smaller than π, a condition that in practice for a static receiver and a normal sampling rate, always is fulfilled.

In Figure 2.12 the between-receiver single difference phase wind-up corrections for two baselines computed with the model above are depicted, viz. for the baseline between the IGS stations Algonquin and Kootwijk with a length of approximately 5,620 km, and for the baseline between Kootwijk and Wettzell with a length of approximately 600 km. For the 5,620 km baseline the maximum double differenced phase wind-up correction is of the order of 0.2 cycle, (4 cm for the L1 phase), whereas for the 600 km baseline the maximum is of the order of 0.02 cycles (4 mm for the L1 phase).

Another phenomenon closely related to the phase wind-up that needs to be corrected for, is the yawing of the satellites when they are in eclipse. In eclipse, the attitude of the satellites with respect to the Sun is not maintained, since the satellite is unable to 'see' the Sun. As a consequence the satellite starts to rotate around the third axis (along the antenna that is pointing towards the geocenter). This will cause an additional phase wind-up, but since it is equal for all observing receivers, it will be absorbed into the estimate for the satellite clock. The error in the range due to the offset of the phase center will in general be different however, for each receiver-satellite combination. This phenomenon will not be treated here, and a correction for it has not been implemented in the software. It has been implemented however in the software suites that are used by the IGS community. For more information we refer to Bar-Sever (1994) and Bar-Sever (1995).

2.9 Computation of Sun and Moon position

The position of the Sun and the Moon as needed for the computation of solid earth tides, as well as for the determination of the attitude of the GPS satellites (Sun only) can be computed using JPL's (Jet Propulsion Laboratory) Planetary and Lunar Ephemerides DE403/LE403 (Standish et al. 1995). The positions are defined in the J2000 reference frame of the International Earth Rotation Service (IERS).

The transformation from the inertial celestial frame J2000 to the Earth-Fixed frame ITRF consists of four separate transformations, viz. a precession rotation P, a nutation rotation N, a siderial time rotation T and a polar motion rotation Z (Bock 1996).

$$r_{\mathrm{ITRF}} = ZTNP\, r_{\mathrm{J2000}} \tag{2.68}$$

Precession and nutation represent the motion of the pole of the rotation axis of the Earth around the pole of the ecliptic, and are thus movements in the inertial celestial system. The rotations due to siderial time and polar motion are movements with respect to the (semi-inertial) terrestrial system itself. Polar motion is the rotation of the true celestial pole as defined by the precession and nutation model with respect to the Z-axis of the terrestrial reference frame. The rotation T around the true celestial pole gives the relation between a rotating, semi-inertial system at the date of epoch and the Earth-Fixed system.

The transformation matrices are computed according to McCarty (1992). Additional data needed for the computation of the polar motion and siderial time matrix are interpolated from Bulletin A or B of the IERS.

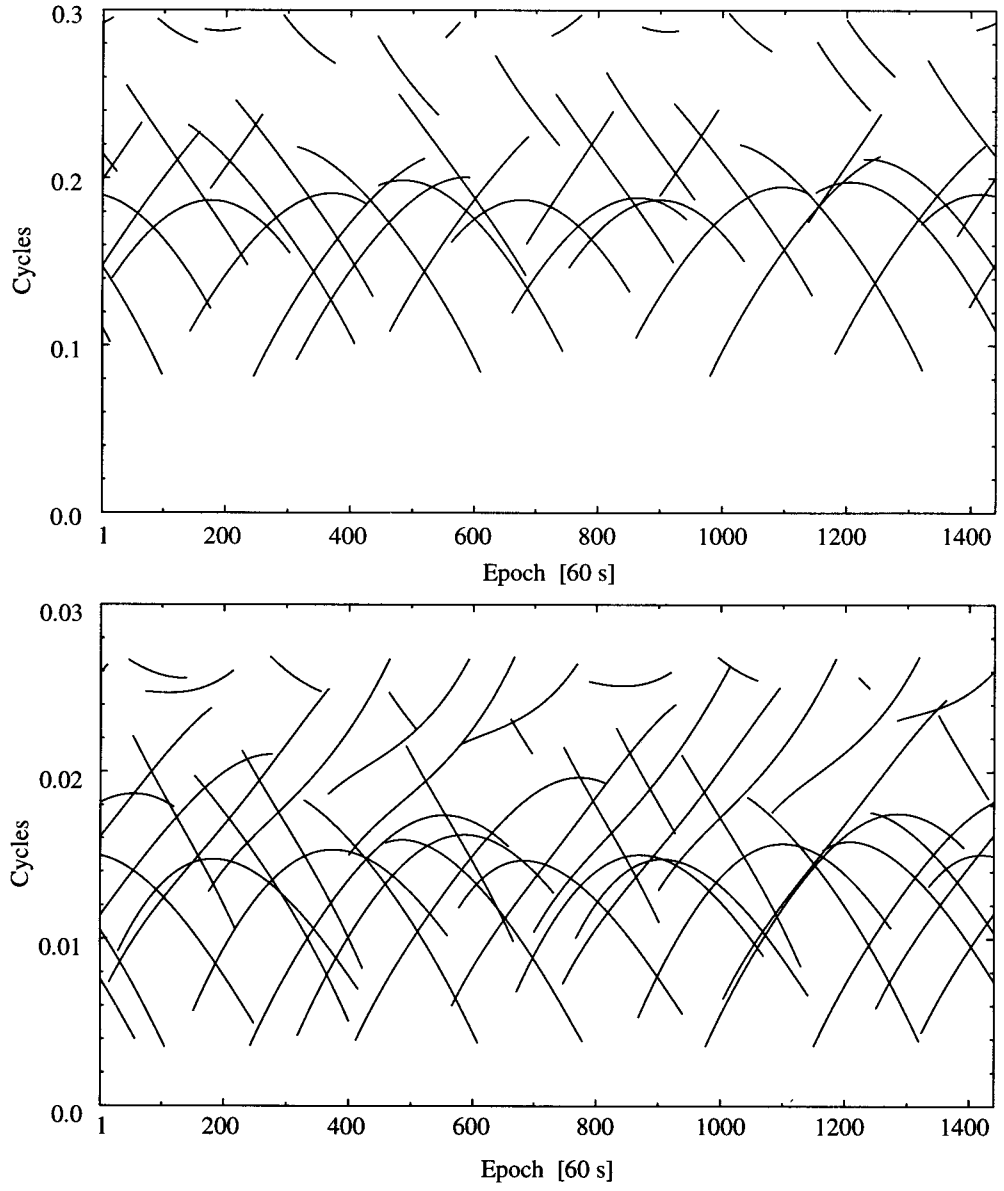

Figure 2.12: Effects of phase wind-up, for between-stations single differences for Algonquin and Kootwijk (above) and Kootwijk and Wettzell (below), for all satellites in view at May 12, 1997 (elevation cut-off of zero degrees).

2.10 Concluding remarks

The tides cause a non-moving antenna, for which we want to determine a set of coordinates for a defined time span, to move around. We want, however, to estimate only one set of coordinates for it.

In Section 2.7 it was indicated how this movement can be modeled. The correction is applied as follows. For each epoch the tide correction is added to the a priori coordinates. These coordinates are used to compute the topocentric range.

The values of the coordinates for the purpose of constraining one or more sets of coordinates to well known a priori coordinates and the computation of partials for the design matrix are not corrected. The correction is not necessary since we already corrected the range.

For the offset of the antenna we have a similar problem. Since the offsets commonly are not equal for both frequencies, there are two sets of coordinates for each antenna, one for the L1 phase center and one for the L2 phase center. Again, we want to estimate only one set of coordinates. We proceed therefore as follows. The topocentric range for the observables on L1 is computed between the L1 phase center and the satellite, the range for the observables on L2 is computed between the L2 phase center and the satellite. The constraining and computation of the partials is made with respect to the L1 phase center.

The list of error sources treated in this chapter is not complete. A prominent error source is e.g. multipath, caused by reflection of the signal in the neighborhood of the transmitting and receiving antenna. It is omitted, since in general it is neither possible to model it a priori (for continuously operating stations some modeling is possible, since the multipath signal repeats after one approximately one day) , nor to estimate it (i.e. not together with the coordinate parameters). Other (small) effects are e.g. (Bock 1996) the displacement of a station due to ocean loading (the elastic response of the Earth's crust to ocean tides) and atmospheric loading (the elastic response of the Earth's crust to a time-varying atmospheric pressure distribution).

References

Bar-Sever, Y. (1995). Performance evaluation of the GPS yaw bias implementation. In *Proceedings of ION GPS-95, 8th International Technical Meeting of the Satellite Division of the Institute of Navigation,* Palm Springs, CA, pp. 599–611. The Institute of Navigation.

Bar-Sever, Y. E. (1994). Improvement to the GPS attitude control subsystem enables predictable attitude during eclipse seasons. IGS Electronic Mail, No. 591.

Bock, Y. (1996). Reference systems. See Kleusberg and Teunissen (1996), Chapter 1, pp. 3–36.

Brouwer, F. J. J., J. van Buren, B. H. W. van Gelder, G. J. Husti, C. D. de Jong, G. de Jong, J. C. de Munck, and H. J. W. van der Vegt (1989). *GPS navigatie en geodetische puntsbepaling met het Global Positioning System.* Faculteit der Geodesie, Delft University of Technology.

Davis, J. L., T. A. Herring, I. I. Shapiro, A. E. E. Rogers, and G. Elgered (1985). Geodesy by radio interferometry: effects of atmospheric modeling errors on estimates of baseline length. *Radio Science 20*(6), 1593–1607.

de Jong, G. (1989). GPS ontvangers. See Brouwer, van Buren, van Gelder, Husti, de Jong, de Jong, de Munck, and van der Vegt (1989), Chapter 4, pp. 4.1–4.64.

Feigl, K. L., R. W. King, T. A. Herring, and M. Rothacher (1991). A scheme for reducing the effect of Selective Availability on precise geodetic measurements from the Global Positioning System. *Geophysical Research Letters 18*(7), 1289–1292.

Georgiadiou, Y. (1994). Modelling the ionosphere for an active control network of GPS stations. LGR-Series 7, Delft Geodetic Computing Centre, Delft University of Technology.

Herring, T. A. (1992). Modeling atmospheric delays in the analysis of space geodetic data. In *Proceedings of the Symposium on Refraction of Transatmospheric Signals in Geodesy,* The Hague, The Netherlands, May 19–22, pp. 157–164.

Hopfield, H. S. (1969). Two-quartic tropospheric refractivity profile for correcting satellite data. *Journal of Geophysical Research 74*(18), 4487–4499.

Kleusberg, A. and P. J. G. Teunissen (Eds.) (1996). *GPS for Geodesy,* Volume 60 of *Lecture Notes in Earth Sciences.* Springer Verlag.

Langley, R. (1996). Propagation of the GPS signals. See Kleusberg and Teunissen (1996), Chapter 3, pp. 103–140.

Lichten, S. M. and J. S. Border (1987). Strategies for high-precision Global Positioning System orbit determination. *Journal of Geophysical Research 92*(B12), 12751–12762.

Marini, J. W. (1972). Correction of satellite tracking data for an arbitrary atmospheric profile. *Radio Science 7*(2), 223–231.

McCarty, D. D. (Ed.) (1992). *IERS Standards (1992),* Number 13 in IERS Technical Note, 61, avenue de l'Observatoire, F-75014 PARIS – France. Central Bureau of IERS – Observatoire de Paris.

McDonald, K. D. (1991). GPS clocks, precise time, and time interval measurement. In *Navstar GPS and GLONASS for engineers.* Navtech Seminars Inc., Arlington, VA, USA.

Mendes, V. B. and R. B. Langley (1994). A comprehensive analysis of mapping functions used in modeling tropospheric propagation delay in space geodetic data. In *Proceedings of International Symposium on Kinematic Systems in Geodesy, Geomatics and Navigation KIS'94,* Banff, Canada, August 30–September 2, pp. 87–98.

Niell, A. E. (1996). Global mapping functions for the atmospheric delay at radio wavelengths. *Journal of Geophysical Research 101*(B2), 3227–3246.

Odijk, D. (1997). Treatment of the ionospheric effect on precise GPS positioning – an inventarisation of existing approaches –. Internal report, Mathematical Geodesy and Positioning.

Parkinson, B. W. and J. J. Spilker Jr. (Eds.) (1996). *Global Positioning System: Theory and Applications Volume I*, Volume 163 of *Progress in Astronautics and Aeronautics*. American Institute of Aeronautics and Astronautics, Inc.

Rocken, C. and C. Meertens (1991). Monitoring selective availability dither frequencies and their effect on GPS data. *Bulletin Géodésique 65*, 162–169.

Rothacher, M. and G. Mader (1996). Combination of antenna phase center offsets and variations.

Saastamoinen, J. (1973). Contributions to the theory of atmospheric refraction. *Bulletin Géodésique 47*(105–107), 279–298, 383–397, 13–34.

Spilker Jr., J. J. (1996). GPS navigation data. See Parkinson and Spilker Jr. (1996), Chapter 4, pp. 121–176.

Standish, E. M., X. X. Newhall, J. G. Williams, and W. M. Folkner (1995). JPL planetary and lunar ephemerides, DE402/LE402. Interoffice memorandum IOM 314.10–27, Jet Propulsion Laboratory.

Teunissen, P. J. G. and H. van der Marel (1992). Lecture notes of the GPS working group. Faculty of Geodetic Engineering, Delft University of Technology, The Netherlands.

Tiberius, C. C. J. M., P. J. G. Teunissen, and P. J. de Jonge (1997). Kinematic GPS: performance and quality control. In *Proceedings of International Symposium on Kinematic Systems in Geodesy, Geomatics and Navigation KIS'97*, Banff, Canada, June 3–6, pp. 289–299.

Vaníček, P. and E. Krakiwsky (1986). *Geodesy: the concepts* (Second ed.). North-Holland/Elsevier.

Wanninger, L. and E. Sardon (1993). Improved data sets of the differential instrumental delays of GPS satellites. IfE-Memo WA-09/93, Institut für Erdmessung, University of Hannover.

Wanninger, L. and E. Sardon (1994). New data sets of the differential instrumental delays of GPS satellites. Electronic mail Canspace, June 3, 1994.

Wu, J. T., S. C. Wu, G. A. Hajj, W. I. Bertiger, and S. M. Lichten (1993). Effects of antenna orientation on GPS carrier phase. *manuscripta geodaetica 18*, 91–98.

Wu, S. C., W. I. Bertiger, and J. T. Wu (1992). Minimizing selective availability error on satellite and ground Global Positioning System measurements. *J. Guidance 15*(5), 1306–1309.

Zumberge, J. F. and W. I. Bertiger (1996). Ephemeris and clock navigation message accuracy. See Parkinson and Spilker Jr. (1996), Chapter 16, pp. 585–599.

Chapter 3

GPS relative positioning: the undifferenced approach

3.1 Introduction

Processing of GPS observables for relative or interferometric positioning is usually done using a 'double differencing' technique. The differencing technique finds its origin in the field of VLBI (Counselman III et al. 1972). In short, the double difference (DD) scheme boils down to elimination of common bias parameters by subtracting one observable from an other. In GPS from four observables, made from two receivers to two satellites, a new DD observable can be formed which is not biased by receiver and satellite clock errors. Coming from VLBI where between-station (single) differences are made, it seems logical to apply the differencing to the GPS observables too. Looking at GPS from the perspective of geodetic adjustment where often large systems with many unknown parameters have to be solved, it seems less logical. We have chosen for the more general technique of using the original or undifferenced observables directly. In this chapter we will show how using a single undifferenced GPS observable type, the unknown parameters of interest can be estimated. In Chapter 4 we will then show how the technique works for more than one observable type.

We will start from the linearized observation equation that was derived in Section 2.1, for the case that atmospheric delays are assumed to be absent. Collecting all observation equations reveals the structure of the design matrix. This design matrix is rank defect, and we will give for a number of models the rank defect and ways to resolve it by adding constraints, or equivalently by specifying an appropriate S-basis. In particular resolving the rank defect caused by the ambiguities will be treated. It will be shown that the S-basis and the resulting estimable functions of parameters can be found in a straightforward way by introducing an associated graph to represent the measurements made between the receivers and satellites.

As a comparison, the DD approach will be treated. It will be shown that the design matrix for the double differences before lumping together the original ambiguities is also rank defect.

With the design matrix as a base the normal matrix and the so-called right-hand side will be given. This information is sufficient to perform the estimation of the parameters we are interested in. The estimation of the parameters is done in two steps: first the local parameters (i.e. the receiver and satellite clocks) are eliminated, and only the global parameters (coordinates and ambiguities) are estimated. In a second step, the local parameters are estimated and the observations are tested for outliers and cycle slips. For the testing we need (parts of) the variance-covariance matrix $Q_{\hat{e}}$ of the residuals. We will show that we can compute the information that is needed in an efficient way. This makes the testing of

sometimes tens of thousands of observations feasible.

In the elimination of the local parameters the projector matrix plays a key role. An efficient way to compute it will be given. In the case of a single baseline, it will be shown that the projector does not need to be computed explicitly.

The chapter will be concluded with a comparison of some double difference generating algorithms with the undifferenced approach on an observation scenario stemming from a global network. It demonstrates that in some cases data has to be discarded in the DD approach, that still can be used in the undifferenced approach.

3.2 Classification of parameters

3.2.1 Global and local parameters

In our estimation process we make a distinction between global and local parameters. Global parameters (x_1) are parameters that are constant over at least some epochs, i.e. coordinates of the receiver, ambiguity parameters, tropospheric delay parameters, and orbit parameters. Orbit parameters will not be treated in this thesis, and in this chapter the global parameters will be restrained to coordinates and ambiguity parameters. Local parameters (x_2) are those parameters that change on an epoch-by-epoch basis, i.e. receiver and satellite clocks, and ionospheric delays.

The distinction between global and local parameters is made since we may treat each group differently: e.g. we can eliminate the local parameters on an epoch-by-epoch basis, as will be described in Section 3.8.

We will denote, as before, the number of receivers as r, the number of satellites as m, and the number of epochs as n. The argument of time (t) is replaced by a subscript $_k$, indicating epoch k. The subscript indicating the observable type is also omitted here, as in this chapter we will use only one observable type, viz. one phase or one code (pseudorange) observable type. From the context it will be clear what observable type is used. For the time being it is assumed that the observation scenario does not change from epoch to epoch.

The system of linearized observation equations reads

$$E\{\begin{bmatrix} y_1 \\ y_2 \\ \vdots \\ y_n \end{bmatrix}\} = \begin{bmatrix} A_{1,1} & A_{2,1} & & \\ A_{1,2} & & A_{2,2} & \\ \vdots & & & \ddots \\ A_{1,n} & & & A_{2,n} \end{bmatrix} \begin{bmatrix} x_1 \\ x_{2,1} \\ x_{2,2} \\ \vdots \\ x_{2,n} \end{bmatrix} \tag{3.1}$$

where y_k are the observations of epoch k

$$y_k = \begin{bmatrix} y_{1,k}^T & y_{2,k}^T & \cdots & y_{r,k}^T \end{bmatrix}^T \tag{3.2}$$

and $y_{i,k}$ the observations at epoch k of receiver i:

$$y_{i,k} = \begin{cases} \Phi_{i,k} = \begin{bmatrix} \Phi_{i,k}^1 & \Phi_{i,k}^2 & \cdots & \Phi_{i,k}^m \end{bmatrix}^T & \text{(Phase)} \\ P_{i,k} = \begin{bmatrix} P_{i,k}^1 & P_{i,k}^2 & \cdots & P_{i,k}^m \end{bmatrix}^T & \text{(Code)} \end{cases} \tag{3.3}$$

The global parameters consist of the coordinates of the receivers and, in case of the carrier phase, the ambiguities:

$$x_1 = \begin{cases} \left[\begin{array}{cccccccccc} r_1^T & r_2^T & \cdots & r_r^T & \lambda N_1^1 & \lambda N_1^2 & \cdots & \lambda N_1^m & \lambda N_2^1 & \cdots & \lambda N_r^m \end{array} \right]^T & \text{(Phase)} \\ \left[\begin{array}{cccc} r_1^T & r_2^T & \cdots & r_r^T \end{array} \right]^T & \text{(Code)} \end{cases} \tag{3.4}$$

The quantity N_i^j is real valued; the integer valued phase ambiguity $\bar{N}_i^j$ has been lumped together with the real valued initial phase delays ϕ_i and ϕ^j.

The local parameters of epoch k consist of the receiver and satellite clocks of that epoch:

$$x_{2,k} = \left[\begin{array}{cccccccc} c\delta t_{1,k} & c\delta t_{2,k} & \cdots & c\delta t_{r,k} & c\delta t^{1,k} & c\delta t^{2,k} & \cdots & c\delta t^{m,k} \end{array} \right]^T \tag{3.5}$$

The geometric part of the design matrix at epoch k consisting of the unit direction vectors from the receivers to the satellites at epoch k is denoted by the rm by $3r$ matrix g_k. The ambiguity part of the design matrix is covered by the identity matrix I_{rm} of dimension rm. The clock part of epoch k is denoted by the rm by $r+m$ sub-matrix d. With this notation the design matrix reads:

$$\underset{nrm \times 3r + rm + n(r+m)}{A} = \left[\begin{array}{c|ccc} A_{1,1} & A_{2,1} & & \\ A_{1,2} & & A_{2,2} & \\ \vdots & & & \ddots \\ A_{1,n} & & & A_{2,n} \end{array} \right] = \left[\begin{array}{cc|ccc} g_1 & I_{rm} & d & & \\ g_2 & I_{rm} & & d & \\ \vdots & \vdots & & & \ddots \\ g_n & I_{rm} & & & d \end{array} \right] \tag{3.6}$$

where

$$\underset{rm \times 3r}{g_k} = \left[\begin{array}{cccc} g_{1,k} & & & \\ & g_{2,k} & & \\ & & \ddots & \\ & & & g_{r,k} \end{array} \right] \text{ with } \underset{m \times 3}{g_{i,k}} = \left[\begin{array}{c} -u_{i,k}^{1^T} \\ -u_{i,k}^{2^T} \\ \vdots \\ -u_{i,k}^{m^T} \end{array} \right] \tag{3.7}$$

↑ only for phase

and $u_{i,k}^j$ the unit direction vector from receiver i to satellite j at epoch k, and

$$\underset{rm \times r+m}{d} = \left[\begin{array}{ccc} e_m & & -I_m \\ & e_m & -I_m \\ & \ddots & \vdots \\ & & e_m \quad -I_m \end{array} \right] \text{ with } \underset{m \times 1}{e_m} = \left[\begin{array}{c} 1 \\ 1 \\ \vdots \\ 1 \end{array} \right] \tag{3.8}$$

3.2.2 Coordinate and bias-parameters

Apart from the distinction between global and local parameters, we can make a distinction between coordinates of the receivers or functions thereof on the one hand (x_I), and bias or nuisance parameters, viz. receiver and satellite clock errors and ambiguity parameters on the other hand (x_{II}). The system of linearized observation equations can then be written as

$$E\{y\} = [A_I A_{II}] \left[\begin{array}{c} x_I \\ x_{II} \end{array} \right] \tag{3.9}$$

with the composed design matrix as

$$[A_I\,|A_{II}] = \left[\begin{array}{c|cccc} g_1 & I_{rm} & d & & \\ g_2 & I_{rm} & & d & \\ \vdots & \vdots & & & \ddots \\ g_n & I_{rm} & & & d \end{array}\right], \qquad (3.10)$$

$\uparrow$ only for phase

the coordinate part of the parameters as

$$x_I = \left[\; r_1^T\, r_2^T\, \cdots\, r_r^T \;\right]^T \qquad (3.11)$$

and the bias part of the parameters as

$$x_{II} = \begin{cases} \left[\; \lambda N_1^1\, \lambda N_1^2 \cdots \lambda N_1^m\, \lambda N_2^1 \cdots \lambda N_r^m x_{2,1}, x_{2,2}, \cdots x_{2,n} \;\right]^T & \text{(Phase)} \\ \left[\; x_{2,1}, x_{2,2}, \cdots x_{2,n} \;\right]^T & \text{(Code)} \end{cases} \qquad (3.12)$$

The reason for making this distinction is that the system (3.10) is not of full rank, but since A_I and A_{II} are complementary (see e.g. Schaffrin and Grafarend (1986)) the rank and the rank defect of both parts can be examined separately. Complementarity of A_I and A_{II} implies that

1. there is no linear combination of the columns of A_I that equals a linear combination of the columns of A_{II}, and that
2. the rank of A equals the rank of A_I plus the rank of A_{II}, and the rank defect of A equals the rank defect of A_I plus the rank defect of A_{II}.

A processing method which annihilates the problem of the large amount of parameters *but not* the rank defect, is differencing of the observations. By differencing twice, we get double differenced observables. Differencing between both receivers and satellites eliminates all receiver and satellite clock terms, but there is still a rank defect that is usually resolved by lumping the original ambiguities into double differenced ambiguities, see Section 3.6.

Another method to process the GPS observations is using undifferenced observations. To be able to do this, we have to investigate what the rank defect is, and how to deal with it, see e.g. Lindlohr and Wells (1985).

A rank defect makes that not all parameters are 'unbiased estimable'; with the help of the theory of the S-transformations (Teunissen 1984), we can investigate what linear functions of parameters are unbiased estimable.

3.3 Resolving the rank defect of the bias parameters

In this section we will investigate the rank of some simple models for relative positioning with GPS, and show how it can be resolved. First we will have a look at the case of pseudoranges; with the one epoch case as starting point the general case of n epochs is derived. From there we go to the case of one epoch using carrier phases (which can only be solved when no

coordinate parameters are included in the model), and the more general case of n epochs of carrier phase.

Pseudo range
The bias part of the observation equations for the pseudorange observable reads:

$$c\delta t_i - c\delta t^j \tag{3.13}$$

Consequently, the bias part of the design matrix for one epoch only reads

$$\underset{rm \times r+m}{A_{II}} = \begin{bmatrix} e_m & & & -I_m \\ & e_m & & -I_m \\ & & \ddots & \vdots \\ & & e_m & -I_m \end{bmatrix} = d \tag{3.14}$$

and is not of full rank. The addition of the first r columns multiplied by -1 gives the same result as addition of the last m columns. There is a rank defect of 1. We have thus the rank deficient system

$$\underset{rm \times 1}{E\{y\}} = \underset{rm \times r+m}{A_{II}} \quad \underset{r+m \times 1}{x_{II}} \tag{3.15}$$

with a rank of $r + m - 1$. To make it uniquely solvable, one constraint of the form

$$\underset{1 \times r+m}{S^{\perp^T}} \quad \underset{r+m \times 1}{x_{II}} = 0, \text{ with } \mathbf{R}^{r+m} = \mathcal{R}(S) \oplus \mathcal{N}(A_{II}) \tag{3.16}$$

has to be added to the model (Teunissen 1984). $S^{\perp^T} x_{II}$ is called the S-basis. Here $\mathbf{R}^p$ denotes the vector space of all p-tuples with real coordinates, $\mathcal{N}(A_{II})$ denotes the null space of A_{II}, which consists of all vectors in $\mathbf{R}^{r+m}$ that are mapped into the null vector in $\mathbf{R}^{rm}$ under A_{II}, i.e.

$$\mathcal{N}(A_{II}) = \{v \mid A_{II}v = 0\} \tag{3.17}$$

and $\mathcal{R}(S)$ is the range space of the $r+m \times r+m-1$ matrix S, which consists of the vectors in $\mathbf{R}^{r+m-1}$ which can be written as Sz for some z in $\mathbf{R}^{r+m}$:

$$\mathcal{R}(S) = \{w \mid w = Sz \text{ for some } z \text{ in } \mathbf{R}^{r+m}\} \tag{3.18}$$

There is an infinite number of bases for $\mathcal{N}(A_{II})$ possible, of which one can arbitrarily choose one; but they all span the same vector space. The base for the null space will be denoted as V, thus $\mathcal{R}(V) = \mathcal{N}(A_{II})$. For the model above we may e.g. choose

$$\underset{r+m \times 1}{V} = [e_{r+m}] \tag{3.19}$$

For S we may also choose from an infinite number of possibilities, e.g.

$$\underset{r+m \times r+m-1}{S} = \begin{bmatrix} 0^T_{r+m-1} \\ I_{r+m-1} \end{bmatrix} \tag{3.20}$$

with 0_q a null-vector with length q, which results in

$$\underset{r+m\times 1}{S^{\perp}} = \begin{bmatrix} q \\ 0_{r+m-1} \end{bmatrix} \tag{3.21}$$

where q can be any real number. The resulting estimable functions are then

$$\left[I_{r+m} - V(S^{\perp^T}V)^{-1}S^{\perp^T}\right] x_{II} = \begin{bmatrix} 0 & 0^T_{r+m-1} \\ -e_{r+m-1} & I_{r+m-1} \end{bmatrix} x_{II} \tag{3.22}$$

or,

$$\begin{matrix} c\delta t_i - c\delta t_1 & i \neq 1 \\ c\delta t^j - c\delta t_1 \end{matrix} \tag{3.23}$$

Usually one takes $q = 1$ (although it has no effect on the eventual estimable functions), which gives an S-basis consisting of the parameter $S^{\perp^T}x_{II}$, viz. in this case $c\delta t_1$.

Other choices for the S-basis may be any of the other clock errors, or e.g. the average of all clock errors or a subset thereof. One could e.g. take the average of the satellite clock errors. With V as before and

$$\underset{r+m\times r+m-1}{S} = \begin{bmatrix} I_r & \\ & -e^T_{m-1} \\ & I_{m-1} \end{bmatrix} \text{ and } \underset{r+m\times 1}{S^{\perp}} = \begin{bmatrix} 0_r \\ e_m \end{bmatrix} \tag{3.24}$$

we get

$$\left[I_{r+m} - V(S^{\perp^T}V)^{-1}S^{\perp^T}\right] x_{II} = \begin{bmatrix} I_r & -\frac{1}{m}E_{r,m} \\ & I_m - \frac{1}{m}E_{m,m} \end{bmatrix} x_{II} \tag{3.25}$$

or

$$\begin{matrix} c\delta t_i - \frac{1}{m}\sum_{j=1}^{m} c\delta t^j \\ c\delta t^j - \frac{1}{m}\sum_{j=1}^{m} c\delta t^j \end{matrix} \tag{3.26}$$

Different choices for the S-basis give different sets of estimable functions of parameters, the coordinate-parameters, however, are not influenced by it.

For n epochs the bias part of the design matrix reads

$$\underset{nrm\times n(r+m)}{A_{II}} = \begin{bmatrix} d & & \\ & d & \\ & & \ddots \\ & & & d \end{bmatrix} \tag{3.27}$$

Since the n parts of A_{II} relating to one epoch are all complementary, the rank defect of A_{II} is n times the rank defect of one epoch:

	1 epoch	n epochs
$nunkA_{II}$	$r+m$	$n(r+m)$
$rnkdA_{II}$	1	n
$rankA_{II}$	$r+m-1$	$n(r+m-1)$

where $nunkA$ is the number of columns of A, or the number of unknowns involved, $rnkdA$ is the rank defect of A, and $rankA$ the rank of A.

The rank defect of n means that one linear combination of clock terms per epoch cannot be estimated. If we take at each epoch the clock of the first receiver $c\delta t_{1,k}$ for the S-basis, the following functions of parameters become unbiased estimable:

$$\begin{matrix} c\delta t_{i,k} - c\delta t_{1,k} & i \neq 1 \\ c\delta t^{j,k} - c\delta t_{1,k} \end{matrix} \tag{3.28}$$

Carrier phase
The bias part of the observation equations for the carrier phase observable reads:

$$\lambda N_i^j + c\delta t_i - c\delta t^j \tag{3.29}$$

which gives for one epoch the following bias part of the design matrix:

$$\underset{rm \times rm+r+m}{A_{II}} = \begin{bmatrix} I_{rm} & d \end{bmatrix} \tag{3.30}$$

There are again $r+m$ clock errors as we saw in the case for the code observable, but there are also rm ambiguities. Besides the rank defect of 1 for the clocks there is an additional rank defect of $r+m-1$ for the ambiguities. Note that to be able to solve this system A_I cannot be present; i.e. the coordinate parameters are assumed to be known. A possible basis for the null space of A_{II} is:

$$\underset{rm+r+m \times r+m}{V} = \begin{bmatrix} -d \\ I_{r+m} \end{bmatrix} \tag{3.31}$$

For S and $S^{\perp}$ we may choose e.g.

$$\underset{rm+r+m \times (r-1)(m-1)+r+m-1}{S} = \begin{bmatrix} S_a & \\ & S_d \end{bmatrix} \tag{3.32}$$

with

$$\underset{rm \times (r-1)(m-1)}{S_a} = \begin{bmatrix} 0_{m,m-1} & & \\ \begin{bmatrix} 0_{m-1}^T \\ I_{m-1} \end{bmatrix} & & \\ & \ddots & \\ & & \begin{bmatrix} 0_{m-1}^T \\ I_{m-1} \end{bmatrix} \end{bmatrix} \tag{3.33}$$

$$\underset{r+m \times r+m-1}{S_d} = \begin{bmatrix} 0_{r+m-1}^T \\ I_{r+m-1} \end{bmatrix} \tag{3.34}$$

and

$$\underset{rm+r+m \times r+m}{S^{\perp}} = \begin{bmatrix} S_a^{\perp} & \\ & S_d^{\perp} \end{bmatrix} \tag{3.35}$$

with

$$\underset{rm \times r+m-1}{S_a^{\perp}} = \begin{bmatrix} I_m & & & \\ & \begin{bmatrix} 1 \\ 0_{m-1} \end{bmatrix} & & \\ & & \ddots & \begin{bmatrix} 1 \\ 0_{m-1} \end{bmatrix} \end{bmatrix} \tag{3.36}$$

$$\underset{r+m \times 1}{S_d^{\perp}} = \begin{bmatrix} 1 \\ 0_{r+m-1} \end{bmatrix} \tag{3.37}$$

The S-basis is thus

$$S^{\perp^T} x_{II} = \begin{cases} \lambda N_i^j & i \neq 1 \vee j \neq 1 \\ c\delta t_1 \end{cases} \tag{3.38}$$

which gives the following unbiased estimable functions of parameters:

$$\left[I_{rm+r+m} - V(S^{\perp^T}V)^{-1}S^{\perp^T}\right] x_{II} = \begin{cases} \lambda(N_i^j - N_i^1 - (N_1^j - N_1^1)) & i \neq 1 \wedge j \neq 1 \\ c\delta t_i - c\delta t_1 - \lambda(N_1^1 - N_i^1) & i \neq 1 \\ c\delta t^j - c\delta t_1 - \lambda N_1^j \end{cases} \tag{3.39}$$

For n epochs the bias part of the design matrix reads:

$$\underset{nrm \times rm+n(r+m)}{A_{II}} = \begin{bmatrix} I_{rm} & d & & \\ I_{rm} & & d & \\ \vdots & & & \ddots \\ I_{rm} & & & d \end{bmatrix} \tag{3.40}$$

For each epoch there are again $r+m$ clock errors, giving a rank defect of 1 per epoch. The inclusion in the model of the rm ambiguities which are common for all epochs, causes an additional rank defect of $r+m-1$, resulting in a total rank defect of $r+m-1+n$:

	1 epoch	n epochs
$nunkA_{II}$	$rm+r+m$	$rm+n(r+m)$
$rnkdA_{II}$	$r+m-1+1$	$r+m-1+n$
$rankA_{II}$	$(r-1)(m-1)+r+m-1$	$(r-1)(m-1)+n(r+m-1)$

A possible basis for the null space of A_{II} is:

$$\underset{rm+n(r+m) \times r+m-1+n}{V} = \begin{bmatrix} -d & & & \\ I_{r+m} & & & \\ I_{r+m} & e_{r+m} & & \\ \vdots & & \ddots & \\ I_{r+m} & & & e_{r+m} \end{bmatrix} \tag{3.41}$$

As before, we have to choose one linear combination of clock terms per epoch, and additionally another $r + m - 1$ parameters for the S-basis. Let us take e.g.

$$\begin{matrix} \lambda N_i^j & i \neq 1 \vee j \neq 1 \\ c\delta t_{1,k} & \end{matrix} \tag{3.42}$$

which corresponds to choices for S and $S^\perp$ as e.g.

$$\underset{rm + n(r+m) \times (r-1)(m-1) + n(r+m-1)}{S} = \begin{bmatrix} S_a & & & \\ & S_d & & \\ & & \ddots & \\ & & & S_d \end{bmatrix} \tag{3.43}$$

and

$$\underset{rm + n(r+m) \times r + m - 1 + n}{S^\perp} = \begin{bmatrix} S_a^\perp & & & \\ & S_d^\perp & & \\ & & \ddots & \\ & & & S_d^\perp \end{bmatrix} \tag{3.44}$$

The unbiased estimable functions of parameters are then:

$$\begin{matrix} \lambda(N_i^j - N_i^1 - (N_1^j - N_1^1)) & i \neq 1 \wedge j \neq 1 \\ c\delta t_{i,k} - c\delta t_{1,k} - \lambda(N_1^1 - N_i^1) & i \neq 1 \\ c\delta t^{j,k} - c\delta t_{1,k} - \lambda N_1^j & \end{matrix} \tag{3.45}$$

In contrast to the individual ambiguities N_i^j, the function of ambiguities $N_i^j - N_i^1 - (N_1^j - N_1^1)$ is integer valued. Since we have defined N_i^j as

$$N_i^j = \bar{N}_i^j + \phi_i - \phi^j \tag{3.46}$$

it is real valued. If however, we substitute Eq. (3.46) into $N_i^j - N_i^1 - (N_1^j - N_1^1)$ we get a function that is integer valued:

$$\begin{aligned} N_i^j - N_i^1 - (N_1^j - N_1^1) = {} & \bar{N}_i^j & & & +\phi_i & & -\phi^j & \\ & -\bar{N}_i^1 & & & -\phi_i & & & +\phi^1 \\ & & -\bar{N}_1^j & & & -\phi_1 & +\phi^j & \\ & & & +\bar{N}_1^1 & & +\phi_1 & & -\phi^1 \\ = {} & \bar{N}_i^j - \bar{N}_i^1 - (\bar{N}_1^j - \bar{N}_1^1) & & & & & & \end{aligned} \tag{3.47}$$

Note that the $(r-1)(m-1)$ functions of ambiguities are equal to the functions one obtains when applying a certain double difference operator ('pivoting' with the first receiver and the first satellite). Therefore we will compare the solution with the undifferenced observations with this DD solution.

3.4 Finding an S-basis for the ambiguities

In Section 3.3 we have seen that to obtain the integer double differenced ambiguities as unbiased estimable function, we have to choose one clock error for each epoch and $r + m - 1$ ambiguities for the S-basis.

In choosing this set of ambiguities one is bounded by some restrictions: each satellite and each receiver should exclusively be represented in the set of S-basis ambiguities. When we say exclusively we mean that if an ambiguity λN_i^j is chosen, it represents either receiver i or satellite j. There is one exception to this rule: one of the S-basis ambiguities represents both the receiver and the satellite. For rm ambiguities, involving r receivers and m satellites, it gives us $r+m-1$ ambiguities for the S-basis, where the -1 comes from the exception above.

Here we have implicitly assumed that the receiver-satellite combinations form one connected component, which is usually the case. One such an occasion might be e.g. two small networks at opposite sides of the Earth, where the set of satellites tracked by the receivers of the first network do not overlap the set of satellites tracked by the receivers of the second network. In such a case two separate S-bases have to be chosen, but it does not make much sense to process the networks together anyhow, since processing the networks separately gives the same results.

There are a large number of ways to choose the set of ambiguities as defined above, each giving a different set of unbiased estimable functions of ambiguities. We can for instance choose the set of ambiguities such that the eventual set of estimated functions of ambiguities becomes equal to the set of double differenced ambiguities one obtains by applying a pivoting scheme in defining the DD combinations. Let us take e.g. the case with $r = 3$ receivers and $m = 4$ satellites,

$$\begin{array}{cccccc} & 1 & 2 & 3 & 4 \\ 1 & \lambda N_1^1 & \lambda N_1^2 & \lambda N_1^3 & \lambda N_1^4 \\ 2 & \lambda N_2^1 & \lambda N_2^2 & \lambda N_2^3 & \lambda N_2^4 \\ 3 & \lambda N_3^1 & \lambda N_3^2 & \lambda N_3^3 & \lambda N_3^4 \end{array} \tag{3.48}$$

We choose as S-basis: $\{\lambda N_1^1, \lambda N_1^2, \lambda N_1^3, \lambda N_1^4, \lambda N_2^1, \lambda N_3^1\}$. In the scheme below we indicate that a receiver or satellite is represented by an ambiguity in the S-basis by putting a box around the sub- or superscript of the ambiguity concerned.

$$\begin{array}{cccccc} & 1 & 2 & 3 & 4 \\ 1 & \lambda N_{\boxed{1}}^{\boxed{1}} & \lambda N_1^{\boxed{2}} & \lambda N_1^{\boxed{3}} & \lambda N_1^{\boxed{4}} \\ 2 & \lambda N_{\boxed{2}}^1 & \lambda N_2^2 & \lambda N_2^3 & \lambda N_2^4 \\ 3 & \lambda N_{\boxed{3}}^1 & \lambda N_3^2 & \lambda N_3^3 & \lambda N_3^4 \end{array} \tag{3.49}$$

It gives us indeed the same double differenced ambiguities we obtain if we form double differenced observables with receiver 1 and satellite 1 as pivot:

$$\begin{array}{ll} \lambda(N_1^1 - N_1^2 - N_2^1 + N_2^2) & \lambda(N_1^1 - N_1^2 - N_3^1 + N_3^2) \\ \lambda(N_1^1 - N_1^3 - N_2^1 + N_2^3) & \lambda(N_1^1 - N_1^3 - N_3^1 + N_3^3) \\ \lambda(N_1^1 - N_1^4 - N_2^1 + N_2^4) & \lambda(N_1^1 - N_1^4 - N_3^1 + N_3^4) \end{array} \tag{3.50}$$

Another valid choice would be: $\{\lambda N_1^1, \lambda N_1^2, \lambda N_2^2, \lambda N_2^3, \lambda N_3^3, \lambda N_3^4\}$.

$$\begin{array}{cccccc} & 1 & 2 & 3 & 4 \\ 1 & \lambda N_{\boxed{1}}^{\boxed{1}} & \lambda N_1^{\boxed{2}} & \lambda N_1^3 & \lambda N_1^4 \\ 2 & \lambda N_2^1 & \lambda N_{\boxed{2}}^2 & \lambda N_2^{\boxed{3}} & \lambda N_2^4 \\ 3 & \lambda N_3^1 & \lambda N_3^2 & \lambda N_{\boxed{3}}^3 & \lambda N_3^{\boxed{4}} \end{array} \tag{3.51}$$

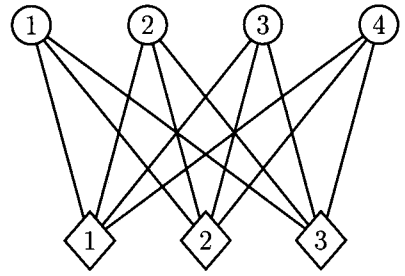

Figure 3.1: Associated graph for the observation scenario of (3.48). Receivers are indicated by diamonds, satellites by circles.

The estimable functions this choice gives are still of integer nature, however they do not all have the form of the classic double differenced ambiguities consisting of 4 ambiguities:

$$\begin{array}{ll} \lambda(-N_1^2+N_1^3+N_2^2-N_2^3) & \lambda(-N_2^3+N_2^4+N_3^3-N_3^4) \\ \lambda(-N_1^2+N_1^4+N_2^2-N_2^3+N_3^3-N_3^4) & \lambda(-N_1^1+N_1^2-N_2^2+N_2^3+N_3^1-N_3^3) \\ \lambda(-N_1^1+N_1^2+N_2^1-N_2^2) & \lambda(-N_2^2+N_2^3+N_3^2-N_3^3) \end{array} \tag{3.52}$$

Which ambiguities may be chosen for the S-basis, and the resulting set of estimable functions, can be determined using an undirected graph to represent the receivers and satellites involved.

A graph $G = G(V, E)$ consists of a set of n nodes or vertices V, together with a set of edges E, where an edge is a pair of nodes belonging to V. If no distinction is made between the edge from node v_1 to node v_2 and the edge from node v_2 to node v_1, the graph is called directed. Two nodes are called adjacent if they are connected by an edge. A path is an ordered set of distinct nodes $(v_1, v_2, \ldots, v_{m+1})$ such that v_k and v_{k+1} are adjacent for $k = 1, 2, \ldots, m$; a path is a cycle when v_1 equals v_{m+1}. A graph is connected if every pair of distinct nodes is connected by at least one path. An undirected graph which is connected, and has no cycles, is called a tree. In a tree there is exactly one path connecting any two nodes (Pissanetzky 1984).

We may define an associated graph for an observation scenario: each receiver and satellite is represented by a node, and each ambiguity belonging to a phase observation made by a receiver to a satellite is represented by an edge. The associated graph for the observation scenario of (3.48) is depicted in Figure 3.1.

We found that the S-basis for the ambiguities can be formed by taking the ambiguities associated to the edges of a so-called 'minimum spanning tree' (MST). A minimum spanning tree is an undirected connected graph consisting of n nodes and $n-1$ edges. It has the property that of all connected graphs the sum of the weights of the edges is minimal. In this case we define the weights of all edges to be equal, and we speak of a 'spanning tree'. An algorithm to build a minimum spanning tree is called Prim's algorithm.

Prim's algorithm for building an MST:

1. Take the edge with the highest weight, and put the two nodes connected by it, in set V_1.
2. Consider the set of edges that connect a node from $V - V_1$ to a node from V_1, and select the edge with the highest weight,
3. Add the node belonging to $V - V_1$ of the edges selected in 2. to V_1.
4. As long as $V - V_1 \neq \emptyset$ go to 2.

In selecting the edge with the highest weight, ties are broken arbitrarily. No matter how ties are broken, the resulting sum of weights is always minimum, although actual trees may differ. In Figure 3.2 two such trees are depicted, the edges of the tree are drawn as solid lines, the remainder of the edges of the associated graph are drawn as dotted lines. The S-basis consists of the ambiguities represented by the edges of the tree, viz. for the tree at left $\{\lambda N_1^1, \lambda N_1^2, \lambda N_1^3, \lambda N_1^4, \lambda N_2^1, \lambda N_3^1\}$ as in the example of (3.49), and for the tree at right $\{\lambda N_1^1, \lambda N_1^2, \lambda N_2^2, \lambda N_2^3, \lambda N_3^3, \lambda N_3^4\}$ as in the example of (3.51).

Each of the estimable functions due to the S-basis consist of one ambiguity not in the S-basis plus a function of ambiguities from the S-basis. This function is found by traversing a path in the spanning tree. For an ambiguity λN_i^j which is not in the S-basis the path to be traversed is the path from receiver i to satellite j, or from satellite j to receiver i. The estimable function consists of ambiguity λN_i^j plus all ambiguities encountered while traversing the path. While traversing the path, the sign for the ambiguities is changed at each edge, starting with a minus sign at the first ambiguity. For the observation scenario of (3.48) with as S-basis the ambiguities associated with the edges of the trees in Figure 3.2 we obtain:

Tree at left:	Tree at right:
$\lambda(N_2^2 - N_2^1 + N_1^1 - N_1^2)$	$\lambda(N_1^3 - N_1^2 + N_2^2 - N_2^3)$
$\lambda(N_2^3 - N_2^1 + N_1^1 - N_1^3)$	$\lambda(N_1^4 - N_1^2 + N_2^2 - N_2^3 + N_3^3 - N_3^4)$
$\lambda(N_2^4 - N_2^1 + N_1^1 - N_1^4)$	$\lambda(N_2^1 - N_2^2 + N_1^2 - N_1^1)$
$\lambda(N_3^2 - N_3^1 + N_1^1 - N_1^2)$	$\lambda(N_2^4 - N_2^3 + N_3^3 - N_3^4)$
$\lambda(N_3^3 - N_3^1 + N_1^1 - N_1^3)$	$\lambda(N_3^1 - N_3^3 + N_2^3 - N_2^2 + N_1^2 - N_1^1)$
$\lambda(N_3^4 - N_3^1 + N_1^1 - N_1^4)$	$\lambda(N_3^2 - N_3^3 + N_2^3 - N_2^2)$

(3.53)

The functions of ambiguities at left can be transformed into those at right by multiplying with the invertible, volume preserving transformation matrix

$$Z = \begin{bmatrix} 1 & -1 & & & & \\ 1 & -1 & & & 1 & -1 \\ -1 & & & & & \\ & -1 & 1 & & 1 & -1 \\ -1 & 1 & & & -1 & \\ -1 & 1 & & 1 & -1 & \end{bmatrix} \tag{3.54}$$

If we denote the S-transformation matrix $[I - V(S_1^{\perp^T}V)^{-1}S_1^{\perp^T}]$ originating from the first S-basis as $\mathcal{S}_1$, and the one originating from the second S-basis as $\mathcal{S}_2 = [I - V(S_2^{\perp^T}V)^{-1}S_2^{\perp^T}]$,

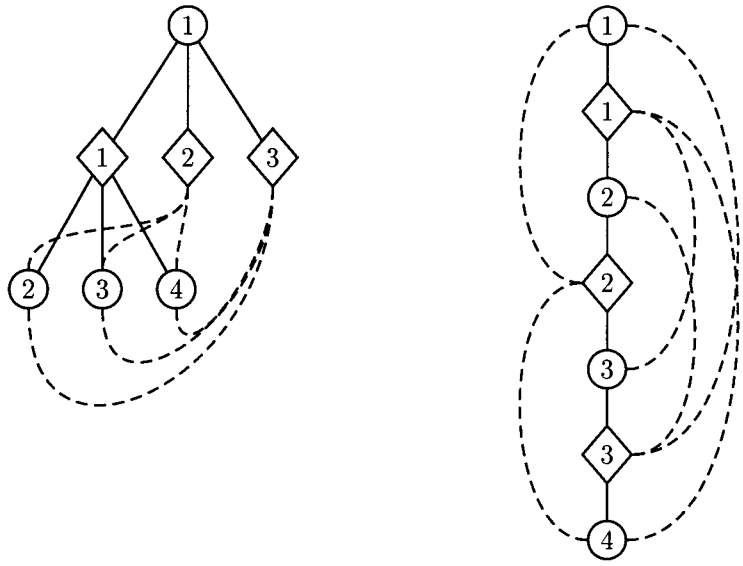

Figure 3.2: Two spanning trees for the observation scenario of (3.48). Receivers are indicated by diamonds, satellites by circles. The edges of the tree are drawn as solid lines, the remainder of the edges of the associated graph are drawn as dashed lines.

the matrix to transform the estimable functions from the first S-basis to the second S-basis is computed as:

$$\mathcal{S}_1\mathcal{S}_2^\dagger \tag{3.55}$$

where † denotes the pseudo inverse ($\mathcal{S}\mathcal{S}^\dagger\mathcal{S} = \mathcal{S}$ and $\mathcal{S}^\dagger\mathcal{S}\mathcal{S}^\dagger = \mathcal{S}^\dagger$).

If we choose one of the receiver or satellite clocks for the S-basis for the clocks, estimable functions are formed consisting of two parts, viz. a differential clock (receiver or satellite clock minus the clock in the S-basis) minus a function of ambiguities. This function of ambiguities can again be determined using the spanning tree.

The two clocks that form the differential clock are the end points of a path in the tree. The function of ambiguities is found by traversing this path, starting at the clock that is part of the S-basis. Again the sign for the ambiguities is changed at each edge, starting with a minus sign at the first ambiguity. If we choose, e.g., the receiver clock of the first receiver for the S-basis, the following estimable functions are obtained:

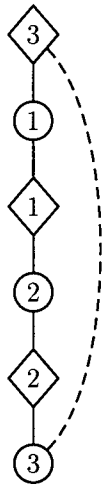

Figure 3.3: Spanning trees for the observation scenario of (3.57). Receivers are indicated by diamonds, satellites by circles. The edges of the tree are drawn as solid lines, the remainder of the edges of the associated graph are drawn as dashed lines.

Tree at left:	Tree at right:
$c(\delta t_{2,k} - \delta t_{1,k}) + \lambda(-N_1^1 + N_2^1)$	$c(\delta t_{2,k} - \delta t_{1,k}) + \lambda(-N_1^2 + N_2^2)$
$c(\delta t_{3,k} - \delta t_{1,k}) + \lambda(-N_1^1 + N_3^1)$	$c(\delta t_{3,k} - \delta t_{1,k}) + \lambda(-N_1^2 + N_2^2 - N_2^3 + N_3^3)$
$c(\delta t^{1,k} - \delta t_{1,k}) - \lambda N_1^1$	$c(\delta t^{1,k} - \delta t_{1,k}) - \lambda N_1^1$
$c(\delta t^{2,k} - \delta t_{1,k}) - \lambda N_2^1$	$c(\delta t^{2,k} - \delta t_{1,k}) - \lambda N_2^1$
$c(\delta t^{3,k} - \delta t_{1,k}) - \lambda N_3^1$	$c(\delta t^{3,k} - \delta t_{1,k}) + \lambda(-N_1^2 + N_2^2 - N_2^3 + N_2^3)$
$c(\delta t^{4,k} - \delta t_{1,k}) - \lambda N_4^1$	$c(\delta t^{4,k} - \delta t_{1,k}) + \lambda(-N_1^2 + N_2^2 - N_2^3 + N_3^3 - N_3^4)$

(3.56)

Also cases as described in e.g. Blewitt (1993), where 3 receivers each track 2 satellites from a total of 3 observed satellites, are easily handled. The ambiguities (and an S-basis chosen by the aforementioned rules) for this case are:

$$\begin{array}{cccc} & 1 & 2 & 3 \\ 1 & \lambda N_{\boxed{1}}^{\boxed{1}} & \lambda N_1^{\boxed{2}} & \\ 2 & & \lambda N_{\boxed{2}}^2 & \lambda N_2^{\boxed{3}} \\ 3 & \lambda N_{\boxed{3}}^1 & & \lambda N_3^3 \end{array} \tag{3.57}$$

The resulting estimable function of ambiguities is then (see Figure 3.3)

$$\lambda(N_1^1 - N_1^2 + N_2^2 - N_2^3 - N_3^1 + N_3^3) \tag{3.58}$$

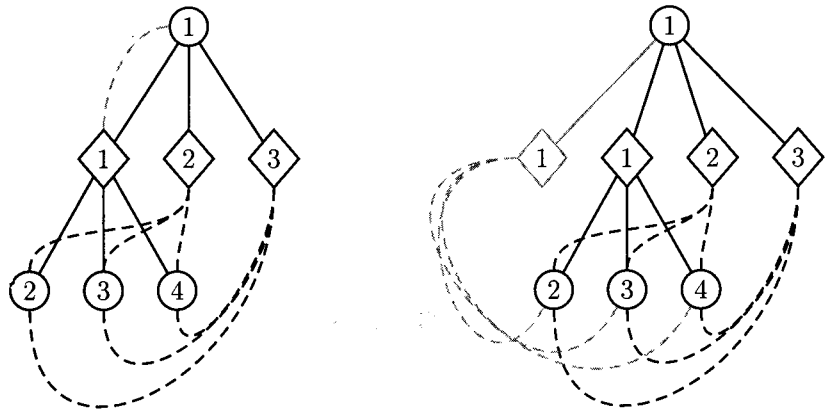

Figure 3.4: Spanning tree for the case of cycle slips in the observation scenario of (3.48). At left a cycle slip occurs in the receiver-satellite combination $\frac{1}{1}$, at right a cycle slip occurs in all combinations of receiver 1. Receivers are indicated by diamonds, satellites by circles. The edges of the tree are drawn as solid lines, the remainder of the edges of the associated graph are drawn as dashed lines. The edges associated with new ambiguities due to a cycle slip are drawn in grey.

There are in this case 6 possible sets of 5 ambiguities, giving 2 functions of ambiguities which differ only by their sign:

$$\left.\begin{array}{lllll} \{ & \lambda N_1^2, & \lambda N_2^2, & \lambda N_2^3, & \lambda N_3^1, \quad \lambda N_3^3\} \\ \{\lambda N_1^1, & \lambda N_1^2, & & \lambda N_2^3, & \lambda N_3^1, \quad \lambda N_3^3\} \\ \{\lambda N_1^1, & \lambda N_1^2, & \lambda N_2^2, & \lambda N_2^3, & \lambda N_3^1 \quad \} \end{array}\right\} \quad \lambda(N_1^1 - N_1^2 + N_2^2 - N_2^3 - N_3^1 + N_3^3)$$

$$\left.\begin{array}{lllll} \{\lambda N_1^1, & & \lambda N_2^2, & \lambda N_2^3, & \lambda N_3^1, \quad \lambda N_3^3\} \\ \{\lambda N_1^1, & \lambda N_1^2, & \lambda N_2^2, & & \lambda N_3^1, \quad \lambda N_3^3\} \\ \{\lambda N_1^1, & \lambda N_1^2, & \lambda N_2^2, & \lambda N_2^3, & \quad \lambda N_3^3\} \end{array}\right\} \quad -\lambda(N_1^1 - N_1^2 + N_2^2 - N_2^3 - N_3^1 + N_3^3)$$

For a more realistic case see Section 3.15.

3.5 Changing observation scenarios

In Section 3.4 we described how to choose an S-basis for the ambiguities assuming that the observation scenario does not change from epoch-to-epoch. In that case the S-basis is determined once at an arbitrary epoch. In practice, due to rising and setting of satellites, and unrepaired cycle slips for which new ambiguity parameters have to be included, we may have different sets of ambiguities for different epochs. The determination of an S-basis is still fairly simple, but it may be necessary to extend it at some epochs.

At the first epoch an S-basis is determined according to the rules given in Section 3.4: each satellite and receiver has to be represented exclusively by one of the ambiguities in the S-basis, with the exception of one ambiguity that represents both a receiver and a satellite.

If there is a change in the observation scenario, it is compared with the scenarios of the previous epochs. The S-basis is extended when

1. a satellite is observed that was not observed in a previous epoch.
2. a receiver starts to observe that did not observe in any of the previous epochs.
3. a slip occurs in all receiver-satellite combinations of a certain satellite. This could e.g. occur when a regional network is observing for 24 hours; then there are time spans that the satellites are not seen by any of the receivers.
4. a slip occurs in all receiver-satellite combinations of a certain receiver. This will happen more frequently: malfunctioning of the receiver or blocking of the signals.

So, if at a certain epoch a receiver-satellite combination is not observed, the S-basis remains as it is, if a new receiver-satellite combination or a slip occurs, the S-basis may be, but not always is, extended.

To clarify the procedure, let us have a look at the observation scenario in (3.48). The first case we will take is a slip in the receiver-satellite combination $\frac{1}{1}$ at an epoch k. None of the cases above applies, and consequently the S-basis need not be extended. In Figure 3.4 the tree and associated graph for this case is depicted. The new ambiguity $N^1_{1,k}$ for epoch k and beyond, is drawn in grey. As far as the ambiguities are concerned, the estimable functions are the ones we already determined for the observation scenario in which no slip occurs, plus

$$\lambda(N^1_{i,k} - N^1_{1,1}) \tag{3.59}$$

which follows from applying the same rules as given in Section 3.4. Note that this is also not a classic double difference ambiguity, but that $N^1_{i,k} - N^1_{1,1}$ is integer valued provided that the size of slip is integer which is usually assumed to be so. The estimable functions involving clocks remain as in the case where no slip occurred.

In a second case we assume a cycle slip in all combinations of receiver 1. Case 4 applies, so one of the ambiguities in the combinations of the first receiver is added to the S-basis. Again, for the ambiguities the estimable functions are the ones already determined for the observation scenario in which no slip occurs plus

$$\begin{aligned}
&\lambda(N^2_{1,k} - N^1_{1,k} + N^1_{1,1} - N^2_{1,1}) \\
&\lambda(N^3_{1,k} - N^1_{1,k} + N^1_{1,1} - N^3_{1,1}) \\
&\lambda(N^4_{1,k} - N^1_{1,k} + N^1_{1,1} - N^4_{1,1})
\end{aligned} \tag{3.60}$$

Again these are not the classic double differences, but they are still integer valued functions, viz. they are differences between the slips of 2 receiver-satellite combinations. As far as the clocks are concerned, from epoch k and beyond we have

$$\begin{aligned}
&c(\delta t_{2,k} - \delta t_{1,k}) + \lambda(-N^1_{1,k} + N^1_{2,1}) \\
&c(\delta t_{3,k} - \delta t_{1,k}) + \lambda(-N^1_{1,k} + N^1_{3,1}) \\
&c(\delta t^{1,k} - \delta t_{1,k}) - \lambda N^1_{1,k} \\
&c(\delta t^{2,k} - \delta t_{1,k}) + \lambda(-N^1_{1,k} + N^1_{1,1} - N^2_{1,1}) \\
&c(\delta t^{3,k} - \delta t_{1,k}) + \lambda(-N^1_{1,k} + N^1_{1,1} - N^3_{1,1}) \\
&c(\delta t^{4,k} - \delta t_{1,k}) + \lambda(-N^1_{1,k} + N^1_{1,1} - N^4_{1,1})
\end{aligned} \tag{3.61}$$

In a third case two new combinations are observed, e.g. $\frac{5}{1}$, and $\frac{5}{2}$. Case 1 applies, so one of the accompanying ambiguities, e.g. $\frac{5}{1}$ is added to the S-basis to represent satellite 5. If in a later epoch, it disappears again and combination $\frac{5}{3}$ is observed instead, the S-basis remains as it is.

3.6 Double differenced approach

To form (single) differences between observations generally two strategies exist, viz. 'pivoting' and 'cycling'. In the pivoting strategy, differences are formed with respect to a chosen 'pivot' receiver or satellite. If we take e.g. as pivot the first receiver or satellite, the differencing process can be denoted as

$$\mathrm{SD}y = R_{q-1}y \tag{3.62}$$

with R_{q-1}

$$\underset{q-1\times q}{R_{q-1}} = \begin{bmatrix} -1 & 1 & & \\ -1 & & 1 & \\ \vdots & & & \ddots \\ -1 & & & 1 \end{bmatrix} \tag{3.63}$$

and q the number of receivers or satellites. Any other receiver or satellite can be used as pivot, as well.

When using the cycling strategy the reference receiver or satellite is obtained by cycling through the range of receiver or satellites; i.e. each difference is formed with respect to a different receiver or satellite. The transformation matrix for the cycling mechanism reads

$$\underset{q-1\times q}{R_{q-1}} = \begin{bmatrix} -1 & 1 & & & \\ & -1 & 1 & & \\ & & & \ddots & \\ & & & -1 & 1 \end{bmatrix} \tag{3.64}$$

In practice also often a combination of the two, or a pivoting scheme with more than one pivot is used (cycling can be seen also as a pivoting scheme with $q-1$ pivots). The whole process of differencing is sometimes also characterized as finding the maximum of $q-1$ independent differences that can be formed out of q observations. Independence of the differences implies that R_{q-1} has full rank, i.e. a rank of $q-1$.

For the analysis that follows the departing point will be the pivoting scheme with the first receiver or satellite as pivot.

Between-receiver SD observables are formed from the original observables through a pre-multiplication by the $(r-1)m \times rm$ matrix $R_{r-1} \otimes I_m$:

$$\mathrm{SD}y = (R_{r-1} \otimes I_m)y \tag{3.65}$$

and from it DD observables are formed through a pre-multiplication by the $(r-1)(m-1) \times (r-1)m$ matrix $I_{r-1} \otimes R_{m-1}$:

$$\begin{aligned} \mathrm{DD}y &= (I_{r-1} \otimes R_{m-1})\mathrm{SD}y \\ &= (I_{r-1} \otimes R_{m-1})(R_{r-1} \otimes I_m)y \\ &= (R_{r-1} \otimes R_{m-1})y \end{aligned} \tag{3.66}$$

Since we have transformed the observables, we also have to transform their variance-covariance matrix. With a variance-covariance matrix Q_{y_k} for the original observables of the form $\frac{1}{w}I$,

the variance-covariance matrix of the double differences becomes:

$$\begin{aligned} Q_{\mathrm{DD}} &= \frac{1}{w}(R_{r-1} \otimes R_{m-1})(R_{r-1} \otimes R_{m-1})^T \\ &= \frac{1}{w}(R_{r-1}R_{r-1}^T) \otimes (R_{m-1}R_{m-1}^T) \end{aligned} \tag{3.67}$$

It can be shown that

$$\begin{aligned} Q_{\mathrm{DD}}^{-1} &= w\left[(R_{r-1} \otimes R_{m-1})(R_{r-1} \otimes R_{m-1})^T\right]^{-1} \\ &= w(R_{r-1}R_{r-1}^T)^{-1} \otimes (R_{m-1}R_{m-1}^T)^{-1} \end{aligned} \tag{3.68}$$

The product $R_{q-1}R_{q-1}^T$ and its inverse are

$$R_{q-1}R_{q-1}^T = (I_{q-1} + E_{q-1}) \tag{3.69}$$

$$\left(R_{q-1}R_{q-1}^T\right)^{-1} = \left(I_{q-1} - \frac{1}{q}E_{q-1}\right) \tag{3.70}$$

So the weight matrix for the double differences equals

$$Q_{\mathrm{DD}}^{-1} = w\left(I_{r-1} - \frac{1}{r}E_{r-1}\right) \otimes \left(I_{m-1} - \frac{1}{m}E_{m-1}\right) \tag{3.71}$$

Assuming the observation scenario does not change, the ambiguity part of the normal matrix is equal for all individual epochs. The system of normal equations for the double differences of epoch k reads then

$$\begin{aligned} &I_{rm}\,(R_{r-1} \otimes R_{m-1})^T \left(I_{r-1} - \frac{1}{r}E_{r-1}\right) \otimes \left(I_{m-1} - \frac{1}{m}E_{m-1}\right)(R_{r-1} \otimes R_{m-1})\, I_{rm}\Delta x_1 = \\ &\qquad I_{rm}\,(R_{r-1} \otimes R_{m-1})^T \left(I_{r-1} - \frac{1}{r}E_{r-1}\right) \otimes \left(I_{m-1} - \frac{1}{m}E_{m-1}\right)(R_{r-1} \otimes R_{m-1})\,\Delta y_k \end{aligned} \tag{3.72}$$

or

$$\begin{aligned} &(R_{r-1} \otimes R_{m-1})^T \left(I_{r-1} - \frac{1}{r}E_{r-1}\right) \otimes \left(I_{m-1} - \frac{1}{m}E_{m-1}\right)(R_{r-1} \otimes R_{m-1})\,\Delta x_1 = \\ &\qquad (R_{r-1} \otimes R_{m-1})^T \left(I_{r-1} - \frac{1}{r}E_{r-1}\right) \otimes \left(I_{m-1} - \frac{1}{m}E_{m-1}\right)\Delta \mathrm{DD} y_k \end{aligned} \tag{3.73}$$

Through the differencing the clock parameters are eliminated, but the transformed design matrix $R_{r-1} \otimes R_{m-1}$ still inhibits a rank defect of $r + m - 1$. This rank defect is usually solved by lumping together of the original ambiguities into double differenced ambiguities. Instead of the rm-vector of original ambiguities

$$\left[\ \lambda N_1^1\ \lambda N_1^2 \cdots \lambda N_1^m\ \lambda N_2^1 \cdots \lambda N_r^m\ \right]^T \tag{3.74}$$

a $(r-1)(m-1)$-vector of double differenced ambiguities

$$\begin{aligned} \big[\ &\lambda(N_1^1 - N_1^2 - N_2^1 + N_2^2) \ \ldots\ \lambda(N_1^1 - N_1^m - N_2^1 + N_2^m) \\ &\lambda(N_1^1 - N_1^2 - N_3^1 + N_3^2) \ \ldots\ \lambda(N_1^1 - N_1^m - N_3^1 + N_3^m) \ \ldots \\ &\lambda(N_1^1 - N_1^2 - N_r^1 + N_r^2) \ \ldots \lambda(N_1^1 - N_1^m - N_r^1 + N_r^m)\ \big]^T \end{aligned} \tag{3.75}$$

is obtained. The design matrix is changed accordingly from the $(r-1)(m-1) \times rm$ matrix $R_{r-1} \otimes R_{m-1}$ to the $(r-1)(m-1) \times (r-1)(m-1)$ matrix $I_{(r-1)(m-1)}$. The resulting system of normal equations is now of full rank:

$$\left(I_{r-1} - \frac{1}{r}E_{r-1}\right) \otimes \left(I_{m-1} - \frac{1}{m}E_{m-1}\right) \Delta x_1 = \left(I_{r-1} - \frac{1}{r}E_{r-1}\right) \otimes \left(I_{m-1} - \frac{1}{m}E_{m-1}\right) \Delta \mathrm{DD} y_k \quad (3.76)$$

The transformation that was applied to the observables is not an invertible one (invertible transformation maintain the information content of the system). In the next section it will be shown why it is still admissible.

3.7 Double differences: an alternative approach

In this section we will show how the system of undifferenced carrier phases

$$E\{\Phi\} = \begin{bmatrix} A_I & A_{II} \end{bmatrix} \begin{bmatrix} x_I \\ x_{II} \end{bmatrix} \quad (3.77)$$

can be transformed by applying invertible transformations (which do not change the information content of the system) only, into

$$E\left\{\begin{bmatrix} \bar{\Phi} \\ \mathrm{DD}\Phi \end{bmatrix}\right\} = \begin{bmatrix} \bar{A}_I & \bar{A}_{II} & 0 \\ \mathrm{DD}A_I & 0 & \mathrm{DD}A_{II} \end{bmatrix} \begin{bmatrix} x_I \\ \bar{x}_{II} \\ \mathrm{DD}x_{II} \end{bmatrix} \quad (3.78)$$

For reasons of legibility, and since here we are mainly interested in the biases, we will only show the transformation of the bias part of the system. Also the expectation operator will be omitted. The superscript ^{M} denotes the whole range of satellites $1, \cdots, m$, the superscript $^{\bar{M}}$ denotes the whole range of satellites except the first one $2, \cdots, m$.

We start with the undifferenced phase observables, modeled by a clock term for the receiver and for the satellite, and an ambiguity term:

$$\begin{bmatrix} \Phi_1^M \\ \Phi_2^M \\ \vdots \\ \Phi_r^M \end{bmatrix} = \begin{bmatrix} e_m & & & -I_m & I_m & & \\ & e_m & & -I_m & & I_m & \\ & & \ddots & \vdots & & & \ddots \\ & & & e_m & -I_m & & & I_m \end{bmatrix} \begin{bmatrix} c\delta t_1 \\ c\delta t_2 \\ \vdots \\ c\delta t_r \\ c\delta t^M \\ \lambda N_1^M \\ \lambda N_2^M \\ \vdots \\ \lambda N_r^M \end{bmatrix} \quad (3.79)$$

In a number of steps we will apply the following invertible transformation to this system of observation equations

$$T_{\mathrm{DD}} = (I_r \otimes \bar{R}_m)(\bar{R}_r \otimes I_m) \quad (3.80)$$

with

$$\bar{R}_q = \left.\begin{bmatrix} 1 & & \\ -1 & 1 & \\ \vdots & & \ddots \\ -1 & & 1 \end{bmatrix}\right\} q \tag{3.81}$$

Applying the second part of (3.80), thus $(\bar{R}_r \otimes I_m)$, to Eq. (3.79) we form single differences between receivers (pivoting with the first receiver as pivot), while retaining the original undifferenced observation equations belonging to the first receiver. In the so formed 'single differenced' (SD) observation equations the satellite clock term has disappeared:

$$\begin{bmatrix} \Phi_1^M \\ \Phi_{21}^M \\ \vdots \\ \Phi_{r1}^M \end{bmatrix} = \begin{bmatrix} e_m & & & -I_m & I_m & & \\ -e_m & e_m & & & -I_m & I_m & \\ \vdots & & \ddots & & \vdots & & \ddots \\ -e_m & & e_m & -I_m & & & I_m \end{bmatrix} \begin{bmatrix} c\delta t_1 \\ c\delta t_2 \\ \vdots \\ c\delta t_r \\ c\delta t^M \\ \lambda N_1^M \\ \lambda N_2^M \\ \vdots \\ \lambda N_r^M \end{bmatrix} \tag{3.82}$$

where $\Phi_{i1}^j = \Phi_i^j - \Phi_1^j$.

In the SD equations we lump together the clock of the first receiver with the clock of the other receivers, and also the ambiguities of the first receiver with the ambiguities of the other receivers:

$$\begin{bmatrix} \Phi_1^M \\ \Phi_{21}^M \\ \vdots \\ \Phi_{r1}^M \end{bmatrix} = \begin{bmatrix} e_m & & & -I_m & I_m & & \\ & e_m & & & & I_m & \\ & & \ddots & & & & \ddots \\ & & e_m & & & & I_m \end{bmatrix} \begin{bmatrix} c\delta t_1 \\ c(\delta t_2 - \delta t_1) \\ \vdots \\ c(\delta t_r - \delta t_1) \\ c\delta t^M \\ \lambda N_1^M \\ \lambda N_{21}^M \\ \vdots \\ \lambda N_{r1}^M \end{bmatrix} \tag{3.83}$$

where $N_{i1}^j = N_i^j - N_1^j$.

Applying the first part of (3.80) to Eq. (3.83) double differences are formed (pivoting with the first satellite as pivot). In the DD observation equations also the receiver clock term

disappears:

$$\begin{bmatrix} \Phi_1^1 \\ \Phi_1^{\bar{M}1} \\ \begin{bmatrix} \Phi_{21}^1 \\ \Phi_{21}^{\bar{M}1} \end{bmatrix} \\ \vdots \\ \begin{bmatrix} \Phi_{r1}^1 \\ \Phi_{r1}^{\bar{M}1} \end{bmatrix} \end{bmatrix} = \begin{bmatrix} 1 & & & -1 & 1 & & & \\ & & & e_{\bar{m}} & -I_{\bar{m}} & -e_{\bar{m}} & I_{\bar{m}} & \\ \begin{bmatrix} 1 \\ 0_{\bar{m}} \end{bmatrix} & & & & & \begin{bmatrix} 1 \\ -e_{\bar{m}} \end{bmatrix} & I_{\bar{m}} & \\ & \ddots & & & & & \ddots & \\ & & \begin{bmatrix} 1 \\ 0_{\bar{m}} \end{bmatrix} & & & & & \begin{bmatrix} 1 \\ -e_{\bar{m}} \end{bmatrix} I_{\bar{m}} \end{bmatrix} \begin{bmatrix} c\delta t_1 \\ c(\delta t_2 - \delta t_1) \\ \vdots \\ c(\delta t_r - \delta t_1) \\ c\delta t^1 \\ c\delta t^{\bar{M}} \\ \lambda N_1^1 \\ \lambda N_1^{\bar{M}} \\ \begin{bmatrix} \lambda N_{21}^1 \\ \lambda N_{21}^{\bar{M}} \end{bmatrix} \\ \vdots \\ \begin{bmatrix} \lambda N_{r1}^1 \\ \lambda N_{r1}^{\bar{M}} \end{bmatrix} \end{bmatrix} \tag{3.84}$$

where $e_{\bar{m}} = e_{m-1}$, $0_{\bar{m}} = 0_{m-1}$, and $I_{\bar{m}} = I_{m-1}$.

In the DD equations the SD ambiguities of the first satellite are lumped together with the SD ambiguities of the other satellites, giving

$$\begin{bmatrix} \Phi_1^1 \\ \Phi_1^{\bar{M}1} \\ \begin{bmatrix} \Phi_{21}^1 \\ \Phi_{21}^{\bar{M}1} \end{bmatrix} \\ \vdots \\ \begin{bmatrix} \Phi_{r1}^1 \\ \Phi_{r1}^{\bar{M}1} \end{bmatrix} \end{bmatrix} = \begin{bmatrix} 1 & & & -1 & 1 & & & \\ & & & e_{\bar{m}} & -I_{\bar{m}} & -e_{\bar{m}} & I_{\bar{m}} & \\ \begin{bmatrix} 1 \\ 0_{\bar{m}} \end{bmatrix} & & & & & \begin{bmatrix} 1 \\ & I_{\bar{m}} \end{bmatrix} & & \\ & \ddots & & & & & \ddots & \\ & & \begin{bmatrix} 1 \\ 0_{\bar{m}} \end{bmatrix} & & & & & \begin{bmatrix} 1 \\ & I_{\bar{m}} \end{bmatrix} \end{bmatrix} \begin{bmatrix} c\delta t_1 \\ c(\delta t_2 - \delta t_1) \\ \vdots \\ c(\delta t_r - \delta t_1) \\ c\delta t^1 \\ c\delta t^{\bar{M}} \\ \lambda N_1^1 \\ \lambda N_1^{\bar{M}} \\ \begin{bmatrix} \lambda N_{21}^1 \\ \lambda N_{21}^{\bar{M}1} \end{bmatrix} \\ \vdots \\ \begin{bmatrix} \lambda N_{r1}^1 \\ \lambda N_{r1}^{\bar{M}1} \end{bmatrix} \end{bmatrix} \tag{3.85}$$

where $N_{i1}^{j1} = N_i^{j1} - N_1^{j1}$. A re-arrangement of the system gives

$$\begin{bmatrix} \Phi_1^1 \\ \Phi_1^{\bar{M}1} \\ \Phi_{21}^1 \\ \vdots \\ \Phi_{r1}^1 \\ \Phi_{21}^{\bar{M}1} \\ \vdots \\ \Phi_{r1}^{\bar{M}1} \end{bmatrix} = \begin{bmatrix} 1 & & -1 & & 1 & & & & \\ & & e_{\bar{m}} & -I_{\bar{m}} & -e_{\bar{m}} & I_{\bar{m}} & & & \\ & 1 & & & & & 1 & & \\ & & \ddots & & & & & \ddots & \\ & & & 1 & & & & & 1 \\ & & & & & & & & & I_{\bar{m}} \\ & & & & & & & & & & \ddots \\ & & & & & & & & & & & I_{\bar{m}} \end{bmatrix} \begin{bmatrix} c\delta t_1 \\ c(\delta t_2 - \delta t_1) \\ \vdots \\ c(\delta t_r - \delta t_1) \\ c\delta t^1 \\ c\delta t^{\bar{M}} \\ \lambda N_1^1 \\ \lambda N_1^{\bar{M}} \\ \lambda N_{21}^1 \\ \vdots \\ \lambda N_{r1}^1 \\ \lambda N_{21}^{\bar{M}1} \\ \vdots \\ \lambda N_{r1}^{\bar{M}1} \end{bmatrix} \tag{3.86}$$

which falls apart into two independent subsystems (although the systems seem to be linked together via the coordinate part, the first part, as we will show below, does not contribute to the estimation of the coordinates):

$$\begin{bmatrix} \Phi_1^1 \\ \Phi_1^{\bar{M}1} \\ \Phi_{21}^1 \\ \vdots \\ \Phi_{r1}^1 \end{bmatrix} = \begin{bmatrix} 1 & & -1 & & 1 & & & \\ & & e_{\bar{m}} & -I_{\bar{m}} & -e_{\bar{m}} & I_{\bar{m}} & & \\ & 1 & & & & & 1 & \\ & & \ddots & & & & & \ddots \\ & & & 1 & & & & & 1 \end{bmatrix} \begin{bmatrix} c\delta t_1 \\ c(\delta t_2 - \delta t_1) \\ \vdots \\ c(\delta t_r - \delta t_1) \\ c\delta t^1 \\ c\delta t^{\bar{M}} \\ \lambda N_1^1 \\ \lambda N_1^{\bar{M}} \\ \lambda N_{21}^1 \\ \vdots \\ \lambda N_{r1}^1 \end{bmatrix} \tag{3.87}$$

$$\begin{bmatrix} \Phi_{21}^{\bar{M}1} \\ \vdots \\ \Phi_{r1}^{\bar{M}1} \end{bmatrix} = \begin{bmatrix} I_{\bar{m}} & & \\ & \ddots & \\ & & I_{\bar{m}} \end{bmatrix} \begin{bmatrix} \lambda N_{21}^{\bar{M}1} \\ \vdots \\ \lambda N_{r1}^{\bar{M}1} \end{bmatrix} \tag{3.88}$$

The second part of the system contains the DD equations modeled by the DD ambiguities. Let us have a closer look at the first part of the system: there we have $r+m-1$ observables, $r+m$ local parameters consisting of functions of the clock parameter, and $r+m$ global parameters consisting of functions of ambiguities. The system is obviously rank defect. By pre-multiplying the system with the matrix

$$\left.\begin{bmatrix} 1 & & \\ 1 & 1 & \\ \vdots & & \ddots \\ 1 & & & 1 \end{bmatrix}\right\} r+m-1 \tag{3.89}$$

we obtain a system with undifferenced equations only:

$$\begin{bmatrix} \Phi_1^1 \\ \Phi_1^{\bar{M}} \\ \Phi_2^1 \\ \vdots \\ \Phi_r^1 \end{bmatrix} = \begin{bmatrix} 1 & & -1 & & 1 & & \\ e_{\bar{m}} & & & -I_{\bar{m}} & I_{\bar{m}} & & \\ 1 & 1 & -1 & & 1 & 1 & \\ \vdots & \ddots & \vdots & & \vdots & & \ddots \\ 1 & & 1 & -1 & 1 & & 1 \end{bmatrix} \begin{bmatrix} c\delta t_1 \\ c(\delta t_2 - \delta t_1) \\ \vdots \\ c(\delta t_r - \delta t_1) \\ c\delta t^1 \\ c\delta t^{\bar{M}} \\ \lambda N_1^1 \\ \lambda N_1^{\bar{M}} \\ \lambda N_{21}^1 \\ \vdots \\ \lambda N_{r1}^1 \end{bmatrix} \tag{3.90}$$

Now we lump together the biased receiver clocks $c(\delta t_i - \delta t_1)$ with the SD ambiguities (λN_{i1}^1), and the satellite clocks $(c\delta t^j)$ with the ambiguities of the first receiver (λN_1^j):

$$\begin{bmatrix} \Phi_1^1 \\ \Phi_1^{\bar{M}} \\ \Phi_2^1 \\ \vdots \\ \Phi_r^1 \end{bmatrix} = \begin{bmatrix} 1 & & -1 & \\ e_{\bar{m}} & & & -I_{\bar{m}} \\ 1 & 1 & -1 & \\ \vdots & \ddots & \vdots & \\ 1 & & 1 & -1 \end{bmatrix} \begin{bmatrix} c\delta t_1 \\ c(\delta t_2 - \delta t_1) + \lambda N_{21}^1 \\ \vdots \\ c(\delta t_r - \delta t_1) + \lambda N_{r1}^1 \\ c\delta t^1 - \lambda N_1^1 \\ c\delta t^{\bar{M}} - \lambda N_1^{\bar{M}} \end{bmatrix} \tag{3.91}$$

In the resulting system there is still a rank defect of 1. To make the system of full rank we lump together the clock error of the first receiver $(c\delta t_1)$ together with the biased satellite clocks $(c\delta t^j - \lambda N_1^j)$:

$$\begin{bmatrix} \Phi_1^1 \\ \Phi_1^{\bar{M}} \\ \Phi_2^1 \\ \vdots \\ \Phi_r^1 \end{bmatrix} = \begin{bmatrix} & & -1 & \\ & & & -I_{\bar{m}} \\ 1 & & -1 & \\ & \ddots & \vdots & \\ & & 1 & -1 \end{bmatrix} \begin{bmatrix} c(\delta t_2 - \delta t_1) + \lambda N_{21}^1 \\ \vdots \\ c(\delta t_r - \delta t_1) + \lambda N_{r1}^1 \\ c(\delta t^1 - \delta t_1) - \lambda N_1^1 \\ c(\delta t^{\bar{M}} - \delta t_1) - \lambda N_1^{\bar{M}} \end{bmatrix} \tag{3.92}$$

The result is a system of full rank, with only local parameters; i.e. at each epoch $r+m-1$ parameters have to be estimated using the $r+m-1$ observables only. These observables are called free variates. The observables in this system do not contribute to the estimation of coordinates or DD ambiguities. If one is not interested in the local parameters, these observables may be discarded.

The local parameters are equal to the unbiased estimable functions of parameters one obtains when in the undifferenced approach the S-basis as in (3.42) is chosen.

3.8 Solution of the normal equations

As we showed in Section 3.3, the rank defect of the bias part of one phase observable type (i.e. the ambiguity parameters and the clock errors) is $r+m+n-1$, so we have to choose

$r+m+n-1$ parameters to form an S-basis. One of the possible choices is to choose one clock in every epoch (we chose the clock of the first receiver), and $r+m-1$ ambiguity parameters.

In practice the choice of the clock of the first receiver means that we skip the columns referring to this parameter. This means that we constrain the value for the clock of the first receiver to zero. By doing this, matrix $A_{2,k}$ is altered into $\bar{A}_{2,k}$:

$$\underset{rm \times (r-1+m)}{\bar{A}_{2,k}} = \begin{bmatrix} & & -I_m \\ e_m & & -I_m \\ & \ddots & \vdots \\ & e_m & -I_m \end{bmatrix} \tag{3.93}$$

With the variance-covariance matrix of the observables as

$$\underset{\times nrm}{Q_y} = \begin{bmatrix} Q_{y_1} & & \\ & \ddots & \\ & & Q_{y_n} \end{bmatrix} \tag{3.94}$$

the normal matrix N and right-hand side h read

$$\underset{\times 3r+rm+n(r+m)}{N} = \begin{bmatrix} \sum_{k=1}^{n} A_{1,k}^T Q_{y_k}^{-1} A_{1,k} & & & \textit{symmetric} \\ \bar{A}_{2,1}^T Q_{y_1}^{-1} A_{1,1} & \bar{A}_{2,1}^T Q_{y_1}^{-1} \bar{A}_{2,1} & & \\ \vdots & & \ddots & \\ \bar{A}_{2,n} Q_{y_n}^{-1} A_{1,n} & & & \bar{A}_{2,n}^T Q_{y_n}^{-1} \bar{A}_{2,n} \end{bmatrix} \tag{3.95}$$

$$\underset{3r+rm+n(r+m)\times 1}{h} = \begin{bmatrix} \sum_{k=1}^{n} A_{1,k}^T Q_{y_k}^{-1} \Delta y_k \\ \bar{A}_{2,1}^T Q_{y_1}^{-1} \Delta y_1 \\ \vdots \\ \bar{A}_{2,n}^T Q_{y_n}^{-1} \Delta y_n \end{bmatrix} \tag{3.96}$$

Since this normal matrix system will become very large for the number of epochs normally involved, the local parameters are first eliminated, and computed in a second step by substitution of the global parameters in the observation equations. The elimination of local parameters and thus the updating of the normal matrix and right-hand side is done epoch-by-epoch, and can symbolically be described as follows:

- $N_0 = 0$; $h_0 = 0$
- for epoch $k = 1$ to n:

$$\begin{aligned} N_k &= N_{k-1} + A_{1,k}^T Q_{y_k}^{-1} A_{1,k} - A_{1,k}^T Q_{y_k}^{-1} \left[\bar{A}_{2,k}(\bar{A}_{2,k}^T Q_{y_k}^{-1} \bar{A}_{2,k})^{-1} \bar{A}_{2,k}^T Q_{y_k}^{-1}\right] A_{1,k} \\ &= N_{k-1} + A_{1,k}^T Q_{y_k}^{-1} \left[I_{rm} - \bar{A}_{2,k}(\bar{A}_{2,k}^T Q_{y_k}^{-1} \bar{A}_{2,k})^{-1} \bar{A}_{2,k}^T Q_{y_k}^{-1}\right] A_{1,k} \\ &= N_{k-1} + A_{1,k}^T Q_{y_k}^{-1} \left[I_{rm} - P_{\bar{A}_{2,k}}\right] A_{1,k} \\ &= N_{k-1} + A_{1,k}^T Q_{y_k}^{-1} P_{\bar{A}_{2,k}}^{\perp} A_{1,k} \end{aligned} \tag{3.97}$$

$$\begin{aligned} h_k &= h_{k-1} + A_{1,k}^T Q_{y_k}^{-1} \Delta y_k - A_{1,k}^T Q_{y_k}^{-1} \left[\bar{A}_{2,k}(\bar{A}_{2,k}^T Q_{y_k}^{-1} \bar{A}_{2,k})^{-1} \bar{A}_{2,k}^T Q_{y_k}^{-1}\right] \Delta y_k \\ &= h_{k-1} + A_{1,k}^T Q_{y_k}^{-1} \left[I_{rm} - \bar{A}_{2,k}(\bar{A}_{2,k}^T Q_{y_k}^{-1} \bar{A}_{2,k})^{-1} \bar{A}_{2,k}^T Q_{y_k}^{-1}\right] \Delta y_k \\ &= h_{k-1} + A_{1,k}^T Q_{y_k}^{-1} \left[I_{rm} - P_{\bar{A}_{2,k}}\right] \Delta y_k \\ &= h_{k-1} + A_{1,k}^T Q_{y_k}^{-1} P_{\bar{A}_{2,k}}^{\perp} \Delta y_k \end{aligned} \tag{3.98}$$

with N_k the normal matrix reduced for the clocks of epoch 1 to k, h_k the right-hand side reduced for the clocks of epoch 1 to k, and Δy_k the vector of 'observed' minus 'computed' of epoch k.

So after n epochs we have the following reduced normal matrix system

$$\sum_{k=1}^{n} A_{1,k}^T Q_{y_k}^{-1} P_{\bar{A}_{2,k}}^{\perp} A_{1,k} \Delta x_1 = \sum_{k=1}^{n} A_{1,k}^T Q_{y_k}^{-1} P_{\bar{A}_{2,k}}^{\perp} \Delta y_k \tag{3.99}$$

In short hand notation we will denote it as

$$N_n \Delta x_1 = h_n \tag{3.100}$$

Since so far we only resolved part of the rank defect, viz. the rank defect relating to the clock parameters, the normal matrix N_n is still singular. The remaining rank defect of $r + m - 1$ is resolved by constraining $r + m - 1$ ambiguities to zero, resulting in an invertible normal matrix $\bar{N}_n$ and matching right-hand side $\bar{h}_n$:

$$\begin{aligned} \bar{N}_n &= S_a^T N_n S_a \\ \bar{h}_n &= S_a^T h_n \end{aligned} \tag{3.101}$$

i.e. if we have chosen an S-basis for the ambiguities consisting of $r + m - 1$ ambiguities, $S_a^T N_n S_a$ is formed by deleting the columns and rows in N_n and the entries in h_n referring to the ambiguities in that S-basis. For the definition of S_a see Eq. (3.33). The selection of the ambiguities is made according to the procedure described in Sections 3.4 and 3.5.

With the exception of global networks, the absolute position of the coordinates is poorly estimable, and thus also the coordinates of one station are constrained to a priori values. This makes that instead of absolute coordinates r_i, relative so-called baseline coordinates $r_i - r_{i0}$, with $i0$ the station whose coordinates are constrained, are estimated. This is however, *not* a real rank defect, so the values at which the coordinates are constrained, influence the estimates.

The global parameters are obtained through solution of the system

$$\bar{N}_n \Delta\bar{x}_1 = \bar{h}_n \tag{3.102}$$

by means of a Cholesky factorization[1] (Golub and Van Loan 1989) of the normal matrix,

$$\bar{N}_n = CC^T \tag{3.103}$$

followed by a forward and backward substitution:

$$Cx_h = \bar{h}_n \tag{3.104}$$

$$C^T \Delta\bar{x}_1 = x_h \tag{3.105}$$

The Cholesky factorization can be made in-place.

After we have computed the global parameters we compute the local parameters by substitution of the global parameters into the 'observed' minus 'computed' quantity:

$$\Delta y_k^{(2)} = \Delta y_k - \bar{A}_{1,k} \Delta\bar{x}_1 \tag{3.106}$$

with

$$\bar{A}_{1,k} = \begin{bmatrix} g_k & S_a \end{bmatrix} \tag{3.107}$$

S_a is formed from I_{rm} by deleting the columns referring to the ambiguities in the S-basis.

The solution of the local parameters $\Delta\bar{x}_{2,k}$ of epoch k follows then from the solution of the system

$$(\bar{A}_{2,k}^T Q_{y_k}^{-1} \bar{A}_{2,k}) \Delta\bar{x}_{2,k} = \bar{A}_{2,k}^T Q_{y_k}^{-1} \Delta y_k^{(2)} \tag{3.108}$$

Or, since $H_{\bar{A}_{2,k}} = (\bar{A}_{2,k}^T Q_{y_k}^{-1} \bar{A}_{2,k})^{-1} \bar{A}_{2,k}^T Q_{y_k}^{-1}$ becomes available during the computation of $P_{\bar{A}_{2,k}}^{\perp}$ (see Section 3.12).

$$\Delta\bar{x}_{2,k} = H_{\bar{A}_{2,k}} \Delta y_k^{(2)} \tag{3.109}$$

3.9 Testing and reliability

In this section we will give a short description of the testing procedures that are employed in all geodetic data processing software of the Section Mathematical Geodesy and Positioning of the Faculty of Civil Engineering and Geosciences of DUT (B-method of testing). For a more extensive description we refer to Teunissen (1989) and Beckers and Kenselaar (1996). In Section 3.10 we will show some examples of these procedures applied to GPS data.

Testing.
The testing procedures are based on the confrontation of the null hypothesis

$$H_0 : y \sim N(Ax, Q_y) \tag{3.110}$$

[1] Devised by André-Louis Cholesky, see (Benoît 1924)

with the alternative hypothesis

$$H_a : y \sim N(Ax + C_y\nabla, Q_y) \tag{3.111}$$

The null hypothesis states that the data fit both the functional and the stochastic model, whereas the alternative hypothesis states that the functional model should be extended, to account for the model error $C_y\nabla$. The observables are assumed to have a normal distribution.

In the GPS data processing three tests are computed, viz. 1. the overall model test (OMT), 2. the test for an outlier in a single observation, and 3. the test for a cycle slip in a carrier phase observation. Slips occur when the receiver miscounts the number of whole cycles. This can occur, e.g., when there is high ionospheric activity, or by some internal failure inside the receiver hard- or software.

The overall model test is a general test on the validity of the chosen model. It analyzes the squared perpendicular distance of the observation vector y to the model Ax. The test statistic reads

$$T_{\text{df}} = \hat{e}^T Q_y^{-1} \hat{e}, \tag{3.112}$$

and has under the null hypothesis a χ^2 distribution with df = 'number of observations'–'rank of the system' degrees of freedom. The null hypothesis is accepted if

$$T_{\text{df}} \leq k_{\text{df}} \tag{3.113}$$

Besides the overall model test, each observation may be tested separately, by specifying a one-dimensional alternative hypothesis for it. The test statistics so obtained are called w-test statistics. For the GPS observable types, two alternative hypotheses are of importance, viz. one that tests if an outlier has occurred in a pseudo range or carrier phase (specified by a conventional alternative hypothesis), and one that tests if a slip occurred in the carrier phase (specified by a non-conventional alternative hypothesis). The w-test statistic for the GPS alternative hypotheses (with $C_y = c_{p,k}$) reads

$$w_{p,k} = \frac{c_{p,k}^T Q_y \hat{e}}{\sqrt{c_{p,k}^T Q_y^{-1} Q_{\hat{e}} Q_y^{-1} c_{p,k}}} \tag{3.114}$$

The choice for $c_{p,k}$ for testing for an outlier, or a cycle slip will be treated in Section 3.10.

The squared w-test statistic has under the null hypothesis a central χ^2 distribution with one degree of freedom. H_0 is accepted if

$$w_{p,k}^2 \leq k_1 \tag{3.115}$$

or consequently, if

$$-\sqrt{k_1} \leq w_{p,k} \leq \sqrt{k_1} \tag{3.116}$$

If H_0 is rejected the estimate for the error $\hat{\nabla}_{p,k}$ reads

$$\hat{\nabla}_{p,k} = \frac{c_{p,k}^T Q_y \hat{e}}{c_{p,k}^T Q_y^{-1} Q_{\hat{e}} Q_y^{-1} c_{p,k}} \tag{3.117}$$

For the case that the size of the error $\|\nabla_{p,k}\|$ is known a priori, the w-test statistic reads (Teunissen 1988)

$$\|w_{p,k}\| = \frac{\|c_{p,k}^T Q_y \hat{e}\|}{\sqrt{c_{p,k}^T Q_y^{-1} Q_{\hat{e}} Q_y^{-1} c_{p,k}}} \tag{3.118}$$

and H_0 is accepted if

$$\|w_{p,k}\| \leq \frac{1}{2}\sqrt{c_{p,k}^T Q_y^{-1} Q_{\hat{e}} Q_y^{-1} c_{p,k}} \ \|\nabla_{p,k}\| \tag{3.119}$$

or

$$\hat{\nabla}_{p,k} \leq \frac{1}{2}\|\nabla_{p,k}\| \tag{3.120}$$

Under the alternative hypothesis the OMT statistic and the squared w-test statistic have a non-central $\chi^2(\mathrm{df}, \lambda_0)$ distribution with λ_0 the non-centrality parameter.

The probability that H_0 is rejected, while it is actually true, is specified by the 'level of significance' of the test α

$$\alpha = P(T > k \mid H_0) = \int_k^\infty \chi^2(\mathrm{df}, t)dt \tag{3.121}$$

The probability that H_0 is rejected, while in fact H_a is true is specified by the 'power' of the test γ

$$\gamma = P(T > k \mid H_a) = \int_k^\infty \chi^2(\mathrm{df}, \lambda_0, t)dt \ . \tag{3.122}$$

In the B-method of testing the power and the non-centrality parameter are set equal for all tests. This guarantees that a model error of a certain size will cause H_0 to be rejected with equal probability for tests of different dimension. The level of significance is different however for tests of different dimension. For all the examples in this thesis, the level of significance for a one-dimensional hypothesis, α_1 was chosen as 0.001, and the power of all tests as 0.80. The critical value k_1 for the one-dimensional tests is then computed from Eq. (3.121) with df=1 as 10.828, and using this value, the non-centrality parameter λ_0 is computed from Eq. (3.122) with df=1 as 17.075. For tests with a different dimension, α_{df} and k_{df} are computed using Eq. (3.121) and Eq. (3.122) (Teunissen 1988).

2. Reliability.

Reliability is defined as the ability of detecting model errors by the testing procedure (internal reliability), and the influence undetected model errors have on the eventual estimates (external reliability). For the computation of the reliability measures we do not need actual data, i.e., they can be computed beforehand in the design stage.

For the one-dimensional hypothesis the size of the so-called minimal detectable bias (MDB) ∇ is computed as

$$\|\nabla_{p,k}\| = \sqrt{\frac{\lambda_0}{c_{p,k}^T Q_y^{-1} Q_{\hat{e}} Q_y^{-1} c_{p,k}}} \tag{3.123}$$

External reliability will not be treated in this thesis, we refer to Kösters (1992).

3.10 Computation of one-dimensional test statistics

For testing the conventional and non-conventional hypotheses we need the variance-covariance matrix of the residuals $Q_{\hat{e}}$. It is defined as

$$Q_{\hat{e}} = Q_y - Q_{\hat{y}} \tag{3.124}$$

With $\hat{y}_k$ defined as

$$\begin{aligned}
\hat{y}_k &= \bar{A}_{1,k}\hat{x}_1 + \bar{A}_{2,k}\hat{x}_{2,k} \\
&= \bar{A}_{1,k}\hat{x}_1 + \bar{A}_{2,k}(\bar{A}_{2,k}^T Q_{y_k}^{-1}\bar{A}_{2,k})^{-1}\bar{A}_{2,k}^T Q_{y_k}^{-1}(y_k - \bar{A}_{1,k}\hat{x}_1) \\
&= \bar{A}_{1,k}\hat{x}_1 + P_{\bar{A}_{2,k}}(y_k - \bar{A}_{1,k}\hat{x}_1) \\
&= P_{\bar{A}_{2,k}}^{\perp}\bar{A}_{1,k}\hat{x}_1 + P_{\bar{A}_{2,k}}y_k
\end{aligned} \tag{3.125}$$

the variance-covariance matrix of the adjusted observables reads:

$$Q_{\hat{y}} = \begin{bmatrix} Q_{\hat{y}_1} & Q_{\hat{y}_1\hat{y}_2} & \cdots & Q_{\hat{y}_1\hat{y}_n} \\ Q_{\hat{y}_2\hat{y}_1} & Q_{\hat{y}_2} & & \vdots \\ \vdots & & \ddots & Q_{\hat{y}_{n-1}\hat{y}_n} \\ Q_{\hat{y}_1\hat{y}_n} & \cdots & Q_{\hat{y}_{n-1}\hat{y}_n} & Q_{\hat{y}_n} \end{bmatrix} \tag{3.126}$$

where

$$\begin{aligned}
Q_{\hat{y}_k} =& P_{\bar{A}_{2,k}}^{\perp}\bar{A}_{1,k}Q_{\hat{x}_1}\bar{A}_{1,k}^T P_{\bar{A}_{2,k}}^{\perp T} + P_{\bar{A}_{2,k}}Q_{y_k}P_{\bar{A}_{2,k}}^T + \\
& P_{\bar{A}_{2,k}}^{\perp}\bar{A}_{1,k}Q_{\hat{x}_1 y_k}P_{\bar{A}_{2,k}}^T + P_{\bar{A}_{2,k}}Q_{y_k\hat{x}_1}\bar{A}_{1,k}^T P_{\bar{A}_{2,k}}^{\perp T} \\
=& P_{\bar{A}_{2,k}}^{\perp}\bar{A}_{1,k}Q_{\hat{x}_1}\bar{A}_{1,k}^T P_{\bar{A}_{2,k}}^{\perp T} + P_{\bar{A}_{2,k}}Q_{y_k}P_{\bar{A}_{2,k}}^T + \\
& P_{\bar{A}_{2,k}}^{\perp}\bar{A}_{1,k}Q_{\hat{x}_1}\bar{A}_{1,k}^T Q_{y_k}^{-1}P_{\bar{A}_{2,k}}^{\perp}Q_{y_k}P_{\bar{A}_{2,k}}^T + P_{\bar{A}_{2,k}}Q_{y_k}P_{\bar{A}_{2,k}}^{\perp T}Q_{y_k}^{-1}\bar{A}_{1,k}Q_{\hat{x}_1}\bar{A}_{1,k}^T P_{\bar{A}_{2,k}}^{\perp T} \\
=& P_{\bar{A}_{2,k}}^{\perp}\bar{A}_{1,k}Q_{\hat{x}_1}\bar{A}_{1,k}^T P_{\bar{A}_{2,k}}^{\perp T} + P_{\bar{A}_{2,k}}Q_{y_k}
\end{aligned} \tag{3.127}$$

and

$$\begin{aligned}
Q_{\hat{y}_k\hat{y}_l} =& P_{\bar{A}_{2,k}}^{\perp}\bar{A}_{1,k}Q_{\hat{x}_1}\bar{A}_{1,l}^T P_{\bar{A}_{2,l}}^{\perp T} + \\
& P_{\bar{A}_{2,k}}^{\perp}\bar{A}_{1,k}Q_{\hat{x}_1 y_l}P_{\bar{A}_{2,l}}^T + P_{\bar{A}_{2,k}}Q_{y_k\hat{x}_1}\bar{A}_{1,l}^T P_{\bar{A}_{2,l}}^{\perp T} \\
=& P_{\bar{A}_{2,k}}^{\perp}\bar{A}_{1,k}Q_{\hat{x}_1}\bar{A}_{1,l}^T P_{\bar{A}_{2,l}}^{\perp T} + \\
& P_{\bar{A}_{2,k}}^{\perp}\bar{A}_{1,k}Q_{\hat{x}_1}\bar{A}_{1,l}^T Q_{y_l}^{-1}P_{\bar{A}_{2,l}}^{\perp}Q_{y_l}P_{\bar{A}_{2,l}}^T + P_{\bar{A}_{2,k}}Q_{y_k}P_{\bar{A}_{2,k}}^{\perp T}Q_{y_k}^{-1}\bar{A}_{1,k}Q_{\hat{x}_1}\bar{A}_{1,l}^T P_{\bar{A}_{2,l}}^{\perp T} \\
=& P_{\bar{A}_{2,k}}^{\perp}\bar{A}_{1,k}Q_{\hat{x}_1}\bar{A}_{1,l}^T P_{\bar{A}_{2,l}}^{\perp T}
\end{aligned} \tag{3.128}$$

(Note that $P_{\bar{A}_{2,k}}Q_{y_k}P_{\bar{A}_{2,k}}^{\perp T} = 0$, and $P_{\bar{A}_{2,l}}^{\perp}Q_{y_l}P_{\bar{A}_{2,l}}^T = 0$.)

In the derivation above we used elements from the variance-covariance matrix of $\hat{x}_1$, and y_k, for $k = 1, \ldots, n$

$$D\{\begin{bmatrix} \hat{x}_1 \\ y_1 \\ \vdots \\ y_n \end{bmatrix}\} = \begin{bmatrix} Q_{\hat{x}_1} & Q_{\hat{x}_1}\bar{A}_{1,1}^T Q_{y_1}^{-1}P_{\bar{A}_{2,1}}^{\perp}Q_{y_1} & \cdots & Q_{\hat{x}_1}\bar{A}_{1,n}^T Q_{y_n}^{-1}P_{\bar{A}_{2,n}}^{\perp}Q_{y_n} \\ Q_{y_1}P_{\bar{A}_{2,1}}^{\perp T}Q_{y_1}^{-1}\bar{A}_{1,1}Q_{\hat{x}_1} & Q_{y_1} & & \\ \vdots & & \ddots & \\ Q_{y_n}P_{\bar{A}_{2,n}}^{\perp T}Q_{y_n}^{-1}\bar{A}_{1,n}Q_{\hat{x}_1} & & & Q_{y_n} \end{bmatrix} \tag{3.129}$$

which follows from applying the propagation law of variances to

$$\begin{bmatrix} \hat{x}_1 \\ y_1 \\ \vdots \\ y_n \end{bmatrix} = \begin{bmatrix} Q_{\hat{x}_1}\bar{A}_{1,1}^T Q_{y_1}^{-1} P_{\bar{A}_{2,1}}^{\perp} & Q_{\hat{x}_1}\bar{A}_{1,2}^T Q_{y_2}^{-1} P_{\bar{A}_{2,2}}^{\perp} & \cdots & Q_{\hat{x}_1}\bar{A}_{1,n}^T Q_{y_n}^{-1} P_{\bar{A}_{2,n}}^{\perp} \\ I & & & \\ & I & & \\ & & \ddots & \\ & & & I \end{bmatrix} \begin{bmatrix} y_1 \\ y_2 \\ \vdots \\ y_n \end{bmatrix} \tag{3.130}$$

where $Q_{\hat{x}_1} = (\sum_{k=1}^{n} \bar{A}_{1,k}^T Q_{y_k}^{-1} \bar{A}_{1,k}^T)^{-1}$.

The corresponding elements of $Q_{\hat{e}}$ read

$$\begin{aligned} Q_{\hat{e}_k} &= Q_{y_k} - P_{\bar{A}_{2,k}}^{\perp} \bar{A}_{1,k} Q_{\hat{x}_1} \bar{A}_{1,k}^T P_{\bar{A}_{2,k}}^{\perp T} - P_{\bar{A}_{2,k}} Q_{y_k} \\ &= - P_{\bar{A}_{2,k}}^{\perp} \bar{A}_{1,k} Q_{\hat{x}_1} \bar{A}_{1,k}^T P_{\bar{A}_{2,k}}^{\perp T} + P_{\bar{A}_{2,k}}^{\perp} Q_{y_k} \qquad (3.131) \\ Q_{\hat{e}_k \hat{e}_l} &= - P_{\bar{A}_{2,k}}^{\perp} \bar{A}_{1,k} Q_{\hat{x}_1} \bar{A}_{1,l}^T P_{\bar{A}_{2,l}}^{\perp T} \qquad (3.132) \end{aligned}$$

The c-vector, belonging to the one-dimensional alternative hypothesis that the p-th observation at epoch k is an outlier, reads

$$\underset{nrm \times 1}{c_{p,k}} = [\overbrace{0_{rm} \cdots 0_{rm}}^{k-1} \; c_p^T \; 0_{rm} \cdots 0_{rm}]^T \tag{3.133}$$

with

$$\underset{rm \times 1}{c_p} = [\overbrace{0 \cdots 0}^{p-1} \; 1 \; 0 \cdots 0]^T \tag{3.134}$$

Consequently the matrix product $c_{p,k}^T Q_y^{-1} Q_{\hat{e}} Q_y^{-1} c_{p,k}$ boils down to picking the p-th element of the diagonal of $Q_{y_k}^{-1} Q_{\hat{e}_k} Q_{y_k}^{-1}$, i.e., from the diagonal of

$$-Q_{y_k}^{-1} P_{\bar{A}_{2,k}}^{\perp} \bar{A}_{1,k} Q_{\hat{x}_1} \bar{A}_{1,k}^T P_{\bar{A}_{2,k}}^{\perp T} Q_{y_k}^{-1} + Q_{y_k}^{-1} P_{\bar{A}_{2,k}}^{\perp} \tag{3.135}$$

The c-vector belonging to the one-dimensional alternative hypothesis that there is a slip in the p-th observation at epoch k, reads

$$\underset{nrm \times 1}{c_{p,k}} [\overbrace{0_{rm} \cdots 0_{rm}}^{k-1} \; c_p^T \; c_p^T \cdots c_p^T]^T \tag{3.136}$$

or, equivalently,

$$\underset{nrm \times 1}{c_{p,k}} = [\overbrace{-c_p^T \cdots -c_p^T}^{k-1} \; 0_{rm} \; 0_{rm} \cdots 0_{rm}]^T \tag{3.137}$$

The computation of the matrix product $c_{p,k}^T Q_y^{-1} Q_{\hat{e}} Q_y^{-1} c_{p,k}$ for this hypothesis is more complicated: we need the sum of $k \times k$ elements of $Q_y^{-1} Q_{\hat{e}} Q_y^{-1}$:

$$c_{p,k}^T Q_y^{-1} Q_{\hat{e}} Q_y^{-1} c_{p,k} = \sum_{i=1}^{k} (Q_{y_i}^{-1} P_{\bar{A}_{2,i}}^{\perp})_{p,p} - \sum_{i=1}^{k} \sum_{j=1}^{k} \left(Q_{y_i}^{-1} P_{\bar{A}_{2,i}}^{\perp} \bar{A}_{1,i} Q_{\hat{x}_1} \bar{A}_{1,j}^T P_{\bar{A}_{2,j}}^{\perp T} Q_{y_j}^{-1} \right)_{p,p} \tag{3.138}$$

A serious threat for the feasibility of the algorithm is that at an epoch k we need the design matrix $\bar{A}_{1,i}$ and projector $P_{\bar{A}_{2,i}}^{\perp}$ of epoch $i = 1, \ldots, k$. It will be clear that this amount of data, even for a modest number of receivers, satellites and epochs will not fit in the core memory. Storing the data on disk will also slow down the processing.

We found a solution for it by recognizing that Eq. (3.138) can be rewritten as

$$c_{p,k}^T Q_y^{-1} Q_{\hat{e}} Q_y^{-1} c_{p,k} = \sum_{i=1}^{k} (Q_{y_i}^{-1} P_{\bar{A}_{2,i}}^{\perp})_{p,p} - \left(\sum_{i=1}^{k} Q_{y_i}^{-1} P_{\bar{A}_{2,i}}^{\perp} \bar{A}_{1,i} Q_{\hat{x}_1} \sum_{j=1}^{k} \bar{A}_{1,j}^T P_{\bar{A}_{2,j}}^{\perp T} Q_{y_j}^{-1} \right)_{p,p} \tag{3.139}$$

(This is also why we use Eq. (3.137) instead of Eq. (3.136) for the specification of the cycle slip hypotheses.) Now we only have to compute and store the three matrices

$$\underset{rm \times rm}{W_{1,k}} = \sum_{i=1}^{k} Q_{y_i}^{-1} P_{\bar{A}_{2,i}}^{\perp} \tag{3.140}$$

$$\underset{rm \times (r-1)(m-1)+3r}{W_{2,k}} = \sum_{i=1}^{k} Q_{y_i}^{-1} P_{\bar{A}_{2,i}}^{\perp} \bar{A}_{1,i} \tag{3.141}$$

$$\underset{rm \times (r-1)(m-1)+3r}{W_{3,k}} = \sum_{i=1}^{k} Q_{y_i}^{-1} P_{\bar{A}_{2,i}}^{\perp} \bar{A}_{1,i} Q_{\hat{x}_1} \tag{3.142}$$

which are updated per epoch. At each epoch k the rm cycle slip hypotheses are computed as

$$c_{p,k}^T Q_y^{-1} Q_{\hat{e}} Q_y^{-1} c_{p,k} = (W_{1,k} - W_{3,k} W_{2,k}^T)_{p,p} \qquad p = 1, \ldots, rm \tag{3.143}$$

Since we have available the Cholesky factorization of the normal matrix $N_n = Q_{\hat{x}}^{-1}$ (see Eq. (3.103)), we can compute $Q_{\hat{x}}$ as

$$Q_{\hat{x}} = C^{-T} C^{-1} \tag{3.144}$$

Using this factorization Eq. (3.143) can be further simplified as

$$c_{p,k}^T Q_y^{-1} Q_{\hat{e}} Q_y^{-1} c_{p,k} = (W_{1,k} - W_{4,k} W_{4,k}^T)_{p,p} \qquad p = 1, \ldots, rm \tag{3.145}$$

with

$$\underset{rm \times (r-1)(m-1)+3r}{W_{4,k}} = \sum_{i=1}^{k} Q_{y_i}^{-1} P_{\bar{A}_{2,i}}^{\perp} \bar{A}_{1,i} C^{-T} \tag{3.146}$$

The efficiency when using one of the two expressions depends among other things on the observable type and the length of the observation time span. In general when the time span is short, and there are not too many changes in the observation scenario, (3.145) is preferred. For larger time spans where inevitably the observation scenario will change many times, (3.143) is the better choice.

3.11 Example of the testing procedure

For an example of how the testing procedure works, we took L1 data collected at a baseline of approximately 2250 m, between station YP01 and YP09. Almost one hour of data was collected (from 19:45:04 to 20:44:04, GPS time) with a sampling interval of 30 seconds giving a total of 119 epochs. Six satellites were observed during the entire time span, while one satellite was observed starting at epoch 17 until the end. The a priori standard deviation of the observables was set to 3 mm.

Internal reliability
In Figures 3.5 and 3.6 the minimal detectable biases for respectively an outlier and a cycle slip are plotted. The value of a MDB for an outlier is primarily a function of the number of satellites that are simultaneously observed. The MDB for a cycle slip however, depends on the time span a satellite is observed, and on the epoch in this time span that it is observed. MDB's for cycle slips in the middle of the time span are smaller than MDB's at the begin or end of the time span. Still the MDB for a cycle slip never exceeds the value of 2 cm, which is far less than the size of one cycle ($\approx$ 19 cm), so it is likely that with this setup we are able to detect possible cycle slips.

Testing
The degrees of freedom for the OMT are 689, the OMT test statistic reads 330.2, with a critical value of 673.9, hence H_0 is accepted. The level of significance for the OMT is 0.653.

In Figures 3.7 and 3.8 the w-test statistics for respectively the test for an outlier and the test for an cycle slip are plotted. Under the null-hypothesis the w-test statistics should be between $-\sqrt{k_1}$ and $\sqrt{k_1} = 3.29$. The largest absolute value of the w-test statistics reads 6.464 for a cycle slip. The corresponding estimated error is however only 0.054 cycle; clearly this cannot be a cycle slip. Instead, the signature of the w-test statistics is probably due to an imperfect functional or stochastic model.

Indeed one is able to squeeze down the signature to within the bounds set by the critical value, by extending the functional model with e.g. a number of tropospheric delay parameters. This would however lead to a decrease of precision of the estimated parameters, and increased values for the MDB's.

In a next case we simulated a cycle slip with a size of one cycle at the third epoch (19:46:04) in the phase observation made at YP09 to PRN01.

The degrees of freedom for the OMT are 689, the OMT test statistic reads 3448.0, with a critical value of 673.9, hence H_0 is rejected. The level of significance for the OMT is 0.653.

In Table 3.1 the ten largest w-test statistics and their corresponding estimated error can be found. The absolute value of largest w-test statistic is 55.842 for the non-conventional hypothesis that a cycle slip occurred at 19:46:04 at the phase observation made at YP01 or YP09 to PRN01. The estimated absolute value for the slip is 0.987 which is larger than 0.5, hence either at YP01 a cycle slip with a size of one cycle, or at YP09 a slip with a size of minus one cycle occurred. These two cases are indistinguishable, at least three stations need to be involved to uniquely determine at which station the slip occurred.

In a subsequent run, an extra ambiguity parameter is introduced for the carrier phase at YP09 to PRN01 at 19:46:04, and the test statistic for the OMT reads now 329.7 with df = 688 (one less than in the previous run, due to the introduction of an extra ambiguity). The critical value is 672.9, hence H_0 is accepted. The level of significance for the OMT is 0.652.

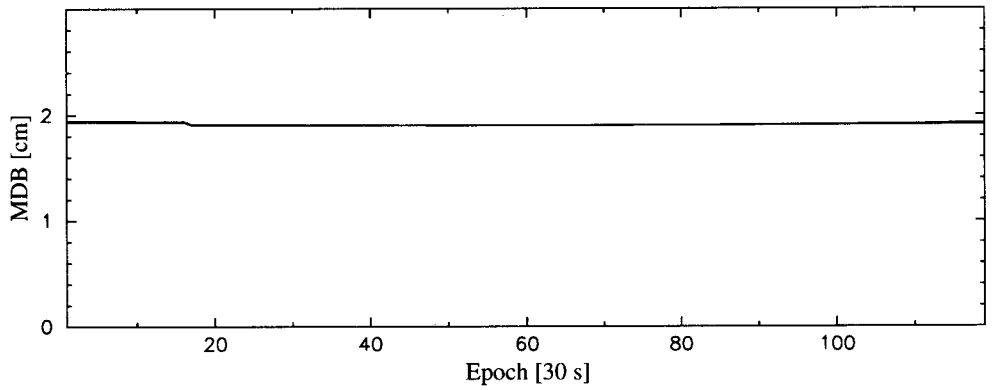

Figure 3.5: Minimal detectable biases for the conventional hypothesis (test for outlier) for all L1 carrier phases at YP09.

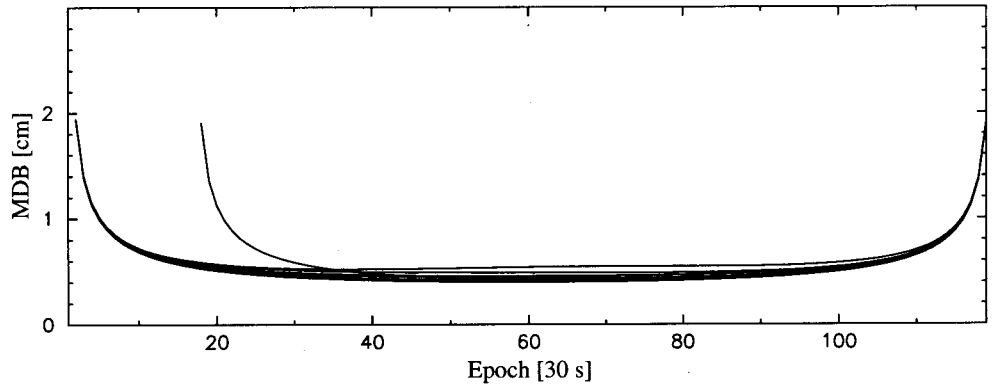

Figure 3.6: Minimal detectable biases for the non-conventional hypothesis (test for cycle slip) for all L1 carrier phases at YP09.

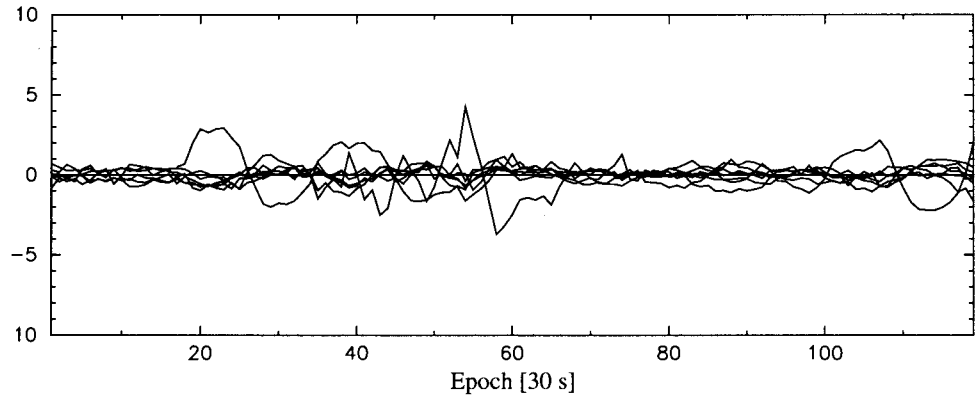

Figure 3.7: Outlier w-test statistics (conventional hypothesis) for for all L1 carrier phases at YP09.

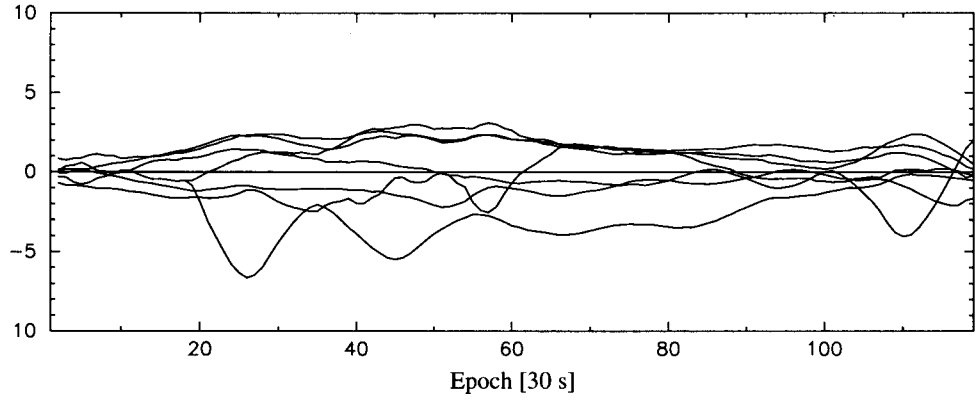

Figure 3.8: Cycle slip w-test statistics (non-conventional hypothesis) for for all L1 carrier phases at YP09.

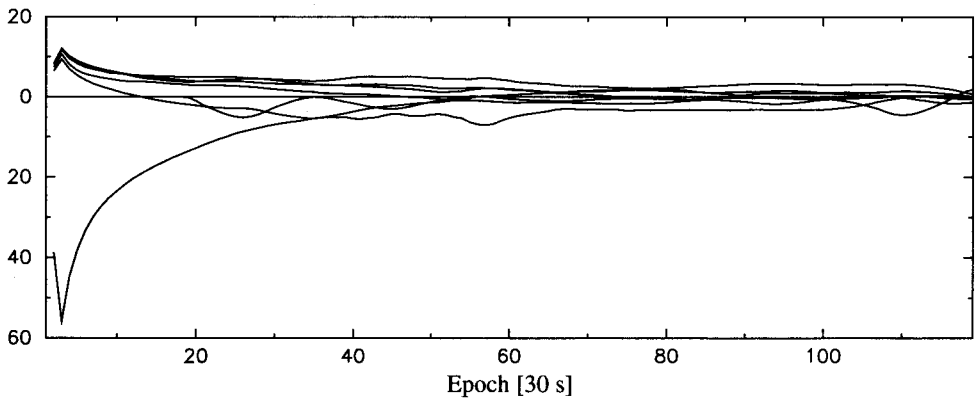

Figure 3.9: Cycle slip w-test statistics (non-conventional hypothesis) for for all L1 carrier phases at YP09, with a simulated cycle slip at the third epoch.

Epoch	$w_{p,k}$	$\hat{\nabla}$ (cycles)	Site ID	PRN	Conventional / Non-conventional
19:46:04	55.842	.987	YP01	01	N
19:46:04	-55.842	-.987	YP09	01	N
19:46:34	44.799	.654	YP01	01	N
19:46:34	-44.799	-.654	YP09	01	N
19:45:34	39.359	.972	YP01	01	C
19:45:34	-39.359	-.972	YP09	01	C
19:45:34	38.698	.956	YP01	01	N
19:45:34	-38.698	-.956	YP09	01	N
19:45:04	-38.698	-.956	YP09	01	C
19:45:04	38.698	.956	YP01	01	C

Table 3.1: Ten largest absolute values for the w-test statistics and estimated error for a simulated cycle slip with a size of one cycle in the carrier phase observation from YP01 to PRN01 at epoch 19:46:04.

3.12 The projector $P_{\bar{d}}^{\perp}$

3.12.1 Introduction

In this section we will have a closer look at the orthogonal projector $P_{\bar{A}_{2,k}}^{\perp}$, for $\bar{A}_{2,k} = \bar{d}$. We will see that if we work out this projector the structure of the reduced normal matrix becomes very simple and fast to compute. We start with the design matrix for the local parameters as in (3.93)

$$\underset{rm \times r+m-1}{\bar{A}_{2,k}} = \begin{bmatrix} & & -I_m \\ e_m & & -I_m \\ & \ddots & \vdots \\ & e_m & -I_m \end{bmatrix} = \bar{d} \tag{3.147}$$

Furthermore we assume that the variance-covariance matrix of the observables is a scaled unit matrix, which is a simplification of what is believed to be the true stochastic model, see e.g. Jin (1996) and (Tiberius 1998), but in accordance with the model used in many other GPS processing softwares. The misspecification of the stochastic model is hardly noticeable in the estimators, but it is likely to be noticeable in their variance-covariance matrix.

$$Q_{y_k} = \frac{1}{w} I \tag{3.148}$$

The product $\bar{d}^T Q_{y_k}^{-1} \bar{d}$ reads then:

$$\underset{\times r+m-1}{\bar{d}^T Q_{y_k}^{-1} \bar{d}} = w \begin{bmatrix} mI_{r-1} & -E_{r-1,m} \\ -E_{m,r-1} & rI_m \end{bmatrix} \tag{3.149}$$

where we introduced $E_{p,q}$ for a p by q matrix filled with 1's. By the choice of the clock of the first receiver for the S-basis, this matrix has become of full rank and thus invertible (see

appendix C):

$$(\bar{d}^T Q_{y_k}^{-1} \bar{d})^{-1} = \frac{1}{w} \begin{bmatrix} \frac{1}{m}(I_{r-1} + E_{r-1}) & \frac{1}{m} E_{r-1,m} \\ \frac{1}{m} E_{m,r-1} & \frac{1}{r}(I_m + \frac{r-1}{m} E_m) \end{bmatrix} \tag{3.150}$$

with $E_q = E_{q,q}$. Using this result, $H_{\bar{d}} = (\bar{d}^T Q_{y_k}^{-1} \bar{d})^{-1} \bar{d}^T Q_{y_k}^{-1}$ can be evaluated:

$$\underset{r+m-1 \times rm}{(\bar{d}^T Q_{y_k}^{-1} \bar{d})^{-1} \bar{d}^T Q_{y_k}^{-1}} = \begin{bmatrix} -\frac{1}{m} e_m^T & \frac{1}{m} e_m^T & & \\ \vdots & & \ddots & \\ -\frac{1}{m} e_m^T & & & \frac{1}{m} e_m^T \\ -\frac{1}{r}(I_m + \frac{r-1}{m} E_m) & -\frac{1}{r}(I_m - \frac{1}{m} E_m) & \cdots & -\frac{1}{r}(I_m - \frac{1}{m} E_m) \end{bmatrix} \tag{3.151}$$

And eventually $P_{\bar{d}}^{\perp} = I_{rm} - \bar{d}(\bar{d}^T Q_{y_k}^{-1} \bar{d})^{-1} \bar{d}^T Q_{y_k}^{-1}$:

$$\underset{\times rm}{P_{\bar{d}}^{\perp}} = \left(I_r - \frac{1}{r} E_r\right) \otimes \left(I_m - \frac{1}{m} E_m\right) \tag{3.152}$$

In this matrix we recognize two basic operators, viz. the identity operator I_q, and the 'average operator' $\frac{1}{q} E_q$. In Section 3.13 it will be shown how this special structure can be used to ones advantage to compute efficiently the solution for a single baseline.

Analogy between $P_{\bar{d}}^{\perp}$ and the weight matrix of the double difference observations.
Since we have chosen to solve for the rank defect of the ambiguities only after the normal matrix has been constructed, the ambiguity part of the normal matrix is singular. We could however also solve the rank defect during the updating of the normal matrix. We will show now that if we do so, the projector is not a projector anymore, and that the ambiguity part of the normal matrix becomes of full rank. Besides that, we will show that the ambiguity part of the normal matrix under some restrictions equals the weight matrix of the DD ambiguities. The restrictions are that the S-basis has to be compatible with the differencing scheme. This means that the unbiased estimable functions resulting from the S-basis choice have to be same as the DD ambiguities resulting from the differencing scheme. If we choose pivoting with the first receiver and first satellite as pivot, the S-basis consists of all ambiguities referring to this receiver and satellite, thus

$$\lambda N_i^j \qquad i \neq 1 \vee j \neq 1 \tag{3.153}$$

In practice it means for the ambiguity part of the normal matrix that the rows and columns associated with the parameters of the S-basis are excluded from the normal matrix system. It is easy to see that the ambiguity part changes from its singular form

$$\underset{\times rm}{N} = \left(I_r - \frac{1}{r} E_r\right) \otimes \left(I_m - \frac{1}{m} E_m\right) \tag{3.154}$$

to its full rank form

$$\underset{\times (r-1)(m-1)}{N} = \left(I_{r-1} - \frac{1}{r} E_{r-1}\right) \otimes \left(I_{m-1} - \frac{1}{m} E_{m-1}\right) \tag{3.155}$$

which equals the DD weight matrix.

3.12.2 The general form of $P_{\bar{d}}^{\perp}$

The orthogonal projector $P_{\bar{d}}^{\perp}$ is based on the following assumptions:

1. All r receivers track the same m satellites.
2. The coefficient for the receiver clock error in the linearized observation equation equals 1.
3. The variance-covariance matrix of the observables is a scaled unit matrix.

1. All r receivers track the same m satellites.
In small networks all receivers generally are tracking the same satellites, however, sometimes there are missing observations due to blocking of the signal, or rejecting an observation. Furthermore rising and setting of satellites does not occur simultaneously for all receivers.

To describe the projector $P_{\bar{d}}^{\perp}$ for the case that not all receivers observe the same set of satellites we introduce the coefficient p_i^j which is defined as $p_i^j = 1$ if satellite j has been tracked by receiver i, and $p_i^j = 0$ if this is not the case (missing observation).

2. The coefficient for the receiver clock error is 1
If one for the computation of the topocentric distance in the observation equation does not regard the receiver clock error as deterministic, the coefficient for the clock error is $(1 - \frac{\partial \varrho}{\partial t}/c)$ instead of 1. To describe the projector $P_{\bar{d}}^{\perp}$ for this case, the coefficient for the clock error of receiver i in the linearized observation equation for observation y_i^j will be denoted as $s_i^j = 1 - \frac{\partial \rho_i^j}{\partial t}/c$. Combining 1. and 2., $\bar{d}$ is denoted as

$$\bar{d} = \begin{bmatrix} \begin{bmatrix} p_2^1 s_2^1 \\ \vdots \\ p_2^m s_2^m \end{bmatrix} & & & \begin{bmatrix} -p_1^1 & & \\ & \ddots & \\ & & -p_1^m \end{bmatrix} \\ & \ddots & & \begin{bmatrix} -p_2^1 & & \\ & \ddots & \\ & & -p_2^m \end{bmatrix} \\ & & \begin{bmatrix} p_r^1 s_r^1 \\ \vdots \\ p_r^m s_r^m \end{bmatrix} & \begin{bmatrix} -p_r^1 & & \\ & \ddots & \\ & & -p_r^m \end{bmatrix} \end{bmatrix} \tag{3.156}$$

3. The variance-covariance matrix of the observables is a scaled unit matrix.
Instead of using $\frac{1}{w}I$ for the variance-covariance matrix of the observables we would like to be able to use an elevation dependent form; i.e. observations with low elevations are considered to be less precise than observations with high elevations, see e.g. Jin (1996). We will denote the variance of observable y_i^j as q_i^j.

With the introduced terminology, we can determine the structure of $\bar{d}^T Q_{y_k}^{-1} \bar{d}$. The resulting matrix preserves a very nice structure; from a computational part of view it is especially convenient that the upper left and the lower right part of the matrix remain diagonal. This

leads to an obvious partitioning of the matrix into:

$$\bar{d}^T Q_{y_k}^{-1} \bar{d} = \left[\begin{array}{ccc|ccc} \sum_{j=1}^{m} p_2^j q_2^j s_2^{j^2} & & & -p_2^1 q_2^1 s_2^1 & \cdots & -p_2^m q_2^m s_2^m \\ & \ddots & & \vdots & & \vdots \\ & & \sum_{j=1}^{m} p_r^j q_r^j s_r^{j^2} & -p_r^1 q_r^1 s_r^1 & \cdots & -p_r^m q_r^m s_r^m \\ \hline -p_2^1 q_2^1 s_2^1 & \cdots & -p_r^1 q_r^1 s_r^1 & \sum_{i=1}^{r} p_i^1 q_i^1 & & \\ \vdots & & \vdots & & \ddots & \\ -p_2^m q_2^m s_2^m & \cdots & -p_r^m q_r^m s_r^m & & & \sum_{i=1}^{r} p_i^m q_i^m \end{array}\right] \tag{3.157}$$

3.12.3 An efficient method to compute the general $P_{\bar{d}}^{\perp}$

With the partitioning of $\bar{d}^T Q_{y_k}^{-1} d$ as

$$\bar{d}^T Q_{y_k}^{-1} \bar{d} = \begin{bmatrix} k_{11} & k_{21}^T \\ k_{21} & k_{22} \end{bmatrix} = K \tag{3.158}$$

we can use the well known matrix inversion lemma:

$$K^{-1} = \begin{bmatrix} k_{11}^{-1} + k_{11}^{-1} k_{21}^T (k_{22} - k_{21} k_{11}^{-1} k_{21}^T)^{-1} k_{21} k_{11}^{-1} & -k_{11}^{-1} k_{21}^T (k_{22} - k_{21} k_{11}^{-1} k_{21}^T)^{-1} \\ -(k_{22} - k_{21} k_{11}^{-1} k_{21}^T)^{-1} k_{21} k_{11}^{-1} & (k_{22} - k_{21} k_{11}^{-1} k_{21}^T)^{-1} \end{bmatrix} \tag{3.159}$$

$$= \begin{bmatrix} (k_{11} - k_{21}^T k_{22}^{-1} k_{21})^{-1} & -(k_{11} - k_{21}^T k_{22}^{-1} k_{21})^{-1} k_{21}^T k_{22}^{-1} \\ -k_{22}^{-1} k_{21} (k_{11} - k_{21}^T k_{22}^{-1} k_{21})^{-1} & k_{22} - k_{22}^{-1} k_{21} (k_{11} - k_{21}^T k_{22}^{-1} k_{21})^{-1} k_{21}^T k_{22}^{-1} \end{bmatrix} \tag{3.160}$$

to compute its inverse. Because the inversion of both k_{11} and k_{22} is trivial since they are diagonal, the main computational load is due to the inversion of either $(k_{11} - k_{21}^T k_{22}^{-1} k_{21})$ with dimension r or $(k_{22} - k_{21} k_{11}^{-1} k_{21}^T)$ with dimension m. So depending on the number of receivers and the number of satellites one of the schemes above may be chosen.

After having computed $(\bar{d}^T Q_{y_k}^{-1} \bar{d})^{-1}$, we compute the projector $I - \bar{d}(\bar{d}^T Q_{y_k}^{-1} \bar{d})^{-1} \bar{d}^T Q_{y_k}^{-1}$. Fortunately, the denial of the assumptions did not change the sparsity of $\bar{d}$, which reduces the computational load.

First we compute $\bar{d}(\bar{d}^T Q_{y_k}^{-1} \bar{d})^{-1}$. Each row of this $(rm) \times (r + m - 1)$ matrix consists of the addition of at most two scaled rows of $(\bar{d}^T Q_{y_k}^{-1} \bar{d})^{-1}$. Remember that $\bar{d}$ is still a sparse matrix with at most two elements per row. Since the latter matrix is symmetric and only the lower triangle has been stored, the most convenient way to build $\bar{d}(\bar{d}^T Q_{y_k}^{-1} \bar{d})^{-1}$ is to find the rows of $(\bar{d}^T Q_{y_k}^{-1} \bar{d})^{-1}$ and the equivalent columns of $\bar{d}$ in increasing order, and add them after scaling to the appropriate row in $\bar{d}(\bar{d}^T Q_{y_k}^{-1} \bar{d})^{-1}$.

The eventual product is computed in a similar way: each column of $\bar{d}(\bar{d}^T Q_{y_k}^{-1} \bar{d})^{-1} \bar{d}^T Q_{y_k}^{-1}$ is again the addition of two scaled columns of $\bar{d}(\bar{d}^T Q_{y_k}^{-1} \bar{d})^{-1}$.

Of course the computation of the actual projector when not all receivers track the same set of satellites will cost more time than the regular situation, but it does not cause a computational burden.

In Beutler et al. (1986) an efficient computing scheme was described to compute the weight matrix of the DD observables in case that not all receivers observe the same set of

satellites. A straightforward approach would need the inversion of a matrix with dimension p, the number of observed double differences. Using the proposed scheme, the matrix to be inverted has dimension q, the number of missing double differences, and since usually $q < p$ this computation method is preferred.

Compared to the effort it costs to construct the projector, however, in most cases the computation of the DD weight matrix will cost more time. On the other hand, the dimension of the projector equals the number of observations, whereas the dimension of the DD weight matrix equals the number of DD ambiguities, which will always be less than the number of observations.

This is however largely compensated by the fact that since a double difference observation always refers to two receivers, one row of the geometric part of the DD design matrix has 2×3 nonzero entries, whereas one row of the geometric part of the design matrix for the undifferenced setup only has 3 nonzero entries.

Consequently, the time needed for the construction of the normal matrix for the undifferenced setup is of the same order as the construction of the DD normal matrix.

3.13 Special case: baseline

If we restrict ourselves to one baseline, i.e., $r = 2$, $P_{\bar{d}}^{\perp}$ becomes

$$\begin{aligned} P_{\bar{d}}^{\perp} &= \left(I_r - \frac{1}{r}E_r\right) \otimes \left(I_m - \frac{1}{m}E_m\right) \\ &= \frac{1}{2}\begin{bmatrix} 1 & -1 \\ -1 & 1 \end{bmatrix} \otimes \left(I_m - \frac{1}{m}E_m\right) \end{aligned} \tag{3.161}$$

Pre-multiplication of a vector w of length m with the projector $P_{\bar{d}}^{\perp}$ yields:

$$\begin{aligned} P_{\bar{d}}^{\perp} w &= w - \frac{1}{m}\sum_{j=1}^{m} w^j \\ &= w - \tilde{w} \end{aligned} \tag{3.162}$$

analogously we have

$$\begin{aligned} w^T P_{\bar{d}}^{\perp} &= w^T - \frac{1}{m}\sum_{j=1}^{m} w^j \\ &= w^T - \tilde{w}^T \end{aligned} \tag{3.163}$$

with $\tilde{w}$ denoting the satellite average of vector w. Let us now have a look at $\sum_{i=1}^{k} P_{\bar{d}}^{\perp} w_k$:

$$\begin{aligned} \sum_{i=1}^{k} P_{\bar{d}}^{\perp} w_k &= \sum_{i=1}^{k} w_k - \sum_{i=1}^{k}\frac{1}{m}\sum_{j=1}^{m} w_k^j \\ &= \sum_{i=1}^{k} w_k - \frac{1}{m}\sum_{j=1}^{m}\sum_{i=1}^{k} w_k^j \\ &= P_{\bar{d}}^{\perp}\sum_{i=1}^{k} w_k \end{aligned} \tag{3.164}$$

As a matrix is a nothing else then a set of vectors this is also true for matrices:

$$\sum_{i=1}^{k} P_{\bar{d}}^{\perp} g_k = P_{\bar{d}}^{\perp} \sum_{i=1}^{k} g_k \tag{3.165}$$

and

$$\sum_{i=1}^{k} g_k^T P_{\bar{d}}^{\perp} = \left(\sum_{i=1}^{k} g_k^T \right) P_{\bar{d}}^{\perp} \tag{3.166}$$

With $Q_{y_k} = \frac{1}{w}$, we get for the reduced normal matrix and right-hand side epoch k:

$$\begin{aligned} N_k &= N_{k-1} + w \begin{bmatrix} g_k^T P_{\bar{d}}^{\perp} g_k & g_k^T P_{\bar{d}}^{\perp} \\ P_{\bar{d}}^{\perp} g_k & P_{\bar{d}}^{\perp} \end{bmatrix} \\ &= N_{k-1} + \frac{w}{2} \begin{bmatrix} {g'_{1,k}}^T g_{1,k} & & & \textit{symmetric} \\ -{g'_{2,k}}^T g_{1,k} & {g'_{2,k}}^T g_{2,k} & & \\ g'_{1,k} & -{g'}_{2,k} & I_m - \frac{1}{m} E_m & \\ -g'_{1,k} & g'_{2,k} & -(I_m - \frac{1}{m} E_m) & I_m - \frac{1}{m} E_m \end{bmatrix} \end{aligned} \tag{3.167}$$

$$\begin{aligned} h_k &= h_{k-1} + w \begin{bmatrix} g_k^T \\ I_{rm} \end{bmatrix} P_{\bar{d}}^{\perp} y_k \\ &= h_{k-1} + \frac{w}{2} \begin{bmatrix} g_{1,k}^T (y'_{1,k} - y'_{2,k}) \\ g_{2,k}^T (-y'_{1,k} + y'_{2,k}) \\ y'_{1,k} - y'_{2,k} \\ -y'_{1,k} + y'_{2,k} \end{bmatrix} \end{aligned} \tag{3.168}$$

with

$$g'_{i,k} = \begin{bmatrix} u_{i,k}^{1^T} - \tilde{u}_{i,k}^T \\ u_{i,k}^{2^T} - \tilde{u}_{i,k}^T \\ \vdots \\ u_{i,k}^{m^T} - \tilde{u}_{i,k}^T \end{bmatrix} \quad \text{and} \quad y'_{i,k} = \begin{bmatrix} y_{i,k}^1 - \tilde{y}_{i,k} \\ y_{i,k}^2 - \tilde{y}_{i,k} \\ \vdots \\ y_{i,k}^m - \tilde{y}_{i,k} \end{bmatrix} \tag{3.169}$$

where $\tilde{}$ denotes the 'satellite average' defined as

$$\tilde{w} = \frac{1}{m} \sum_{j=1}^{m} w^j \tag{3.170}$$

Using the intermediate quantities $g'_{i,k}$ and $y'_{i,k}$, the construction of the reduced normal matrix and right-hand side can thus be computed very efficiently.

The solution of the local parameters of epoch k

$$\Delta \bar{x}_{2,k} = H_{\bar{A}_{2,k}} \Delta y_k^{(2)} \tag{3.171}$$

is with

$$H_{\bar{A}_{2,k}} = \begin{bmatrix} -\frac{1}{m} e_m^T & \frac{1}{m} e_m^T \\ -\frac{1}{2}(I_m + \frac{1}{m} E_m) & -\frac{1}{2}(I_m - \frac{1}{m} E_m) \end{bmatrix} \tag{3.172}$$

very simple computed as

$$c\delta t_{2,k} - c\delta t_{1,k} - \lambda(N_1^1 - N_2^1) = -\Delta\tilde{y}_{1,k}^{(2)} + \Delta\tilde{y}_{2,k}^{(2)}$$
$$c\delta t^{j,k} - c\delta t_{1,k} - \lambda N_1^j = -\frac{1}{2}\left(\Delta y_{1,k}^{j\ (2)} + \Delta\tilde{y}_{1,k}^{(2)} + \Delta y_{2,k}^{j\ (2)} - \Delta\tilde{y}_{2,k}^{(2)}\right) \tag{3.173}$$

In principle also networks solutions could be computed in a similar simple manner, but all receivers should track the same set of satellites, which is not always the case. For a single baseline it is, due to the prerequisite that a satellite has to be observed by at least two receivers.

3.14 DD generating algorithms

In the literature several approaches to form double difference observations are proposed (Bock et al. 1985), (Bock et al. 1986), (Goad and Mueller 1988), (Mervart et al. 1994), (Rothacher and Mervart 1996).

In most double differenced approaches the first step is the formation of single differences between receivers; this is usually done only once before the adjustment, by producing $r-1$ single difference (SD) files. If the set of observed satellites of one file does not exactly match the set of the second file, the data to the satellites that do not match are lost.

A simple strategy to use as much data as possible is to look at the number of single differences that can be formed between every combination of receivers, and choose those $r-1$ combinations that give the highest number. The choice is restricted by the conditions that each receiver has to be included in at least one single difference, and that the resulting sequence of between-receiver differences must be connected.

A method to do this is to build a minimum spanning tree. As in this case we are looking for the maximum number of single difference to be formed, we will make a 'maximum spanning tree' instead.[2] The weight between two receivers is defined as number of single differences that can be formed.

The minimum spanning tree algorithm is also described in Mervart et al. (1994), to find all 'independent' baselines and in Rothacher and Mervart (1996) where it is called the minimum path method.

The minimum spanning tree algorithm can also be used to find the set of independent baselines with minimum total length. This is sometimes done to improve the precision of the ambiguities. As we will see in Chapter 5 it is not necessary to do this since the precision of the ambiguities can be improved by applying a more general decorrelating transformation to it.

The method mentioned in Bock et al. (1985) and Bock et al. (1986) finds the maximum number of double differences per epoch, and for large networks usually discards less data than the schemes based on the spanning tree concept. In Section 3.15 we will show a comparison of the two double difference generating methods with the undifferenced approach.

[2]There is no essential difference between the construction of a minimum and a maximum spanning tree. Commonly the minimum spanning tree is introduced for nodes with weights equal to the Euclidian distance in the 2-dimensional space of the edges between them. A minimum spanning tree is then planar, i.e. edges do not cross when the graph is displayed at a plane.

Site ID	PRN code																					
	01	02	03	04	05	06	09	10	14	15	16	17	18	21	22	23	24	25	26	27	29	31
ALGO			**b**				**b**					**b**		**b**		**b**			**b**			
GOLD	**b**		**b**									b		b		b						
GOL2	**b**		b			**b**						b		b		b						
TIDB									**b**	**b**	**b**				**b**			**b**			**b**	
MADR		**b**						**b**											**b**	**b**		
FAIR			**b**									b		b		b			b	b		**b**
HART		**b**		**b**	**b**			b			b		**b**				**b**					
KOKB	**b**		b							**b**		b		b	b	b						b
KOSG		**b**					b	b				b				b			b	b		b
SANT	**b**			b	b	b	b										b	b				
WETT		**b**						b											b	b		b
YAR1									**b**	b	b		b		b						b	
YELL			**b**									b		b		b			b	b		b
TROM		**b**																	b	b		b

Table 3.2: Observations made on L2 by the 13 IGS core stations plus station GOL2 at May 12, 1997, 02:47:30.0, GPS time. Only satellites observed by at least two receivers have been included. Legend: b: observed, **b**: S-basis.

3.15 The undifferenced approach compared to DD generating algorithms

In this section we will assess different methods to deal with the rank defect system of the GPS phase observation equations using an existing observation scenario with stations spread over the entire Earth. The assessment will be made with respect to the amount of data that is used. The methods that will be used are the undifferenced approach as described in Section 3.4, the DD generating algorithm as described in Bock et al. (1985) and Bock et al. (1986) implemented in the GAMIT (GPS At MIT) software, and the DD generating algorithm as described in Mervart et al. (1994) and Rothacher and Mervart (1996) implemented in the Bernese software.

For the comparison we took an arbitrary epoch of L2 data of the 13 fiducial stations of the IGS, plus an extra station at Goldstone (GOL2). The epoch is May 12, 1997, 02:47:30.0, GPS time.

The observations that were made can be found in Table 3.2; only observations to satellites observed by at least two receivers have been included. The minimum spanning tree used to find the S-basis and the estimable functions for the undifferenced approach, is depicted in Figure 3.10. The number of receiver-satellite combinations and thus the number of ambiguities, is 86, and the dimension of the S-basis for the ambiguities is 35. Consequently, the undifferenced approach forms $86 - 35 = 51$ integer functions of ambiguities, and all observations are used. The estimable functions and the S-basis for the ambiguities can be found in Table 3.4. Not all functions consist of 4 ambiguities as in the case of the classic double differences; there are functions formed consisting of 4 (29 times), 6 (14 times), 8 (3 times), 10 (3 times), 12 (once), and 14 (once) ambiguities.

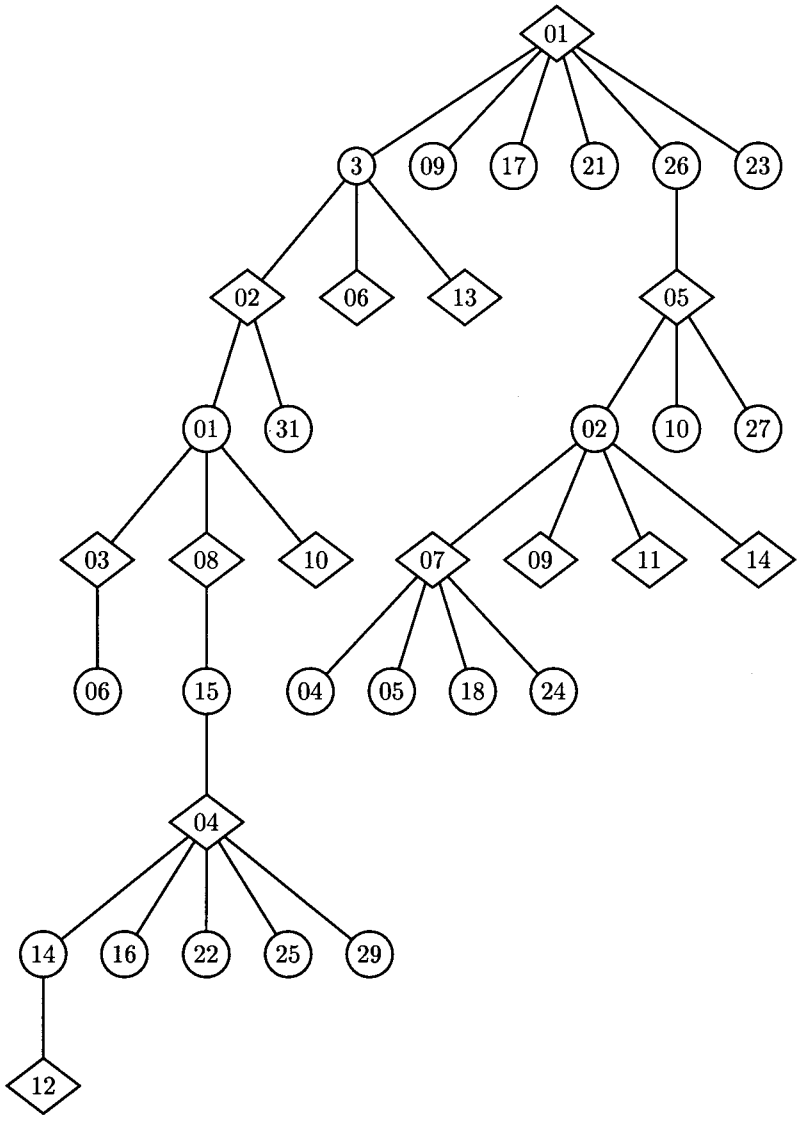

Figure 3.10: Minimum spanning tree for the observation scenario of Table 3.2.

Site ID (short)	Site ID (IGS)	Name	Country
1	ALGO	Algonquin	Canada
2	GOLD	Goldstone	USA
3	GOL2	Goldstone	USA
4	TIDB	Tidbinbilla	Australia
5	MADR	Madrid	Spain
6	FAIR	Fairbanks	USA
7	HART	Hartebeesthoek	South-Africa
8	KOKB	Kokee-Park	USA (Hawaii)
9	KOSG	Kootwijk	The Netherlands
10	SANT	Santiago	Chile
11	WETT	Wettzell	Germany
12	YAR1	Yarragadee	Australia
13	YELL	Yellowknife	Canada
14	TROM	Tromsö	Norway

Table 3.3: Stations used for the analysis in this section.

In Table 3.5 the between-receiver single differences that may be recognized in the resulting set of observable functions of ambiguities can be found, and in Figure 3.11 the polyhedron formed by these baselines is depicted.

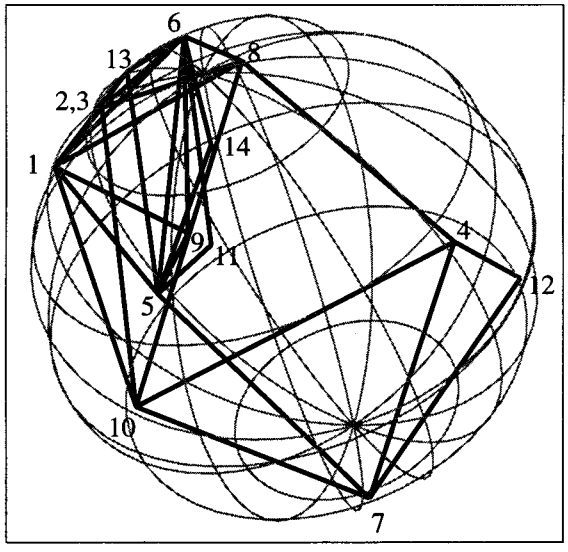

Figure 3.11: Polyhedron consisting of the between-receiver single differences formed in the undifferenced approach. The WGS-84 ellipsoid is visualized by depicting some of its meridians and parallels.

1. λN_1^3 : S-basis λN_1^9 : S-basis λN_1^{17} : S-basis λN_1^{21} : S-basis λN_1^{23} : S-basis λN_1^{26} : S-basis	$\lambda(N_1^3 - N_1^{26} - N_6^3 + N_6^{26})$ $\lambda(N_1^3 - N_1^{26} + N_5^{26} - N_5^{27} - N_6^3 + N_6^{27})$ λN_6^{31} : S-basis	$\lambda(N_1^3 - N_1^{26} + N_2^1 - N_2^3 - N_5^2 + N_5^{26}$ $+N_7^2 - N_7^5 - N_{10}^1 + N_{10}^5)$ $\lambda(N_3^1 - N_3^6 - N_{10}^1 + N_{10}^6)$ $\lambda(N_1^3 - N_1^9 + N_2^1 - N_2^3 - N_{10}^1 + N_{10}^9)$ $\lambda(N_1^3 - N_1^{26} + N_2^1 - N_2^3 - N_5^2 + N_5^{26}$ $+N_7^2 - N_7^{24} - N_{10}^1 + N_{10}^{24})$ $\lambda(N_4^{15} - N_4^{25} + N_8^1 - N_8^{15} - N_{10}^1 + N_{10}^{25})$
2. λN_2^1 : S-basis λN_2^3 : S-basis $\lambda(N_1^3 - N_1^{17} - N_2^3 + N_2^{17})$ $\lambda(N_1^3 - N_1^{21} - N_2^3 + N_2^{21})$ $\lambda(N_1^3 - N_1^{23} - N_2^3 + N_2^{23})$	7. λN_7^2 : S-basis λN_7^4 : S-basis λN_7^5 : S-basis $\lambda(N_5^2 - N_5^{10} - N_7^2 + N_7^{10})$ $\lambda(-N_1^3 + N_1^{26} - N_2^1 + N_2^3 + N_4^{15} - N_4^{16}$ $+N_5^2 - N_5^{26} - N_7^2 + N_7^{16} + N_8^1 - N_8^{15})$ λN_7^{18} : S-basis λN_7^{24} : S-basis	11. λN_{11}^2 : S-basis $\lambda(N_5^2 - N_5^{10} - N_{11}^2 + N_{11}^{10})$ $\lambda(N_5^2 - N_5^{26} - N_{11}^2 + N_{11}^{26})$ $\lambda(N_5^2 - N_5^{27} - N_{11}^2 + N_{11}^{27})$ $\lambda(-N_1^3 + N_1^{26} + N_5^2 - N_5^{26} + N_6^3 - N_6^{31}$ $-N_{11}^2 + N_{11}^{31})$
3. λN_3^1 : S-basis $\lambda(N_2^1 - N_2^3 - N_3^1 + N_3^3)$ λN_3^6 : S-basis $\lambda(N_1^3 - N_1^{17} + N_2^1 - N_2^3 - N_3^1 + N_3^{17})$ $\lambda(N_1^3 - N_1^{21} + N_2^1 - N_2^3 - N_3^1 + N_3^{21})$ $\lambda(N_1^3 - N_1^{23} + N_2^1 - N_2^3 - N_3^1 + N_3^{23})$	8. λN_8^1 : S-basis $\lambda(N_2^1 - N_2^3 - N_8^1 + N_8^3)$ λN_8^{15} : S-basis $\lambda(N_1^3 - N_1^{17} + N_2^1 - N_2^3 - N_8^1 + N_8^{17})$ $\lambda(N_1^3 - N_1^{21} + N_2^1 - N_2^3 - N_8^1 + N_8^{21})$ $\lambda(N_4^{15} - N_4^{22} - N_8^{15} + N_8^{22})$ $\lambda(N_1^3 - N_1^{23} + N_2^1 - N_2^3 - N_8^1 + N_8^{23})$ $\lambda(N_2^1 - N_2^3 + N_6^3 - N_6^{31} - N_8^1 + N_8^{31})$	12. λN_{12}^{14} : S-basis $\lambda(N_4^{14} - N_4^{15} - N_{12}^{14} + N_{12}^{15})$ $\lambda(N_4^{14} - N_4^{16} - N_{12}^{14} + N_{12}^{16})$ $\lambda(N_1^3 - N_1^{26} + N_2^1 - N_2^3 + N_4^{14} - N_4^{15} - N_5^2$ $+N_5^{26} + N_7^2 - N_7^{18} - N_8^1 + N_8^{15} - N_{12}^{14} + N_{12}^{18})$ $\lambda(N_4^{14} - N_4^{22} - N_{12}^{14} + N_{12}^{22})$ $\lambda(N_4^{14} - N_4^{29} - N_{12}^{14} + N_{12}^{29})$
4. λN_4^{14} : S-basis λN_4^{15} : S-basis λN_4^{16} : S-basis λN_4^{22} : S-basis λN_4^{25} : S-basis λN_4^{29} : S-basis	9. λN_9^2 : S-basis $\lambda(-N_1^9 + N_1^{26} + N_5^2 - N_5^{26} - N_9^2 + N_9^9)$ $\lambda(N_5^2 - N_5^{10} - N_9^2 + N_9^{10})$ $\lambda(-N_1^{17} + N_1^{26} + N_5^2 - N_5^{26} - N_9^2 + N_9^{17})$ $\lambda(-N_1^{23} + N_1^{26} + N_5^2 - N_5^{26} - N_9^2 + N_9^{23})$ $\lambda(N_5^2 - N_5^{26} - N_9^2 + N_9^{26})$ $\lambda(N_5^2 - N_5^{27} - N_9^2 + N_9^{27})$ $\lambda(-N_1^3 + N_1^{26} + N_5^2 - N_5^{26} + N_6^3 - N_6^{31}$ $-N_9^2 + N_9^{31})$	13. λN_{13}^3 : S-basis $\lambda(N_1^3 - N_1^{17} - N_{13}^3 + N_{13}^{17})$ $\lambda(N_1^3 - N_1^{21} - N_{13}^3 + N_{13}^{21})$ $\lambda(N_1^3 - N_1^{23} - N_{13}^3 + N_{13}^{23})$ $\lambda(N_1^3 - N_1^{26} - N_{13}^3 + N_{13}^{26})$ $\lambda(N_1^3 - N_1^{26} + N_5^{26} - N_5^{27} - N_{13}^3 + N_{13}^{27})$ $\lambda(N_6^3 - N_6^{31} - N_{13}^3 + N_{13}^{31})$
5. λN_5^2 : S-basis λN_5^{10} : S-basis λN_5^{26} : S-basis λN_5^{27} : S-basis	10. λN_{10}^1 : S-basis $\lambda(N_1^3 - N_1^{26} + N_2^1 - N_2^3 - N_5^2 + N_5^{26}$ $+N_7^2 - N_7^4 - N_{10}^1 + N_{10}^4)$ *continued in next column*	14. λN_{14}^2 : S-basis $\lambda(N_5^2 - N_5^{26} - N_{14}^2 + N_{14}^{26})$ $\lambda(N_5^2 - N_5^{27} - N_{14}^2 + N_{14}^{27})$ $\lambda(-N_1^3 + N_1^{26} + N_5^2 - N_5^{26} + N_6^3 - N_6^{31}$ $-N_{14}^2 + N_{14}^{31})$
6. λN_6^3 : S-basis $\lambda(N_1^3 - N_1^{17} - N_6^3 + N_6^{17})$ $\lambda(N_1^3 - N_1^{21} - N_6^3 + N_6^{21})$ $\lambda(N_1^3 - N_1^{23} - N_6^3 + N_6^{23})$ *continued in next column*		

Table 3.4: Possible set of estimable functions of parameters when using the undifferenced approach.

Single difference	PRN codes of satellites involved	Single difference	PRN codes of satellites involved
ALGO-GOLD	03,17,21,23	ALGO-GOL2	17,21,23
ALGO-MADR	26	ALGO-FAIR	03,17,21,23,26
ALGO-KOKB	17,21,23	ALGO-KOSG	09,17,23
ALGO-SANT	09	ALGO-YELL	03,17,21,23,26
GOLD-GOL2	01,03	GOLD-FAIR	03
GOLD-KOKB	01,03	GOLD-SANT	01
GOL2-SANT	01,06		
TIDB-HART	16	TIDB-KOKB	15,22
TIDB-SANT	25	TIDB-YAR1	14,15,16,22,29
MADR-FAIR	27	MADR-HART	02,10
MADR-KOSG	02,10,26,27	MADR-WETT	02,10,26,27
MADR-YELL	27	MADR-TROM	02,26,27
FAIR-KOKB	31	FAIR-KOSG	31
FAIR-WETT	31	FAIR-YELL	03,31
FAIR-TROM	31		
HART-SANT	04,05,24	HART-YAR1	18
KOKB-SANT	01		

Table 3.5: Between-receiver single differences implicitly formed in the undifferenced approach.

ALGO											
3402	GOLD										
3402	0	GOL2									
12090	10589	10589	TIDB								
5616	8390	8390	12515	MADR							
4476	3807	3807	10527	7399	FAIR						
10969	12261	12261	9589	7525	11998	HART					
7193	4305	4305	7769	10671	4728	12723	KOKB				
5620	8141	8141	12273	1512	6494	8195	10104	KOSG			
8105	8260	8260	9928	9430	10696	8426	9835	10301	SANT		
6155	8583	8583	12157	1655	6857	7832	10358	603	10461	WETT	
12549	11808	11808	3197	11547	10968	7847	9498	11253	10918	10991	YAR1
2913	2986	2986	11224	6680	1631	11795	5440	6013	9867	6473	11707 YELL
5388	7337	7337	11820	3480	4899	9426	8884	2055	11055	2296	10978 4776 TROM

Table 3.6: Slope distances between the stations of Table 3.2. A grey-boxed distance signifies that this between-receiver single difference is formed in the undifferenced approach.

The method to find the maximum number of double differences implemented in the GAMIT software (Bock et al. 1985), (Bock et al. 1986), produces 47 double differences. Of the total number of 86 observations, the following 3 are not used {TIDB–PRN25, SANT–PRN25, SANT–PRN09}. And consequently, none of the observations made to PRN25 are used.

The formation of double differences in the Bernese software is based on between-receiver single differences. The optimal set of single differences is found by building a minimum spanning tree. The weights may be defined in several ways, one of it being the maximum number of single differences that may be formed, thus aiming to use as much data as possible. The number of between-receiver single differences that can be formed from the data in Table 3.2, can be found in Table 3.11.

In Table 3.8 one of the possible sets of between-receiver single differences produced by the MST algorithm can be found. The corresponding MST is depicted in Figure 3.12. The total of single differences formed in this way amounts to 57, and from it $57-13 = 44$ double differenced observations can be formed. From the total of 86 observations, 10 have to be discarded because they are not used in the forming of the single differenced observations. The set of unused observations is {ALGO–PRN09, KOSG–PRN09, TIDB–PRN25, YAR1–PRN18, SANT–PRN09, SANT–PRN25, HART–PRN02, HART–PRN10, HART–PRN16, HART–PRN18}. None of the observations made to PRN09, PRN18 and PRN25 are used.

Another option is to construct an MST with as weights the distance between the stations. This is sometimes done to improve the performance of the ambiguity resolution (i.e. if no decorrelating transformation is applied). The inter-station distances for the stations of Table 3.2 can be found in Table 3.6, and the between-receiver single differences formed in this way in Table 3.9. It gives a total of 52 single differences, of which one has to be discarded, since only one satellite is related to it. From the remainder $51 - 12 = 39$ double differences can be formed. Only 66 observations are used, and no observations are used made from station SANT, or to PRN04, PRN05, PRN06, PRN09, PRN18, PRN24 and PRN25.

Instead of selecting $r - 1$ between-receiver single differences combinations we could also choose $m-1$ between-satellite single difference combinations, by applying the MST algorithm to Table 3.12 (this is not an option in the Bernese software, there only between-receiver single differences are formed).

A possible outcome of Prim's algorithm with as input the between-satellite single differences can be found in Table 3.10. The corresponding MST is depicted in Figure 3.13. It gives a total of 67 single differences. The single differences between satellite 17 and 22, satellite 2 and 5 and between satellite 1 and 25 have to be discarded since they only involve one station and consequently no between-receiver difference can be made. That gives then a total of 64 single differences from which $64 - 18 = 46$ double difference combinations can be formed. One observation involved in the three single differences that are discarded (SANT-PRN25) is not part of any other single difference, and thus also has to be discarded. There are 3 observations that are not involved in any single difference, which makes the set of unused observations {TIDB–PRN25, KOSG–PRN31, SANT–PRN09, SANT–PRN25}. None of the observations made to PRN25 are used. The results for the different methods to form integer functions of ambiguities are summarized in Table 3.7.

Method	Number of observations	Number of receivers	Number of satellites	Number of functions
Undifferenced	86	14	22	51
GAMIT	83	14	21	47
Between-satellite SD	82	14	21	46
Between-receiver SD	76	14	19	44
Minimum distance	66	13	15	39

Table 3.7: Results for the methods to form integer functions of ambiguities.

3.16 Concluding remarks

Although the DD approach at first sight seems to be advantageous over the undifferenced setup since less parameters are involved, this advantage is to a large extent cosmetic.

The differencing scheme obscures the rank defect inherent to the relative positioning setup with GPS, and sometimes not all available data are used.

When the clocks are modeled as shown in this chapter, and when an appropriate S-basis is chosen, the undifferenced approach is equivalent to the DD approach when the same data is used. However, using the undifferenced approach alternative choices for modeling the clocks are still possible (e.g. using polynomials or spline functions).

As far as the computational load for determining the global parameters is concerned, the undifferenced approach can compete with the DD approach.

The undifferenced approach has the advantage that individual observations can be tested, and if more than two receivers simultaneously track the same satellite, possible errors in the data can uniquely be located. It also opens the possibility for e.g. the estimation of variance components per satellite or per receiver.

Single difference	Number of satellites involved	PRN codes of satellites involved
YELL-FAIR	7	03,17,21,23,26,27,31
ALGO-FAIR	5	03,17,21,23,26
KOKB-FAIR	5	03,17,21,23,31
KOSG-FAIR	5	17,23,26,27,31
GOLD-KOKB	5	01,03,17,21,23
GOL2-KOKB	5	01,03,17,21,23
WETT-KOSG	5	02,10,26,27,31
MADR-KOSG	4	02,10,26,27
TROM-KOSG	4	02,26,27,31
TIDB-KOKB	3	15,22,23
YAR1-TIDB	5	14,15,16,22,29
SANT-GOL2	2	01,06
HART-SANT	3	04,05,24

Table 3.8: Between-receiver single differences formed by Prim's algorithm, with weights based on maximum possible single differences.

Single difference	Number of satellites involved	Distance
GOLD-GOL2	5	0
GOLD-YELL	4	2986
YELL-FAIR	7	1631
YELL-ALGO	5	2931
GOLD-KOKB	5	4305
YELL-TROM	3	4776
TROM-KOSG	4	2055
KOSG-WETT	5	603
KOSG-MADR	4	1512
MADR-HART	2	7525
KOKB-TIDB	2	7769
TIDB-YAR1	5	3197
ALGO-SANT	1	8105

Table 3.9: Between-receiver single differences formed by Prim's algorithm, with weights based on inter-station distance.

Single difference	Number of stations involved	Site ID's of stations involved
17 - 23	7	ALGO,GOLD,GOL2,FAIR,KOKB,KOSG,YELL
17 - 03	6	ALGO,GOLD,GOL2,FAIR,KOKB,YELL
17 - 21	6	ALGO,GOLD,GOL2,FAIR,KOKB,YELL
17 - 26	4	ALGO,FAIR,KOSG,YELL
26 - 27	6	MADR,FAIR,KOSG,WETT,YELL,TROM
26 - 31	5	FAIR,KOSG,WETT,YELL,TROM
26 - 02	4	MADR,KOSG,WETT,TROM
02 - 10	4	MADR,HART,KOSG,WETT
17 - 01	3	GOLD,GOL2,KOKB
17 - 09	2	ALGO,KOSG
01 - 06	2	GOL2,SANT
17 - 22	1	KOKB
22 - 15	3	TIDB,KOKB,YAR1
22 - 14	2	TIDB,YAR1
22 - 29	2	TIDB,YAR1
22 - 16	2	TIDB,YAR1
16 - 18	2	HART,YAR1
02 - 05	1	HART
05 - 04	2	HART,SANT
05 - 24	2	HART,SANT
01 - 25	1	SANT

Table 3.10: Between-satellite single differences formed by Prim's algorithm, with weights based on maximum possible single differences.

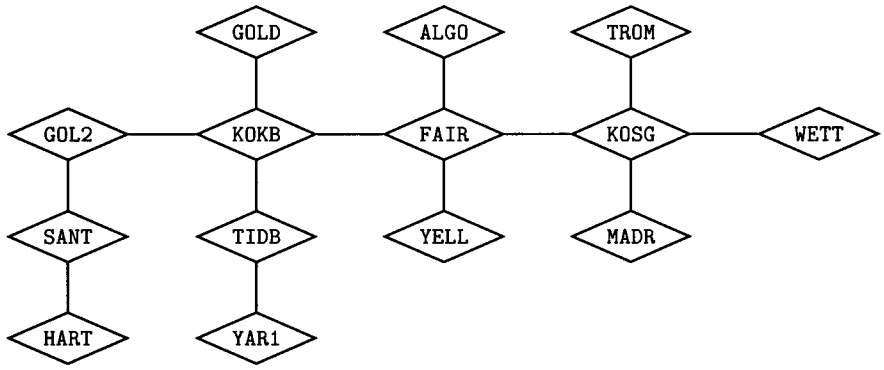

Figure 3.12: Minimum spanning tree to form maximum of between-receiver single differences.

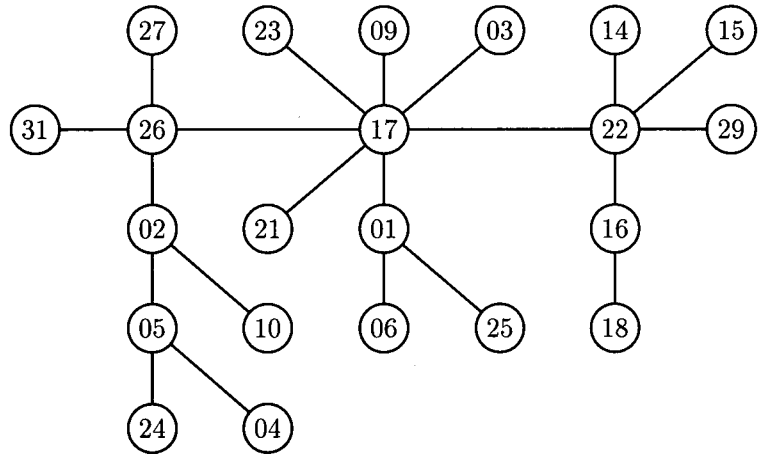

Figure 3.13: Minimum spanning tree to form maximum of between-satellite single differences.

ALGO												
4	GOLD											
4	5	GOL2										
0	0	0	TIDB									
1	0	0	0	MADR								
5	4	4	0	2	FAIR							
0	0	0	1	2	0	HART						
4	5	5	2	0	5	0	KOKB					
4	2	2	0	4	5	2	3	KOSG				
1	1	2	1	0	0	3	1	1	SANT			
1	0	0	0	4	3	2	1	5	0	WETT		
0	0	0	5	0	0	2	2	0	0	0	YAR1	
5	4	4	0	2	7	0	5	5	0	3	0	YELL
1	0	0	0	3	3	1	1	4	0	4	0	3 TROM

Table 3.11: The number of possible between-receiver single differences for the observation scenario in Table 3.2.

PRN01																									
0	PRN02																								
3	0	PRN03																							
1	1	0	PRN04																						
1	1	0	2	PRN05																					
2	0	1	1	1	PRN06																				
1	1	1	1	1	1	PRN09																			
0	4	0	1	1	0	1	PRN10																		
0	0	0	0	0	0	0	0	PRN14																	
1	0	1	0	0	0	0	0	2	PRN15																
0	1	0	1	1	0	0	1	2	2	PRN16															
3	1	6	0	0	1	2	1	0	1	0	PRN17														
0	1	0	1	1	0	0	1	1	1	2	0	PRN18													
3	0	6	0	0	1	1	0	0	1	0	6	0	PRN21												
1	0	1	0	0	0	0	0	2	3	2	1	1	1	PRN22											
3	1	6	0	0	1	2	1	0	1	0	7	0	6	1	PRN23										
1	1	0	2	2	1	1	1	0	0	1	0	1	0	0	0	PRN24									
1	0	0	1	1	1	1	0	1	1	1	0	0	0	1	0	1	PRN25								
0	4	3	0	0	0	2	3	0	0	0	4	0	3	0	4	0	0	PRN26							
0	4	2	0	0	0	1	3	0	0	0	3	0	2	0	3	0	0	6	PRN27						
0	0	0	0	0	0	0	0	2	2	2	0	1	0	2	0	0	1	0	0	PRN29					
1	3	3	0	0	0	1	2	0	1	0	4	0	3	1	4	0	0	5	5	0	PRN31				

Table 3.12: The number of possible between-satellite single differences for the observation scenario in Table 3.2.

References

Beckers, G. W. J. and F. Kenselaar (1996). Adjust 3.3. Technical report, Delft Geodetic Computing Centre, Delft University of Technology.

Benoît, E. (1924). Note sur une méthode de résolution des équations normales provenant de l'application de la méthode des moindres carrés a un système d'équations linéaires en nombre inférieur a celui des inconnues. – Application de la méthode a la résolution d'un système defini d'équations linéaires. *Bulletin Géodésique* (2), 67–77. (Procédé du Commandant Cholesky).

Beutler, G., W. Gurtner, I. Bauersima, and M. Rothacher (1986). Efficient computation of the inverse of the covariance matrix of simultaneous GPS carrier phase difference observations. *manuscripta geodaetica 11*, 249–255.

Blewitt, G. (1993). Advances in Global Positioning System technology for geodynamics investigations: 1978–1992. In D. E. Smith and D. L. Turcotte (Eds.), *Crustal Dynamics*, Volume 25 of *Contributions of Space Geodesy to Geodynamics*. AGU.

Bock, Y., R. I. Abbot, C. C. Counselman III, R. W. King, and S. A. Gourevitch (1985). Three-dimensional geodetic control by interferometry with GPS: processing of GPS phase observables. In C. C. Goad (Ed.), *Proceedings of the First International Symposium on Precise Positioning with the Global Positioning System*, Rockville, Maryland, pp. 255–261. National Geodetic Survey.

Bock, Y., S. A. Gourevitch, C. C. Councelman III, R. W. King, and R. I. Abbot (1986). Interferometric analysis of GPS phase observations. *manuscripta geodaetica 11*, 282–288.

Counselman III, C. C., H. F. Hinteregger, and I. I. Shapiro (1972). Astronomical applications of differential interferometry. *Science 178*, 607–608.

Goad, C. C. and A. Mueller (1988). An automated procedure for generating an optimum set of independent double difference observables using Global Positioning System carrier phase measurements. *manuscripta geodaetica 13*, 365–369.

Golub, G. H. and C. F. Van Loan (1989). *Matrix Computations, second edition*. Johns Hopkins Series in the Mathematical Sciences. The Johns Hopkins University Press.

Jin, X.-X. (1996). *Theory of Carrier Adjusted DGPS Positioning Approach and Some Experimental Results*. Ph. D. thesis, Delft University of Technology.

Kösters, A. J. M. (1992). Some aspects of a 3-dimensional reference system for surveying in the netherlands – quality analysis of GPS phase observations. Technical Report 92.1, Section Mathematical and Physical Geodesy, Department of Geodetic Engineering, Delft University of Technology.

Lindlohr, W. and D. Wells (1985). GPS design using undifferenced carrier beat phase observations. *manuscripta geodaetica 10*, 255–281.

Mervart, L., G. Beutler, M. Rothacher, and U. Wild (1994). Ambiguity resolution strategies using the results of the International GPS Geodynamics Service (IGS). *Bulletin Géodésique 68*, 29–38.

Pissanetzky, S. (1984). *Sparse matrix technology*. Academic Press, London.

Rothacher, M. and L. Mervart (1996). Bernese GPS software version 4.0. Technical report, Astronomical Institute University of Berne.

Schaffrin, B. and E. Grafarend (1986). Generating classes of equivalent linear models by nuisance parameter elimination. Applications to GPS observations. *manuscripta geodaetica 11*, 262–271.

Teunissen, P. J. G. (1984). Generalized inverses, adjustment, the datum problem and S-transformations. Technical Report 84.1, Faculty of Geodetic Engineering, Dept. of Mathematical and Physical Geodesy. Delft University of Technology, The Netherlands.

Teunissen, P. J. G. (1988). Toetsing en betrouwbaarheid voor een bekende ∇. Internal research memo, Mathematical Geodesy and Positioning.

Teunissen, P. J. G. (1989). Mathematische Geodesie II. Inleiding Toetsingstheorie. Lecture Notes (in English) GE-31b, Faculty of Geodetic Engineering, Delft University of Technology, The Netherlands.

Tiberius, C. C. J. M. (1998). *Recursive data processing for kinematic GPS surveying.* Ph. D. thesis, Delft University of Technology.

Chapter 4

Relative positioning using multiple GPS observable types

4.1 Introduction

In Chapter 3 we described the estimation process for a single GPS observable type using the undifferenced approach. In this chapter we will describe the estimation for more than one observable type. When using more than one observable type at different frequencies, it is possible to estimate first order ionospheric delays, due to the dispersive character of the ionosphere. The ionospheric delay may be modeled by some function of the latitude of the sub-ionospheric point and the local hour angle of the Sun, or by modeling a slant delay for each receiver-satellite combination at each epoch. Only modeling by slant delays will be treated in this chapter. Depending on the observable types that are employed it may introduce an additional rank defect.

In this chapter we will investigate this rank defect for a number of models and show how it can be resolved by an appropriate choice of S-basis. The alternative method is again to take certain differences, or linear combinations of the observable types. We will show that some of these linear combinations have their counterpart in the undifferenced approach, while others do not preserve the information content of the system, and hence should be used with care.

We will also show that although the number of observations and unknowns in the undifferenced approach is much larger than in the case of using linear combinations, the computational load can be reduced to the same level as the latter, by making use of the intrinsic symmetric properties of the product of the weight matrix of the observables and the $P_{\bar{A}_2}^{\perp}$ projector.

As the normal matrices arising from the processing of large time spans may be sparse, the influence of the ordering of the parameters on preserving the sparsity in the subsequent Cholesky factorization will be shown.

As said before, we will treat four different cases to handle the clocks and the ionospheric delays. These cases with their corresponding system of linearized observation equations for all four basic GPS observable types are given below.

1. No estimation of ionosphere, distinct clocks for each observable type

$$E\{\begin{bmatrix}\Phi^j_{i,\mathrm{L1}}\\ \Phi^j_{i,\mathrm{L2}}\\ P^j_{i,\mathrm{P1}}\\ P^j_{i,\mathrm{P2}}\end{bmatrix}\} = \begin{bmatrix} g & I & & d & & \\ g & & I & & d & \\ g & & & & & d \\ g & & & & & d \end{bmatrix} \begin{bmatrix} r_i \\ \lambda_1 N^j_{i,\mathrm{L1}} \\ \lambda_2 N^j_{i,\mathrm{L2}} \\ \begin{bmatrix} c\delta t_{i,\mathrm{L1}} \\ c\delta t^{j,\mathrm{L1}} \end{bmatrix} \\ \begin{bmatrix} c\delta t_{i,\mathrm{L2}} \\ c\delta t^{j,\mathrm{L2}} \end{bmatrix} \\ \begin{bmatrix} c\delta t_{i,\mathrm{P1}} \\ c\delta t^{j,\mathrm{P1}} \end{bmatrix} \\ \begin{bmatrix} c\delta t_{i,\mathrm{P2}} \\ c\delta t^{j,\mathrm{P2}} \end{bmatrix} \end{bmatrix} \tag{4.1}$$

2. No estimation of ionosphere, common clocks

$$E\{\begin{bmatrix}\Phi^j_{i,\mathrm{L1}}\\ \Phi^j_{i,\mathrm{L2}}\\ P^j_{i,\mathrm{P1}}\\ P^j_{i,\mathrm{P2}}\end{bmatrix}\} = \begin{bmatrix} g & I & & d \\ g & & I & d \\ g & & & d \\ g & & & d \end{bmatrix} \begin{bmatrix} r_i \\ \lambda_1 N^j_{i,\mathrm{L1}} \\ \lambda_2 N^j_{i,\mathrm{L2}} \\ \begin{bmatrix} c\delta t_i \\ c\delta t^j \end{bmatrix} \end{bmatrix} \tag{4.2}$$

3. Estimation of ionosphere, distinct clocks for each observable type

$$E\{\begin{bmatrix}\Phi^j_{i,\mathrm{L1}}\\ \Phi^j_{i,\mathrm{L2}}\\ P^j_{i,\mathrm{P1}}\\ P^j_{i,\mathrm{P2}}\end{bmatrix}\} = \begin{bmatrix} g & I & & d & & & \eta_1 I \\ g & & I & & d & & \eta_2 I \\ g & & & & & d & \eta_3 I \\ g & & & & & d & \eta_4 I \end{bmatrix} \begin{bmatrix} r_i \\ \lambda_1 N^j_{i,\mathrm{L1}} \\ \lambda_2 N^j_{i,\mathrm{L2}} \\ \begin{bmatrix} c\delta t_{i,\mathrm{L1}} \\ c\delta t^{j,\mathrm{L1}} \end{bmatrix} \\ \begin{bmatrix} c\delta t_{i,\mathrm{L2}} \\ c\delta t^{j,\mathrm{L2}} \end{bmatrix} \\ \begin{bmatrix} c\delta t_{i,\mathrm{P1}} \\ c\delta t^{j,\mathrm{P1}} \end{bmatrix} \\ \begin{bmatrix} c\delta t_{i,\mathrm{P2}} \\ c\delta t^{j,\mathrm{P2}} \end{bmatrix} \\ \mathcal{I}^j_i \end{bmatrix} \tag{4.3}$$

4. Estimation of ionosphere, common clocks

$$E\{\begin{bmatrix}\Phi^j_{i,\mathrm{L1}}\\ \Phi^j_{i,\mathrm{L2}}\\ P^j_{i,\mathrm{P1}}\\ P^j_{i,\mathrm{P2}}\end{bmatrix}\} = \begin{bmatrix} g & I & & d & \eta_1 I \\ g & & I & d & \eta_2 I \\ g & & & d & \eta_3 I \\ g & & & d & \eta_4 I \end{bmatrix} \begin{bmatrix} r_i \\ \lambda_1 N^j_{i,\mathrm{L1}} \\ \lambda_2 N^j_{i,\mathrm{L2}} \\ \begin{bmatrix} c\delta t_i \\ c\delta t^j \end{bmatrix} \\ \mathcal{I}^j_i \end{bmatrix} \tag{4.4}$$

Note that in this chapter the dimension of the unit matrix is only indicated by a subscript if its dimension is not clear from the context. To facilitate the translation of models in this

Case	DD equivalent distinct clock?	DD equivalent common clocks?
P1 or P2	yes	n/a
L1 or L2	yes	n/a
P1 and P2	yes	no
L1 and L2	yes	no
(L1 or L2) and (P1 or P2)	yes	no
L1 and L2 and (P1 or P2)	yes	no
(L1 or L2) and P1 and P2	yes	no
L1 and L2 and P1 and P2	yes	no
p phase and $q-p$ pseudo-range observable types	yes	no

Table 4.1: Overview of the possible models without estimation of ionosphere using the undifferenced approach and their possible DD equivalents.

chapter to the terminology the reader may be using, the ionospheric delay is denoted here as $\eta_1\mathcal{I}$ for P1, $\eta_2\mathcal{I}$ for P2, $\eta_3\mathcal{I}$ for L1 and $\eta_4\mathcal{I}$ for L2, where $\eta_1 = -\eta_3$, $\eta_2 = -\eta_4$, and $\eta_2/\eta_1 = \gamma = {f_1}^2/{f_2}^2$.

Throughout this chapter, (no) estimation of ionosphere refers to (no) estimation of ionospheric *slant delays*.

The fourth case is only included for the sake of completeness. As we will show it should not be applied to the GPS, but it might be applied to GPS-like systems where no ionospheric delays are expected, e.g. in-house GPS-like systems (Malagodi et al. 1995), and ground based pseudolites-only systems.

For the models where no ionospheric delays are estimated, we may use any set of GPS observable types with a minimum of one type. For the models where ionospheric delays are estimated the minimum number of observable types is two.

Some, but not all, models have a DD equivalent. An overview of the possible models using the undifferenced approach and their DD equivalents can be found in Tables 4.1 and 4.2.

4.2 Resolving the rank defect of the bias parameters

4.2.1 Introduction

In this section we will give the rank defect, and a way to resolve it by choosing an appropriate S-basis, for the models of the previous section.

The most straightforward case is the model where no ionospheric delays are estimated, and each observable type has its own clocks. The rank defect is then the sum of the individual rank defects of the observable types, i.e. the part of the design matrix of the bias parameters referring to one observable type are complementary to the parts referring to the bias parameters of the other observable types, see Section 3.2.

Rank defect and S-basis are given for the case where all receivers track the same set of satellites. For observation scenarios where this is not the case we refer to Section 3.5.

Case	DD equivalent distinct clock?	DD equivalent common clocks?
P1 and P2	yes	yes
L1 and L2	yes	yes
(L1 or L2) and (P1 or P2)	no	no
L1 and L2 and (P1 or P2)	no	no
(L1 or L2) and P1 and P2	no	no
L1 and L2 and P1 and P2	yes	no
p phase and $q-p$ pseudorange observable types	for some p and q	no

Table 4.2: Overview of the possible models with estimation of ionosphere using the undifferenced approach and their possible DD equivalents.

In Table 4.3 the number of unknown bias parameters and rank defect for the models without estimation of ionosphere is given, for the cases of distinct clocks and common clocks. In Table 4.4 the same is done for the models with estimation of ionosphere. S-basis and resulting estimable functions are given in Tables 4.5–4.8. The S-basis is always chosen such that, when applicable, double difference like estimable functions are produced by it. This is important since they may possibly be constrained to an integer value in a subsequent integer estimation step, which will in general improve the precision of the non-ambiguity parameters. The integer estimation will be treated in Chapter 5.

As far as clock terms are concerned, always the clock of the first receiver is included in the S-basis. This is done to prevent very long expressions for the estimable functions. Sometimes one prefers to have an S-basis consisting of the average of the satellite clock terms. If the a priori satellite clock model from the broadcast ephemerides is applied, for pseudorange observable types the resulting bias due to the satellite clocks will then consist of the average of the mismodeling of the clock model, the SA effect, and effects due to group delays. This is e.g. applied to get (almost) unbiased estimates for the receiver clocks to correct the receiver time tag.

It can be easily constructed by subtracting the average of the biased satellite clocks, from all estimable functions in which the clock of the first receiver occurs. It is also subtracted from the estimate for the clock term of the first receiver itself (which by being part of the S-basis is set to zero).

The estimable functions that are affected by this change of S-basis are only those that refer to clocks or ionosphere terms. The functions of ambiguities are not affected.

Although usually receiver clock, satellite clock and ionosphere terms are not separately estimable, differences in time sometimes are. Again these functions are easily constructed by subtracting the estimable function at one epoch from all subsequent epochs. This will give the development in time of e.g. the ionospheric delay, or a clock. Likewise one can make divided differences to find the derivative of ionospheric delays or clocks. Again the ambiguities are not affected.

Model	$nunkA_{II}$	$rnkdA_{II}$
Distinct clocks:		
P1 or P2	$n(r+m)$	n
L1 or L2	$n(r+m)+rm$	$n+(r+m-1)$
P1 and P2	$2n(r+m)$	$2n$
L1 and L2	$2n(r+m)+2rm$	$2n+2(r+m-1)$
(L1 or L2) and (P1 or P2)	$2n(r+m)+rm$	$2n+(r+m-1)$
L1 and L2 and (P1 or P2)	$3n(r+m)+2rm$	$3n+2(r+m-1)$
(L1 or L2) and P1 and P2	$3n(r+m)+rm$	$3n+(r+m-1)$
L1 and L2 and P1 and P2	$4n(r+m)+2rm$	$4n+2(r+m-1)$
p phase and $q-p$ pseudo range observable types	$qn(r+m)+prm$	$qn+p(r+m-1)$
Common clocks:		
P1 and P2	$n(r+m)$	n
L1 and L2	$n(r+m)+2rm$	$n+(r+m-1)$
(L1 or L2) and (P1 or P2)	$n(r+m)+rm$	n
L1 and L2 and (P1 or P2)	$n(r+m)+2rm$	n
(L1 or L2) and P1 and P2	$n(r+m)+rm$	n
L1 and L2 and P1 and P2	$n(r+m)+2rm$	n
p phase and $q-p$ pseudo range observable types	$n(r+m)+prm$	$\begin{cases} n & p=0 \\ n+(r+m-1) & p>0 \end{cases}$

Table 4.3: Number of unknown bias parameters ($nunkA_{II}$), and rank defect for it ($rnkdA_{II}$) for the models without estimation of ionosphere.

Code	$nunkA_{II}$	$rnkdA_{II}$
Distinct clocks:		
P1 and P2	$2n(r+m)+nrm$	$n+n(r+m)$
L1 and L2	$2n(r+m)+2rm+nrm$	$n+n(r+m)+(r+m-1)+rm$
(L1 or L2) and (P1 or P2)	$2n(r+m)+rm+nrm$	$n+n(r+m)+(r+m-1)$
L1 and L2 and (P1 or P2)	$3n(r+m)+2rm+nrm$	$2n+n(r+m)+2(r+m-1)$
(L1 or L2) and P1 and P2	$3n(r+m)+rm+nrm$	$2n+n(r+m)+(r+m-1)$
L1 and L2 and P1 and P2	$4n(r+m)+2rm+nrm$	$3n+n(r+m)+2(r+m-1)$
p phase and $q-p$ pseudo range observable types	$qn(r+m)+prm+nrm$	$(q-1)n+n(r+m)+p(r+m-1)$
Common clocks:		
P1 and P2	$n(r+m)+nrm$	n
L1 and L2	$n(r+m)+2rm+nrm$	$n+(r+m-1)+rm$
(L1 or L2) and (P1 or P2)	$n(r+m)+rm+nrm$	$n+(r+m-1)$
L1 and L2 and (P1 or P2)	$n(r+m)+2rm+nrm$	$n+(r+m-1)$
(L1 or L2) and P1 and P2	$n(r+m)+rm+nrm$	$n+(r+m-1)$
L1 and L2 and P1 and P2	$n(r+m)+2rm+nrm$	n
p phase and $q-p$ pseudo range observable types	$n(r+m)+prm+nrm$	$\begin{cases} n & p=0 \\ n+(r+m-1)+(p-1)rm & p=q \\ n+(r+m-1) & p\neq 0 \wedge p\neq q \end{cases}$

Table 4.4: Number of unknown bias parameters ($nunkA_{II}$), and rank defect for it ($rnkdA_{II}$) for the models with estimation of ionosphere.

4.2.2 No estimation of ionospheric slant delays

This model is the standard model for short (up to 10 km) inter-station distances. Modeling of ionosphere is not needed since the ionospheric delays are (almost) equal at the two stations, and consequently are absorbed by the satellite clock term (see Section 4.2.6).

Distinct clocks:
In Table 4.5 a possible S-basis and the resulting estimable function of parameters for the models with distinct clocks and no estimation of ionosphere are given. Due to the complementarity of the observable types, it is given for the case of one single pseudorange or carrier phase observable. When observable types are combined one may add S-basis and estimable functions of the individual observable types.

As far as ambiguities are concerned, for each carrier phase observable type involved, DD-like functions of ambiguities may be estimated. Taking the average of the satellite clocks as S-basis for the pseudorange clocks will, as explained above, give estimates for the receiver clock error that are only biased by the SA effect, mismodeling of the clock, and effects due to group delays. This will be explained in detail in Section 4.2.5.

Common clocks:
In Table 4.6 the same is done for the case that common clocks are used. When only one observable type is used, S-basis and estimable functions are of course equal to those for the model with distinct clocks. When more than one observable type is involved, then there is no complementarity anymore. Therefore in Table 4.6 also combinations of observable types are included. As mentioned before, these models cannot be applied to the GPS, but only to systems that employ signals not affected by the ionosphere.

4.2.3 Estimation of ionospheric slant delays

For distances larger than approximately 10 km, the ionospheric delays are no longer absorbed by the satellite clock terms, and hence have to modeled.

Distinct clocks:
In Table 4.7 a possible S-basis and resulting estimable functions for the models with distinct clocks and estimation of ionosphere are given, and in Table 4.8 for the models with a common clock and estimation of ionosphere.

Although models with one carrier phase observable type and one or more pseudorange observable types are also included, these models are not adequate for use with the GPS, due to poor precision of the pseudoranges compared to the carrier phases. They are merely included for the sake of completeness.

Integer double difference like functions of ambiguities can only be estimated if at least one pseudorange observable type is included. Otherwise, only linear combinations of the L1 and L2 ambiguities, which are not integers anymore, can be estimated. They are of the form

$$\lambda_1(N^j_{i,\mathrm{L1}} - N^1_{i,\mathrm{L1}} - N^j_{1,\mathrm{L1}} + N^1_{1,\mathrm{L1}}) - \frac{\eta_1}{\eta_2}\lambda_2(N^j_{i,\mathrm{L2}} - N^1_{i,\mathrm{L2}} - N^j_{1,\mathrm{L2}} + N^1_{1,\mathrm{L2}}) =$$
$$\lambda_1\{(N^j_{i,\mathrm{L1}} - N^1_{i,\mathrm{L1}} - N^j_{1,\mathrm{L1}} + N^1_{1,\mathrm{L1}}) - \frac{\eta_1}{\eta_2}\frac{\lambda_2}{\lambda_1}(N^j_{i,\mathrm{L2}} - N^1_{i,\mathrm{L2}} - N^j_{1,\mathrm{L2}} + N^1_{1,\mathrm{L2}})\} =$$
$$\lambda_1\{(N^j_{i,\mathrm{L1}} - N^1_{i,\mathrm{L1}} - N^j_{1,\mathrm{L1}} + N^1_{1,\mathrm{L1}}) - \frac{f_2}{f_1}(N^j_{i,\mathrm{L2}} - N^1_{i,\mathrm{L2}} - N^j_{1,\mathrm{L2}} + N^1_{1,\mathrm{L2}})\} \tag{4.5}$$

Although

$$(N^j_{i,\mathrm{L1}} - N^1_{i,\mathrm{L1}} - N^j_{1,\mathrm{L1}} + N^1_{1,\mathrm{L1}}) - \frac{f_2}{f_1}(N^j_{i,\mathrm{L2}} - N^1_{i,\mathrm{L2}} - N^j_{1,\mathrm{L2}} + N^1_{1,\mathrm{L2}}) \tag{4.6}$$

is not an integer valued function, it still is a rational valued function, and hence can be transformed into a integer function. Multiplication of (4.6) by 77 and dividing λ_1 by the same number, transforms (4.5) into

$$\frac{\lambda_1}{77}\{77(N^j_{i,\mathrm{L1}} - N^1_{i,\mathrm{L1}} - N^j_{1,\mathrm{L1}} + N^1_{1,\mathrm{L1}}) - 60(N^j_{i,\mathrm{L2}} - N^1_{i,\mathrm{L2}} - N^j_{1,\mathrm{L2}} + N^1_{1,\mathrm{L2}})\} \tag{4.7}$$

Now we have obtained an integer function, which in principle could be integer estimated. Unfortunately its synthetic wavelength is very small ($\approx$ 2.5 mm) compared to the standard deviation of the phase observables ($\approx$ 3 mm), which renders a successful integer estimation virtually impossible.

Common clocks:
In Table 4.8 S-basis and resulting estimable functions for the models with a common clock and estimation of ionosphere are given. If only two observable types are used, rank and estimates for the non-bias parameters equal those of the models with distinct clocks.

A nice property of this model when applied to pseudorange observable types, is that for the clocks and for the ionospheric delay estimable functions are obtained that are almost unbiased (see Section 4.2.5).

When applied to carrier phase observable types, or a combination of these with pseudorange observable types, clocks and ionospheric delays are biased. However, since the biases consist of functions of ambiguities, by taking differences in time, the behaviour in time of these parameters can be monitored.

4.2.4 Constraining of ionospheric slant delays

Estimation of ionospheric delay parameters per receiver-satellite combination, per epoch, or equivalently per epoch elimination of these parameters (the ionosphere-free solution, see Section 4.3.1) implies that only a linear combination of the L1 and L2 ambiguity, which is not integer anymore, can be estimated.

In Bock et al. (1986) it is shown that inclusion of stochastic constraints on the size of the ionospheric delays, results again in DD like integer functions of ambiguities.

The constraints are implemented by adding pseudo observables of the form

$$E\{l^j_i\} = \eta_0 \mathcal{I}^j_i \quad \text{with} \quad D\{l^j_i\} = \sigma^2_{l^j_i} = \frac{1}{w_0} \tag{4.8}$$

Case S-basis	Estimable functions	
P1 or P2 $c\delta t_{1,\mathrm{P}l}$	$c(\delta t_{i,\mathrm{P}l} - \delta t_{1,\mathrm{P}l})$ $c(\delta t^{j,\mathrm{P}l} - \delta t_{1,\mathrm{P}l})$	$i \neq 1$
L1 or L2 $c\delta t_{1,\mathrm{L}l}$ $\lambda_l N^j_{i,\mathrm{L}l} \quad i = 1 \vee j = 1$	$c(\delta t_{i,\mathrm{L}l} - \delta t_{1,\mathrm{L}l}) - \lambda_l(N^1_{1,\mathrm{L}l} - N^1_{i,\mathrm{L}l})$ $c(\delta t^{j,\mathrm{L}l} - \delta t_{1,\mathrm{L}l}) - \lambda_l N^j_{1,\mathrm{L}l}$ $\lambda_l(N^j_{i,\mathrm{L}l} - N^1_{i,\mathrm{L}l} - N^j_{1,\mathrm{L}l} + N^1_{1,\mathrm{L}l})$	$i \neq 1$ $i \neq 1 \wedge j \neq 1$

Table 4.5: Possible S-basis and resulting estimable functions for some models with distinct clocks and no estimation of ionosphere.

Case S-basis	Estimable functions	
P1 and P2 $c\delta t_1$	$c(\delta t_i - \delta t_1)$ $c(\delta t^j - \delta t_1)$	$i \neq 1$
L1 and L2 $c\delta t_1$ $\lambda_1 N^j_{i,\mathrm{L1}} \quad i = 1 \vee j = 1$	$c(\delta t_i - \delta t_1) - \lambda_1(N^1_{1,\mathrm{L1}} - N^1_{i,\mathrm{L1}})$ $c(\delta t^j - \delta t_1) - \lambda_1 N^j_{1,\mathrm{L1}}$ $\lambda_2 N^j_{i,\mathrm{L2}} - \lambda_1(N^1_{i,\mathrm{L1}} - N^j_{1,\mathrm{L1}} + N^1_{1,\mathrm{L1}})$ $\lambda_2 N^j_{i,\mathrm{L2}} - \lambda_1 N^j_{i,\mathrm{L1}}$ $\lambda_1(N^j_{i,\mathrm{L1}} - N^1_{i,\mathrm{L1}} - N^j_{1,\mathrm{L1}} + N^1_{1,\mathrm{L1}})$	$i \neq 1$ $i \neq 1 \wedge j \neq 1$ $i = 1 \vee j = 1$ $i \neq 1 \wedge j \neq 1$
L1 and L2 and P1 $c\delta t_1$	$c(\delta t_i - \delta t_1)$ $c(\delta t^j - \delta t_1)$ $\lambda_1 N^j_{i,\mathrm{L1}}$ $\lambda_2 N^j_{i,\mathrm{L2}}$	$i \neq 1$
L1 and L2 and P1 and P2 $c\delta t_1$	$c(\delta t_i - \delta t_1)$ $c(\delta t^j - \delta t_1)$ $\lambda_1 N^j_{i,\mathrm{L1}}$ $\lambda_2 N^j_{i,\mathrm{L2}}$	$i \neq 1$

Table 4.6: Possible S-basis and resulting estimable functions for some models with common clocks and no estimation of ionosphere.

Case S-basis	Estimable functions	
P1 and P2	$c(\delta t_{i,\mathrm{P2}} - \delta t_{1,\mathrm{P2}}) - \frac{\eta_4}{\eta_3} c(\delta t_{i,\mathrm{P1}} - \delta t_{1,\mathrm{P1}})$	$i \neq 1$
$c\delta t_{i,\mathrm{P1}}$ $c\delta t^{j,\mathrm{P1}}$	$c(\delta t^{j,\mathrm{P2}} - \delta t_{1,\mathrm{P2}}) - \frac{\eta_4}{\eta_3} c(\delta t^{j,\mathrm{P1}} - \delta t_{1,\mathrm{P1}})$	
$c\delta t_{1,\mathrm{P2}}$	$\mathcal{I}_i^j + \frac{1}{\eta_3} c(\delta t_{i,\mathrm{P1}} - \delta t^{j,\mathrm{P1}})$	
L1 and L2	$c(\delta t_{i,\mathrm{L2}} - \delta t_{1,\mathrm{L2}}) - \lambda_2(N^1_{1,\mathrm{L2}} - N^1_{i,\mathrm{L2}}) - \frac{\eta_2}{\eta_1}\{c(\delta t_{i,\mathrm{L1}} - \delta t_{1,\mathrm{L1}}) - \lambda_1(N^1_{1,\mathrm{L1}} - N^1_{i,\mathrm{L1}})\}$	$i \neq 1$
$c\delta t_{i,\mathrm{L1}}$ $c\delta t^{j,\mathrm{L1}}$	$c(\delta t^{j,\mathrm{L2}} - \delta t_{1,\mathrm{L2}}) - \lambda_2 N^j_{1,\mathrm{L2}} - \frac{\eta_2}{\eta_1}\{c(\delta t^{j,\mathrm{L1}} - \delta t_{1,\mathrm{L1}}) - \lambda_1 N^j_{1,\mathrm{L1}}\}$	
$c\delta t_{1,\mathrm{L2}}$	$\mathcal{I}_i^j + \frac{1}{\eta_1}\{c(\delta t_{i,\mathrm{L1}} - \delta t^{j,\mathrm{L1}}) + \lambda_1 N^i_{j,\mathrm{L1}}\}$	$i = 1 \vee j = 1$
$\lambda_1 N^j_{i,\mathrm{L1}}$ $i = 1 \vee j = 1$	$\mathcal{I}_i^j + \frac{1}{\eta_1}\{c(\delta t_{i,\mathrm{L1}} - \delta t^{j,\mathrm{L1}}) + \lambda_1(N^1_{i,\mathrm{L1}} + N^j_{1,\mathrm{L1}} - N^1_{1,\mathrm{L1}})\}$	
	$+ \frac{1}{\eta_2}\lambda_2(N^j_{i,\mathrm{L2}} - N^1_{i,\mathrm{L2}} - N^j_{1,\mathrm{L2}} + N^1_{1,\mathrm{L2}})$	$i \neq 1 \wedge j \neq 1$
$\lambda_2 N^j_{i,\mathrm{L2}}$	$\lambda_1(N^j_{i,\mathrm{L1}} - N^1_{i,\mathrm{L1}} - N^j_{1,\mathrm{L1}} + N^1_{1,\mathrm{L1}}) - \frac{\eta_1}{\eta_2}\lambda_2(N^j_{i,\mathrm{L2}} - N^1_{i,\mathrm{L2}} - N^j_{1,\mathrm{L2}} + N^1_{1,\mathrm{L2}})$	$i \neq 1 \wedge j \neq 1$
L1 and P1	$c(\delta t_{i,\mathrm{P1}} - \delta t_{1,\mathrm{P1}}) - \frac{\eta_3}{\eta_1}\{c(\delta t_{i,\mathrm{L1}} - \delta t_{1,\mathrm{L1}}) - \lambda_1(N^1_{1,\mathrm{L1}} - N^1_{i,\mathrm{L1}})\}$	$i \neq 1$
$c\delta t_{i,\mathrm{L1}}$ $c\delta t^{j,\mathrm{L1}}$	$c(\delta t^{j,\mathrm{P1}} - \delta t_{1,\mathrm{P1}}) - \frac{\eta_3}{\eta_1}\{c(\delta t^{j,\mathrm{L1}} - \delta t_{1,\mathrm{L1}}) - \lambda_1 N^j_{1,\mathrm{L1}}\}$	
$c\delta t_{1,\mathrm{P1}}$	$\mathcal{I}_i^j + \frac{1}{\eta_1}\{c(\delta t_{i,\mathrm{L1}} - \delta t^{j,\mathrm{L1}}) + \lambda_1 N^i_{j,\mathrm{L1}}\}$	$i = 1 \vee j = 1$
$\lambda_1 N^j_{i,\mathrm{L1}}$ $i = 1 \vee j = 1$	$\mathcal{I}_i^j + \frac{1}{\eta_1}\{c(\delta t_{i,\mathrm{L1}} - \delta t^{j,\mathrm{L1}}) + \lambda_1(N^1_{i,\mathrm{L1}} + N^j_{1,\mathrm{L1}} - N^1_{1,\mathrm{L1}})\}$	$i \neq 1 \wedge j \neq 1$
	$\lambda_1(N^j_{i,\mathrm{L1}} - N^1_{i,\mathrm{L1}} - N^j_{1,\mathrm{L1}} + N^1_{1,\mathrm{L1}})$	$i \neq 1 \wedge j \neq 1$
L1 and L2 and P1	$c(\delta t_{i,\mathrm{L2}} - \delta t_{1,\mathrm{L2}}) - \lambda_2(N^1_{1,\mathrm{L2}} - N^1_{i,\mathrm{L2}}) - \frac{\eta_2}{\eta_1}\{c(\delta t_{i,\mathrm{L1}} - \delta t_{1,\mathrm{L1}}) - \lambda_1(N^1_{1,\mathrm{L1}} - N^1_{i,\mathrm{L1}})\}$	$i \neq 1$
$c\delta t_{i,\mathrm{L1}}$ $c\delta t^{j,\mathrm{L1}}$	$c(\delta t^{j,\mathrm{L2}} - \delta t_{1,\mathrm{L2}}) - \lambda_2 N^j_{1,\mathrm{L2}} - \frac{\eta_2}{\eta_1}\{c(\delta t^{j,\mathrm{L1}} - \delta t_{1,\mathrm{L1}}) - \lambda_1 N^j_{1,\mathrm{L1}}\}$	
$c\delta t_{1,\mathrm{L2}}$	$c(\delta t_{i,\mathrm{P1}} - \delta t_{1,\mathrm{P1}}) - \frac{\eta_3}{\eta_1}\{c(\delta t_{i,\mathrm{L1}} - \delta t_{1,\mathrm{L1}}) - \lambda_1(N^1_{1,\mathrm{L1}} - N^1_{i,\mathrm{L1}})\}$	$i \neq 1$
$c\delta t_{1,\mathrm{P1}}$	$c(\delta t^{j,\mathrm{P1}} - \delta t_{1,\mathrm{P1}}) - \frac{\eta_3}{\eta_1}\{c(\delta t^{j,\mathrm{L1}} - \delta t_{1,\mathrm{L1}}) - \lambda_1 N^j_{1,\mathrm{L1}}\}$	
$\lambda_1 N^j_{i,\mathrm{L1}}$ $i = 1 \vee j = 1$	$\mathcal{I}_i^j + \frac{1}{\eta_1}\{c(\delta t_{i,\mathrm{L1}} - \delta t^{j,\mathrm{L1}}) + \lambda_1 N^i_{j,\mathrm{L1}}\}$	$i = 1 \vee j = 1$

(Continued on next page)

Table 4.7: Possible S-basis and resulting estimable functions for some models with distinct clocks and estimation of ionosphere.

Case. S-basis	Estimable functions	
L1 and L2 and P1	*(Continued from previous page)*	
$\lambda_2 N^j_{i,\mathrm{L2}}$ $i=1 \vee j=1$	$\mathcal{I}^j_i + \frac{1}{\eta_1}\{c(\delta t_{i,\mathrm{L1}} - \delta t^{j,\mathrm{L1}}) + \lambda_1(N^1_{i,\mathrm{L1}} + N^j_{1,\mathrm{L1}} - N^1_{1,\mathrm{L1}})\}$	$i \neq 1 \wedge j \neq 1$
	$\lambda_1(N^j_{i,\mathrm{L1}} - N^1_{i,\mathrm{L1}} - N^j_{1,\mathrm{L1}} + N^1_{1,\mathrm{L1}})$	$i \neq 1 \wedge j \neq 1$
	$\lambda_2(N^j_{i,\mathrm{L2}} - N^1_{i,\mathrm{L2}} - N^j_{1,\mathrm{L2}} + N^1_{1,\mathrm{L2}})$	$i \neq 1 \wedge j \neq 1$
L1 and P1 and P2	$c(\delta t_{i,\mathrm{P1}} - \delta t_{1,\mathrm{P1}}) - \frac{\eta_3}{\eta_1}\{c(\delta t_{i,\mathrm{L1}} - \delta t_{1,\mathrm{L1}}) - \lambda_1(N^1_{1,\mathrm{L1}} - N^1_{i,\mathrm{L1}})\}$	$i \neq 1$
$c\delta t_{i,\mathrm{L1}}$ $c\delta t^{j,\mathrm{L1}}$	$c(\delta t^{j,\mathrm{P1}} - \delta t_{1,\mathrm{P1}}) - \frac{\eta_3}{\eta_1}\{c(\delta t^{j,\mathrm{L1}} - \delta t_{1,\mathrm{L1}}) - \lambda_1 N^j_{1,\mathrm{L1}}\}$	
$c\delta t_{1,\mathrm{P1}}$	$c(\delta t_{i,\mathrm{P2}} - \delta t_{1,\mathrm{P2}}) - \frac{\eta_4}{\eta_1}\{c(\delta t_{i,\mathrm{L1}} - \delta t_{1,\mathrm{L1}}) - \lambda_1(N^1_{1,\mathrm{L1}} - N^1_{i,\mathrm{L1}})\}$	$i \neq 1$
$c\delta t_{1,\mathrm{P2}}$	$c(\delta t^{j,\mathrm{P2}} - \delta t_{1,\mathrm{P2}}) - \frac{\eta_4}{\eta_1}\{c(\delta t^{j,\mathrm{L1}} - \delta t_{1,\mathrm{L1}}) - \lambda_1 N^j_{1,\mathrm{L1}}\}$	
$\lambda_1 N^j_{i,\mathrm{L1}}$ $i=1 \vee j=1$	$\mathcal{I}^j_i + \frac{1}{\eta_1}\{c(\delta t_{i,\mathrm{L1}} - \delta t^{j,\mathrm{L1}}) + \lambda_1 N^i_{j,\mathrm{L1}}\}$	$i=1 \vee j=1$
	$\mathcal{I}^j_i + \frac{1}{\eta_1}\{c(\delta t_{i,\mathrm{L1}} - \delta t^{j,\mathrm{L1}}) + \lambda_1(N^1_{i,\mathrm{L1}} + N^j_{1,\mathrm{L1}} - N^1_{1,\mathrm{L1}})\}$	$i \neq 1 \wedge j \neq 1$
	$\lambda_1(N^j_{i,\mathrm{L1}} - N^1_{i,\mathrm{L1}} - N^j_{1,\mathrm{L1}} + N^1_{1,\mathrm{L1}})$	$i \neq 1 \wedge j \neq 1$
L1 and L2 and P1 and P2	$c(\delta t_{i,\mathrm{L3}} - \delta t_{1,\mathrm{L2}}) - \lambda_2(N^1_{1,\mathrm{L2}} - N^1_{i,\mathrm{L2}}) - \frac{\eta_2}{\eta_1}\{c(\delta t_{i,\mathrm{L1}} - \delta t_{1,\mathrm{L1}}) - \lambda_1(N^1_{1,\mathrm{L1}} - N^1_{i,\mathrm{L1}})\}$	$i \neq 1$
$c\delta t_{i,\mathrm{L1}}$ $c\delta t^{j,\mathrm{L1}}$	$c(\delta t^{j,\mathrm{L2}} - \delta t_{1,\mathrm{L2}}) - \lambda_2 N^j_{1,\mathrm{L2}} - \frac{\eta_2}{\eta_1}\{c(\delta t^{j,\mathrm{L1}} - \delta t_{1,\mathrm{L1}}) - \lambda_1 N^j_{1,\mathrm{L1}}\}$	
$c\delta t_{1,\mathrm{L2}}$	$c(\delta t_{i,\mathrm{P1}} - \delta t_{1,\mathrm{P1}}) - \frac{\eta_3}{\eta_1}\{c(\delta t_{i,\mathrm{L1}} - \delta t_{1,\mathrm{L1}}) - \lambda_1(N^1_{1,\mathrm{L1}} - N^1_{i,\mathrm{L1}})\}$	$i \neq 1$
$c\delta t_{1,\mathrm{P1}}$	$c(\delta t^{j,\mathrm{P1}} - \delta t_{1,\mathrm{P1}}) - \frac{\eta_3}{\eta_1}\{c(\delta t^{j,\mathrm{L1}} - \delta t_{1,\mathrm{L1}}) - \lambda_1 N^j_{1,\mathrm{L1}}\}$	
$c\delta t_{1,\mathrm{P2}}$	$c(\delta t_{i,\mathrm{P2}} - \delta t_{1,\mathrm{P2}}) - \frac{\eta_4}{\eta_1}\{c(\delta t_{i,\mathrm{L1}} - \delta t_{1,\mathrm{L1}}) - \lambda_1(N^1_{1,\mathrm{L1}} - N^1_{i,\mathrm{L1}})\}$	$i \neq 1$
$\lambda_1 N^j_{i,\mathrm{L1}}$ $i=1 \vee j=1$	$c(\delta t^{j,\mathrm{P2}} - \delta t_{1,\mathrm{P2}}) - \frac{\eta_4}{\eta_1}\{c(\delta t^{j,\mathrm{L1}} - \delta t_{1,\mathrm{L1}}) - \lambda_1 N^j_{1,\mathrm{L1}}\}$	
$\lambda_2 N^j_{i,\mathrm{L2}}$ $i=1 \vee j=1$	$\mathcal{I}^j_i + \frac{1}{\eta_1}\{c(\delta t_{i,\mathrm{L1}} - \delta t^{j,\mathrm{L1}}) + \lambda_1 N^i_{j,\mathrm{L1}}\}$	$i=1 \vee j=1$
	$\mathcal{I}^j_i + \frac{1}{\eta_1}\{c(\delta t_{i,\mathrm{L1}} - \delta t^{j,\mathrm{L1}}) + \lambda_1(N^1_{i,\mathrm{L1}} + N^j_{1,\mathrm{L1}} - N^1_{1,\mathrm{L1}})\}$	$i \neq 1 \wedge j \neq 1$
	$\lambda_1(N^j_{i,\mathrm{L1}} - N^1_{i,\mathrm{L1}} - N^j_{1,\mathrm{L1}} + N^1_{1,\mathrm{L1}})$	$i \neq 1 \wedge j \neq 1$
	$\lambda_2(N^j_{i,\mathrm{L2}} - N^1_{i,\mathrm{L2}} - N^j_{1,\mathrm{L2}} + N^1_{1,\mathrm{L2}})$	$i \neq 1 \wedge j \neq 1$

Table 4.7: Possible S-basis and resulting estimable functions for some models with distinct clocks and estimation of ionosphere.

Case S-basis	Estimable functions	
P1 and P2 $c\delta t_1$	$c(\delta t_i - \delta t_1)$ $c(\delta t^j - \delta t_1)$ $\mathcal{I}_i^j$	$i \neq 1$
L1 and L2 $c\delta t_1$ $\lambda_1 N_{i,\mathrm{L1}}^j \quad i = 1 \vee j = 1$ $\lambda_2 N_{i,\mathrm{L2}}^j$	$c(\delta t_i - \delta t_1) + \frac{\eta_1}{\eta_2 - \eta_1}\lambda_2(N_{1,\mathrm{L2}}^1 - N_{i,\mathrm{L2}}^1) - \frac{\eta_2}{\eta_2 - \eta_1}\lambda_1(N_{1,\mathrm{L1}}^1 - N_{i,\mathrm{L1}}^1)$ $c(\delta t^j - \delta t_1) + \frac{\eta_1}{\eta_2 - \eta_1}\lambda_2 N_{1,\mathrm{L2}}^j - \frac{\eta_2}{\eta_2 - \eta_1}\lambda_1 N_{1,\mathrm{L1}}^j$ $\mathcal{I}_i^j + \frac{1}{\eta_2 - \eta_1}(\lambda_2 N_{i,\mathrm{L2}}^j - \lambda_1 N_{i,\mathrm{L1}}^j)$ $\mathcal{I}_i^j + \frac{1}{\eta_2 - \eta_1}\{\lambda_1(-N_{i,\mathrm{L1}}^1 - N_{1,\mathrm{L1}}^j + N_{1,\mathrm{L1}}^1) - \frac{\eta_1}{\eta_2}\lambda_2(-N_{i,\mathrm{L2}}^1 - N_{1,\mathrm{L2}}^j + N_{1,\mathrm{L2}}^1)\}$ $+ \frac{1}{\eta_2}\lambda_2 N_{i,\mathrm{L2}}^j$ $\lambda_1(N_{i,\mathrm{L1}}^j - N_{i,\mathrm{L1}}^1 - N_{1,\mathrm{L1}}^j + N_{1,\mathrm{L1}}^1) - \frac{\eta_1}{\eta_2}\lambda_2(N_{i,\mathrm{L2}}^j - N_{i,\mathrm{L2}}^1 - N_{1,\mathrm{L2}}^j + N_{1,\mathrm{L2}}^1)$	$i \neq 1$ $i = 1 \vee j = 1$ $i \neq 1 \wedge j \neq 1$ $i \neq 1 \wedge j \neq 1$
L1 and L2 and (P1 or P2) $c\delta t_1$ $\lambda_1 N_{i,\mathrm{L1}}^j \quad i = 1 \vee j = 1$ $\lambda_2 N_{i,\mathrm{L2}}^j$	$c(\delta t_i - \delta t_1) - \frac{\eta_2}{\eta_2 - \eta_1}\lambda_1(N_{1,\mathrm{L1}}^1 - N_{i,\mathrm{L1}}^1)$ $c(\delta t^j - \delta t_1) - \frac{\eta_2}{\eta_2 - \eta_1}\lambda_1 N_{1,\mathrm{L1}}^j$ $\mathcal{I}_i^j + \frac{1}{\eta_2 - \eta_1}\lambda_1 N_{i,\mathrm{L1}}^j$ $\mathcal{I}_i^j + \frac{1}{\eta_2 - \eta_1}\lambda_1(N_{i,\mathrm{L1}}^1 + N_{1,\mathrm{L1}}^j - N_{1,\mathrm{L1}}^1)$ $\lambda_1(N_{i,\mathrm{L1}}^j - N_{i,\mathrm{L1}}^1 - N_{1,\mathrm{L1}}^j + N_{1,\mathrm{L1}}^1)$	$i \neq 1$ $i = 1 \vee j = 1$ $i \neq 1 \wedge j \neq 1$ $i \neq 1 \wedge j \neq 1$
L1 and L2 and P1 and P2 $c\delta t_1$	$c(\delta t_i - \delta t_1)$ $c(\delta t^j - \delta t_1)$ $\mathcal{I}_i^j$ $\lambda_1 N_{i,\mathrm{L1}}^j$ $\lambda_2 N_{i,\mathrm{L2}}^j$	$i \neq 1$

Table 4.8: Possible S-basis and resulting estimable functions for some models with common clocks and estimation of ionosphere.

The weights for the pseudo observables are chosen such that they reflect the size and variability of the ionospheric delay, which depend on geographic location, time of day, and sun spot cycle.

The rank defect and resulting estimable functions equal those of the models where no ionosphere is estimated, i.e. we have again DD like integer functions of ambiguities.

The precision of the estimates depends on the precision of the ionospheric pseudo observables. For $\sigma^2_{l_i^j} = 0$, the precision equals that of the estimates from the model without estimation of ionosphere, for $\sigma^2_{l_i^j} = \infty$ it equals that of the model with estimation of ionosphere. In the latter case, no integer DD ambiguities are estimated.

If these ionospheric constraints are included, the minimum number of GPS observable types is one, as in the case where no ionospheric delays are estimated.

4.2.5 Group delays

Estimation of satellite clock errors at the Control Segment (CS).
Although in Eqs. (2.3) and (2.4) no group delays (also called instrumental delay biases, or equipment delays) are included since they are not estimated in our processing setup, they are in principle present. These delays are assumed to be constant, but different for P1 and P2. They occur both in the receiver and the satellite. If we denote the receiver group delay for Pl as $\mathrm{d}_{i,\mathrm{P}l}$ and the satellite group delay for Pl as $\mathrm{d}^{j,\mathrm{P}l}$, the augmented observation equations for P1 and P2 for the model with common clocks and in which ionospheric delays are included, read

$$P^j_{i,\mathrm{P1}} = \rho^j_i + c\delta t_i - c\delta t^j + \mathcal{I}^j_i + \mathrm{d}_{i,\mathrm{P1}} + \mathrm{d}^{j,\mathrm{P1}} + \varepsilon_{P^j_{i,\mathrm{P1}}} \tag{4.9}$$

$$P^j_{i,\mathrm{P2}} = \rho^j_i + c\delta t_i - c\delta t^j + \gamma\mathcal{I}^j_i + \mathrm{d}_{i,\mathrm{P2}} + \mathrm{d}^{j,\mathrm{P2}} + \varepsilon P^j_{i,\mathrm{P2}} \tag{4.10}$$

Inclusion of the group delays in the model causes an additional rank defect of $2(r+m)$, i.e. the group delays itself are not estimable. If we choose for the S-basis all group delays and the clock of one receiver, the resulting estimable functions are

$$\begin{aligned} & c(\delta t_i - \delta t_1) - \frac{\gamma}{1-\gamma}(\mathrm{d}_{i,\mathrm{P1}} - \mathrm{d}_{1,\mathrm{P1}}) + \frac{1}{1-\gamma}(\mathrm{d}_{i,\mathrm{P2}} - \mathrm{d}_{1,\mathrm{P2}}) \qquad i \neq 1 \\ & c(\delta t^j - \delta t_1) + \frac{\gamma}{1-\gamma}(\mathrm{d}^{j,\mathrm{P1}} + \mathrm{d}_{1,\mathrm{P1}}) - \frac{1}{1-\gamma}(\mathrm{d}^{j,\mathrm{P2}} + \mathrm{d}_{1,\mathrm{P2}}) \\ & \mathcal{I}^j_i + \frac{1}{1-\gamma}(\mathrm{d}^{j,\mathrm{P1}} + \mathrm{d}_{i,\mathrm{P1}} - \mathrm{d}^{j,\mathrm{P2}} - \mathrm{d}_{i,\mathrm{P2}}) \end{aligned} \tag{4.11}$$

Assuming the receiver clock errors and group delays are known, which e.g. for the receivers of the CS is a valid assumption, we have:

$$E\{c\hat{\delta t}^j\} = c\delta t^j + \frac{\gamma}{1-\gamma}\mathrm{d}^{j,\mathrm{P1}} - \frac{1}{1-\gamma}\mathrm{d}^{j,\mathrm{P2}} \tag{4.12}$$

$$E\{\hat{\mathcal{I}}^j_i\} = \mathcal{I}^j_i + \frac{1}{1-\gamma}(\mathrm{d}^{j,\mathrm{P1}} - \mathrm{d}^{j,\mathrm{P2}}) \tag{4.13}$$

The polynomial clock model in the broadcast ephemerides is based on Eq. (4.12). To enable a meaningful physical interpretation of the estimates of the clock error and ionospheric

delays, this clock model has to be corrected. For this purpose in the broadcast ephemerides for each satellite the parameter T_{GD}^{j} is provided, which is defined as (Spilker Jr. 1996)

$$T_{\mathrm{GD}}^{j} = \frac{1}{1-\gamma}(\mathrm{d}^{j,\mathrm{P1}} - \mathrm{d}^{j,\mathrm{P2}}) \tag{4.14}$$

No estimation of ionosphere, distinct clocks.
If we correct P1 and P2 using the polynomial clock model only, we have

$$\begin{aligned}\bar{P}_{i,\mathrm{P1}}^{j} &= \rho_i^j + c\delta t_{i,\mathrm{P1}} - c\bar{\delta}t^{j,\mathrm{P1}} + \mathrm{d}_{i,\mathrm{P1}} + \mathrm{d}^{j,\mathrm{P1}} + \frac{\gamma}{1-\gamma}\mathrm{d}^{j,\mathrm{P1}} - \frac{1}{1-\gamma}\mathrm{d}^{j,\mathrm{P2}} + \varepsilon_{\bar{P}_{i,\mathrm{P1}}^{j}} \\ &= \rho_i^j + c\delta t_{i,\mathrm{P1}} - c\bar{\delta}t^{j,\mathrm{P1}} + \mathrm{d}_{i,\mathrm{P1}} + \mathrm{d}^{j} + \varepsilon_{\bar{P}_{i,\mathrm{P1}}^{j}} \end{aligned} \tag{4.15}$$

$$\begin{aligned}\bar{P}_{i,\mathrm{P2}}^{j} &= \rho_i^j + c\delta t_{i,\mathrm{P2}} - c\bar{\delta}t^{j,\mathrm{P2}} + \mathrm{d}_{i,\mathrm{P2}} + \mathrm{d}^{j,\mathrm{P2}} + \frac{\gamma}{1-\gamma}\mathrm{d}^{j,\mathrm{P1}} - \frac{1}{1-\gamma}\mathrm{d}^{j,\mathrm{P2}} + \varepsilon_{\bar{P}_{i,\mathrm{P2}}^{j}} \\ &= \rho_i^j + c\delta t_{i,\mathrm{P2}} - c\bar{\delta}t^{j,\mathrm{P2}} + \mathrm{d}_{i,\mathrm{P2}} + \gamma\mathrm{d}^{j} + \varepsilon_{\bar{P}_{i,\mathrm{P2}}^{j}} \end{aligned} \tag{4.16}$$

with

$$d^{j} = \frac{1}{1-\gamma}(\mathrm{d}^{j,\mathrm{P1}} - \mathrm{d}^{j,\mathrm{P2}}) \tag{4.17}$$

which equals the definition of the correction term T_{GD}^{j}. The term $c\bar{\delta}t^{j,\mathrm{P}l}, l = 1,2$ contains the mismodeling of the satellite clock by the CS, the SA effect, and part of the atmospheric delays. (Since these delays are not modeled they are absorbed by the parameters that are.)

The resulting estimable functions for an S-basis consisting of the average of all satellite clocks are then

$$\begin{aligned} &c(\delta t_{i,\mathrm{P1}} - \frac{1}{m}\sum_{j=1}^{m}\bar{\delta}t^{j,\mathrm{P1}}) + \mathrm{d}_{i,\mathrm{P1}} + \mathrm{d}^{j} \\ &c(\bar{\delta}t^{j,\mathrm{P1}} - \frac{1}{m}\sum_{j=1}^{m}\bar{\delta}t^{j,\mathrm{P1}}) \end{aligned} \tag{4.18}$$

$$\begin{aligned} &c(\delta t_{i,\mathrm{P2}} - \frac{1}{m}\sum_{j=1}^{m}\bar{\delta}t^{j,\mathrm{P2}}) + \mathrm{d}_{i,\mathrm{P2}} + \gamma\mathrm{d}^{j} \\ &c(\bar{\delta}t^{j,\mathrm{P2}} - \frac{1}{m}\sum_{j=1}^{m}\bar{\delta}t^{j,\mathrm{P2}}) \end{aligned} \tag{4.19}$$

If we correct P1 and P2 using the polynomial clock model plus the correction term T_{GD}^{j}, we have

$$\begin{aligned}\bar{P}_{i,\mathrm{P1}}^{j} &= \rho_i^j + c\delta t_{i,\mathrm{P1}} - c\bar{\delta}t^{j,\mathrm{P1}} + \mathrm{d}_{i,\mathrm{P1}} + \mathrm{d}^{j,\mathrm{P1}} + \frac{\gamma}{1-\gamma}\mathrm{d}^{j,\mathrm{P1}} - \frac{1}{1-\gamma}\mathrm{d}^{j,\mathrm{P2}} - T_{\mathrm{GD}}^{j} + \varepsilon_{\bar{P}_{i,\mathrm{P1}}^{j}} \\ &= \rho_i^j + c\delta t_{i,\mathrm{P1}} - c\bar{\delta}t^{j,\mathrm{P1}} + \mathrm{d}_{i,\mathrm{P1}} + \varepsilon_{\bar{P}_{i,\mathrm{P1}}^{j}} \end{aligned} \tag{4.20}$$

$$\begin{aligned}\bar{P}_{i,\mathrm{P2}}^{j} &= \rho_i^j + c\delta t_{i,\mathrm{P2}} - c\bar{\delta}t^{j,\mathrm{P2}} + \mathrm{d}_{i,\mathrm{P2}} + \mathrm{d}^{j,\mathrm{P2}} + \frac{\gamma}{1-\gamma}\mathrm{d}^{j,\mathrm{P1}} - \frac{1}{1-\gamma}\mathrm{d}^{j,\mathrm{P2}} - \gamma T_{\mathrm{GD}}^{j} + \varepsilon_{\bar{P}_{i,\mathrm{P2}}^{j}} \\ &= \rho_i^j + c\delta t_{i,\mathrm{P2}} - c\bar{\delta}t^{j,\mathrm{P2}} + \mathrm{d}_{i,\mathrm{P2}} + \varepsilon_{\bar{P}_{i,\mathrm{P2}}^{j}} \end{aligned} \tag{4.21}$$

The resulting estimable functions for an S-basis consisting of the average of all satellite clocks are then ($l = 1, 2$):

$$\begin{aligned} & c(\delta t_{i,\mathrm{P}l} - \frac{1}{m}\sum_{j=1}^{m}\bar{\delta}t^{j,\mathrm{P}l}) + \mathrm{d}_{i,\mathrm{P}l} \\ & c(\bar{\delta}t^{j,\mathrm{P}l} - \frac{1}{m}\sum_{j=1}^{m}\bar{\delta}t^{j,\mathrm{P}l}) \end{aligned} \tag{4.22}$$

Estimation of ionosphere, common clocks.
If we correct P1 and P2 using the polynomial clock model only, we have

$$\begin{aligned} \bar{P}^j_{i,\mathrm{P1}} &= \rho^j_i + c\delta t_i - c\bar{\delta}t^j + \mathcal{I}^j_i + \mathrm{d}_{i,\mathrm{P1}} + \mathrm{d}^{j,\mathrm{P1}} + \frac{\gamma}{1-\gamma}\mathrm{d}^{j,\mathrm{P1}} - \frac{1}{1-\gamma}\mathrm{d}^{j,\mathrm{P2}} + \varepsilon_{\bar{P}^j_{i,\mathrm{P1}}} \\ &= \rho^j_i + c\delta t_i - c\bar{\delta}t^j + \mathcal{I}^j_i + \mathrm{d}_{i,\mathrm{P1}} + \mathrm{d}^j + \varepsilon_{\bar{P}^j_{i,\mathrm{P1}}} \end{aligned} \tag{4.23}$$

$$\begin{aligned} \bar{P}^j_{i,\mathrm{P2}} &= \rho^j_i + c\delta t_i - c\bar{\delta}t^j + \gamma\mathcal{I}^j_i + \mathrm{d}_{i,\mathrm{P2}} + \mathrm{d}^{j,\mathrm{P2}} + \frac{\gamma}{1-\gamma}\mathrm{d}^{j,\mathrm{P1}} - \frac{1}{1-\gamma}\mathrm{d}^{j,\mathrm{P2}} + \varepsilon_{\bar{P}^j_{i,\mathrm{P2}}} \\ &= \rho^j_i + c\delta t_i - c\bar{\delta}t^j + \gamma\mathcal{I}^j_i + \mathrm{d}_{i,\mathrm{P2}} + \gamma\mathrm{d}^j + \varepsilon_{\bar{P}^j_{i,\mathrm{P2}}} \end{aligned} \tag{4.24}$$

The term $c\bar{\delta}t^j$ contains now only the mismodeling of the satellite clock by the CS plus the SA effect.

The resulting estimable functions for an S-basis consisting of the average of all satellite clocks are then

$$\begin{aligned} & c(\delta t_i - \frac{1}{m}\sum_{j=1}^{m}\bar{\delta}t^j) - \frac{\gamma}{1-\gamma}\mathrm{d}_{i,\mathrm{P1}} + \frac{1}{1-\gamma}\mathrm{d}_{i,\mathrm{P2}} \\ & c(\bar{\delta}t^j - \frac{1}{m}\sum_{j=1}^{m}\bar{\delta}t^j) \\ & \mathcal{I}^j_i + \frac{1}{1-\gamma}(\mathrm{d}_{i,\mathrm{P1}} - \mathrm{d}_{i,\mathrm{P2}}) + \mathrm{d}^j \end{aligned} \tag{4.25}$$

This shows that as far as the satellite clock terms are concerned, applying the correction term T^j_{GD} is not needed. To remove the bias in the estimates for the ionospheric delay one should apply it, though.

If we correct P1 and P2 using the polynomial clock model plus the correction term T^j_{GD} we have:

$$\begin{aligned} \bar{P}^j_{i,\mathrm{P1}} &= \rho^j_i + c\delta t_i - c\bar{\delta}t^j + \mathcal{I}^j_i + \mathrm{d}_{i,\mathrm{P1}} + \mathrm{d}^{j,\mathrm{P1}} + \frac{\gamma}{1-\gamma}\mathrm{d}^{j,\mathrm{P1}} - \frac{1}{1-\gamma}\mathrm{d}^{j,\mathrm{P2}} - T^j_{\mathrm{GD}} + \varepsilon_{\bar{P}^j_{i,\mathrm{P1}}} \\ &= \rho^j_i + c\delta t_i - c\bar{\delta}t^j + \mathcal{I}^j_i + \mathrm{d}_{i,\mathrm{P1}} + \varepsilon_{\bar{P}^j_{i,\mathrm{P1}}} \end{aligned} \tag{4.26}$$

$$\begin{aligned} \bar{P}^j_{i,\mathrm{P2}} &= \rho^j_i + c\delta t_i - c\bar{\delta}t^j + \gamma\mathcal{I}^j_i + \mathrm{d}_{i,\mathrm{P2}} + \mathrm{d}^{j,\mathrm{P2}} + \frac{\gamma}{1-\gamma}\mathrm{d}^{j,\mathrm{P1}} - \frac{1}{1-\gamma}\mathrm{d}^{j,\mathrm{P2}} - \gamma T^j_{\mathrm{GD}} + \varepsilon_{\bar{P}^j_{i,\mathrm{P2}}} \\ &= \rho^j_i + c\delta t_i - c\bar{\delta}t^j + \gamma\mathcal{I}^j_i + \mathrm{d}_{i,\mathrm{P2}} + \varepsilon_{\bar{P}^j_{i,\mathrm{P2}}} \end{aligned} \tag{4.27}$$

The resulting estimable functions for an S-basis consisting of the average of all satellite clocks are then

$$\begin{aligned} & c(\delta t_i - \frac{1}{m}\sum_{j=1}^{m}\bar{\delta}t^j) - \frac{\gamma}{1-\gamma}\mathrm{d}_{i,\mathrm{P1}} + \frac{1}{1-\gamma}\mathrm{d}_{i,\mathrm{P2}} \\ & c(\bar{\delta}t^j - \frac{1}{m}\sum_{j=1}^{m}\bar{\delta}t^j) \\ & \mathcal{I}_i^j + \frac{1}{1-\gamma}(\mathrm{d}_{i,\mathrm{P1}} - \mathrm{d}_{i,\mathrm{P2}}) \end{aligned} \tag{4.28}$$

In Figure 4.1 we plotted the estimates for the correction to the satellite clock delay as defined in (4.28) for all GPS satellites for the time spans during April 20, 1997 they were visible by at least two stations out of the set Kootwijk, Brussels and Herstmonceux.

Between approximately 6:00 and 20:00 GPS time, SA was switched off or significantly reduced for most satellites. In Figure 4.2 an enlargement of Figure 4.1 for `PRN14` and `PRN15` for the time span 16:00-24:00 is shown. One can clearly see the transition from SA off to SA on, at approximately 20:00. For these two satellites we see that with SA off the nominal noise level of the clock delays is of the order of a few meters, which corresponds to approximately 10 ns for the clock errors. The SA effect on `PRN15` is comparatively small, an observation which is confirmed by others, see e.g. Langley (1997).

4.2.6 Absorbing of atmospheric delays by the satellite clock

For short inter-station distances atmospheric delays are usually not modeled. Although the coordinate and possible ambiguity parameters are not, or hardly influenced by omitting the atmospheric delays from the model, the satellite clock parameters are. The tropospheric and ionospheric delays are, depending on the inter-station distance, fully or partly absorbed by the satellite clock parameters.

The observation equations for the L1 and L2 phase observables read (we do not apply a mapping function for the tropospheric delay here)

$$\begin{aligned} \Phi_{i,\mathrm{L1}}^j &= \rho_i^j + c\delta t_{i,\mathrm{L1}} - c\delta t^{j,\mathrm{L1}} + T_i^j - \mathcal{I}_i^j + \lambda_1 N_{i,\mathrm{L1}}^j + \varepsilon_{\Phi_{i,\mathrm{L1}}^j} \\ \Phi_{i,\mathrm{L2}}^j &= \rho_i^j + c\delta t_{i,\mathrm{L2}} - c\delta t^{j,\mathrm{L2}} + T_i^j - \gamma\mathcal{I}_i^j + \lambda_2 N_{i,\mathrm{L2}}^j + \varepsilon_{\Phi_{i,\mathrm{L2}}^j} \end{aligned} \tag{4.29}$$

In the extreme case, viz. a zero baseline, the tropospheric and ionospheric delays sensed by both receivers are by definition equal, since the signals are received by the same antenna. Therefore the observation equations can be rewritten as

$$\begin{aligned} \Phi_{i,\mathrm{L1}}^j &= \rho_i^j + c\delta t_{i,\mathrm{L1}} - c\delta t^{j,\mathrm{L1}} + T^j - \mathcal{I}^j + \lambda_1 N_{i,\mathrm{L1}}^j + \varepsilon_{\Phi_{i,\mathrm{L1}}^j} \\ \Phi_{i,\mathrm{L2}}^j &= \rho_i^j + c\delta t_{i,\mathrm{L2}} - c\delta t^{j,\mathrm{L2}} + T^j - \gamma\mathcal{I}^j + \lambda_2 N_{i,\mathrm{L2}}^j + \varepsilon_{\Phi_{i,\mathrm{L2}}^j} \end{aligned} \tag{4.30}$$

Note that the tropospheric and ionospheric delays are equal for a certain satellite for both receivers (hence $\mathcal{I}^j$ and T^j instead of $\mathcal{I}_i^j$ and T_i^j). Since we have taken into account both the initial phase at receiver and satellite (they are included in the definition for N_i^j) and the

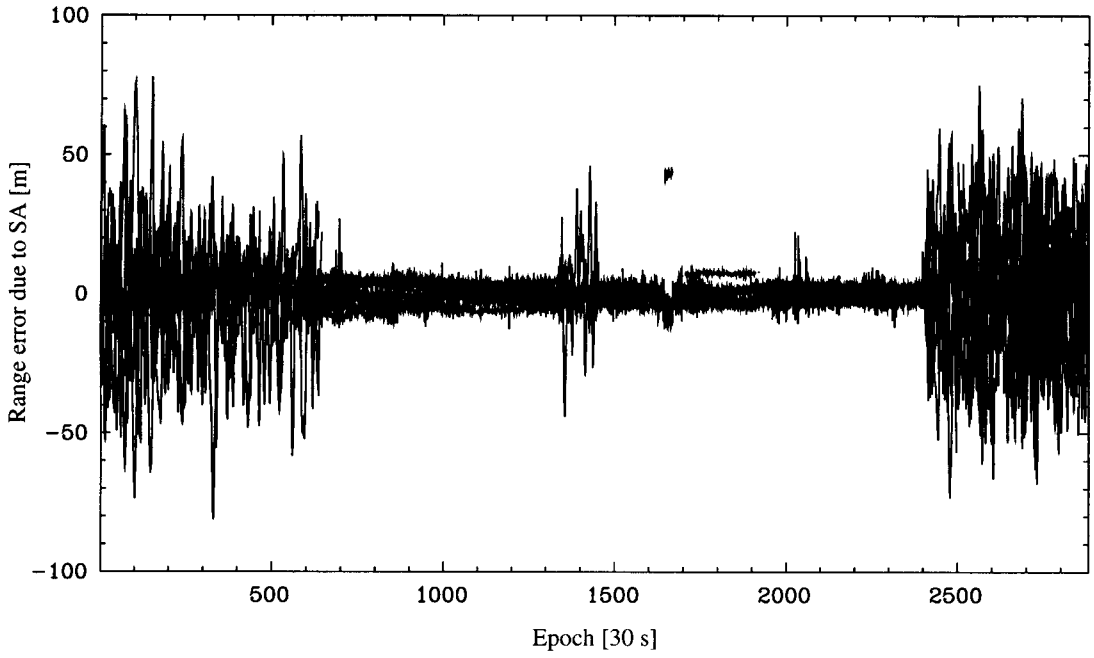

Figure 4.1: Range errors due to SA for all GPS satellites visible from Kootwijk, Brussels and Herstmonceux at April 20, 1997.

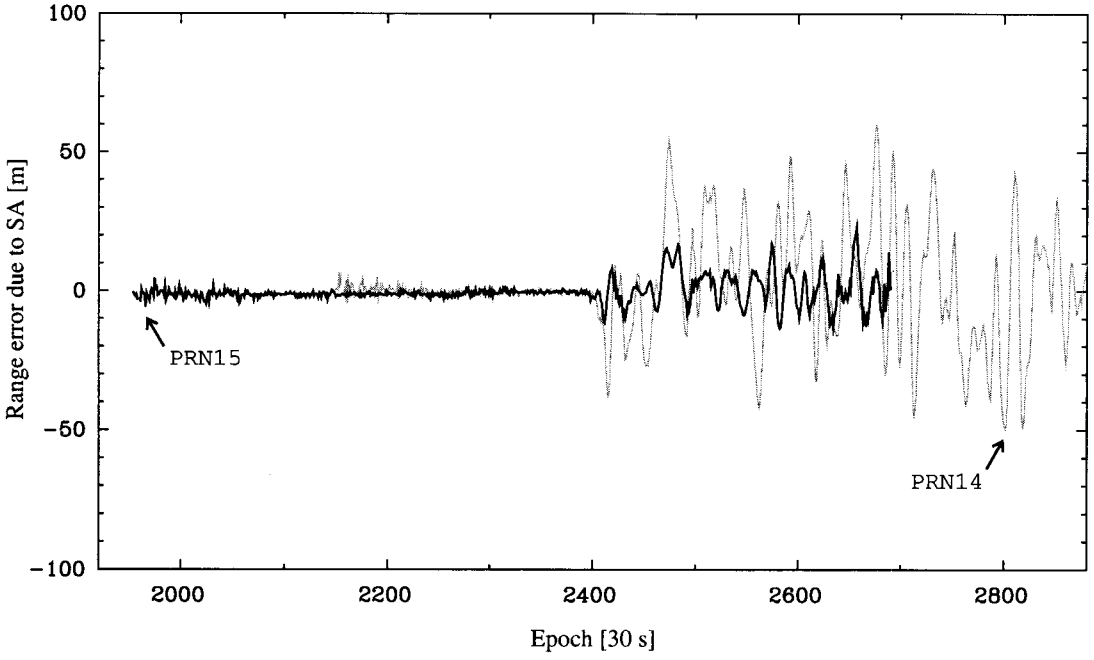

Figure 4.2: Range errors due to SA for PRN14 and PRN15 on April 20, 1997, for the time span 16:00-24:00 (GPS time).

atmospheric delays, we may replace the distinct clock errors $\delta t^{j,\mathrm{L1}}$ and $\delta t^{j,\mathrm{L2}}$ by a common clock error δt^j:

$$\begin{aligned}\Phi^j_{i,\mathrm{L1}} &= \rho^j_i + c\delta t_{i,\mathrm{L1}} - \overbrace{\left(c\delta t^j - T^j + \mathcal{I}^j\right)}^{c\delta t^{j,\mathrm{L1}}} + \lambda_1 N^j_{i,\mathrm{L1}} + \varepsilon_{\Phi^j_{i,\mathrm{L1}}} \\ \Phi^j_{i,\mathrm{L2}} &= \rho^j_i + c\delta t_{i,\mathrm{L2}} - \underbrace{\left(c\delta t^j - T^j + \gamma\mathcal{I}^j\right)}_{c\delta t^{j,\mathrm{L2}}} + \lambda_2 N^j_{i,\mathrm{L2}} + \varepsilon_{\Phi^j_{i,\mathrm{L2}}}\end{aligned} \tag{4.31}$$

This leads to the structure of the L1 and L2 model with distinct clocks without estimation of ionospheric slant delay parameters. It has a rank defect of $2n+2(r+m-1)$, see Tables 4.3 and 4.6.

In Figure 4.3 the differences between the L1 and L2 phase clock delay estimates for a zero baseline are plotted. They result from a zero baseline test using Trimble 4000 SSI receivers. A solution was computed for the whole time span of 3596 seconds, with L1 and L2 phase data. The estimated parameters were coordinates, receiver and satellite clocks, and ambiguities. The time tags were corrected using clocks from a previous pseudorange solution, satellite clock errors were corrected using the model in the broadcast ephemerides and an a priori correction for the troposphere was computed using the Saastamoinen model. As S-basis the average of the satellite clocks on L1 and the average of the satellite clocks on L2 was chosen. As far as the receiver clocks of the first receiver is concerned, the resulting estimable functions are then

$$c\delta t_{1,\mathrm{L1}} - \frac{1}{m}\sum_{j=1}^{m}(c\delta t^j - T^j + \mathcal{I}^j) + \lambda_1\frac{1}{m}\sum_{j=1}^{m}N^j_{1,\mathrm{L1}} \tag{4.32}$$

$$c\delta t_{1,\mathrm{L2}} - \frac{1}{m}\sum_{j=1}^{m}(c\delta t^j - T^j + \gamma\mathcal{I}^j) + \lambda_2\frac{1}{m}\sum_{j=1}^{m}N^j_{1,\mathrm{L2}} \tag{4.33}$$

Using the same argument as we used for the satellite clocks, we may replace the distinct receiver clocks $\delta t_{i,\mathrm{L1}}$ and $\delta t_{i,\mathrm{L2}}$ by a common clock δt_i. Subtracting (4.33) from (4.32) gives then

$$-(1-\gamma)\frac{1}{m}\sum_{j=1}^{m}\mathcal{I}^j + \lambda_1\frac{1}{m}\sum_{j=1}^{m}N^j_{1,\mathrm{L1}} - \lambda_2\frac{1}{m}\sum_{j=1}^{m}N^j_{1,\mathrm{L2}} \tag{4.34}$$

To get rid of the bias due to the ambiguities, the value of the first epoch was subtracted from the values of the subsequent epochs, which gives

$$-(1-\gamma)\left(\frac{1}{m}\sum_{j=1}^{m}\mathcal{I}^{j,k} - \frac{1}{m}\sum_{j=1}^{m}\mathcal{I}^{j,1}\right) \tag{4.35}$$

As long as the same set of satellites is tracked, and no slips occur, the obtained differences are all biased by the same unknown value, which is a function of the ambiguities. Since changes did occur, three time spans were selected where the configuration remained constant. Note that each time span is biased by a different value, that was set arbitrarily to zero in the plot. For this example, the maximum difference between the two clocks can be as large as approximately 4 cm. These differences are mainly due to the unmodeled ionospheric delay. The size of this effect is different for the two carrier phases because of the ionosphere's

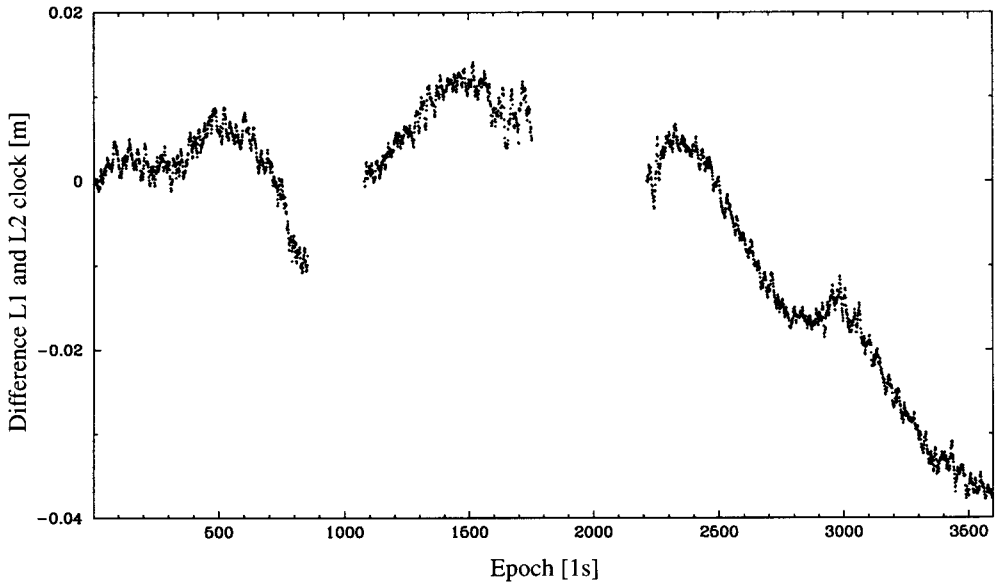

Figure 4.3: Biased difference between L1 and L2 (phase) clock delay estimates for a zero baseline.

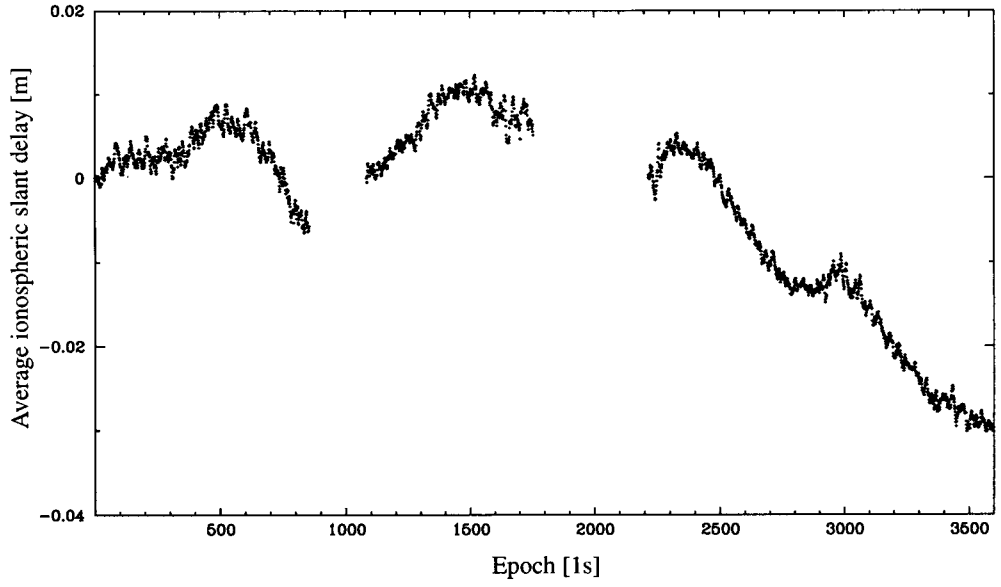

Figure 4.4: Biased average ionospheric slant delay estimates from an L1 and L2 (phase) solution with common clocks, for a zero baseline.

dispersive character. Subtracting the two delays gives $-(1-\gamma) \approx 0.65$ times the ionospheric delay at the L1 phase carrier.

The receiver clock errors are therefore biased by the average of the ionospheric delays. Another effect that may play a role here are time varying, dispersive delays in the receiver and satellite hardware.

As a comparison we processed the same data using a model in which ionospheric slant delays are estimated, and where a common clock for the L1 and L2 is assumed. The resulting estimates for the ionospheric slant delays are then biased by some function of the ambiguities. Again this function remains constant as long as no change of configuration or cycle slip occurs. In Figure 4.4 the average over the satellites of these estimates are plotted, for the same three time spans as in Figure 4.3. The average of the ionospheric delays for the first receiver reads

$$\frac{1}{m}\sum_{j=1}^{m}\mathcal{I}^j + \frac{1}{1-\gamma}\left(\lambda_2\frac{1}{m}\sum_{j=1}^{m}N^j_{1,\mathrm{L2}} - \lambda_1\frac{1}{m}\sum_{j=1}^{m}N^j_{1,\mathrm{L1}}\right) \tag{4.36}$$

Again the unknown biases for each time span are set to zero analogously to what we did for the plot of the difference of the clock errors. To facilitate comparison with Figure 4.3, the delays are multiplied by $-(1-\gamma)$, giving

$$-(1-\gamma)\left(\frac{1}{m}\sum_{j=1}^{m}\mathcal{I}^{j,k} - \frac{1}{m}\sum_{j=1}^{m}\mathcal{I}^{j,1}\right) \tag{4.37}$$

Comparing the two plots we see that the details in both plots are similar.

4.3 Linear combinations of observable types

In the DD setup, usually transformations to the original observable types are applied to eliminate model parameters (e.g. ionospheric slant delays), or to transform ambiguity parameters (e.g. wide lane transformation).

Some of these transformations maintain the information content of the system since they are invertible, but also transformations are used that do not. The latter should be used with care, since information that contributes to the parameters of interest is lost.

In this section some of these transformations will be treated, and the connection with the undifferenced approach will be shown (if existing).

4.3.1 The ionosphere-free linear combination

The equivalent of the model with distinct clocks and estimation of ionosphere is the ionosphere-free linear combination. It is constructed from the L1 and L2 carrier phase observable types (denoted as L3 or LC linear combination), or from the P1 and P2 pseudorange observable types. As the name already indicates, the new observable type is not affected anymore by the ionosphere.

We will show here the construction of the carrier phase ionosphere-free linear combination. The construction of the pseudorange ionosphere-free linear combination is done analogously. Starting with the non-linear observation equations for both carrier phases

$$\begin{aligned}\Phi^j_{i,\mathrm{L1}} &= \rho^j_i + \lambda_1 N^j_{i,\mathrm{L1}} + c\delta t_{i,\mathrm{L1}} - c\delta t^{j,\mathrm{L1}} + \eta_1\mathcal{I}^j_i + \varepsilon_{\Phi^j_{i,\mathrm{L1}}}\\ \Phi^j_{i,\mathrm{L2}} &= \rho^j_i + \lambda_2 N^j_{i,\mathrm{L2}} + c\delta t_{i,\mathrm{L2}} - c\delta t^{j,\mathrm{L2}} + \eta_2\mathcal{I}^j_i + \varepsilon_{\Phi^j_{i,\mathrm{L2}}}\end{aligned} \tag{4.38}$$

the system of linearized observation equations reads

$$E\{\begin{bmatrix}\Phi^j_{i,\mathrm{L1}}\\ \Phi^j_{i,\mathrm{L2}}\end{bmatrix}\} = \begin{bmatrix} g & I & & d & & \eta_1 I\\ g & & I & & d & \eta_2 I\end{bmatrix}\begin{bmatrix} r_i\\ \lambda_1 N^j_{i,\mathrm{L1}}\\ \lambda_2 N^j_{i,\mathrm{L2}}\\ \begin{bmatrix} c\delta t_{i,\mathrm{L1}}\\ c\delta t^{j,\mathrm{L1}}\end{bmatrix}\\ \begin{bmatrix} c\delta t_{i,\mathrm{L2}}\\ c\delta t^{j,\mathrm{L2}}\end{bmatrix}\\ \mathcal{I}^j_i\end{bmatrix} \tag{4.39}$$

The ionospheric delays can be eliminated by applying the transformation

$$\begin{bmatrix}\frac{\eta_2}{\eta_2-\eta_1} & \frac{-\eta_1}{\eta_2-\eta_1}\end{bmatrix}\otimes I = \begin{bmatrix}\frac{{f_1}^2}{{f_1}^2-{f_2}^2} & \frac{-{f_2}^2}{{f_1}^2-{f_2}^2}\end{bmatrix}\otimes I \tag{4.40}$$

This transformation is not invertible, and thus it seems that information is lost. That it is still allowed can be seen by looking at the extended invertible transformation

$$\begin{bmatrix}1 & \\ \frac{\eta_2}{\eta_2-\eta_1} & \frac{-\eta_1}{\eta_2-\eta_1}\end{bmatrix}\otimes I \tag{4.41}$$

The transformed system reads then:

$$E\{\begin{bmatrix}\Phi^j_{i,\mathrm{L1}}\\ \frac{\eta_2}{\eta_2-\eta_1}\Phi^j_{i,\mathrm{L1}} - \frac{\eta_1}{\eta_2-\eta_1}\Phi^j_{i,\mathrm{L2}}\end{bmatrix}\} =$$

$$\begin{bmatrix} g & I & & d & & \eta_1 I\\ g & \frac{\eta_2}{\eta_2-\eta_1}I & \frac{-\eta_1}{\eta_2-\eta_1}I & \frac{\eta_2}{\eta_2-\eta_1}d & \frac{-\eta_1}{\eta_2-\eta_1}d & \end{bmatrix}\begin{bmatrix} r_i\\ \lambda_1 N^j_{i,\mathrm{L1}}\\ \lambda_2 N^j_{i,\mathrm{L2}}\\ \begin{bmatrix} c\delta t_{i,\mathrm{L1}}\\ c\delta t^{j,\mathrm{L1}}\end{bmatrix}\\ \begin{bmatrix} c\delta t_{i,\mathrm{L2}}\\ c\delta t^{j,\mathrm{L2}}\end{bmatrix}\\ \mathcal{I}^j_i\end{bmatrix} \tag{4.42}$$

Lumping together the ambiguities and clocks of L1 with the ionospheric delays in the first set of equations, and in the second set of equations the clocks of L1 with the clocks of L2, and the ambiguities of L1 with those of L2, gives:

$$E\{\begin{bmatrix}\Phi^j_{i,\mathrm{L1}}\\ \frac{\eta_2}{\eta_2-\eta_1}\Phi^j_{i,\mathrm{L1}} - \frac{\eta_1}{\eta_2-\eta_1}\Phi^j_{i,\mathrm{L2}}\end{bmatrix}\} =$$

$$\begin{bmatrix} g & & & \eta_1 I\\ g & \frac{-\eta_1}{\eta_2-\eta_1}I & \frac{-\eta_1}{\eta_2-\eta_1}d & \end{bmatrix}\begin{bmatrix} r_i\\ \lambda_2 N^j_{i,\mathrm{L2}} - \frac{\eta_2}{\eta_1}\lambda_1 N^j_{i,\mathrm{L1}}\\ \begin{bmatrix} c\delta t_{i,\mathrm{L2}} - \frac{\eta_2}{\eta_1}c\delta t_{i,\mathrm{L1}}\\ c\delta t^{j,\mathrm{L2}} - \frac{\eta_2}{\eta_1}c\delta t^{j,\mathrm{L1}}\end{bmatrix}\\ \mathcal{I}^j_i + \frac{1}{\eta_1}(\lambda_1 N^j_{i,\mathrm{L1}} + c\delta t_{i,\mathrm{L1}} - c\delta t^{j,\mathrm{L1}})\end{bmatrix} \tag{4.43}$$

In the first set of equations we have for each observable one unknown function of bias parameters. These observables are free variates since they do not contribute to the coordinates nor to the bias parameters involved in the second set of equations. If we are not interested in the function of bias parameters of the first set of equations, we can discard this set. It can easily be seen that we would have obtained the same result if we would have applied the non-invertible transformation of (4.40).

The second set of equations has the form we saw already in Chapter 3, and can be transformed in the same way as the ordinary phase observation equations into DD observation equations.

4.3.2 The wide lane linear combination

To improve ambiguity resolution, often the wide lane linear combination (also called L5 or LW linear combination) is formed from the L1 and L2 carrier phase observable types. The transformation matrix reads

$$T = \begin{bmatrix} \frac{f_1}{f_1-f_2} & -\frac{f_2}{f_1-f_2} \end{bmatrix} \otimes I \tag{4.44}$$

Again this transformation matrix is not invertible; an invertible transformation matrix might read e.g.

$$T = \begin{bmatrix} 1 & \\ \frac{f_1}{f_1-f_2} & -\frac{f_2}{f_1-f_2} \end{bmatrix} \otimes I \tag{4.45}$$

Usually this transformation is applied to the short baseline model, where the ionospheric delays are omitted. The system of linearized observation equations reads

$$E\{\begin{bmatrix} \Phi^j_{i,\mathrm{L1}} \\ \Phi^j_{i,\mathrm{L2}} \end{bmatrix}\} = \begin{bmatrix} g & I & & d & \\ g & & I & & d \end{bmatrix} \begin{bmatrix} r_i \\ \lambda_1 N^j_{i,\mathrm{L1}} \\ \lambda_2 N^j_{i,\mathrm{L2}} \\ \begin{bmatrix} c\delta t_{i,\mathrm{L1}} \\ c\delta t^{j,\mathrm{L1}} \end{bmatrix} \\ \begin{bmatrix} c\delta t_{i,\mathrm{L2}} \\ c\delta t^{j,\mathrm{L2}} \end{bmatrix} \end{bmatrix} \tag{4.46}$$

Applying (4.45) to it gives the transformed system

$$E\{\begin{bmatrix} \Phi^j_{i,\mathrm{L1}} \\ \frac{f_1}{f_1-f_2}\Phi^j_{i,\mathrm{L1}} - \frac{f_2}{f_1-f_2}\Phi^j_{i,\mathrm{L2}} \end{bmatrix}\} = \begin{bmatrix} g & I & & d & \\ g & \frac{f_1}{f_1-f_2}I & -\frac{f_2}{f_1-f_2}I & \frac{f_1}{f_1-f_2}d & -\frac{f_2}{f_1-f_2}d \end{bmatrix} \begin{bmatrix} r_i \\ \lambda_1 N^j_{i,\mathrm{L1}} \\ \lambda_2 N^j_{i,\mathrm{L2}} \\ \begin{bmatrix} c\delta t_{i,\mathrm{L1}} \\ c\delta t^{j,\mathrm{L1}} \end{bmatrix} \\ \begin{bmatrix} c\delta t_{i,\mathrm{L2}} \\ c\delta t^{j,\mathrm{L2}} \end{bmatrix} \end{bmatrix} \tag{4.47}$$

Lumping together in the second set of equations the clocks of L1 and L2 and the ambiguities of L1 and L2 gives:

$$E\{\begin{bmatrix} \Phi^j_{i,\mathrm{L1}} \\ \frac{f_1}{f_1-f_2}\Phi^j_{i,\mathrm{L1}} - \frac{f_2}{f_1-f_2}\Phi^j_{i,\mathrm{L2}} \end{bmatrix}\} = \begin{bmatrix} g & I & & d & \\ g & & I & & d \end{bmatrix} \begin{bmatrix} r_i \\ \lambda_1 N^j_{i,\mathrm{L1}} \\ \frac{c}{f_1-f_2}(N^j_{i,\mathrm{L1}} - N^j_{i,\mathrm{L2}}) \\ \begin{bmatrix} c\delta t_{i,\mathrm{L1}} \\ c\delta t^{j,\mathrm{L1}} \end{bmatrix} \\ \frac{f_1}{f_1-f_2}\begin{bmatrix} c\delta t_{i,\mathrm{L1}} \\ c\delta t^{j,\mathrm{L1}} \end{bmatrix} - \frac{f_2}{f_1-f_2}\begin{bmatrix} c\delta t_{i,\mathrm{L2}} \\ c\delta t^{j,\mathrm{L2}} \end{bmatrix} \end{bmatrix} \tag{4.48}$$

In contrast to what we saw with the ionosphere-free linear combination, the two sets of transformed observation equations can *not* be treated separately, since they have the geometric parameters in common.

4.3.3 The Melbourne-Wübbena linear combination

The Melbourne-Wübbena linear combination (Melbourne 1985), (Wübbena 1985) is a linear combination of the L1 and L2 carrier phase plus the P1 and P2 pseudorange. Geometry, troposphere, and ionosphere are eliminated by it.

The Melbourne-Wübbena transformation is usually applied to the system of non-linear observation equations. The system of non-linear observation equations reads

$$E\{\begin{bmatrix} \Phi^j_{i,\mathrm{L1}} \\ \Phi^j_{i,\mathrm{L2}} \\ P^j_{i,\mathrm{P1}} \\ P^j_{i,\mathrm{P2}} \end{bmatrix}\} = \begin{bmatrix} I & I & & d & & & \eta_1 I \\ I & & I & & d & & \eta_2 I \\ I & & & & & d & -\eta_1 I \\ I & & & & & d & -\eta_2 I \end{bmatrix} \begin{bmatrix} \rho^j_i \\ \lambda_1 N^j_{i,\mathrm{L1}} \\ \lambda_2 N^j_{i,\mathrm{L2}} \\ \begin{bmatrix} c\delta t_{i,\mathrm{L1}} \\ c\delta t^{j,\mathrm{L1}} \end{bmatrix} \\ \begin{bmatrix} c\delta t_{i,\mathrm{L2}} \\ c\delta t^{j,\mathrm{L2}} \end{bmatrix} \\ \begin{bmatrix} c\delta t_{i,\mathrm{P1}} \\ c\delta t^{j,\mathrm{P1}} \end{bmatrix} \\ \begin{bmatrix} c\delta t_{i,\mathrm{P2}} \\ c\delta t^{j,\mathrm{P2}} \end{bmatrix} \\ \mathcal{I}^j_i \end{bmatrix} \tag{4.49}$$

(Note that we have replaced here the coefficients for the ionospheric delay for the pseudoranges η_3 and η_4, by $-\eta_1$ and $-\eta_2$.) Construction of this linear combination starts with the following transformation matrix

$$\begin{aligned} T &= \begin{bmatrix} 1 & & -\frac{\eta_2+\eta_1}{\eta_2-\eta_1} & \frac{2\eta_1}{\eta_2-\eta_1} \\ & 1 & -\frac{2\eta_2}{\eta_2-\eta_1} & \frac{\eta_2+\eta_1}{\eta_2-\eta_1} \end{bmatrix} \otimes I \\ &= \begin{bmatrix} 1 & & -\frac{{f_1}^2+{f_2}^2}{{f_1}^2-{f_2}^2} & \frac{2{f_2}^2}{{f_1}^2-{f_2}^2} \\ & 1 & -\frac{2{f_1}^2}{{f_1}^2-{f_2}^2} & \frac{{f_1}^2+{f_2}^2}{{f_1}^2-{f_2}^2} \end{bmatrix} \otimes I \end{aligned} \tag{4.50}$$

Again this is not an invertible transformation. An extended transformation matrix that is

invertible might e.g. read

$$T = \begin{bmatrix} & \frac{\eta_2}{\eta_2-\eta_1} & -\frac{\eta_1}{\eta_2-\eta_1} \\ & \frac{1}{\eta_2-\eta_1} & -\frac{1}{\eta_2-\eta_1} \\ 1 & -\frac{\eta_2+\eta_1}{\eta_2-\eta_1} & \frac{2\eta_1}{\eta_2-\eta_1} \\ & -\frac{2\eta_2}{\eta_2-\eta_1} & \frac{\eta_2+\eta_1}{\eta_2-\eta_1} \end{bmatrix} \otimes I \tag{4.51}$$

Applying (4.51) to (4.49) gives

$$E\{\begin{bmatrix} \frac{\eta_2}{\eta_2-\eta_1}P^j_{i,\mathrm{P1}} - \frac{\eta_1}{\eta_2-\eta_1}P^j_{i,\mathrm{P2}} \\ \frac{1}{\eta_2-\eta_1}P^j_{i,\mathrm{P1}} - \frac{1}{\eta_2-\eta_1}P^j_{i,\mathrm{P2}} \\ \Phi^j_{i,\mathrm{L1}} - \frac{\eta_2+\eta_1}{\eta_2-\eta_1}P^j_{i,\mathrm{P1}} + \frac{2\eta_1}{\eta_2-\eta_1}P^j_{i,\mathrm{P2}} \\ \Phi^j_{i,\mathrm{L2}} - \frac{2\eta_2}{\eta_2-\eta_1}P^j_{i,\mathrm{P1}} + \frac{\eta_2+\eta_1}{\eta_2-\eta_1}P^j_{i,\mathrm{P2}} \end{bmatrix}\} =$$

$$\begin{bmatrix} I & & & \frac{\eta_2}{\eta_2-\eta_1}d & -\frac{\eta_1}{\eta_2-\eta_1}d & \\ & & & \frac{1}{\eta_2-\eta_1}d & -\frac{1}{\eta_2-\eta_1}d & I \\ & I & d & -\frac{\eta_2+\eta_1}{\eta_2-\eta_1}d & \frac{2\eta_1}{\eta_2-\eta_1}d & \\ & & I \quad d & -\frac{2\eta_2}{\eta_2-\eta_1}d & \frac{\eta_2+\eta_1}{\eta_2-\eta_1}d & \end{bmatrix} \begin{bmatrix} \rho^j_i \\ \lambda_1 N^j_{i,\mathrm{L1}} \\ \lambda_2 N^j_{i,\mathrm{L2}} \\ \begin{bmatrix} c\delta t_{i,\mathrm{L1}} \\ c\delta t^{j,\mathrm{L1}} \end{bmatrix} \\ \begin{bmatrix} c\delta t_{i,\mathrm{L2}} \\ c\delta t^{j,\mathrm{L2}} \end{bmatrix} \\ \begin{bmatrix} c\delta t_{i,\mathrm{P1}} \\ c\delta t^{j,\mathrm{P1}} \end{bmatrix} \\ \begin{bmatrix} c\delta t_{i,\mathrm{P2}} \\ c\delta t^{j,\mathrm{P2}} \end{bmatrix} \\ \mathcal{I}^j_i \end{bmatrix} \tag{4.52}$$

Lumping together the clocks of the two pseudorange observable types with the topocentric distances in the first set of equations, and in the second set of equations the ionospheric delays together with the two pseudorange observable types gives

$$E\{\begin{bmatrix} \frac{\eta_2}{\eta_2-\eta_1}P^j_{i,\mathrm{P1}} - \frac{\eta_1}{\eta_2-\eta_1}P^j_{i,\mathrm{P2}} \\ \frac{1}{\eta_2-\eta_1}P^j_{i,\mathrm{P1}} - \frac{1}{\eta_2-\eta_1}P^j_{i,\mathrm{P2}} \\ \Phi^j_{i,\mathrm{L1}} - \frac{\eta_2+\eta_1}{\eta_2-\eta_1}P^j_{i,\mathrm{P1}} + \frac{2\eta_1}{\eta_2-\eta_1}P^j_{i,\mathrm{P2}} \\ \Phi^j_{i,\mathrm{L2}} - \frac{2\eta_2}{\eta_2-\eta_1}P^j_{i,\mathrm{P1}} + \frac{\eta_2+\eta_1}{\eta_2-\eta_1}P^j_{i,\mathrm{P2}} \end{bmatrix}\} = \begin{bmatrix} I & & & \\ & & & I \\ & I & d & \\ & & I & d \end{bmatrix}$$

$$\begin{bmatrix} \rho^j_i + \frac{1}{\eta_2-\eta_1}\left(\eta_2\left(c\delta t_{i,\mathrm{P1}} - c\delta t^{j,\mathrm{P1}}\right) - \eta_1\left(c\delta t_{i,\mathrm{P2}} - c\delta t^{j,\mathrm{P2}}\right)\right) \\ \lambda_1 N^j_{i,\mathrm{L1}} \\ \lambda_2 N^j_{i,\mathrm{L2}} \\ \begin{bmatrix} c\delta t_{i,\mathrm{L1}} \\ c\delta t^{j,\mathrm{L1}} \end{bmatrix} - \frac{\eta_2+\eta_1}{\eta_2-\eta_1}\begin{bmatrix} c\delta t_{i,\mathrm{P1}} \\ c\delta t^{j,\mathrm{P1}} \end{bmatrix} + \frac{2\eta_1}{\eta_2-\eta_1}\begin{bmatrix} c\delta t_{i,\mathrm{P2}} \\ c\delta t^{j,\mathrm{P2}} \end{bmatrix} \\ \begin{bmatrix} c\delta t_{i,\mathrm{L2}} \\ c\delta t^{j,\mathrm{L2}} \end{bmatrix} - \frac{2\eta_2}{\eta_2-\eta_1}\begin{bmatrix} c\delta t_{i,\mathrm{P1}} \\ c\delta t^{j,\mathrm{P1}} \end{bmatrix} + \frac{\eta_2+\eta_1}{\eta_2-\eta_1}\begin{bmatrix} c\delta t_{i,\mathrm{P2}} \\ c\delta t^{j,\mathrm{P2}} \end{bmatrix} \\ \mathcal{I}^j_i + \frac{1}{\eta_2-\eta_1}\left(\left(c\delta t_{i,\mathrm{P1}} - c\delta t^{j,\mathrm{P1}}\right) - \left(c\delta t_{i,\mathrm{P2}} - c\delta t^{j,\mathrm{P2}}\right)\right) \end{bmatrix} \tag{4.53}$$

The system separates into four systems, each of which may be treated independently. As this transformation is applied for the estimation of ambiguities, in a processing step prior

or parallel to the estimation of geometric parameters, one usually discards the two first sets of equations. This is again allowed since they do not contribute to the estimation of the ambiguities. It means that it is allowed to use the transformation matrix in (4.50) even though it is not invertible.

$$E\{\begin{bmatrix} \Phi^j_{i,\mathrm{L1}} - \frac{\eta_2+\eta_1}{\eta_2-\eta_1} P^j_{i,\mathrm{P1}} + \frac{2\eta_1}{\eta_2-\eta_1} P^j_{i,\mathrm{P2}} \\ \Phi^j_{i,\mathrm{L2}} - \frac{2\eta_2}{\eta_2-\eta_1} P^j_{i,\mathrm{P1}} + \frac{\eta_2+\eta_1}{\eta_2-\eta_1} P^j_{i,\mathrm{P2}} \end{bmatrix}\} =$$

$$\begin{bmatrix} I & & d & \\ & I & & d \end{bmatrix} \begin{bmatrix} \lambda_1 N^j_{i,\mathrm{L1}} \\ \lambda_2 N^j_{i,\mathrm{L2}} \\ \begin{bmatrix} c\delta t_{i,\mathrm{L1}} \\ c\delta t^{j,\mathrm{L1}} \end{bmatrix} - \frac{\eta_2+\eta_1}{\eta_2-\eta_1} \begin{bmatrix} c\delta t_{i,\mathrm{P1}} \\ c\delta t^{j,\mathrm{P1}} \end{bmatrix} + \frac{2\eta_1}{\eta_2-\eta_1} \begin{bmatrix} c\delta t_{i,\mathrm{P2}} \\ c\delta t^{j,\mathrm{P2}} \end{bmatrix} \\ \begin{bmatrix} c\delta t_{i,\mathrm{L2}} \\ c\delta t^{j,\mathrm{L2}} \end{bmatrix} - \frac{2\eta_2}{\eta_2-\eta_1} \begin{bmatrix} c\delta t_{i,\mathrm{P1}} \\ c\delta t^{j,\mathrm{P1}} \end{bmatrix} + \frac{\eta_2+\eta_1}{\eta_2-\eta_1} \begin{bmatrix} c\delta t_{i,\mathrm{P2}} \\ c\delta t^{j,\mathrm{P2}} \end{bmatrix} \end{bmatrix} \tag{4.54}$$

As a last step a wide lane transformation, see Eq. (4.45) is applied to them, giving

$$E\{\begin{bmatrix} \Phi^j_{i,\mathrm{L1}} - \frac{\eta_2+\eta_1}{\eta_2-\eta_1} P^j_{i,\mathrm{P1}} + \frac{2\eta_1}{\eta_2-\eta_1} P^j_{i,\mathrm{P2}} \\ \frac{f_1}{f_1-f_2}\Phi^j_{i,\mathrm{L1}} - \frac{f_2}{f_1-f_2}\Phi^j_{i,\mathrm{L2}} - \frac{f_1}{f_1+f_2} P^j_{i,\mathrm{P1}} - \frac{f_2}{f_1+f_2} P^j_{i,\mathrm{P2}} \end{bmatrix}\} =$$

$$\begin{bmatrix} I & & d & \\ \frac{f_1}{f_1-f_2} I & -\frac{f_2}{f_1-f_2} I & \frac{f_1}{f_1-f_2} d & -\frac{f_2}{f_1-f_2} d \end{bmatrix} \begin{bmatrix} \lambda_1 N^j_{i,\mathrm{L1}} \\ \lambda_2 N^j_{i,\mathrm{L2}} \\ \begin{bmatrix} c\delta t_{i,\mathrm{L1}} \\ c\delta t^{j,\mathrm{L1}} \end{bmatrix} - \frac{\eta_2+\eta_1}{\eta_2-\eta_1} \begin{bmatrix} c\delta t_{i,\mathrm{P1}} \\ c\delta t^{j,\mathrm{P1}} \end{bmatrix} + \frac{2\eta_1}{\eta_2-\eta_1} \begin{bmatrix} c\delta t_{i,\mathrm{P2}} \\ c\delta t^{j,\mathrm{P2}} \end{bmatrix} \\ \begin{bmatrix} c\delta t_{i,\mathrm{L2}} \\ c\delta t^{j,\mathrm{L2}} \end{bmatrix} - \frac{2\eta_2}{\eta_2-\eta_1} \begin{bmatrix} c\delta t_{i,\mathrm{P1}} \\ c\delta t^{j,\mathrm{P1}} \end{bmatrix} + \frac{\eta_2+\eta_1}{\eta_2-\eta_1} \begin{bmatrix} c\delta t_{i,\mathrm{P2}} \\ c\delta t^{j,\mathrm{P2}} \end{bmatrix} \end{bmatrix} \tag{4.55}$$

Lumping together in the last set of equations the ambiguities on L1 and L2, and the clock terms gives eventually

$$E\{\begin{bmatrix} \Phi^j_{i,\mathrm{L1}} - \frac{\eta_2+\eta_1}{\eta_2-\eta_1} P^j_{i,\mathrm{P1}} + \frac{2\eta_1}{\eta_2-\eta_1} P^j_{i,\mathrm{P2}} \\ \frac{f_1}{f_1-f_2}\Phi^j_{i,\mathrm{L1}} - \frac{f_2}{f_1-f_2}\Phi^j_{i,\mathrm{L2}} - \frac{f_1}{f_1+f_2} P^j_{i,\mathrm{P1}} - \frac{f_2}{f_1+f_2} P^j_{i,\mathrm{P2}} \end{bmatrix}\} = \begin{bmatrix} I & & d & \\ & I & & d \end{bmatrix}$$

$$\begin{bmatrix} \lambda_1 N^j_{i,\mathrm{L1}} \\ \frac{c}{f_1-f_2}(N^j_{i,\mathrm{L1}} - N^j_{i,\mathrm{L2}}) \\ \begin{bmatrix} c\delta t_{i,\mathrm{L1}} \\ c\delta t^{j,\mathrm{L1}} \end{bmatrix} - \frac{\eta_2+\eta_1}{\eta_2-\eta_1} \begin{bmatrix} c\delta t_{i,\mathrm{P1}} \\ c\delta t^{j,\mathrm{P1}} \end{bmatrix} + \frac{2\eta_1}{\eta_2-\eta_1} \begin{bmatrix} c\delta t_{i,\mathrm{P2}} \\ c\delta t^{j,\mathrm{P2}} \end{bmatrix} \\ \frac{f_1}{f_1-f_2} \begin{bmatrix} c\delta t_{i,\mathrm{L1}} \\ c\delta t^{j,\mathrm{L1}} \end{bmatrix} - \frac{f_1}{f_1-f_2} \begin{bmatrix} c\delta t_{i,\mathrm{L2}} \\ c\delta t^{j,\mathrm{L2}} \end{bmatrix} - \frac{f_1}{f_1+f_2} \begin{bmatrix} c\delta t_{i,\mathrm{P1}} \\ c\delta t^{j,\mathrm{P1}} \end{bmatrix} - \frac{f_2}{f_1+f_2} \begin{bmatrix} c\delta t_{i,\mathrm{P2}} \\ c\delta t^{j,\mathrm{P2}} \end{bmatrix} \end{bmatrix} \tag{4.56}$$

These two sets of equations can be transformed in the same way as the ordinary phase observation equations into DD observation equations. Usually one only estimates the wide lane ambiguities, although in this case this is not allowed, due to the correlation between the L1 ambiguities and the wide lane ambiguities.

Moreover, other transformations may be applied to the ambiguities that give a more favorable set of ambiguities in terms of precision and correlation (Teunissen 1996), (Jonkman 1998).

Frequently one even does the estimation per DD ambiguity. This can be done due to the very weak correlation between the DD ambiguities and their homogeneous precision, contrary to the case where one parameterizes in baseline coordinates.

In Section 6.4 we will show that when certain receiver-satellite combinations are observed less than others, as is usually the case for receivers in large networks that are continuously observing, precision of the DD ambiguities is much more heterogeneous.

4.3.4 The linear combinations used in GAMIT

In Section 4.2.4 we stated that inclusion of constraints on the ionospheric slant delays in the form of pseudo observables makes it possible to estimate integer DD-like functions of ambiguities. In Schaffrin and Bock (1988) a transformation of the two phase observable types on L1 and L2 and this ionospheric pseudo observable type is given that produces two orthogonal linear combinations, in which the ionospheric delay is eliminated.

Starting with the original three sets of non-linear observation equations

$$\begin{aligned} l_i^j &= \eta_0 \mathcal{I}_i^j + \varepsilon_{l_i^j} \\ \Phi_{i,\mathrm{L1}}^j &= \rho_i^j + \lambda_1 N_{i,\mathrm{L1}}^j + c\delta t_{i,\mathrm{L1}} - c\delta t^{j,\mathrm{L1}} + \eta_1 \mathcal{I}_i^j + \varepsilon_{\Phi_{i,\mathrm{L1}}^j} \\ \Phi_{i,\mathrm{L2}}^j &= \rho_i^j + \lambda_2 N_{i,\mathrm{L2}}^j + c\delta t_{i,\mathrm{L2}} - c\delta t^{j,\mathrm{L2}} + \eta_2 \mathcal{I}_i^j + \varepsilon_{\Phi_{i,\mathrm{L2}}^j} \end{aligned} \tag{4.57}$$

the system of linearized observation equations reads

$$E\{\begin{bmatrix} l_i^j \\ \Phi_{i,\mathrm{L1}}^j \\ \Phi_{i,\mathrm{L2}}^j \end{bmatrix}\} = \begin{bmatrix} g & I & & d & & \eta_0 I \\ g & & I & & d & \eta_1 I \\ g & & I & & d & \eta_2 I \end{bmatrix} \begin{bmatrix} r_i \\ \lambda_1 N_{i,\mathrm{L1}}^j \\ \lambda_2 N_{i,\mathrm{L2}}^j \\ c\delta t_{i,\mathrm{L1}} \\ c\delta t^{j,\mathrm{L1}} \\ c\delta t_{i,\mathrm{L2}} \\ c\delta t^{j,\mathrm{L2}} \\ \mathcal{I}_i^j \end{bmatrix} \tag{4.58}$$

In Schaffrin and Bock (1988) the following transformation matrix is proposed:

$$T = \begin{bmatrix} 0 & \frac{\eta_2}{\eta_2-\eta_1} & -\frac{\eta_1}{\eta_2-\eta_1} \\ -\frac{\eta_1^2+\eta_2^2}{\eta_0(\eta_1+\eta_2)} & \frac{\eta_1}{\eta_1+\eta_2} & \frac{\eta_2}{\eta_1+\eta_2} \end{bmatrix} \otimes I \tag{4.59}$$

(Note that in (ibid.) the transformation is given for the observation equations expressed in cycles.) Since the transformation matrix is not invertible, it is extended with an extra row, which will produce a third orthogonal linear combination.

$$T = \begin{bmatrix} 0 & \frac{\eta_2}{\eta_2-\eta_1} & -\frac{\eta_1}{\eta_2-\eta_1} \\ -\frac{\eta_1^2+\eta_2^2}{\eta_0(\eta_1+\eta_2)} & \frac{\eta_1}{\eta_1+\eta_2} & \frac{\eta_2}{\eta_1+\eta_2} \\ \frac{\eta_0}{\eta_1+\eta_2} & \frac{\eta_1}{\eta_1+\eta_2} & \frac{\eta_2}{\eta_1+\eta_2} \end{bmatrix} \otimes I \tag{4.60}$$

Applying (4.60) to (4.58) gives

$$E\{\begin{bmatrix} \frac{\eta_2}{\eta_2-\eta_1}\Phi^j_{i,\mathrm{L1}} - \frac{\eta_1}{\eta_2-\eta_1}\Phi^j_{i,\mathrm{L2}} \\ -\frac{\eta_1^2+\eta_2^2}{\eta_0(\eta_1+\eta_2)}l_i^j + \frac{\eta_1}{\eta_1+\eta_2}\Phi^j_{i,\mathrm{L1}} + \frac{\eta_2}{\eta_1+\eta_2}\Phi^j_{i,\mathrm{L2}} \\ \frac{\eta_0}{\eta_1+\eta_2}l_i^j + \frac{\eta_1}{\eta_1+\eta_2}\Phi^j_{i,\mathrm{L1}} + \frac{\eta_2}{\eta_1+\eta_2}\Phi^j_{i,\mathrm{L2}} \end{bmatrix}\} =$$

$$\begin{bmatrix} g & \frac{\eta_2}{\eta_2-\eta_1}I & -\frac{\eta_1}{\eta_2-\eta_1}I & \frac{\eta_2}{\eta_2-\eta_1}d & -\frac{\eta_1}{\eta_2-\eta_1}d & \\ g & \frac{\eta_1}{\eta_1+\eta_2}I & \frac{\eta_2}{\eta_1+\eta_2}I & \frac{\eta_1}{\eta_1+\eta_2}d & \frac{\eta_2}{\eta_1+\eta_2}d & \\ g & \frac{\eta_1}{\eta_1+\eta_2}I & \frac{\eta_2}{\eta_1+\eta_2}I & \frac{\eta_1}{\eta_1+\eta_2}d & \frac{\eta_2}{\eta_1+\eta_2}d & \frac{\eta_0^2+\eta_1^2+\eta_2^2}{\eta_1+\eta_2}I \end{bmatrix} \begin{bmatrix} r_i \\ \lambda_1 N^j_{i,\mathrm{L1}} \\ \lambda_2 N^j_{i,\mathrm{L2}} \\ \begin{bmatrix} c\delta t_{i,\mathrm{L1}} \\ c\delta t^{j,\mathrm{L1}} \end{bmatrix} \\ \begin{bmatrix} c\delta t_{i,\mathrm{L2}} \\ c\delta t^{j,\mathrm{L2}} \end{bmatrix} \\ \mathcal{I}_i^j \end{bmatrix} \tag{4.61}$$

Lumping together the ambiguities on L1 and L2 and the clock errors at L1 and L1 in all three sets of equations gives

$$E\{\begin{bmatrix} \frac{\eta_2}{\eta_2-\eta_1}\Phi^j_{i,\mathrm{L1}} - \frac{\eta_1}{\eta_2-\eta_1}\Phi^j_{i,\mathrm{L2}} \\ -\frac{\eta_1^2+\eta_2^2}{\eta_0(\eta_1+\eta_2)}l_i^j + \frac{\eta_1}{\eta_1+\eta_2}\Phi^j_{i,\mathrm{L1}} + \frac{\eta_2}{\eta_1+\eta_2}\Phi^j_{i,\mathrm{L2}} \\ \frac{\eta_0}{\eta_1+\eta_2}l_i^j + \frac{\eta_1}{\eta_1+\eta_2}\Phi^j_{i,\mathrm{L1}} + \frac{\eta_2}{\eta_1+\eta_2}\Phi^j_{i,\mathrm{L2}} \end{bmatrix}\} =$$

$$\begin{bmatrix} g & I & & d & \\ g & & I & & d \\ g & & I & & d & \frac{\eta_0^2+\eta_1^2+\eta_2^2}{\eta_1+\eta_2}I \end{bmatrix} \begin{bmatrix} r_i \\ \frac{\eta_2}{\eta_2-\eta_1}\lambda_1 N^j_{i,\mathrm{L1}} - \frac{\eta_1}{\eta_2-\eta_1}\lambda_2 N^j_{i,\mathrm{L2}} \\ \frac{\eta_1}{\eta_1+\eta_2}\lambda_1 N^j_{i,\mathrm{L1}} + \frac{\eta_2}{\eta_1+\eta_2}\lambda_2 N^j_{i,\mathrm{L2}} \\ \frac{\eta_2}{\eta_2-\eta_1}\begin{bmatrix} c\delta t_{i,\mathrm{L1}} \\ c\delta t^{j,\mathrm{L1}} \end{bmatrix} - \frac{\eta_1}{\eta_2-\eta_1}\begin{bmatrix} c\delta t_{i,\mathrm{L2}} \\ c\delta t^{j,\mathrm{L2}} \end{bmatrix} \\ \frac{\eta_1}{\eta_1+\eta_2}\begin{bmatrix} c\delta t_{i,\mathrm{L1}} \\ c\delta t^{j,\mathrm{L1}} \end{bmatrix} + \frac{\eta_2}{\eta_1+\eta_2}\begin{bmatrix} c\delta t_{i,\mathrm{L2}} \\ c\delta t^{j,\mathrm{L2}} \end{bmatrix} \\ \mathcal{I}_i^j \end{bmatrix} \tag{4.62}$$

Since the three newly formed linear combinations are orthogonal they are uncorrelated, and since the ionospheric delays are only involved in the last set of observation equations, and therefore these linear combinations do not contribute to the estimation of the other parameters, they are free variates, and can be omitted from the system if one is not interested in the value of the ionospheric delay.

It means that we may use the transformation matrix in (4.59) even though it is not invertible. This gives then

$$E\{\begin{bmatrix} \frac{\eta_2}{\eta_2-\eta_1}\Phi^j_{i,\mathrm{L1}} - \frac{\eta_1}{\eta_2-\eta_1}\Phi^j_{i,\mathrm{L2}} \\ -\frac{\eta_1^2+\eta_2^2}{\eta_0(\eta_1+\eta_2)}l_i^j + \frac{\eta_1}{\eta_1+\eta_2}\Phi^j_{i,\mathrm{L1}} + \frac{\eta_2}{\eta_1+\eta_2}\Phi^j_{i,\mathrm{L2}} \end{bmatrix}\} =$$

$$\begin{bmatrix} g & I & & d \\ g & & I & & d \end{bmatrix} \begin{bmatrix} r_i \\ \frac{\eta_2}{\eta_2-\eta_1}\lambda_1 N^j_{i,\mathrm{L1}} - \frac{\eta_1}{\eta_2-\eta_1}\lambda_2 N^j_{i,\mathrm{L2}} \\ \frac{\eta_1}{\eta_1+\eta_2}\lambda_1 N^j_{i,\mathrm{L1}} + \frac{\eta_2}{\eta_1+\eta_2}\lambda_2 N^j_{i,\mathrm{L2}} \\ \frac{\eta_2}{\eta_2-\eta_1}\begin{bmatrix} c\delta t_{i,\mathrm{L1}} \\ c\delta t^{j,\mathrm{L1}} \end{bmatrix} - \frac{\eta_1}{\eta_2-\eta_1}\begin{bmatrix} c\delta t_{i,\mathrm{L2}} \\ c\delta t^{j,\mathrm{L2}} \end{bmatrix} \\ \frac{\eta_1}{\eta_1+\eta_2}\begin{bmatrix} c\delta t_{i,\mathrm{L1}} \\ c\delta t^{j,\mathrm{L1}} \end{bmatrix} + \frac{\eta_2}{\eta_1+\eta_2}\begin{bmatrix} c\delta t_{i,\mathrm{L2}} \\ c\delta t^{j,\mathrm{L2}} \end{bmatrix} \end{bmatrix} \tag{4.63}$$

These two sets of equations can be transformed in the same way as the ordinary phase observation equations into DD observation equations.

In the GAMIT (GPS At MIT) software these linear combinations are implemented to constrain the ionosphere for the purpose of ambiguity resolution (see Chapter 6).

4.4 Solution of the normal equations

In this section we will show how the system of normal equations for more than one observable type can be computed in an efficient way. The part for the global parameters of the design matrix for q observable types (p phase observable types and $q-p$ code observable types) for the case that all q observable types are available for each receiver-satellite combination reads

$$A_{1,k} = \begin{bmatrix} \overbrace{\begin{matrix} g_k & I \\ \vdots & \ddots \\ g_k & I \\ \vdots & \\ g_k & \end{matrix}}^{p} \end{bmatrix} \quad q \tag{4.64}$$

When besides coordinate parameters also other types of global parameters are involved, as e.g. tropospheric zenith delays, ionospheric model parameters, or orbital parameters they are added as extra columns next to g_k. Apart from enlarging the system of normal equations it will have no effect on the solution method for the system.

For the variance-covariance matrix of the observables we take:

$$Q_k = \begin{bmatrix} \frac{1}{w_1} & & & \\ & \frac{1}{w_2} & & \\ & & \ddots & \\ & & & \frac{1}{w_q} \end{bmatrix} \otimes Q_{y_k} \tag{4.65}$$

Note that this definition of the variance-covariance matrix makes e.g. elevation dependent standard deviation for the observables possible, or even a full variance-covariance matrix for each observable type.

The updated normal matrix system for n epochs reads:

$$\sum_{k=1}^{n} A_{1,k}^T Q_k^{-1} P_{\bar{A}_{2,k}}^{\perp} A_{1,k}^T \Delta x_1 = \sum_{k=1}^{n} A_{1,k}^T Q_k^{-1} P_{\bar{A}_{2,k}}^{\perp} \Delta y_k \tag{4.66}$$

In Table 4.10 $Q_k^{-1} P_{\bar{A}_{2,k}}^{\perp}$ for the four models for the temporal parameters as defined in Section 4.1 can be found. A more detailed derivation of them is given in Appendix D.

For the models with distinct clocks $Q_k^{-1} P_{\bar{A}_{2,k}}^{\perp}$ can be written as

$$Q_k^{-1} P_{\bar{A}_{2,k}}^{\perp} = U \otimes Q_{y_k}^{-1} P_{\bar{d}}^{\perp} \tag{4.67}$$

with U a $q \times q$ matrix. In short hand notation Eq. (4.66) reads

$$N_n \Delta x_1 = h_n \tag{4.68}$$

Using Eq. (4.67) the normal matrix N_n and right-hand side h_n can be written as:

$$N_n = \sum_{k=1}^{n} \begin{bmatrix} \sum_{i=1}^{q}\sum_{j=1}^{q} U_{(i,j)} g_k^T Q_{y_k}^{-1} P_{\bar{d}_k}^{\perp} g_k & \sum_{i=1}^{q} U_{(i,1)} g_k^T Q_{y_k}^{-1} P_{\bar{d}_k}^{\perp} & \cdots & \sum_{i=1}^{q} U_{(i,p)} g_k^T Q_{y_k}^{-1} P_{\bar{d}_k}^{\perp} \\ \sum_{j=1}^{q} U_{(1,j)} Q_{y_k}^{-1} P_{\bar{d}_k}^{\perp} g_k & U_{(1,1)} Q_{y_k}^{-1} P_{\bar{d}_k}^{\perp} & \cdots & U_{(1,p)} Q_{y_k}^{-1} P_{\bar{d}_k}^{\perp} \\ \vdots & \vdots & \ddots & \vdots \\ \sum_{j=1}^{q} U_{(p,j)} Q_{y_k}^{-1} P_{\bar{d}_k}^{\perp} g_k & U_{(p,1)} Q_{y_k}^{-1} P_{\bar{d}_k}^{\perp} & \cdots & U_{(p,p)} Q_{y_k}^{-1} P_{\bar{d}_k}^{\perp} \end{bmatrix}$$

$$= \begin{bmatrix} \sum_{i=1}^{q}\sum_{j=1}^{q} U_{(i,j)} \sum_{k=1}^{n} g_k^T Q_{y_k}^{-1} P_{\bar{d}_k}^{\perp} g_k & \sum_{i=1}^{q} U_{(i,1)} \sum_{k=1}^{n} g_k^T Q_{y_k}^{-1} P_{\bar{d}_k}^{\perp} & \cdots & \sum_{i=1}^{q} U_{(i,p)} \sum_{k=1}^{n} g_k^T Q_{y_k}^{-1} P_{\bar{d}_k}^{\perp} \\ \sum_{j=1}^{q} U_{(1,j)} \sum_{k=1}^{n} Q_{y_k}^{-1} P_{\bar{d}_k}^{\perp} g_k & U_{(1,1)} \sum_{k=1}^{n} Q_{y_k}^{-1} P_{\bar{d}_k}^{\perp} & \cdots & U_{(1,p)} \sum_{k=1}^{n} Q_{y_k}^{-1} P_{\bar{d}_k}^{\perp} \\ \vdots & \vdots & \ddots & \vdots \\ \sum_{j=1}^{q} U_{(p,j)} \sum_{k=1}^{n} Q_{y_k}^{-1} P_{\bar{d}_k}^{\perp} g_k & U_{(p,1)} \sum_{k=1}^{n} Q_{y_k}^{-1} P_{\bar{d}_k}^{\perp} & \cdots & U_{(p,p)} \sum_{k=1}^{n} Q_{y_k}^{-1} P_{\bar{d}_k}^{\perp} \end{bmatrix} \tag{4.69}$$

$$h_n = \sum_{k=1}^{n} \begin{bmatrix} \sum_{i=1}^{q}\sum_{j=1}^{q} U_{(i,j)} g_k^T Q_{y_k}^{-1} P_{\bar{d}_k}^{\perp} \Delta y_{j,k} \\ \sum_{j=1}^{q} U_{(1,j)} Q_{y_k}^{-1} P_{\bar{d}_k}^{\perp} \Delta y_{j,k} \\ \vdots \\ \sum_{j=1}^{q} U_{(p,j)} Q_{y_k}^{-1} P_{\bar{d}_k}^{\perp} \Delta y_{j,k} \end{bmatrix} = \begin{bmatrix} \sum_{j=1}^{q} \left(\sum_{i=1}^{q} U_{(i,j)} \sum_{k=1}^{n} g_k^T Q_{y_k}^{-1} P_{\bar{d}_k}^{\perp} \Delta y_{j,k} \right) \\ \sum_{j=1}^{q} U_{(1,j)} \left(\sum_{k=1}^{n} Q_{y_k}^{-1} P_{\bar{d}_k}^{\perp} \Delta y_{j,k} \right) \\ \vdots \\ \sum_{j=1}^{q} U_{(p,j)} \left(\sum_{k=1}^{n} Q_{y_k}^{-1} P_{\bar{d}_k}^{\perp} \Delta y_{j,k} \right) \end{bmatrix} \tag{4.70}$$

This means that to construct the normal matrix, irrespective of the number of observable types used, we only have to compute at each epoch

$$Q_{y_k}^{-1} P_{\bar{d}_k}^{\perp} \quad , \quad g_k^T Q_{y_k}^{-1} P_{\bar{d}_k}^{\perp} \quad , \quad g_k^T Q_{y_k}^{-1} P_{\bar{d}_k}^{\perp} g_k \tag{4.71}$$

For the right-hand side we have to compute at each epoch for all observable types ($j = 1, \cdots, q$)

$$Q_{y_k}^{-1} P_{\bar{d}_k}^{\perp} \Delta y_{j,k} \quad , \quad g_k^T Q_{y_k}^{-1} P_{\bar{d}_k}^{\perp} \Delta y_{j,k} \tag{4.72}$$

$$\mu_1 = \sum_{j=1}^{q} w_j \qquad \mu_2 = \sum_{j=1}^{q} w_j \eta_j$$

$$\mu_3 = \sum_{j=1}^{q} w_j \eta_j^2 \qquad \mu_4 = \sum_{i=1}^{q} \sum_{j=1}^{i} w_i w_j (\eta_i - \eta_j)^2$$

$$h_{i,j} = \frac{w_j}{\mu_3 \mu_4}(\mu_3 - \mu_2 \eta_i)(\mu_3 - \mu_2 \eta_j) \qquad H_{\bar{d}} = (\bar{d}^T Q_y^{-1} \bar{d})^{-1} \bar{d}^T Q_y^{-1}$$

$$k_{i,j} = w_j \eta_i \eta_j + h_{i,j} \qquad P_{\bar{d}} = \bar{d}(\bar{d}^T Q_y^{-1} \bar{d})^{-1} \bar{d}^T Q_y^{-1}$$

$$= \frac{w_j}{\mu_4} \sum_{k=1}^{q} w_k (\eta_i - \eta_k)(\eta_j - \eta_k) \qquad P_{\bar{d}}^{\perp} = I - \bar{d}(\bar{d}^T Q_y^{-1} \bar{d})^{-1} \bar{d}^T Q_y^{-1}$$

Table 4.9: Legend for Tables 4.10 and 4.11.

When no ionosphere is estimated, $U_{(i,j)} = 0$ for $i \neq j$, so,

$$\begin{aligned} \sum_{i=1}^{q} U_{(i,j)} &= w_j \\ \sum_{j=1}^{q} U_{(i,j)} &= w_i \\ \sum_{i=1}^{q} \sum_{j=1}^{q} U_{(i,j)} &= \mu_1 \end{aligned} \tag{4.73}$$

When ionosphere is estimated, we have

$$\begin{aligned} \sum_{i=1}^{q} U_{(i,j)} &= \frac{1}{\mu_3}(w_j \mu_3 - \sum_{i=1}^{q} w_i \eta_i w_j \eta_j) = \frac{(\mu_3 - \eta_j \mu_2) w_j}{\mu_3} \\ \sum_{j=1}^{q} U_{(i,j)} &= \frac{1}{\mu_3}(w_i \mu_3 - \sum_{i=1}^{q} w_i \eta_i w_j \eta_j) = \frac{(\mu_3 - \eta_i \mu_2) w_i}{\mu_3} \\ \sum_{i=1}^{q} \sum_{j=1}^{q} U_{(i,j)} &= \frac{1}{\mu_3}(\mu_1 \mu_3 - \mu_2^2) = \frac{\mu_4}{\mu_3} \end{aligned} \tag{4.74}$$

For the models with common clocks $Q_k^{-1} P_{\bar{A}_{2,k}}^{\perp}$ can be written as

$$Q_k^{-1} P_{\bar{A}_{2,k}}^{\perp} = U \otimes Q_{y_k}^{-1} P_{\bar{d}}^{\perp} + U_e \otimes Q_{y_k}^{-1} \tag{4.75}$$

with U and U_e $q \times q$ matrices. The normal matrix system can be written as a sum of two systems of the form as in Eqs. (4.69–4.70). Fortunately, only the parts of $U_e \otimes Q_{y_k}^{-1}$ referring

$\bar{A}_{2,k}$	$Q_k^{-1}P^{\perp}_{\bar{A}_{2,k}} = Q_k^{-1}(I - \bar{A}_{2,k}(\bar{A}_{2,k}^T Q_k^{-1} \bar{A}_{2,k})^{-1}\bar{A}_{2,k}^T Q_k^{-1})$

No estimation of ionosphere, distinct clocks for each observable type

$$\begin{bmatrix} \bar{d}_1 & & & \\ & \bar{d}_2 & & \\ & & \ddots & \\ & & & \bar{d}_q \end{bmatrix} \quad \begin{bmatrix} w_1 Q_{y_k}^{-1} P^{\perp}_{\bar{d}_1} & & & \\ & w_2 Q_{y_k}^{-1} P^{\perp}_{\bar{d}_2} & & \\ & & \ddots & \\ & & & w_q Q_{y_k}^{-1} P^{\perp}_{\bar{d}_q} \end{bmatrix}$$

No estimation of ionosphere, common clocks

$$\begin{bmatrix} \bar{d} \\ \bar{d} \\ \vdots \\ \bar{d} \end{bmatrix} \quad \begin{matrix} \frac{1}{\mu_1} \begin{bmatrix} w_1^2 & w_1 w_2 & \cdots & w_1 w_q \\ w_2 w_1 & w_2^2 & \cdots & w_2 w_q \\ \vdots & \vdots & \ddots & \vdots \\ w_q w_1 & w_q w_2 & \cdots & w_q^2 \end{bmatrix} \otimes Q_{y_k}^{-1} P^{\perp}_{\bar{d}} + \\ \frac{1}{\mu_1} \begin{bmatrix} w_1(\mu_1 - w_1) & -w_1 w_2 & \cdots & -w_1 w_q \\ -w_2 w_1 & w_2(\mu_1 - w_2) & \cdots & -w_2 w_q \\ \vdots & \vdots & \ddots & \vdots \\ -w_q w_1 & -w_q w_2 & \cdots & w_q(\mu_1 - w_q) \end{bmatrix} \otimes Q_{y_k}^{-1} \end{matrix}$$

Estimation of ionosphere, distinct clocks for each observable type
(clock of first observable type in S-basis)

$$\begin{bmatrix} & & \eta_1 I \\ \bar{d} & & \eta_2 I \\ & \ddots & \vdots \\ & \bar{d} & \eta_q I \end{bmatrix} \quad \frac{1}{\mu_3} \begin{bmatrix} w_1(\mu_3 - w_1\eta_1^2) & -w_1\eta_1 w_2\eta_2 & \cdots & -w_1\eta_1 w_q\eta_q \\ -w_2\eta_2 w_1\eta_1 & w_2(\mu_3 - w_2\eta_2^2) & & -w_2\eta_2 w_q\eta_q \\ \vdots & & \ddots & \\ -w_q\eta_q w_1\eta_1 & -w_q\eta_q w_2\eta_2 & & w_q(\mu_3 - w_q\eta_q^2) \end{bmatrix} \otimes Q_{y_k}^{-1} P^{\perp}_{\bar{d}}$$

Estimation of ionosphere, common clocks

$$\begin{bmatrix} \bar{d} & \eta_1 I \\ \bar{d} & \eta_2 I \\ \vdots & \vdots \\ \bar{d} & \eta_q I \end{bmatrix} \quad \begin{matrix} \begin{bmatrix} w_1 h_{1,1} & w_1 h_{1,2} & \cdots & w_1 h_{1,q} \\ w_2 h_{2,1} & w_2 h_{2,2} & \cdots & w_2 h_{2,q} \\ \vdots & \vdots & \ddots & \vdots \\ w_q h_{q,1} & w_q h_{q,2} & \cdots & w_q h_{q,q} \end{bmatrix} \otimes Q_{y_k}^{-1} P^{\perp}_{\bar{d}} + \\ \begin{bmatrix} w_1 - w_1 k_{1,1} & -w_1 k_{1,2} & \cdots & -w_1 k_{1,q} \\ -w_2 k_{2,1} & w_2 - w_2 k_{2,2} & & -w_2 k_{2,q} \\ \vdots & & \ddots & \\ -w_q k_{q,1} & -w_q k_{q,2} & & w_q - w_q k_{q,q} \end{bmatrix} \otimes Q_{y_k}^{-1} \end{matrix}$$

Table 4.10: $Q^{-1}P^{\perp}_{\bar{A}_{2,k}}$ for different models for the temporal parameters (Legend in Table 4.9).

to the ambiguities may be nonzero, since all summations of elements of U_e equal zero, as we will show below.

When no ionosphere is estimated we have

$$\begin{aligned} \sum_{i=1}^{q} U_{(i,j)} &= \frac{1}{\mu_1} \sum_{i=1}^{q} w_i w_j = w_j \\ \sum_{j=1}^{q} U_{(i,j)} &= \frac{1}{\mu_1} \sum_{j=1}^{q} w_i w_j = w_i \\ \sum_{i=1}^{q} \sum_{j=1}^{q} U_{(i,j)} &= \mu_1 \end{aligned} \tag{4.76}$$

and

$$\begin{aligned} \sum_{i=1}^{q} U_{e(i,j)} &= \frac{1}{\mu_1}(w_j \mu_1 - \sum_{i=1}^{q} w_i w_j) = 0 \\ \sum_{j=1}^{q} U_{e(i,j)} &= \frac{1}{\mu_1}(w_i \mu_1 - \sum_{j=1}^{q} w_i w_j) = 0 \\ \sum_{i=1}^{q} \sum_{j=1}^{q} U_{e(i,j)} &= 0 \end{aligned} \tag{4.77}$$

When ionosphere is estimated we have

$$\begin{aligned} \sum_{i=1}^{q} U_{(i,j)} &= \sum_{i=1}^{q} w_i h_{i,j} = \frac{(\mu_3 - \eta_j \mu_2) w_j}{\mu_3} \\ \sum_{j=1}^{q} U_{(i,j)} &= \sum_{j=1}^{q} w_i h_{i,j} = \frac{(\mu_3 - \eta_i \mu_2) w_i}{\mu_3} \\ \sum_{i=1}^{q} \sum_{j=1}^{q} U_{(i,j)} &= \frac{\mu_1 \mu_3 - \mu_2^2}{\mu_3} = \frac{\mu_4}{\mu_3} \end{aligned} \tag{4.78}$$

and

$$\begin{aligned} \sum_{i=1}^{q} U_{e(i,j)} &= (w_j - \sum_{i=1}^{q} w_i k_{i,j}) = 0 \\ \sum_{j=1}^{q} U_{e(i,j)} &= (w_i - \sum_{j=1}^{q} w_i k_{i,j}) = 0 \\ \sum_{i=1}^{q} \sum_{j=1}^{q} U_{e(i,j)} &= 0 \end{aligned} \tag{4.79}$$

In addition for the case of two observable types we have

$$U_{e(i,i)} = w_i - w_i k_{i,i} = 0 \quad , \quad U_{e(1,2)} = -w_1 k_{1,2} = 0 \quad , \quad U_{e(2,1)} = -w_2 k_{2,1} = 0 \tag{4.80}$$

The similarity of the structure of the normal matrix systems for different models enables us to compute normal matrix systems for several models at almost no extra cost. Note that this is only true if all observations are available for a particular receiver-satellite combination. This is however not a severe restriction, since for most of the models with estimation of ionosphere this is already a condition, since otherwise the ionospheric parameters can either not be estimated or the observables involved will act as free variates, and thus do not contribute to the estimation of the global parameters.

For the models without estimation of ionosphere it may be fruitful to apply all observations, irrespective of the circumstance that all observations for a certain receiver-satellite combination are available. Then for *each* observable type we need to compute a normal equation system as in Eqs. (4.69–4.70) and add them together after all epochs have been processed. Usually, however, these models are applied to only a few receivers, and hence the size of the matrices is relatively small.

The system of normal equations is solved in a similar fashion as described in Eqs. (3.102–3.105) for one observable type, with the rank defect resolved as described in Section 4.2.

The temporal parameters, which now besides clock parameters may consist also of ionospheric slant delays, are computed according to the procedure in Eqs. (3.108–3.109). The vector of 'observed' minus 'computed' now of course consists of more than one observable type. In Table 4.11 for the four models for the temporal parameters as defined in Section 4.1 an expression for $H_{\bar{A}_{2,k}}$ is given. A more detailed derivation of them is given in Appendix D.

Changing observation scenarios

Every epoch k the normal matrix system of that epoch is added to the system of the previous epochs (N_{k-1}, h_{k-1}). If at epoch k there is a change in the set of parameters involved, N_{k-1} and h_{k-1} are permuted such, that the parameters of epoch k are in front. In this way, the system of epoch k can be easily added to the existing normal matrix system. If N is stored as a full triangular matrix, the permutation can be made in-place.

In Figure 4.5 the number of parameters per epoch for a time span of 24 hours for a model where we have L1 and L2 ambiguities, coordinates, tropospheric zenith delays (1 per station per hour), and orbital parameters (8 per satellite), for a global network of which the characteristics can be found in Table 4.12 is given (upper black curve). The total number of global parameters is 1369.

The normal matrix for one epoch is a full matrix, i.e. it does not contain zero entries. It is a symmetric matrix, hence only the lower triangular part is computed and stored. Since the set of parameters may change per epoch, the stacked normal matrix of all epochs, may not be a full matrix. Especially when the observation time span is long (several hours to days), a considerable part of the normal matrix may be zero. This is due to the fact that satellites rise and set, and the limited time for which the tropospheric zenith delays are defined (e.g. one hour).

A matrix that contains a substantial number of zero entries is called a sparse matrix. If one uses appropriate algorithms and data structures, one can benefit from the sparsity of the matrix; i.e. the same data can be processed in less time using less core memory. In Section 4.6 we will show the gain in efficiency when applying sparse matrix techniques to the normal matrices occurring in the GPS data processing,

$\bar{A}_{2,k}$	$H_{\bar{A}_{2,k}} = (\bar{A}_{2,k}^T Q^{-1} \bar{A}_{2,k})^{-1} \bar{A}_{2,k}^T Q^{-1}$

No estimation of ionosphere, distinct clocks for each observable type

$$\begin{bmatrix} \bar{d}_1 & & & \\ & \bar{d}_2 & & \\ & & \ddots & \\ & & & \bar{d}_q \end{bmatrix} \qquad \begin{bmatrix} H_{\bar{d}_1} & & & \\ & H_{\bar{d}_2} & & \\ & & \ddots & \\ & & & H_{\bar{d}_q} \end{bmatrix}$$

No estimation of ionosphere, common clocks

$$\begin{bmatrix} \bar{d} \\ \bar{d} \\ \vdots \\ \bar{d} \end{bmatrix} \qquad \frac{1}{\mu_1} \begin{bmatrix} w_1 H_{\bar{d}} & w_2 H_{\bar{d}} & \cdots & w_q H_{\bar{d}} \end{bmatrix}$$

Estimation of ionosphere, distinct clocks for each observable type

$$\begin{bmatrix} & & \eta_1 I \\ \bar{d} & & \eta_2 I \\ & \ddots & \vdots \\ & \bar{d} & \eta_q I \end{bmatrix} \qquad \begin{bmatrix} -\frac{\eta_2}{\eta_1} H_{\bar{d}} & H_{\bar{d}} & & \\ \vdots & & \ddots & \\ -\frac{\eta_q}{\eta_1} H_{\bar{d}} & & & H_{\bar{d}} \\ \frac{1}{\eta_1}(I - \frac{\mu_3 - w_1 \eta_1^2}{\mu_3} P_{\bar{d}}^{\perp}) & \frac{w_2 \eta_2}{\mu_3} P_{\bar{d}}^{\perp} & \cdots & \frac{w_q \eta_q}{\mu_3} P_{\bar{d}}^{\perp} \end{bmatrix}$$

Estimation of ionosphere, common clocks

$$\begin{bmatrix} \bar{d} & \eta_1 I \\ \bar{d} & \eta_2 I \\ \vdots & \vdots \\ \bar{d} & \eta_q I \end{bmatrix} \qquad \begin{bmatrix} H_{1,1} & H_{1,2} & \cdots & H_{1,q} \\ H_{2,1} & H_{2,2} & \cdots & H_{2,q} \end{bmatrix}$$

where

$$H_{1,j} = -\frac{w_j}{\mu_4}(\eta_j \mu_2 - \mu_3) H_{\bar{d}}$$
$$H_{2,j} = \frac{w_j \eta_j}{\mu_3} I + \frac{w_j \mu_2 (\eta_j \mu_2 - \mu_3)}{\mu_4 \mu_3} P_{\bar{d}}$$

Table 4.11: $H_{\bar{A}_{2,k}}$ for different models for the temporal parameters (Legend in Table 4.9).

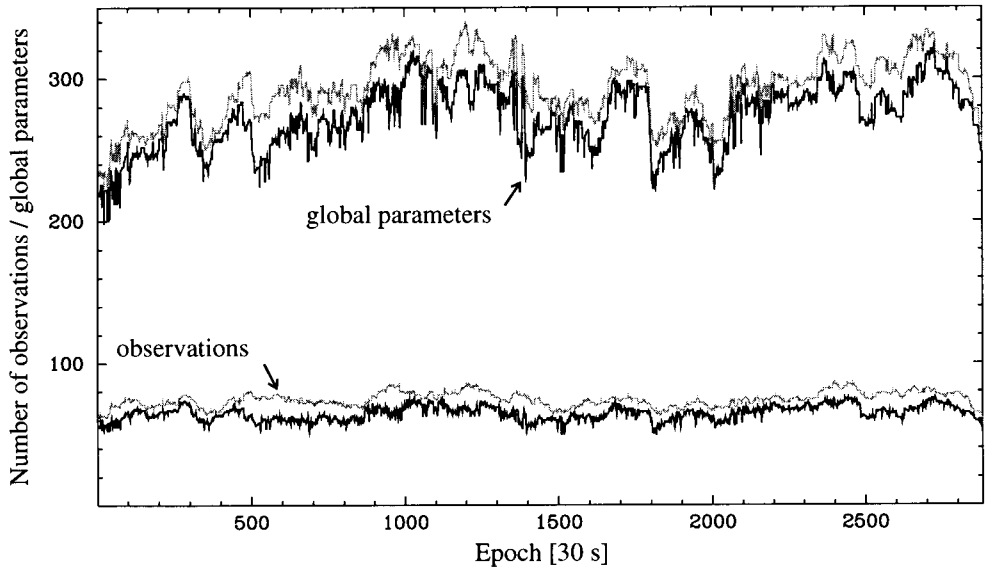

Figure 4.5: Number of parameters per epoch (black, upper curve), idem, maximum (grey, upper curve), and number of observations per epoch (black, lower curve), idem, maximum (grey, lower curve) for the global network.

Global Network (Pol)		Californian Network (Cal)	
Site ID (IGS)	Name	Site ID (IGS)	Name
ALGO	Algonquin	GOLD	Goldstone
GOLD	Goldstone	CHIL	Chilao Flats
MADR	Madrid	VNDP	Vandenberg
FAIR	Fairbanks	DAM1	Pacoima Dam
HART	Hartebeesthoek	DAM2	Pacoima Dam
KOKB	Kokee Park	CMP9	Fire Camp 9
KOSG	Kootwijk	LEEP	Mount Lee
SANT	Santiago	LONG	Longdon Yard
WETT	Wettzell	TABL	Table Mountain
YELL	Yellowknife	HOLP	Hollydale
TROM	Tromsö	GOL2	Goldstone

Table 4.12: Stations included in the global network (Pol), and stations included in the Californian network (Cal).

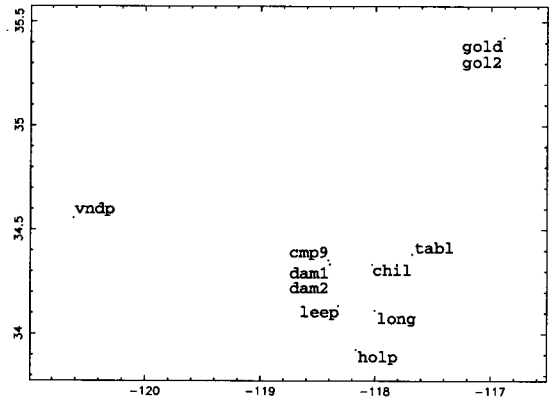

Figure 4.6: Map of the stations of the Californian network. The distance between VNDP and GOLD is approximately 350 km, the distance between HOLP and GOLD is approximately 200 km.

4.5 Computation of the one-dimensional test statistics

In Section 3.10 we showed how the one-dimensional test statistics can be computed when there is only one observable type .

In the general case of p phase observable types and a total of q observable types, we want to specify alternative hypotheses for outliers in all q types, and for slips in the p phase observable types. Although we have a system referring to more than one observable type, the computation of the test statistics is still fairly simple, since the hypotheses only refer to a single observable type at a time.

For an alternative hypothesis that there is an outlier in the l-th observation of epoch k we have

$$c_{l,k}^T Q_y^{-1} Q_{\hat{e}} Q_y^{-1} c_{l,k} = -Q_{y_k}^{-1} P_{\bar{A}_{2,k}}^{\perp} \bar{A}_{1,k} Q_{\hat{x}_1} \bar{A}_{1,k}^T P_{\bar{A}_{2,k}}^{\perp T} Q_{y_k}^{-1} + Q_{y_k}^{-1} P_{\bar{A}_{2,k}}^{\perp} \tag{4.81}$$

$$= -V_{3,k} V_{2,k}^T + Q_{y_k}^{-1} P_{\bar{A}_{2,k}}^{\perp} \tag{4.82}$$

With

$$\bar{A}_{1,i} = \begin{bmatrix} q \begin{cases} g_k & \overbrace{S_a}^{p} \\ \vdots & \ddots \\ g_k & S_a \\ \vdots & \\ g_k & \end{cases} \end{bmatrix} \tag{4.83}$$

(for the definition of S_a see Eq. (3.33)), we compute $V_{2,k} = Q_{y_k}^{-1} P_{\bar{A}_{2,k}}^{\perp} \bar{A}_{1,k}$ as

$$V_{2,k} = \begin{bmatrix} \sum_{j=1}^{q} U_{(1,j)} Q_{y_k}^{-1} P_{\bar{A}_{2,k}}^{\perp} g_k & U_{(1,1)} Q_{y_k}^{-1} P_{\bar{A}_{2,k}}^{\perp} S_a & \cdots & U_{(1,p)} Q_{y_k}^{-1} P_{\bar{A}_{2,k}}^{\perp} S_a \\ \sum_{j=2}^{q} U_{(1,j)} Q_{y_k}^{-1} P_{\bar{A}_{2,k}}^{\perp} g_k & U_{(2,1)} Q_{y_k}^{-1} P_{\bar{A}_{2,k}}^{\perp} S_a & \cdots & U_{(2,p)} Q_{y_k}^{-1} P_{\bar{A}_{2,k}}^{\perp} S_a \\ \vdots & \vdots & \ddots & \vdots \\ \sum_{j=1}^{q} U_{(q,j)} Q_{y_k}^{-1} P_{\bar{A}_{2,k}}^{\perp} g_k & U_{(q,1)} Q_{y_k}^{-1} P_{\bar{A}_{2,k}}^{\perp} S_a & \cdots & U_{(q,p)} Q_{y_k}^{-1} P_{\bar{A}_{2,k}}^{\perp} S_a \end{bmatrix} \tag{4.84}$$

For the computation of $-Q_{y_k}^{-1} P_{\bar{A}_{2,k}}^{\perp} \bar{A}_{1,k} Q_{\hat{x}_1} \bar{A}_{1,k}^T P_{\bar{A}_{2,k}}^{\perp T} Q_{y_k}^{-1}$ we need only the part of $Q_{\hat{x}_1}$ which refers to the parameters involved in the current epoch. This part corresponds always to a nonzero part of the normal matrix. Using sparse matrix techniques, (see Section 4.6) we can compute a sparse inverse of the normal matrix which will contain the needed part.

For the example of the global network we have a total of $n_t = 1369$ parameters. For one particular epoch the number of parameters n_e varies from 198 to 322 with an average of approximately 273, see Figure 4.5. The number of observations for one observable type varies from 49 to 76, with an average of 64. This means that for the example of the global network, the maximal dimension of $V_{2,k}$ is $76q \times 322$.

The matrix products $V_{2,k} = Q_{y_k}^{-1} P_{\bar{A}_{2,k}}^{\perp} \bar{A}_{1,k}$ and $V_{3,k} = Q_{y_k}^{-1} P_{\bar{A}_{2,k}}^{\perp} \bar{A}_{1,k} Q_{\hat{x}_1}$ can be computed in parallel for all observable types involved, i.e. we only have to compute one mega-row of $V_{2,k}$ and $V_{3,k}$ where we take care to pass the appropriate (sum of) entries of $U_{(i,j)}$ for each observable type. We compute only the diagonal of $-V_{3,k} V_{2,k}^T + Q_{y_k}^{-1} P_{\bar{A}_{2,k}}^{\perp}$ since that is the only part we need to compute the alternative hypotheses.

As in the case of only one observable type, the alternative hypotheses for a cycle slip can be computed efficiently from three matrices that are updated per epoch. Recalling these matrices:

$$\underset{rm \times rm}{W_{1,k}} = \sum_{i=1}^{k} Q_{y_i}^{-1} P_{\bar{A}_{2,i}}^{\perp} \tag{4.85}$$

$$\underset{rm \times (r-1)(m-1)+3r}{W_{2,k}} = \sum_{i=1}^{k} Q_{y_i}^{-1} P_{\bar{A}_{2,i}}^{\perp} \bar{A}_{1,i} \tag{4.86}$$

$$\underset{rm \times (r-1)(m-1)+3r}{W_{3,k}} = \sum_{i=1}^{k} Q_{y_i}^{-1} P_{\bar{A}_{2,i}}^{\perp} \bar{A}_{1,i} Q_{\hat{x}_1} \tag{4.87}$$

For an alternative hypothesis that there is a slip in the l-th observation of epoch k we have

$$c_{l,k}^T Q_y^{-1} Q_{\hat{e}} Q_y^{-1} c_{l,k} = (W_{1,k} - W_{3,k} W_{2,k}^T)_{ll} \qquad l = 1, \ldots, rm \tag{4.88}$$

Matrices $W_{1,k}, W_{2,k}$ and $W_{3,k}$ are updated with the already computed $Q_{y_k}^{-1} P_{\bar{A}_{2,k}}^{\perp}$, $V_{2,k}$ and $V_{3,k}$. Here we have to take care that it is possible that though a certain receiver-satellite combination is not observed in this epoch, it may have been observed at an earlier epoch and will be observed again at a later epoch. This might e.g. occur when the number of receivers observing a certain satellite, drops temporarily below two. Matrices $W_{1,k}, W_{2,k}$ and

$W_{3,k}$ should thus contain slots for all receiver-satellite combinations that were observed in a previous epoch, and for which the elevation is still larger than the elevation cut-off. In Figure 4.5 the maximum number of parameters and observations due to this condition for the global network are plotted as the grey curves.

4.6 Sparsity considerations

For the solution of the system of normal equations there exist a number of methods. Three of these will be described here since they are used in one of the large GPS software suites (or should be used).

1. Direct inversion of the normal matrix.
The most straightforward way to solve the system of normal equations is to invert the normal matrix, and multiply the right-hand side by it:

$$\hat{x} = N^{-1}h \qquad Q_{\hat{x}} = N^{-1} \tag{4.89}$$

An algorithm for the inversion of a symmetric semi-definite matrix is given in (Rutishauser 1963). The inversion is done in-place, and the number of floating point operations or flops (one flop being defined as one multiplicative and one additive operation) is of the order $\mathcal{O}(\frac{1}{2}n^3)$ where n is the dimension of the matrix. This operation count does not take into account the administration part of the computation, nor the operations for the pivot search needed for stability reasons. The operation count for the multiplication of the inverse of the normal matrix with the right-hand side is of the order $\mathcal{O}(n^2)$. This method is the only one that needs a pivot search.

The two other methods are based on a Cholesky factorization of the normal matrix:

$$N = CC^T \tag{4.90}$$

with C a lower triangular matrix. The Cholesky factorization can be done in-place and the operation count is of the order $\mathcal{O}(\frac{1}{6}n^3)$.

2. Inversion of the Cholesky factor.
Using this method the Cholesky factor is first inverted. This can be done in-place (see Dongarra et al. (1979)) and the operation count is of the order $\mathcal{O}(\frac{1}{6}n^3)$:

$$C \rightarrow C^{-1} \tag{4.91}$$

From the inverted Cholesky factor the inverse of the normal matrix is then computed as

$$N^{-1} = Q_{\hat{x}} = C^{-T}C^{-1} \tag{4.92}$$

It can also be done in-place and has an operation count of the order $\mathcal{O}(\frac{1}{6}n^3)$. The solution is eventually computed as in Eq. (4.89).

	Number of flops
Cholesky factorization	$\frac{1}{6}n^3$
Inverse from Cholesky	$\frac{1}{3}n^3$
Inverting triangular matrix	$\frac{1}{6}n^3$
Multiplication C^TC	$\frac{1}{6}n^3$
Direct inversion	$\frac{1}{2}n^3$

Table 4.13: Operation count (flops) for some operations on a full matrix.

3. Forward and backward substitution.
In the third method the solution is computed by forward and backward substitution:

$$\begin{aligned} CC^Tx &= h && \text{Cholesky factorization of the normal matrix} \\ Cu &= h && \text{Computation of auxiliary vector } u \text{ via forward substitution} \\ C^Tx &= u && \text{Computation of } x \text{ via backward substitution} \end{aligned} \tag{4.93}$$

The forward and backward substitution can be done in-place (at the location of h), and the operation count is of the order $\mathcal{O}(n^2)$. The variance-covariance matrix $Q_{\hat{x}}$ is computed column wise by a sequence of forward and backward substitutions on the columns of the unit matrix of dimension n:

$$CC^TQ_{\hat{x}} = I_n \tag{4.94}$$

This again can be done in-place and the operation count for it is of the order $\mathcal{O}(\frac{1}{3}n^3)$.

Until now we only discussed solution techniques for full normal matrices, i.e. all entries are treated as nonzeros and hence have to operated upon. Many normal matrices encountered when solving problems within geodesy have a substantial number of nonzero entries. Geodetic examples are e.g. the photogrammetric block-bundle adjustment, the adjustment of classic geodetic (i.e. established by measuring directions and distances) networks.

Using the outer product formulation of the Cholesky factorization, it can be shown that the number of nonzeros in the Cholesky factor is greater than or equal to the number of nonzeros in the normal matrix, and that entries that are nonzero in the normal matrix remain nonzero in the Cholesky factor, assuming that exact numerical cancellation does not occur.[1] The gain in the number of nonzeros is called fill-in.

The amount of fill-in and its location depends on the order of the unknown parameters. As for the Cholesky factorization we do not need to permute parameters for stability reasons, we are free to apply a permutation specifically aiming at reducing fill-in. So, instead of solving the system

$$Nx = h \tag{4.95}$$

the equivalent permuted system

$$(PNP^T)(Px) = Ph \tag{4.96}$$

[1]This assumption is made, since it is generally not predictable if, when or where it occurs.

is solved. The permutation matrix P is orthogonal, thus $P^{-1} = P^T$. The solution vector Px is identical to the solution of (4.95), except for the order of the parameters in the solution vector.

Summarizing, we have three methods for computing the solution vector x and its variance-covariance matrix $Q_{\hat{x}}$, with, for a non-sparse matrix, equal operation count. However since the direct inversion method needs a pivot search and does not profit from the presence of zeros in the matrix, this alternative is dropped.

The second method (inversion of the Cholesky factor) needs always the full inverse of the normal matrix to be computed, and inversion of the factor and computation of the inverse of the normal matrix will only in special cases profit from zeros in the normal matrix.

The third method (forward and backward substitution) has an operation count for computation of the *solution only* of the order $\mathcal{O}(n^2)$. Computation of the solution as well as computation of its variance-covariance matrix (or parts thereof) take advantage of the sparsity of the normal matrix.

Since the late sixties, research has been directed to the problem of establishing good a priori orderings for the unknown parameters. For an overview see George and Liu (1980), Pissanetzky (1984).

For some problems that exhibit a regular structure, simple a priori orderings can be constructed (e.g. the determination of star abscissae on a great circle from data collected by the astrometric ESA satellite Hipparcos, see van der Marel (1988)). For other problems one has to use a heuristic algorithm. Among the most efficient and well-known algorithms are the minimum-degree, the (nested) dissection, the reverse Cuthill-McKee (Cuthill and McKee 1969) and the family of banker's algorithms (King 1970), (Levy 1971), (Snay 1976). For an extensive description of the first three methods see George and Liu (1980), for a description of the bankers's methods (and comparison with the other methods when applied to geodetic normal matrices) see de Jonge (1991) and de Jonge (1992).

The algorithms for minimizing fill-in can be divided into three groups, viz. those that strive directly for a minimization of the fill-in (minimum degree), those that try to find divisors that cut the matrix into independent parts (dissection methods) and those that try to concentrate the nonzeros in the normal matrix around the diagonal (reverse Cuthill-McKee and banker's).

The a priori ordering we will describe below belongs to the last type. The reason that it is beneficial when the nonzeros of the normal matrix are clustered around the diagonal is that fill-in only occurs in the region defined by

$$N_{(i,j)} \quad \text{with} \quad \min\{k \mid N_{(i,k)} \neq 0\} < j < i \quad \text{for} \quad i = 1, \ldots, n \tag{4.97}$$

This region is called the envelope of a matrix, and the number of elements containing it is called the profile. All elements inside the envelope, zero and nonzeros alike, are stored and operated upon, and the matrix is called a profile matrix.

The number of elements in the intersection of column i with the envelope is called the ith frontwidth, denoted by ω_i. The sum of ω_i for $i = 1$ to n equals the profile. For a full symmetric matrix of dimension n, ω_i equals $n - i$. Using the frontwidth, the operation count for the Cholesky factorization of a profile matrix can be given (see Table 4.14).

Forward and backward substitution also profit form the sparsity of the Cholesky factor. Furthermore it is possible to compute only those elements of the inverse of the normal matrix that correspond to the nonzero entries in the Cholesky factor (Golub and Plemmons 1980).

scheme	multiplicative operation count	additive operation count	storage (excl. administration)
Full	$\frac{1}{6}n^3 + \frac{1}{2}n^2 - \frac{2}{3}n$	$\frac{1}{6}n^3 - \frac{1}{6}n$	$\frac{1}{2}n^2 + \frac{1}{2}n$
Profile	$\frac{1}{2}\sum_{i=1}^{n-1}\omega_i(\omega_i + 3)$	$\frac{1}{2}\sum_{i=1}^{n-1}\omega_i(\omega_i + 1)$	$n + \sum_{i=1}^{n-1}\omega_i$

Table 4.14: Operation count and storage for Cholesky factorization of a full and a profile matrix (Pissanetzky 1984).

This inverse is denoted as sparse inverse. Depending on the sparsity of the Cholesky factor the sparse inverse can be computed more efficiently than the full inverse.

Instead of using one of the heuristic algorithms to reduce the fill-in in the Cholesky factor of the normal matrix originating from the processing of GPS data for relative positioning, we use an optimal or near optimal ordering that can be defined a priori. In the sequel this ordering will be denoted by 'd3', and is determined as follows.

For each parameter we know at which epoch it starts to be active and at which epoch it stops being active. For the coordinate parameters of a network that is continuously observed for one day with an interval of 30 seconds, we have e.g. that they are active from epoch 1 to 2880. If we define tropospheric zenith delays, for each hour, we have for each station 24 parameters that are active for 120 epochs, i.e. for epochs [1-120], [121-240], ... , [2661-2880]. Ambiguities are active for time spans that may vary considerably. In Figure 4.7 for the ambiguities of both the global and the Californian network of Table 4.12, the length of the time span for all ambiguities, sorted after increasing length of the time span is plotted. The length of the time span for the global network varies from 1 to 842 epochs, with an average of approximately 387 epochs. For the Californian network the length varies from 3 to 878, with an average of 426.

If we denote the first epoch that a parameter is active by ζ_1, and the last epoch that it is active by ζ_2, a near optimal ordering was found by first sorting the parameters in increasing order of ζ_1. If there are several parameters with equal ζ_1, this batch is again sorted in increasing order of ζ_2. The ordering was applied to four normal matrices:

Cal Californian network, L1 and L2, with ionospheric slant delays constrained via pseudo observables.

Pol Global network, L1 and L2, with ionospheric slant delays constrained via pseudo observables.

Poli Global network, L1 and L2, and estimation of ionospheric slant delays (non-constrained).

Poln Global network, L1 and L2, with ionospheric slant delays constrained via pseudo observables, and coordinates, tropospheric zenith delays and orbits constrained to a priori values (from e.g. the solution of Poli).

Both networks were observed for one day with an interval of 30 seconds, and had per station, per hour a tropospheric zenith delay modeled. The orbits were modeled by 8 parameters per satellite.

In Table 4.15 for these normal matrices the CPU time is listed that was needed to compute

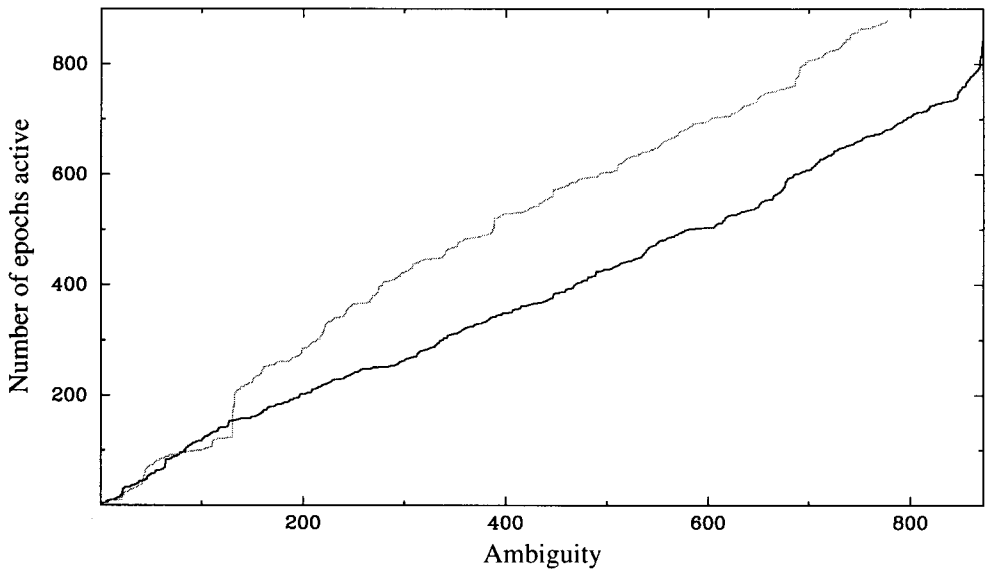

Figure 4.7: Length of time span that an ambiguity is active for the ambiguities of the global network (black curve), and the Californian network (grey curve). The ambiguities are sorted according to the length of this time span.

1. the full Cholesky factor and the full inverse from it,
2. a profile Cholesky factor from the normal matrix ordered by d3, and the full inverse from it,
3. a profile Cholesky factor from the normal matrix ordered by d3, and the sparse inverse from it.

All timing was done on a Pentium 100 MHz PC.

For 'Pol', 'Poli' and 'Poln', it was found that the ordering according to ζ_2 was arbitrary. Except for 'Poln', the d3 ordering is not optimal in the sense that it produced a small amount of fill-in. It gave however a smaller fill-in than the heuristic algorithms. Whether there exist an optimal ordering is impossible to say, see Garey and Johnson (1979).

The nonzero structures of the normal matrices of 'Cal' and 'Pol' are depicted in Figures 4.8 and 4.9. The parameters are ordered as L1 ambiguities, L2 ambiguities, coordinates, tropospheric zenith delays, orbit parameters. One tropospheric delay per station per hour was modeled, i.e. 24 delays per station. The orbits were modeled with 8 parameters per satellite. With 25 satellites observed, the total number of global parameters is 1275 for 'Cal', and 1369 for 'Pol'.

Figure 4.10 shows for 'Pol' in the lower triangle the lower triangular part of the normal matrix ordered by d3, and in the upper triangle the resulting (transposed) Cholesky factor. There is some, though not much, fill-in in the Cholesky factor, and all of it is contained within the envelope. Figure 4.11 shows the same for the normal matrix 'Poli'. As ionospheric slant delays were modeled, the number of ambiguities equals half the number of ambiguities in 'Pol'. The total number of parameters is 933.

	Cal	Pol	Poli	Poln
C full	120.0	148.9	46.3	37.5
N^{-1} full from C full	240.0	297.8	92.6	75.0
Total	360.0	446.7	138.9	112.5
C profile	14.0	21.8	9.8	1.8
N^{-1} from C profile	123.1	169.2	60.1	26.5
Total	137.1	191.0	69.9	28.3
C profile	14.0	21.8	9.8	1.8
Sparse N^{-1} from C profile	49.4	78.6	34.6	4.8
Total	63.4	100.4	44.4	6.6

Table 4.15: CPU time (in seconds on a Pentium 100 MHz PC) for some operations on the normal matrix from the Californian network, and the global network. For the operations on the profile matrix, the parameters were ordered according to a priori ordering d3.

Figure 4.12 shows the normal matrix and resulting Cholesky factor for the normal matrix 'Poln', where we only have ambiguities. The number of ambiguity parameters is 872. At right the normal matrix is in the original ordering, at left it is ordered by d3. For the ordering by d3, there is no fill-in.

These examples show that when the time span is large, and hence satellites set and rise during the time span, it is worthwhile to order the parameters in order to minimize the fill-in in the Cholesky factor and thereby reducing CPU time. A prerequisite is then of course that the solution is computed via Cholesky factorization followed by forward and backward substitution instead of direct inversion or inversion of the Cholesky factor.

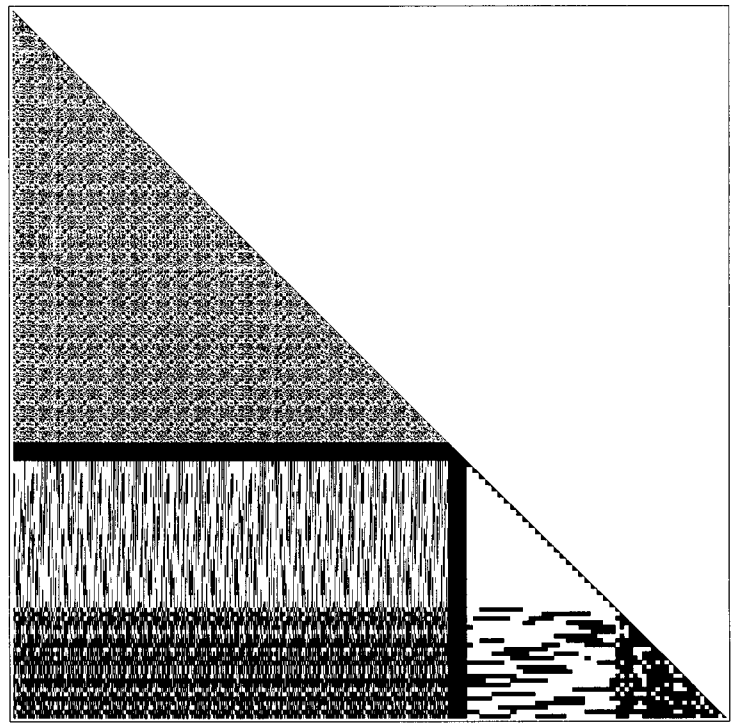

Figure 4.8: Nonzero structure of the lower triangular part of the normal matrix of the network in California (Cal), original ordering (1275 parameters).

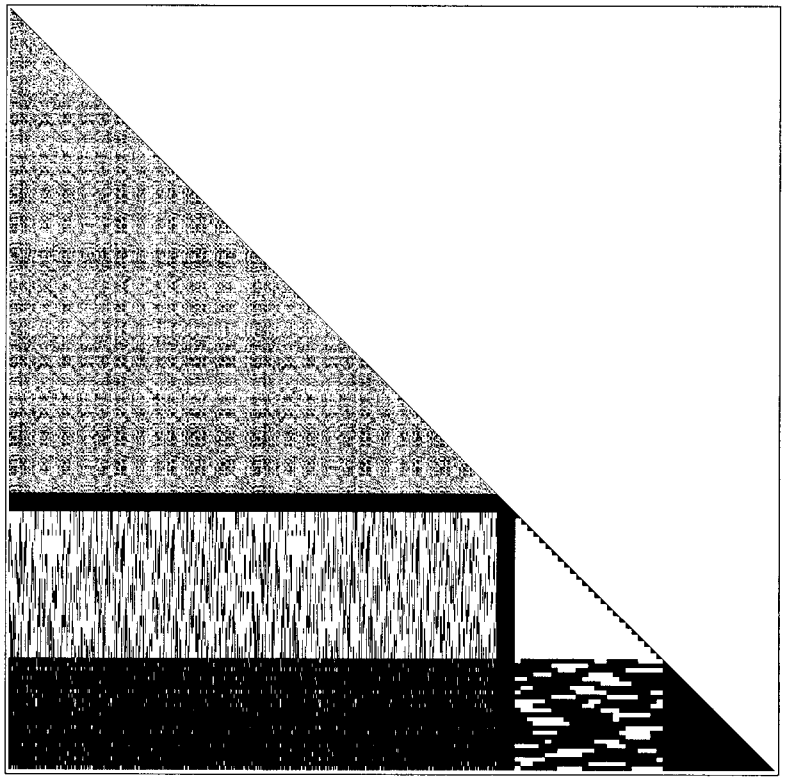

Figure 4.9: Nonzero structure of the lower triangular part of the normal matrix of the global network (Pol), original ordering (1369 parameters).

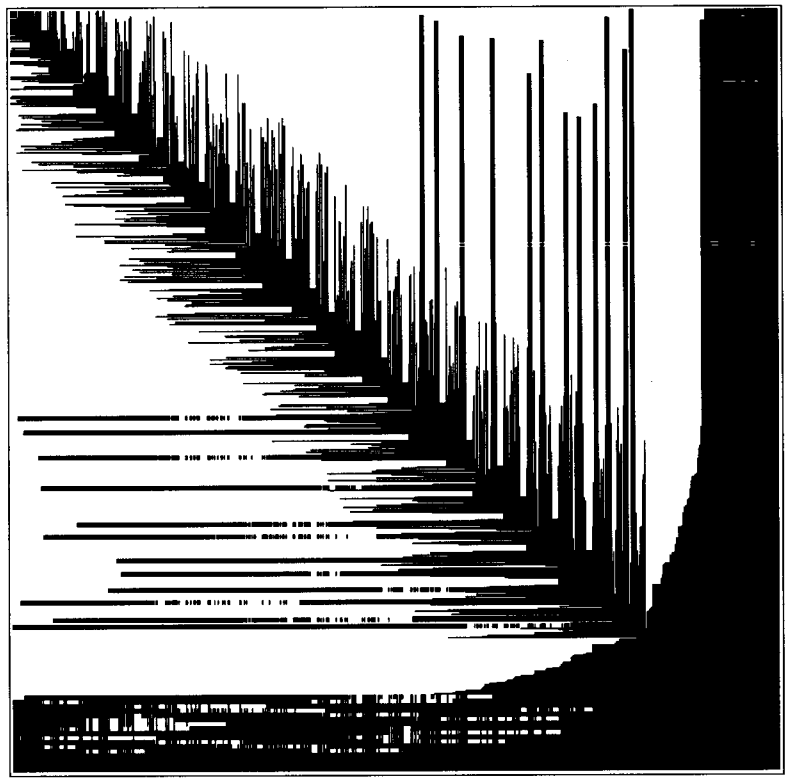

Figure 4.10: Nonzero structure of the lower triangular part of the normal matrix of the global network (Pol) ordered by d3, and the resulting (transposed) Cholesky factor (1369 parameters).

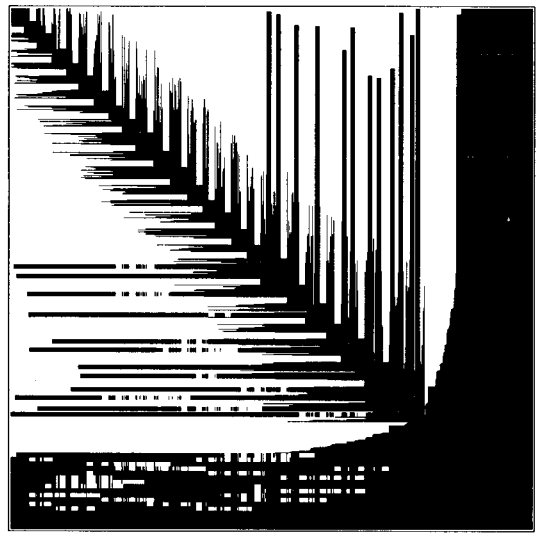

Figure 4.11: Nonzero structure of the lower triangular part of the normal matrix of the global network (Poli), ordered by d3, and the resulting (transposed) Cholesky factor (933 parameters).

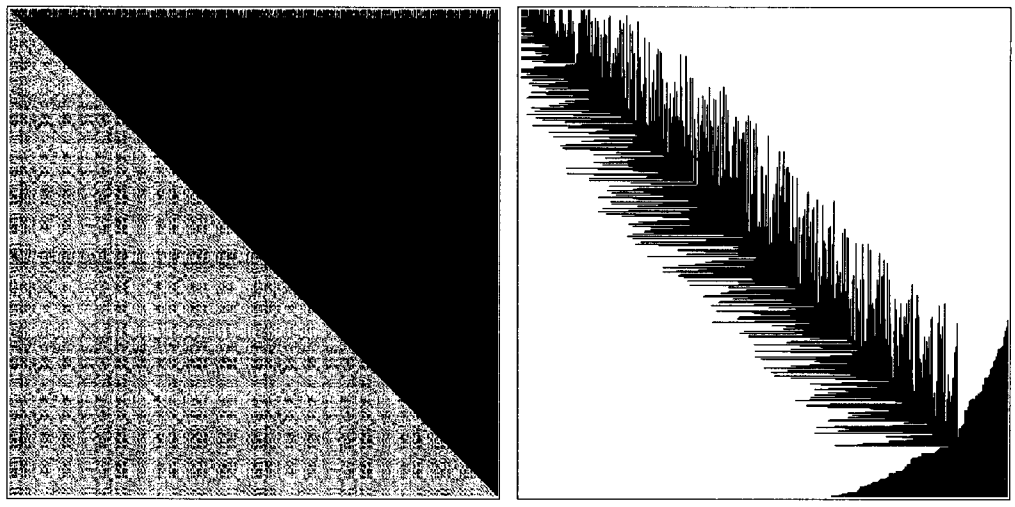

Figure 4.12: Nonzero structure of the lower triangular part of the ambiguity part of the normal matrix of the global network (Poln), and the resulting (transposed) Cholesky factor. Left: original ordering, right: ordered by d3 (872 parameters).

References

Bock, Y., S. A. Gourevitch, C. C. Councelman III, R. W. King, and R. I. Abbot (1986). Interferometric analysis of GPS phase observations. *manuscripta geodaetica 11*, 282–288.

Cuthill, E. and J. McKee (1969). Reducing the bandwidth of sparse symmetric matrices. In *Proceedings 24th National Conference ACM*. Brandon Systems Press, NJ. ACM publication no. P-69.

de Jonge, P. J. (1991). An analysis of ordering schemes for the unknowns during the solving of geodetic least squares systems. Technical Report 91.4, Faculty of Geodetic Engineering, Dept. of Mathematical and Physical Geodesy. Delft University of Technology, The Netherlands.

de Jonge, P. J. (1992). A comparative study of algorithms for reducing the fill-in during Cholesky factorization. *Bulletin Géodésique 66*(3), 296–305.

Dongarra, J. J., J. R. Bunch, C. B. Moler, and G. W. Stewart (1979). *LINPACK user's guide.* SIAM Publications, Philadelphia, USA.

Garey, M. R. and D. D. Johnson (1979). *Computers and Intractability. A Guide to the Theory of NP-Completeness.* W. H. Freeman and Company, New York.

George, A. and J. W. Liu (1980). *Computer solution of large sparse positive systems.* Prentice-Hall, Englewood Cliffs, NJ.

Goad, C. C. (Ed.) (1985). *Proceedings of the First International Symposium on Precise Positioning with the Global Positioning System*, Rockville, Maryland. National Geodetic Survey.

Golub, G. H. and R. J. Plemmons (1980). Large-scale geodetic least-squares adjustment by dissection and orthogonal decomposition. *Linear Algebra and its Applications 34*, 3–28.

Jonkman, N. F. (1998). Integer GPS-ambiguity estimation without the receiver-satellite geometry. LGR-Series 18, Delft Geodetic Computing Centre, Delft University of Technology.

King, I. P. (1970). An automatic reordering scheme for simultaneous equations derived from network systems. *International Journal Numerical Methods Engineering 2*, 497–509.

Langley, R. B. (1997). Navstar GPS constellation status (97-02-15). Canspace mail.

Levy, R. (1971). Restructuring of the structural stiffness matrix to improve computational efficiency. *Jet Propulsion Laboratory Technical Review* (1), 61–70.

Malagodi, M. S., K. M. Mostafa, T. A. Oblak, and R. N. Zeigler (1995). A radio frequency carrier phase measurement technique to enable non-invasive spinal/pelvic alignment monitoring for individuals seated in personal wheeled mobility devices. In *1995 IEEE Engineering in Medicine & Biology 17th Annual Conference & 21st Canadian Medical and Biological Engineering Conference*, Montreal, Web Edition. Paper 5.7.4.24.

Melbourne, W. G. (1985). The case for ranging in GPS based geodetic systems. See Goad (1985), pp. 373–386.

Pissanetzky, S. (1984). *Sparse matrix technology.* Academic Press, London.

Rutishauser, H. (1963). SYMINV2 (ACM Calgo algorithm 150). *Communications of the ACM 6*(2), 67–68.

Schaffrin, B. and Y. Bock (1988). A unified scheme for processing GPS dual-band phase observations. *Bulletin Géodésique 62*, 144–160.

Snay, R. A. (1976). Reducing the profile of sparse symmetric matrices. *Bulletin Géodésique 50*, 341–352.

Spilker Jr., J. J. (1996). GPS navigation data. In J. J. Spilker Jr. and B. W. Parkinson (Eds.), *Global Positioning System: Theory and Applications Volume I*, Volume 163 of *Progress in Astronautics and Aeronautics*, Chapter 4, pp. 121–176. American Institute of Aeronautics and Astronautics, Inc.

Teunissen, P. J. G. (1996). On the geometry of the ambiguity search space with and without ionosphere. *Zeitschrift für Vermessungswesen 121*(7), 332–341.

van der Marel, H. (1988). *On the great circle reduction in the data analysis for the astrometric satellite Hipparcos.* Ph. D. thesis, Delft University of Technology, Faculty of Geodetic Engineering.

Wübbena, G. (1985). Software developments for geodetic positioning with GPS using TI-4100 code and carrier measurements. See Goad (1985), pp. 403–412.

Chapter 5

Integer ambiguity estimation

5.1 Introduction

High precision relative GPS positioning is based on the very precise carrier phase measurements. As we saw in Chapter 2 these carrier phase observations are ambiguous, and hence extra model parameters, the carrier phase ambiguities, are introduced.

For short time spans, these ambiguities are strongly correlated, and the estimates for the geometric parameters have a poor precision (float solution). To achieve highest precision the integer nature of the DD ambiguities has to be exploited, i.e. one has to constrain the ambiguity parameters to their integer values (fixed solution).

As an example, Figure 5.1 shows, for a baseline of 12.7 km, by how much the precision of the baseline can improve, once one fixes the ambiguities. The three-dimensional scatter-plots shown, concern instantaneous positioning (single epoch baseline solutions) using dual frequency code and phase data (standard deviation code 30 cm, phase 3 mm). The coordinates are expressed in a local North, East, Height system. One hundred experiments were carried out (one at every 30 seconds) each represented by an asterisk; the dots are the projections on the walls of the grid. The scatter-plot at left contains the float solutions, the one at right the corresponding fixed solutions. Thus in the first case, the carrier phase ambiguities were treated as real numbers, whereas in the second case, they were solved for as integers. The figure clearly shows the dramatic improvement in precision with ambiguity resolution (note the difference in scale). The empirical standard deviation of the baseline coordinates before ambiguity fixing are $\sigma_N = 35$ cm, $\sigma_E = 20$ cm and $\sigma_U = 63$ cm and after $\sigma_N = 4.4$ mm, $\sigma_E = 3.8$ mm and $\sigma_U = 11.4$ mm. So, for this example, by fixing the ambiguities, the precision of the position coordinates improves by a factor of more than 50.

Although the improvement for short time spans is largest, an improvement in precision of the geometric parameters is achieved even for time spans up to 24 hours, see e.g. Mervart (1995).

Unfortunately, the estimation of the integer values for the ambiguities has proven to be a particularly hard and time-consuming problem, and several methods to tackle the problem have been proposed.

Traditionally, these methods have been developed for two different applications. On the one hand methods have been devised for applications where a multiple of stations are occupied for several hours until several days, and maximum inter-station distance can be of the order of thousands of kilometers, (Dong and Bock 1989), (Blewitt 1989), (Mervart 1995). On the other hand methods have been developed for rapid-static and navigation applications, where usually only two stations are involved, the maximum distance is some tens of kilometers, and time of occupation is of the order of seconds to minutes, or the receiver is moving: the Ambiguity Function Method (AFM) (Counselman and Gourevitch 1981), the Least-

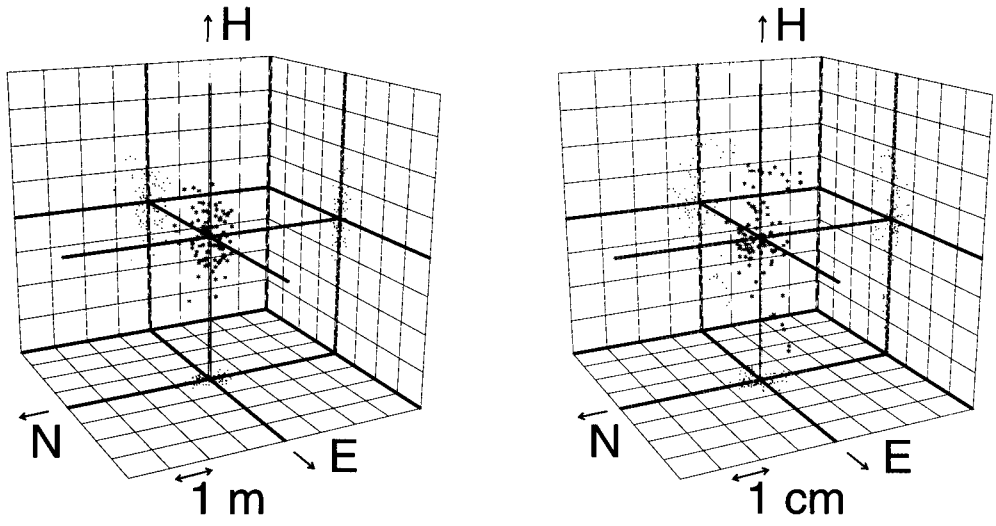

Figure 5.1: Scatter of float (left) and fixed solution (right) for a 12.7 km baseline (differential atmospheric delays assumed to be zero). The sampling rate was 1 second, and one epoch of dual frequency code and phase data of 7 satellites was used every 30 seconds during 50 minutes for instantaneous positioning. First sample at 14:10:00 (GPS time) on December 22, 1996.

Squares Ambiguity Search Technique (LSAST) (Hatch 1990), the Fast Ambiguity Resolution Approach (FARA) (Frei 1991), optimized search using Cholesky (Euler and Landau 1992) and the Least-squares AMBiguity Decorrelation Adjustment LAMBDA (Teunissen 1993).

At first sight it seems that ambiguity estimation for regional networks is treated as an entirely different problem, although conceptually there is no real difference with the short baseline case, as far as the estimation of the integer ambiguities is concerned. Of course, for longer inter-station distances more adequate mathematical models for e.g. tropospheric and ionospheric delays, as well for the orbital parameters have to be employed.

For regional networks applies that, due to their hybrid character with inter-station distances from some to several thousands of kilometers, and with some receiver-satellite combinations less well observed than others, the probability to find a valid integer solution for the complete vector of ambiguities is decreased. Consequently one sometimes has to resort to a proper subset for which such a solution exists.

Another difference between the regional network and the short baseline algorithms, is that in the former no validation step is involved, other than repeatability of the fixed coordinates between the days. The baseline algorithms that are used in rapid static and navigation applications have some sort of validation step which is based on the data itself, and thus can be computed and evaluated as soon as the data are collected and processed. It usually needs next to the best solution, the second best solution.

There are, however, similarities between some of the algorithms applied to the regional networks, and some of those applied to the short baselines. The methods described in Dong and Bock (1989), Blewitt (1989) as well as the 'sigma' and QIF (Quasi-Ionosphere Free) methods (Rothacher and Mervart 1996) all use a sequential conditioning (fixing) of ambiguities. The conditioning makes subsequent ambiguities become more precise, and usually

pushes the values of the ambiguities conditioned at the previous ambiguities towards integer values. The schemes differ in the criteria that are used for selecting the next ambiguity to be fixed, and in the way parameters are modeled and constrained in the preceding float solution.

This principle of conditioning of ambiguities is also found in the sequential conditional least-squares adjustment which is part of the LAMBDA method, which will be the main focus of this chapter. The latter differs from the methods above in the sense that if the resolution or adjustment is finished with a complete or partial vector of integer ambiguities, it is guaranteed that this vector minimizes the integer least-squares criterion, i.e. it guarantees that the fixed solution is an integer least-squares solution.

In Teunissen (1993) it was shown that the DD ambiguities are strongly correlated, especially when the observation time span is short, due to the small change in the receiver-satellite geometry. Since this correlation makes the estimation of the integer ambiguities via a sequential conditioning of the ambiguities far from efficient, a method to construct a decorrelating transformation for the ambiguities was proposed in (ibid). Alternative decorrelating methods can be found in Han and Rizos (1995), and in Li and Gao (1997), where it is also shown that decorrelating the ambiguities often has a favorable influence on the efficiency of other resolution methods too.

The ambiguities of the one day solutions for the large regional networks are less correlated, but still can be improved upon. This most likely will produce more ambiguities that will pass the criteria that allow them to be fixed, thereby further improving the eventual fixed solution. Possibly it could also reduce the time span for which a fixed solution can be computed. For monitoring coseismic and postseismic deformation with magnitudes up to several decimeters, and several mm/day, respectively, shortening these time spans would be very useful. The integer estimation in regional networks will be the topic of Chapter 6.

In this chapter, the LAMBDA method will be treated. The method can be divided into two parts. The first part consists of a general decorrelation of the ambiguities materialized in a so-called Z-matrix. The second part consists of the sequential conditional least-squares adjustment materialized by a depth-first search in the hyper-ellipsoid formed by the variance-covariance matrix of the ambiguities. Depending on the application at hand, if may be more efficient to compute the Z-matrix implicitly. The construction of the Z-matrix (explicitly and implicitly) and the search are derived, and described in detail.

Timing results for the integer estimation are given for a short baseline and for a small network with three of the four stations allowed to be moving.

5.2 The least-squares ambiguity decorrelation adjustment

The LAMBDA method has been developed for efficiently estimating the integer values of the GPS double difference ambiguities or DD-like functions of ambiguities. The method was introduced in Teunissen (1993), and fast positioning results using it were given in Teunissen (1994), de Jonge and Tiberius (1994) and Tiberius and de Jonge (1995).

The two main features of the method are

1. the decorrelation of the ambiguities, realized by a transformation of the original ambiguities, and

2. the actual integer ambiguity estimation

By the transformation, the existing large correlation between the ambiguities is reduced to a great extent. The construction of this decorrelating transformation, is the most time-consuming part of the method (albeit still very modest compared with other methods for ambiguity resolution, see Han (1995)).

The actual integer estimation is made for the transformed ambiguities. In practice this amounts to a search over grid points inside the n-dimensional ambiguity hyper-ellipsoid (with n the number of ambiguities), defined by the variance-covariance matrix of the ambiguities.

The shape and orientation of the ellipsoid are governed by the variance-covariance matrix of the ambiguities; the decorrelation realizes an ellipsoid that is very much more sphere-like than the original one, and therefore can be searched more efficiently.

The volume of the ellipsoid, which can be computed prior to the search, gives an indication of the number of candidates contained in the ellipsoid. Therefore, a limited number of candidates may be output of which one is the integer least-squares estimate for the vector of ambiguities.

The efficiency of the method through the decorrelation step has been explained in detail by analysis of the precision and correlation of the GPS double difference ambiguities in Teunissen and Tiberius (1994), Teunissen et al. (1994) and Teunissen (1995c).

5.3 The three-step estimation procedure

In Section 3.2 we divided the parameters into two groups, viz. global parameters x_1 and local parameters x_2. The system of linearized observation equations reads

$$E\{y\} = \begin{bmatrix} A_1 & A_2 \end{bmatrix} \begin{bmatrix} x_1 \\ x_2 \end{bmatrix} \tag{5.1}$$

For the purpose of the integer estimation of the ambiguity parameters the *global* parameters are again subdivided into two groups, viz. n_b parameters b that remain real valued, and n double difference ambiguity parameters a that may take integer values.

Parameters belonging to the first group are the parameters that are functions of the station and/or satellite coordinates (e.g. station coordinates, tropospheric zenith delays, ionospheric model parameters, and orbit parameters).

The system of linearized observation equations reads then

$$E\{y\} = \begin{bmatrix} A_b & A_a & A_2 \end{bmatrix} \begin{bmatrix} b \\ a \\ x_2 \end{bmatrix} \tag{5.2}$$

The design matrix $\begin{bmatrix} A_b & A_a & A_2 \end{bmatrix}$ is assumed to have full rank, i.e. the rank defect has been resolved (see Section 4.2), and the redundancy is greater than or equal to zero. The vector of observations may include all of the available GPS observable types, with at least one carrier phase type present. All of the models of Section 4.1 may be applied, as long as in the set of estimable functions, integer (or at least rational) DD-like functions of ambiguities occur. In the following the DD-like functions of ambiguities will be denoted as 'DD ambiguities' or simply 'ambiguities'.

The least-squares principle is used to compute estimates for the real valued parameters and the *integer* valued ambiguities:

$$\min_{b,a,x_2} \|y - A_b b - A_a a - A_2 x_2\|^2_{Q_y^{-1}} \text{ with } b \in \mathbf{R}^{n_b}, x_2 \in \mathbf{R}^{n_{x_2}} \text{ and } a \in \mathbf{Z}^n \tag{5.3}$$

The parameter estimation is carried out in three steps, see Teunissen (1995b). These steps are: 1. the computation of the float solution, 2. the integer ambiguity estimation and 3. the computation of the fixed solution.

1. Float solution
First the minimization (5.3) is carried out with $b \in \mathbf{R}^{n_b}, x_2 \in \mathbf{R}^{n_{x_2}}, a \in \mathbf{R}^n$. Real valued estimates for the ambiguities will be obtained. This full rank least-squares problem is solved via a Cholesky factorization of the normal matrix reduced for the local parameters x_2 (see Section 3.8).

If the system of normal equations is small and hence there is no need for ordering the unknowns for reasons of sparsity, the parameters are ordered as: 1. real valued parameters, 2. ambiguity parameters.

The system of normal equations for (5.2) reads then

$$\begin{bmatrix} N_b & N_{ba} \\ N_{ab} & N_a \end{bmatrix} \begin{bmatrix} b \\ a \end{bmatrix} = \begin{bmatrix} h_b \\ h_a \end{bmatrix} \tag{5.4}$$

The estimates and the variance-covariance matrix for the global parameters are:

$$\begin{bmatrix} \hat{b} \\ \hat{a} \end{bmatrix} \quad ; \quad \begin{bmatrix} Q_{\hat{b}} & Q_{\hat{b}\hat{a}} \\ Q_{\hat{a}\hat{b}} & Q_{\hat{a}} \end{bmatrix} \tag{5.5}$$

2. Integer ambiguity estimation
The second step consists of

$$\min_a \|\hat{a} - a\|^2_{Q_{\hat{a}}^{-1}} \text{ with } a \in \mathbf{Z}^n \tag{5.6}$$

This minimization yields the integer least-squares estimate for the vector of ambiguities: $\check{a}$. The computation of the integer estimate will be treated in detail in Section 5.5.

Due to the strong correlation that exists between the ambiguities, a decorrelating transformation is applied to them:

$$z = Z^T a \tag{5.7}$$

This is done by a systematic pair-wise decorrelation of the ambiguities. The construction of this transformation is treated in detail in Section 5.4. Through this so-called Z-transformation the variance-covariance matrix is transformed accordingly:

$$Q_{\hat{z}} = Z^T Q_{\hat{a}} Z \tag{5.8}$$

The actual integer minimization is made upon the transformed ambiguities. In practice the minimization (5.6) (but now for the transformed ambiguities z), amounts to a search

over grid points inside the n-dimensional ambiguity hyper-ellipsoid, defined by the variance-covariance matrix of the ambiguities

$$(\hat{z} - z)^T Q_{\hat{z}}^{-1} (\hat{z} - z) \leq \chi^2 \tag{5.9}$$

The search results in the grid point that is nearest to the real valued estimate, with nearness measured in the metric of the variance-covariance matrix, see Teunissen (1993). χ^2 is a positive constant which should be chosen such that at least one (or two if one also needs the second best solution) grid point is contained in the ellipsoid. On the other hand not too many more grid points should be contained in the ellipsoid, since that would slow down the search. Methods to determine a suitable χ^2 will be given in Section 5.6.

Depending of the computation scheme that is used, the integer estimate $\check{z}$ has to be back-transformed to $\check{a}$. It is however also possible to continue with $\check{z}$. In Section 5.9 we will show in which circumstances what computation scheme should be chosen.

3. Fixed solution
The final solution $\check{b} = \hat{b}|\check{a}$, with the ambiguities fixed to their integer least-squares estimates $\check{a}$, reads

$$\begin{aligned} \check{b} &= \hat{b} - Q_{\hat{b}\hat{a}} Q_{\hat{a}}^{-1} (\hat{a} - \check{a}) \\ \check{x}_2 &= \hat{x}_2 - Q_{\hat{x}_2\hat{a}} Q_{\hat{a}}^{-1} (\hat{a} - \check{a}) \end{aligned} \tag{5.10}$$

The least-squares estimates $\check{b}, \check{a}$, and $\check{x}_2$ are the solution to the constrained minimization (5.3). Note that in practice $\check{b}$ is not computed using (5.10), see Section 5.9, and $\check{x}_2$ is often not computed at all.

5.4 Integer ambiguity estimation: transformation

5.4.1 The decorrelating or Z-transformation, introduction

To explain the concept of the decorrelating transformation we decompose the variance-covariance matrix $Q_{\hat{a}}$ into

$$Q_{\hat{a}} = L^{-T} D^{-1} L^{-1} \tag{5.11}$$

Note that this corresponds to the inverse of the LDL^T decomposition of $Q_{\hat{a}}^{-1}$ which is easily derived from the already computed Cholesky factor, see Eq. (5.17). The principle of the decorrelation is to find a matrix Z, which is an integer approximation of matrix L. If we would be able to find a matrix Z that fulfills the requirements in Teunissen (1995a) i.e. all entries of Z as well of its inverse are integer valued ($\Rightarrow |Z|$ and $|Z^{-1}| = \pm 1$), and that exactly equals L, then with (5.8)

$$Q_{\hat{z}} = Z^T Q_{\hat{a}} Z = Z^T L^{-T} D^{-1} L^{-1} Z = D^{-1} \tag{5.12}$$

The transformed ambiguities $\hat{z}$ are fully decorrelated and the integer minimization reduces to a simple rounding of the real valued estimates, see Teunissen (1995b). In practice, a matrix with integer entries that transforms the variance-covariance matrix to a diagonal matrix is seldom found, and hence the transformed ambiguities are still (weakly) correlated.

The result of the decorrelation process is the square $n \times n$ transformation matrix Z. The estimate $\hat{z}$ follows from $\hat{z} = Z^T\hat{a}$. The factors of the variance-covariance matrix are updated in the decorrelation process: $\tilde{D}^{-1}$ and $\tilde{L}^{-1}$. They satisfy

$$Q_{\hat{z}} = \tilde{L}^{-T}\tilde{D}^{-1}\tilde{L}^{-1} \tag{5.13}$$

The problem (5.6) has now been transformed into the following minimization

$$\min_z \|\hat{z} - z\|^2_{Q_{\hat{z}}^{-1}} \text{ with } z \in \mathbf{Z}^n \tag{5.14}$$

Inversion of $\tilde{L}^{-1}$ yields $\tilde{L}$ and inversion of $\tilde{D}^{-1}$ yields $\tilde{D}$. They satisfy

$$Q_{\hat{z}}^{-1} = \tilde{L}\tilde{D}\tilde{L}^T \tag{5.15}$$

This decomposition into $\tilde{L}$ and $\tilde{D}$ is then used in the search, see Section 5.5.

5.4.2 Decomposition of the variance-covariance matrix

The ambiguity decorrelating transformation can be computed in several ways depending on the matrix one starts with, and on the type of factorization one uses. One can either use the variance-covariance matrix of the ambiguities, or its inverse, and the factorization can be either an LDL^T, or an L^TDL factorization. Schematic we have

$$\begin{array}{llll}
Q_{\hat{a}}^{-1} = L_1 D_1 L_1^T & ; & Q_{\hat{a}} = L_1^{-T} D_1^{-1} L_1^{-1} & \text{cf. (Teunissen 1993)} \\
Q_{\hat{a}}^{-1} = L_2^T D_2 L_2 & ; & Q_{\hat{a}} = L_2^{-1} D_2^{-1} L_2^{-T} & \\
Q_{\hat{a}} = L_3^T D_3 L_3 & ; & Q_{\hat{a}}^{-1} = L_3^{-1} D_3^{-1} L_3^{-T} & \\
Q_{\hat{a}} = L_4 D_4 L_4^T & ; & Q_{\hat{a}}^{-1} = L_4^{-T} D_4^{-1} L_4^{-1} & \text{cf. (Teunissen 1995b)}
\end{array} \tag{5.16}$$

where:

L_i is a unit lower triangular matrix (i.e. with ones on the diagonal) and

D_i is a diagonal matrix with elements $d_1, \ldots, d_n$

Note that $L_1 = L_3^{-1}, L_2 = L_4^{-1}$ and that $D_1 = D_3^{-1}, D_2 = D_4^{-1}$. In Teunissen (1993) the LDL^T factorization of the inverse of the variance-covariance matrix is used, and in Teunissen (1995b) the LDL^T factorization of the variance-covariance matrix itself.

Here we depart from the LDL^T factorization of the inverse of the variance-covariance matrix. The reason for it is, that depending on the chosen computation scheme, the Cholesky factor C_a of the inverse of the variance-covariance matrix of the ambiguities is already available in the float solution. With the Cholesky factor C of the normal matrix referring to the global parameters partitioned as

$$C = \begin{bmatrix} C_b & 0 \\ C_{ab} & C_a \end{bmatrix} \tag{5.17}$$

with C_a a lower triangular matrix of dimension n, we have $Q_{\hat{a}}^{-1} = C_a C_a^T$. The Cholesky factor C_a becomes thus available at no extra cost in the float solution.

The LDL^T decomposition of $Q_{\hat{a}}^{-1}$ is easily constructed from the Cholesky factor. It holds that

$$C_a = L\sqrt{D} \tag{5.18}$$

Note that matrix $Q_{\hat{a}}^{-1}$ is symmetric positive definite: for the diagonal elements of D it holds that $d_i > 0 \; \forall \; i = 1, \ldots, n$.

The corresponding factorization of the variance-covariance matrix reads

$$Q_{\hat{a}} = L^{-T} D^{-1} L^{-1} \tag{5.19}$$

An interpretation can be given to the elements of matrix D^{-1}, see Teunissen (1993): they are the conditional variances of the double difference ambiguities.

$$d_i^{-1} = \sigma^2_{\hat{a}_{i|i+1,\ldots,n}} \tag{5.20}$$

Conditioned means here that one or more ambiguities are constrained (conditioned) at an in principle arbitrary value. In the context of integer ambiguity estimation this value will be the integer found for a particular ambiguity. The conditional estimate for ambiguity i, conditioned at ambiguities $i+1, \ldots, n$, is denoted by

$$\hat{a}_{i|i+1,\ldots,n} \tag{5.21}$$

Instead of inverting the LDL^T decomposition, one can compute $Q_{\hat{a}} = L^{-T} D^{-1} L^{-1}$ directly. This should be done when the factor L is not already available. An algorithm for this factorization in an outer product formulation which is used to explain some features of the construction of the transformation matrix Z in Section 5.4.3, reads in stylized MATLAB notation:

Given the symmetric positive definite matrix Q, an $L^T DL$ factorization is computed by the outer product method. Matrix L may over write matrix Q; the latter is destroyed during the computation. Only the lower triangular part of Q is accessed.

for $i = n : -1 : 1$
  $D(i,i) = Q(i,i)$
  $L(i, 1:i) = Q(i, 1:i)/\sqrt{Q(i,i)}$
  for $j = 1 : i-1$
    $Q(j, 1:j) = Q(j, 1:j) - L(i, 1:j)L(i,j)$
  end
  $L(i, 1:i) = L(i, 1:i)/L(i,i)$.
end

5.4.3 Modifying the decomposition

Note: the construction of the transformation matrix Z is based on the variance-covariance matrix $Q_{\hat{a}}$. To simplify notation we will assume for the remainder of this section that we have the L^TDL factorization of $Q_{\hat{a}}$ (the third option of (5.16) instead of the first), thus $d_i = \sigma^2_{\hat{a}_{i|i+1,\ldots,n}}$.

The construction of the $n \times n$ Z matrix in (5.8) consists of a sequence of integer approximated Gauss transformations (see Section 5.4.4) and permutations. Both are admissible ambiguity transformations, see e.g. Teunissen (1995a). The actual decorrelation is carried out by the integer Gauss transformation. If necessary the ambiguities are reordered to allow for further decorrelation.

Before we continue, we will discuss the triangular decomposition after transformation, analogously to the decomposition discussed in Teunissen (1995b) (Eqs. 47–49 at page 79).

The unit lower triangular matrix L and the diagonal matrix D are partitioned into

$$L = \begin{bmatrix} L_{11} & & \\ L_{21} & L_{22} & \\ L_{31} & L_{32} & L_{33} \end{bmatrix} \text{ and } D = \begin{bmatrix} D_{11} & & \\ & D_{22} & \\ & & D_{33} \end{bmatrix} \tag{5.22}$$

Sub-matrix L_{22} is of order 2, L_{11} of order $i-1$, and L_{33} of order $n-i-1$. The dimension of the other sub-matrices in L and D are determined accordingly. If we apply a two-dimensional ambiguity transformation to the i-th and the $(i+1)$-th ambiguity, with the block-diagonal matrix

$$Z = \begin{bmatrix} I_{i-1} & & \\ & Z_{22} & \\ & & I_{n-i-1} \end{bmatrix} \tag{5.23}$$

with Z_{22} a square and full rank 2×2 matrix, we get the new triangular decomposition $L'^T D' L'$, with

$$L' = \begin{bmatrix} L_{11} & & \\ \bar{L}_{21} & \bar{L}_{22} & \\ L_{31} & \bar{L}_{32} & L_{33} \end{bmatrix} \text{ and } D' = \begin{bmatrix} D_{11} & & \\ & \bar{D}_{22} & \\ & & D_{33} \end{bmatrix} \tag{5.24}$$

The fact that only L_{21}, L_{22}, L_{32} and D_{22} change, can be explained by looking at the outer product form of the L^TDL factorization as given in Section 5.4.2. We have (the variance-covariance matrix is symmetric):

$$Z^T Q_{\hat{a}} Z = \begin{bmatrix} Q_{11} & & \\ Z_{22}^T Q_{21} & Z_{22}^T Q_{22} Z_{22} & \\ Q_{31} & Q_{32} Z_{22} & Q_{33} \end{bmatrix} = \begin{bmatrix} Q_{11} & & \\ \bar{Q}_{21} & \bar{Q}_{22} & \\ Q_{31} & \bar{Q}_{32} & Q_{33} \end{bmatrix} \tag{5.25}$$

Let us look at the updating step of the algorithm i.e. the part where an outer product is subtracted from the matrix. The parts of the outer product that are affected by Z always coincide with the parts of Q affected by Z. So the 'reduced' Q has the same structure as in (5.25). Since L is basically obtained from extracting rows from the reduced Q divided by the square root of the corresponding diagonal element, and D is set equal to the diagonal element, the modified decomposition will be as indicated in (5.24).

The modified factor can be related to the original one. We know that

$$L'^T D' L' = Z^T L^T D L Z \tag{5.26}$$

From this relation we easily derive for $\bar{L}_{32}$

$$L_{33}^T D_{33} \bar{L}_{32} = L_{33}^T D_{33} L_{32} Z_{22} \tag{5.27}$$

or,

$$\bar{L}_{32} = L_{32} Z_{22} \tag{5.28}$$

For $\bar{L}_{22}$ holds that

$$\bar{L}_{22}^T \bar{D}_{22} \bar{L}_{22} + \bar{L}_{32}^T D_{33} \bar{L}_{32} = Z_{22}^T (L_{22}^T D_{22} L_{22} + L_{32}^T D_{33} L_{32}) Z_{22} \tag{5.29}$$

or, using (5.28)

$$\bar{L}_{22}^T \bar{D}_{22} \bar{L}_{22} = Z_{22}^T (L_{22}^T D_{22} L_{22}) Z_{22} \tag{5.30}$$

And for $\bar{L}_{21}$ holds that

$$\bar{L}_{22}^T D_{22} \bar{L}_{21} + \bar{L}_{32}^T D_{33} L_{31} = Z_{22}^T (L_{22}^T D_{22} L_{21} + L_{32}^T D_{33} L_{31}) \tag{5.31}$$

from which can be derived after substituting (5.28)

$$\bar{L}_{22}^T \bar{D}_{22} \bar{L}_{21} = Z_{22}^T L_{22}^T D_{22} L_{21} \tag{5.32}$$

Using the relation $Z_{22}^T L_{22}^T D_{22} = \bar{L}_{22}^T \bar{D}_{22} \bar{L}_{22} (L_{22} Z_{22})^{-1}$ which follows from Eq. (5.30) we finally get

$$\bar{L}_{21} = \bar{L}_{22} (L_{22} Z_{22})^{-1} L_{21} \tag{5.33}$$

Thus, once matrix Q is factored as $Q = L^T D L$, the factorization of $Z^T Q Z$ with Z defined in (5.23), can be efficiently computed from the existing factorization. In the unit lower triangular matrix L only the rows i and $i+1$ and the columns i and $i+1$ change. The modification of the diagonal matrix D is limited to the elements (i,i) and $(i+1,i+1)$. The transformation of the variance-covariance matrix can be realized by updating the factors L and D.

5.4.4 The integer Gauss transformation

The relations found in Section 5.4.3 (Eqs. (5.28), (5.30), and (5.33)) can be further simplified if we restrict the transformation (sub-)matrix to a single Gauss-transformation (see Golub and Van Loan (1989) Section 3.2.1):

$$Z_{22} = \begin{bmatrix} 1 & 0 \\ \alpha & 1 \end{bmatrix} \tag{5.34}$$

Then

$$\bar{L}_{32} = \begin{bmatrix} l_{i+2,i} + \alpha l_{i+2,i+1} & l_{i+2,i+1} \\ l_{i+3,i} + \alpha l_{i+3,i+1} & l_{i+3,i+1} \\ \vdots & \vdots \\ l_{n,i} + \alpha l_{n,i+1} & l_{n,i+1} \end{bmatrix} \tag{5.35}$$

$$\bar{L}_{22} = \begin{bmatrix} 1 & 0 \\ l_{i+1,i} + \alpha & 1 \end{bmatrix} \text{ and } \bar{D}_{22} = \begin{bmatrix} d_i & 0 \\ 0 & d_{i+1} \end{bmatrix} \tag{5.36}$$

$$\bar{L}_{21} = L_{21} \tag{5.37}$$

We see that only the unit lower triangular matrix L changes. The diagonal matrix D is left unchanged by a single Gauss transformation. In other words: the conditional variances do not change, only the conditional covariances and thus the unconditional variances change. This can intuitively be understood since the order of ambiguities was not changed.

To achieve full decorrelation we would like to choose $\alpha = -l_{i+1,i}$. In general $l_{i+1,i} \notin \mathbf{Z}$. To meet the requirements for the construction of the Z-matrix, α is approximated by $-nint(l_{i+1,i})$, where *nint* stands for the nearest integer operator. With this integer approximation, we can make the absolute value of any non-diagonal element of L less than or equal to $\frac{1}{2}$. The integer Gauss transformation was discussed in Teunissen (1994) and Teunissen (1995a).

In general, if we take for Z the unit matrix with an additional α at position (i, j), with $i > j$, the elements that change are

$$\begin{aligned} l'_{i,j} &= l_{i,j} + \alpha \\ l'_{k,j} &= l_{k,j} + \alpha l_{k,i} \quad \text{for} \quad k = i+1, \ldots, n \end{aligned} \tag{5.38}$$

The detailed algorithm for the computation of a Z-transformation matrix, that will make the absolute value of all non-diagonal elements of L less than or equal to $\frac{1}{2}$, can be found in de Jonge and Tiberius (1996). Given the unit lower triangular factor L from the $L^T DL$ factorization of the variance-covariance matrix $Q_{\hat{a}}$, it computes a Z-transformation matrix. Z will be lower triangular on output if set to the unit matrix on input. The computation of this matrix is performed column wise from n to 1. Instead of decorrelating all n columns, one can apply the algorithm to only one column. The vector with estimates $\hat{a}$ is transformed to $\hat{z} = Z^T \hat{a}$. The original factor L is transformed to $L' = LZ$ for which holds: $L'^T DL' = Q_{\hat{z}}$. Factor L remains lower triangular.

5.4.5 Reordering of the ambiguities

As was explained in Teunissen et al. (1994) and Teunissen (1995b), the signature of the conditional variances shows, in the case of a single baseline, a distinctive discontinuity when passing from the third to the fourth ambiguity encountered in the search or conditioning process (see Figure 5.2). In general for a network of r receivers with the coordinates of one receiver fixed, this discontinuity is found when passing from the $(3r-3)$-th to the $(3r-2)$-th ambiguity (see Figure 5.3). The size of this discontinuity is governed by the length of the observation time span. In Section 5.5.3 it will be shown that it is this discontinuity in the signature that causes the search to be highly inefficient. Carrying out the integer estimation (5.6) will be a very time-consuming task (Teunissen et al. 1994), (Teunissen 1995c).

As we saw in Section 5.4.4, the integer Gauss transformation decorrelates the ambiguities, but it leaves the conditional variances, and thus the discontinuity, intact. Looking at the definition of conditional variance, it seems logical to change the order of the ambiguities if we want to change the signature. In Teunissen et al. (1994), Teunissen et al. (1995) and

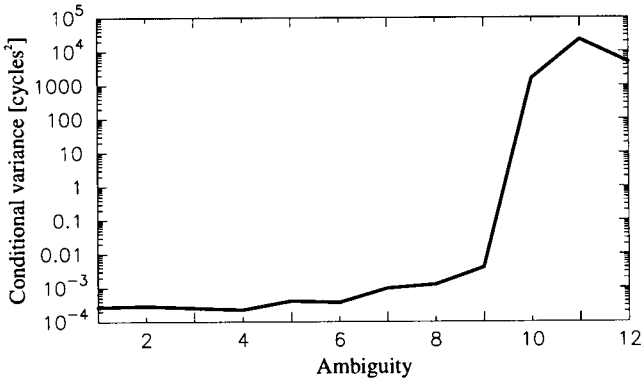

Figure 5.2: Conditional variances of the L1 and L2 ambiguities for a single baseline, with 7 satellites observed and a time span of 1 second.

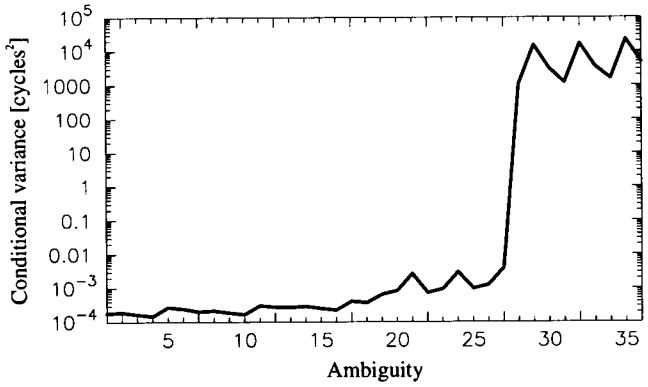

Figure 5.3: Conditional variances of the L1 and L2 ambiguities for a 4-station network, with 7 satellites observed and a time span of 1 second.

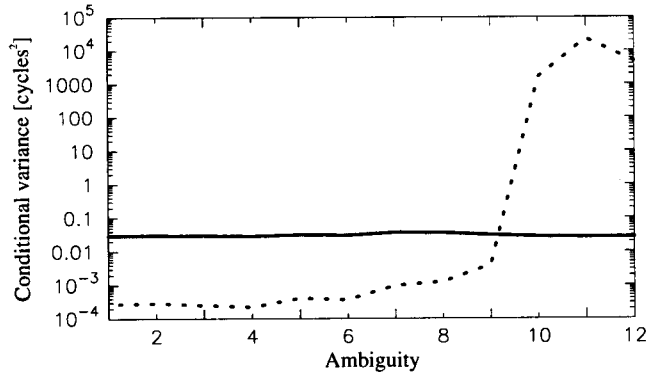

Figure 5.4: Conditional variances of the L1 and L2 ambiguities for a single baseline before (dotted line, cf. Figure 5.2) and after transformation (solid line).

Teunissen (1996) this problem, and the solution for it, is explained geometrically in terms of the form and orientation of the ambiguity search space.

To change the order of the i-th and the $(i+1)$-th ambiguity we again apply a local transformation but now using the 2-by-2 permutation matrix P for Z_{22}. With (5.28), (5.30) and (5.33) we have

$$\bar{L}_{32} = L_{32}P \tag{5.39}$$

$$\bar{L}_{22}^T \bar{D}_{22} \bar{L}_{22} = P^T L_{22}^T D_{22} L_{22} P \tag{5.40}$$

$$\bar{L}_{21} = \bar{L}_{22}(L_{22}P)^{-1} L_{21} \tag{5.41}$$

where

$$P = P^T = \begin{bmatrix} 0 & 1 \\ 1 & 0 \end{bmatrix} \tag{5.42}$$

Working out these relations we get

$$\bar{L}_{32} = \begin{bmatrix} l_{i+2,i+1} & l_{i+2,i} \\ l_{i+3,i+1} & l_{i+3,i} \\ \vdots & \vdots \\ l_{n,i+1} & l_{n,i} \end{bmatrix} \tag{5.43}$$

$$\bar{L}_{22} = \begin{bmatrix} 1 & 0 \\ l'_{i+1,i} & 1 \end{bmatrix} = \begin{bmatrix} 1 & 0 \\ \frac{l_{i+1,i} d_{i+1}}{d_i + l_{i+1,i}^2 d_{i+1}} & 1 \end{bmatrix} \tag{5.44}$$

$$\bar{D}_{22} = \begin{bmatrix} d'_i & 0 \\ 0 & d'_{i+1} \end{bmatrix} = \begin{bmatrix} d_{i+1} - \frac{l_{i+1,i}^2 d_{i+1}^2}{d_i + l_{i+1,i}^2 d_{i+1}} & 0 \\ 0 & d_i + l_{i+1,i}^2 d_{i+1} \end{bmatrix} \tag{5.45}$$

$$\bar{L}_{21} = \begin{bmatrix} -l_{i+1,i} & 1 \\ \frac{-l_{i+1,i}^2 d_{i+1}}{d_i + l_{i+1,i}^2 d_{i+1}} + 1 & \frac{l_{i+1,i} d_{i+1}}{d_i + l_{i+1,i}^2 d_{i+1}} \end{bmatrix} L_{21} \tag{5.46}$$

Simplifying Eqs. (5.44–5.46) gives

$$d'_{i+1} = d_i + l_{i+1,i}^2 d_{i+1} \tag{5.47}$$

$$d'_i = \frac{d_i}{d'_{i+1}} d_{i+1} \tag{5.48}$$

$$l'_{i+1,i} = \frac{d_{i+1}}{d'_{i+1}} l_{i+1,i} \tag{5.49}$$

and

$$\bar{L}_{21} = \begin{bmatrix} -l_{i+1,i} & 1 \\ \frac{d_i}{d'_{i+1}} & l'_{i+1,i} \end{bmatrix} L_{21} \tag{5.50}$$

The factors L and D are updated, as shown in (5.24) and (5.25), as to correspond to the transformed (permuted) ambiguities.

5.4.6 Putting it all together

For the actual integer minimization we strive for largely decorrelated ambiguities, and furthermore we want to have the most precise ambiguity at position n where the search starts (see Section 5.5.3). In other words, we strive for

$$d_n \leq \ldots \leq d_1 \text{ with } d_i \text{ from } D \text{ of } Q_{\hat{a}} = L^T D L \tag{5.51}$$

and therefore we interchange two conditional variances if

$$d'_{i+1} < d_{i+1} \tag{5.52}$$

Alternatingly we will have a decorrelation and a reordering step. We start with the last ambiguity and we try to reach the first one. At each step i we check whether the interchange of d_i and d_{i+1} will decrease the value for the latter. After each interchange we start again at the last ambiguity. The algorithm ends if during one sweep from n to 1 no further interchanges can be performed.

The algorithm requires element $l_{i+1,i}$ to be as small as possible. Therefore we take care that the absolute values of the off-diagonal elements of columns $i \ldots n$ are less than or equal to $\frac{1}{2}$, by applying the column wise decorrelating Z-transformation of Section 5.4.4. Figure 5.4 shows the signature of conditional variances before and after decorrelation for a single baseline case. The decorrelating transformation has effectively removed the discontinuity in the signature, thereby enabling a much more efficient search.

In Teunissen (1994) the ambiguity decorrelation number was introduced as a measure for the decorrelation between the ambiguities. With the correlation matrix of $Q_{\hat{a}}$ defined as

$$R_{\hat{a}} = \{diag(Q_{\hat{a}})\}^{-\frac{1}{2}} Q_{\hat{a}} \{diag(Q_{\hat{a}})\}^{-\frac{1}{2}} \tag{5.53}$$

where $diag(Q_{\hat{a}})$ is a diagonal matrix with elements equal to those of the diagonal of $Q_{\hat{a}}$, it reads

$$r_{\hat{a}} = \sqrt{|R_{\hat{a}}|} \tag{5.54}$$

By definition $0 \leq r_{\hat{a}} \leq 1$. When the ambiguities are uncorrelated $r_{\hat{a}}$ equals 1; the more correlation exists between the ambiguities, the smaller the ambiguity decorrelation number becomes. Alternatively, the ambiguity decorrelation number is computed as

$$r_{\hat{a}} = \prod_{i=1}^{n} \frac{\sigma_{\hat{a}_{i|i+1,\ldots,n}}}{\sigma_{\hat{a}_i}} \tag{5.55}$$

If the ambiguities are uncorrelated, $\sigma_{\hat{a}_{i|i+1,\ldots,n}} = \sigma_{\hat{a}_i}$, and hence $r_{\hat{a}} = 1$. The ambiguity decorrelation number can be used to compare the measure of correlation of two variance-covariance matrices of the *same* dimension, i.e. it may be used to compare the correlation between the ambiguities before and after the decorrelating transformation.

As an illustration of the Z-transformation we will apply it to an artificial three-dimensional example. The synthetic variance covariance matrix results from the addition of a scaled unit matrix and a rank-2 matrix with elements that are significantly larger than the scale factor of the first matrix, see also Teunissen et al. (1994).

$$Q_{\hat{a}} = \begin{bmatrix} 6.290 & 5.978 & 0.544 \\ 5.978 & 6.292 & 2.340 \\ 0.544 & 2.340 & 6.288 \end{bmatrix} \tag{5.56}$$

The ambiguities have large variances and in particular a_1 and a_2 are strongly correlated.

$$\begin{array}{ll} \sigma_{\hat{a}_1} = 2.508 & \rho_{\hat{a}_1\hat{a}_2} = 0.950 \\ \sigma_{\hat{a}_2} = 2.508 & \rho_{\hat{a}_1\hat{a}_3} = 0.086 \\ \sigma_{\hat{a}_3} = 2.508 & \rho_{\hat{a}_2\hat{a}_3} = 0.372 \end{array} \tag{5.57}$$

The matrix Z^T reads

$$Z^T = \begin{bmatrix} 1 & -1 & 0 \\ -2 & 3 & -1 \\ 3 & -3 & 1 \end{bmatrix} \tag{5.58}$$

Note that the matrix Z^T given here is not unique. Reflections (change of sign) and permutations (reordering) of the ambiguities do not change the amount of correlation between the ambiguities.

Matrix Z^T indeed has integer elements and $|Z^T| = 1$. The variance covariance matrix of the transformed ambiguities z reads

$$Q_{\hat{z}} = \begin{bmatrix} 0.626 & 0.230 & 0.082 \\ 0.230 & 4.476 & 0.334 \\ 0.082 & 0.334 & 1.146 \end{bmatrix} \tag{5.59}$$

and it can be seen that the ambiguities are largely decorrelated.

$$\begin{array}{ll} \sigma_{\hat{z}_1} = 0.791 & \rho_{\hat{z}_1\hat{z}_2} = 0.137 \\ \sigma_{\hat{z}_2} = 2.116 & \rho_{\hat{z}_1\hat{z}_3} = 0.097 \\ \sigma_{\hat{z}_3} = 1.071 & \rho_{\hat{z}_2\hat{z}_3} = 0.147 \end{array} \tag{5.60}$$

5.4.7 Back transformation

Once the transformed integer minimization problem (5.14) has been solved, we have to back transform the integer estimate $\check{z}$, in order to obtain the integer least-squares estimate $\check{a}$. The relation reads

$$Z^T\check{a} = \check{z} \tag{5.61}$$

The inverse of the matrix Z^T does not need to be computed explicitly. Matrix Z^T has only integer elements, has full rank, with $|Z^T| = \pm 1$, and is square and usually dense, as the transformation is truly a multi-satellite transformation (Teunissen 1995a). Therefore an LU factorization can be made by Gaussian elimination with partial pivoting, see Chapter 3 of Golub and Van Loan (1989) and Chapter 1 of Dongarra et al. (1979) (the LINPACK routines DGEFA and DGESL). Then the integer least-squares estimate $\check{a}$ is obtained via forward and backward substitution. Note that the intermediate result, after the forward substitution, is in general *not* an integer vector. The forward and backward substitution can be repeated for any other candidate, e.g. the second best $\check{a}'$.

One can also compute instead of Z, the matrix Z^{-T} directly, it involves only a minor change in the algorithm, and takes the same number of operations to compute.

With other alternatives, the transformation is constructed in an implicit manner. The fixed solution (5.10) can be computed using the transformed integer ambiguities $\check{z}$ directly, cf. Eq. (3) in Teunissen (1995b). Instead of starting with $Z = I$ on the input and computing matrix Z, one can insert matrix $Q_{\hat{b}\hat{a}}$ and transform it into $Q_{\hat{b}\hat{z}}$. Matrix $Q_{\hat{z}}^{-1}$ is obtained from the updated factors L and D (see Section 5.9).

5.5 Integer ambiguity estimation: search

5.5.1 Introduction

In this section the actual integer ambiguity estimation will be discussed. The integer estimation is also referred to as search. Based on the results of the float solution a search will be performed in order to come up with the most likely integer candidate[1] for the vector of ambiguities.

Decorrelating the ambiguities, as discussed in the previous section, is not a prerequisite for the integer ambiguity estimation. The search can be performed on the original ambiguities a as well, instead of on the transformed ambiguities z. The decorrelation, however, is highly beneficial to the efficiency of the search. In the sequel the ambiguities are denoted by a, whether or not they represent transformed ambiguities.

The implementation of the search is based on the correspondence of the LDL^T decomposition of matrix $Q_{\hat{a}}^{-1}$ (the first option of (5.16)) and the sequential conditional least-squares estimation, see section 5 of Teunissen (1993). The input of this step consists of matrices L and D and the real valued estimate $\hat{a}$. The output is the integer least-squares estimate $\check{a}$.

5.5.2 Sequential conditional least-squares estimation

As discussed in Teunissen (1993), no standard techniques are available for solving (5.6). A discrete search is employed instead. An ellipsoidal region in $\mathbf{R}^n$ is taken, on the basis of which a search is performed for the minimizer of (5.6):

$$(\hat{a} - a)^T Q_{\hat{a}}^{-1} (\hat{a} - a) \leq \chi^2 \tag{5.62}$$

For a discussion on the value for χ^2, the constant that controls the size of the ellipsoidal region, see Section 5.6, and also Teunissen et al. (1996).

With the LDL^T decomposition of matrix $Q_{\hat{a}}^{-1}$, expanding (5.62) gives

$$\sum_{i=1}^{n} d_i \left[(a_i - \hat{a}_i) + \sum_{j=i+1}^{n} l_{ji} (a_j - \hat{a}_j) \right]^2 \leq \chi^2 \tag{5.63}$$

Equation (5.63) is just an algebraic development of (5.62). In Section 5.5.3 we will continue this development, as the algorithm for the integer estimation is based on (5.63).

As mentioned above, the search can also be given a statistical interpretation: the sequential conditional adjustment. The term between the square brackets is the difference of a_i and $\hat{a}_{i|i+1,\ldots,n}$ and together with (5.20), (5.63) can be rewritten in

$$\sum_{i=1}^{n} \frac{(a_i - \hat{a}_{i|i+1,\ldots,n})^2}{\sigma^2_{\hat{a}_{i|i+1,\ldots,n}}} \leq \chi^2 \tag{5.64}$$

[1] What is a candidate? It is a grid point that is inside or on the ambiguity search ellipsoid; it satisfies Eq. (5.62).

see also Eq. (25) of Teunissen (1993). The conditional estimate $\hat{a}_{i|i+1,\ldots,n}$ is the estimate for a_i conditioned at a_j with $j = i+1, \ldots, n$. The conditional estimate for ambiguity i thus reads

$$\hat{a}_{i|i+1,\ldots,n} = \hat{a}_i - \sum_{j=i+1}^{n} l_{ji}(a_j - \hat{a}_j) \tag{5.65}$$

Equation (5.65) clearly shows that conditioning on a_j for $j = i+1, \ldots, n$ affects the estimate for a_i due to the correlation between the ambiguities. Only in case there is no correlation, $L = I$, we have

$$\hat{a}_{i|i+1,\ldots,n} = \hat{a}_i \tag{5.66}$$

In the integer ambiguity estimation using the sequential conditional least-squares adjustment, the ambiguities a_j are conditioned at integers. The variance of the conditional estimator equals $\sigma^2_{\hat{a}_{i|i+1,\ldots,n}} = d_i^{-1}$, see (5.20).

5.5.3 Computation of the bounds

By means of a sequential conditional adjustment, the full ellipsoid will be searched for candidates for the vector of ambiguities. From (5.63) we can construct the following bounds for ambiguity a_{i+1}; the ambiguities a_n through a_{i+2} are already conditioned, the ambiguities a_i through a_1 are not conditioned yet.

$$\underbrace{\left[(a_{i+1} - \hat{a}_{i+1}) + \sum_{j=i+2}^{n} l_{j,i+1}(a_j - \hat{a}_j)\right]^2}_{left_{i+1}} \leq$$

$$\underbrace{\frac{\chi^2}{d_{i+1}} - \frac{1}{d_{i+1}} \sum_{l=i+2}^{n} d_l \left[(a_l - \hat{a}_l) + \sum_{j=l+1}^{n} l_{jl}(a_j - \hat{a}_j)\right]^2}_{right_{i+1}} \tag{5.67}$$

Once ambiguity $i+1$ has been fixed to integer a_{i+1}, we compute the bounds for ambiguity i:

$$\underbrace{\left[(a_i - \hat{a}_i) + \sum_{j=i+1}^{n} l_{ji}(a_j - \hat{a}_j)\right]^2}_{left_i} \leq$$

$$\underbrace{\frac{\chi^2}{d_i} - \frac{1}{d_i} \sum_{l=i+1}^{n} d_l \left[(a_l - \hat{a}_l) + \sum_{j=l+1}^{n} l_{jl}(a_j - \hat{a}_j)\right]^2}_{right_i} \tag{5.68}$$

Equations (5.67) and (5.68) hold for $i \in [1, n-1]$. To show that the bounds can be computed recursively, we split off the term $l = i+1$ from the summation on the right-hand side of (5.68),

$$\underbrace{\left[(a_i - \hat{a}_i) + \sum_{j=i+1}^{n} l_{ji}\,(a_j - \hat{a}_j)\right]^2}_{left_i} \leq$$

$$\frac{d_{i+1}}{d_i}\{\frac{\chi^2}{d_{i+1}} - \frac{1}{d_{i+1}} \sum_{l=i+2}^{n} d_l \underbrace{\left[(a_l - \hat{a}_l) + \sum_{j=l+1}^{n} l_{jl}\,(a_j - \hat{a}_j)\right]^2}_{right_{i+1}}$$

$$- \underbrace{\left[(a_{i+1} - \hat{a}_{i+1}) + \sum_{j=i+2}^{n} l_{j,i+1}\,(a_j - \hat{a}_j)\right]^2}_{left_{i+1}}\} \quad (5.69)$$

Recognizing on the right-hand side the terms $right_{i+1}$, see (5.67) and $left_{i+1}$, the equation can be simplified to

$$\underbrace{\left[(a_i - \hat{a}_i) + \sum_{j=i+1}^{n} l_{ji}(a_j - \hat{a}_j)\right]^2}_{left_i} \leq \underbrace{\frac{d_{i+1}}{d_i}(right_{i+1} - left_{i+1})}_{right_i} \quad (5.70)$$

This shows that, in the sequential conditional adjustment, the bounds for the ambiguities $n-1$ through 1 can be computed recursively. The recursion starts with the conditioning of a_n (substitution of $i = n$ in (5.63)):

$$\underbrace{(a_n - \hat{a}_n)^2}_{left_n} \leq \underbrace{\frac{\chi^2}{d_n}}_{right_n} \quad (5.71)$$

The interval with valid integers for ambiguity a_i follows now from elaboration on (5.70)

$$\|(a_i - \hat{a}_i) + \sum_{j=i+1}^{n} l_{ji}(a_j - \hat{a}_j)\| \leq \sqrt{right_i} \quad (5.72)$$

or

$$-\sqrt{right_i} \leq (a_i - \hat{a}_i) + \sum_{j=i+1}^{n} l_{ji}(a_j - \hat{a}_j) \leq \sqrt{right_i} \quad (5.73)$$

Equation (5.73) can be further developed into

$$-\sqrt{right_i} - \sum_{j=i+1}^{n} l_{ji}(a_j - \hat{a}_j) \leq a_i - \hat{a}_i \leq \sqrt{right_i} - \sum_{j=i+1}^{n} l_{ji}(a_j - \hat{a}_j) \quad (5.74)$$

and

$$\hat{a}_i - \sqrt{right_i} - \sum_{j=i+1}^{n} l_{ji}(a_j - \hat{a}_j) \leq a_i \leq \hat{a}_i + \sqrt{right_i} - \sum_{j=i+1}^{n} l_{ji}(a_j - \hat{a}_j) \tag{5.75}$$

This defines the interval for ambiguity i. It will be searched in a straightforward manner from left to right, i.e. from the lower to the upper bound. Once a valid integer is found, the adjustment proceeds with the next ambiguity a_{i-1} (the so-called depth-first search). If for a certain ambiguity a_l no valid integers can be found, one returns to the previous ambiguity a_{l+1} and takes the next valid integer for this ambiguity. Once an integer is encountered that satisfies interval (5.75) for ambiguity a_1, a full candidate vector is found. The search terminates when all valid integers encountered, have been treated and one is back at the last ambiguity a_n. The full ellipsoid has been searched.

To summarize: the sequential adjustment starts with a conditioning on a_n and ends with a conditioning on a_1. In this way the bounds for the ambiguities a_n through a_1 are constructed in a recursive way. When the sequential adjustment is at ambiguity i, with the definition of the conditional estimate (5.65), the interval (5.73) can be rewritten into

$$-\sqrt{right_i} \leq (a_i - \hat{a}_{i|i+1,\ldots,n}) \leq \sqrt{right_i} \tag{5.76}$$

which shows that the interval for a_i is centered at the conditional estimate $\hat{a}_{i|i+1,\ldots,n}$. At this moment the integer nearest to the conditional estimate, $nint(\hat{a}_{i|i+1,\ldots,n})$, is the most likely candidate for ambiguity i. From (5.64) it can be seen that the conditional variances play a decisive role in the bounds for the ambiguities. The smaller the conditional variance, the smaller the interval (5.75).

Since in the case of the original ambiguities, the conditional variances of the first three ambiguities encountered in the search, are usually of a large order, the bounds for these first three ambiguities will be rather loose. This implies that quite a number of integer triples satisfy these bounds. For all these triples one has to compute the bounds for the fourth ambiguity. The bounds for the fourth ambiguity, however, are very tight due to the steep decrease in value of the conditional variances, and hence we have a high likelihood that no integer is contained by them. The potential of halting is therefore significant when one goes from the third to the fourth ambiguity in the search. As a consequence a large number of incomplete candidates are generated, for which bounds have to computed, before one is able to move on to the next ambiguity.

In case the search is performed on the original ambiguities a, they should be ordered according to their conditional precision (Teunissen 1993):

$$\sigma^2_{\hat{a}_{1|2,\ldots,n}} \geq, \ldots, \geq \sigma^2_{\hat{a}_n} \tag{5.77}$$

The sequential adjustment should start with the most precise ambiguity.

5.5.4 Computation of the norm

In the previous section the full ellipsoid was searched and as a result we have available all grid points that are inside the ellipsoid. One of them, the one which yields the minimum for (5.6), is the integer least-squares estimate $\check{a}$.

The squared norm $t(a) = \|\hat{a} - a\|^2_{Q_{\hat{a}}^{-1}}$ of a candidate can be computed by substitution of a into (5.62). It can also be computed from the bounds for ambiguity a_1 at the moment the candidate is encountered in the search. The squared norm, the left-hand side of (5.63), can be rewritten into (by respectively adding and subtracting χ^2 and splitting off the first term)

$$\begin{aligned} t(a) &= \sum_{i=1}^{n} d_i \left[(a_i - \hat{a}_i) + \sum_{j=i+1}^{n} l_{ji}(a_j - \hat{a}_j) \right]^2 \\ &= \chi^2 - d_1 \{ \underbrace{\frac{\chi^2}{d_1} - \frac{1}{d_1} \sum_{i=2}^{n} d_i \left[(a_i - \hat{a}_i) + \sum_{j=i+1}^{n} l_{ji}(a_j - \hat{a}_j) \right]^2}_{right_1} \\ &\quad - \underbrace{\left[(a_1 - \hat{a}_1) + \sum_{j=2}^{n} l_{j1}(a_j - \hat{a}_j) \right]^2}_{left_1} \} \end{aligned} \tag{5.78}$$

The squared norm $t(a)$ is less or equal to χ^2, as the grid point is on or inside the ellipsoid.

If, at level $i = 1$, more than one candidate is available, the squared norm of successive candidate vectors a' can be computed very easily once the squared norm of one candidate a has been computed already. This is because $a'_i = a_i$ for $i = 2, \ldots, n$ and $a'_1 = a_1 + \nabla$ (where ∇ can be chosen to be any integer). So now the squared norm becomes

$$t(a') = t(a) + d_1 \{ 2\nabla [\underbrace{(a_1 - \hat{a}_1)}_{dist_1} + \underbrace{\sum_{j=2}^{n} l_{j1}(a_j - \hat{a}_j)}_{lef_1}] + \nabla^2 \} \tag{5.79}$$

5.6 Integer ambiguity estimation: setting the volume

In this section we will elaborate on how to control, prior to the search, the size of the ambiguity search space. We will recognize the relation between the volume of the ellipsoid and the number of candidates contained. By this relation, the straightforward search is an effective instrument in solving the minimization problem (5.6).

5.6.1 The volume of the ellipsoidal region

The volume, expressed in [cycles^n], of the ellipsoidal region (5.62) is given by

$$E_n = \chi^n \sqrt{|Q_{\hat{a}}|} V_n \tag{5.80}$$

see Apostol (1969). The volume function in (5.80) is

$$V_n = \frac{2}{n} \frac{\pi^{\frac{n}{2}}}{\Gamma(\frac{n}{2})} \tag{5.81}$$

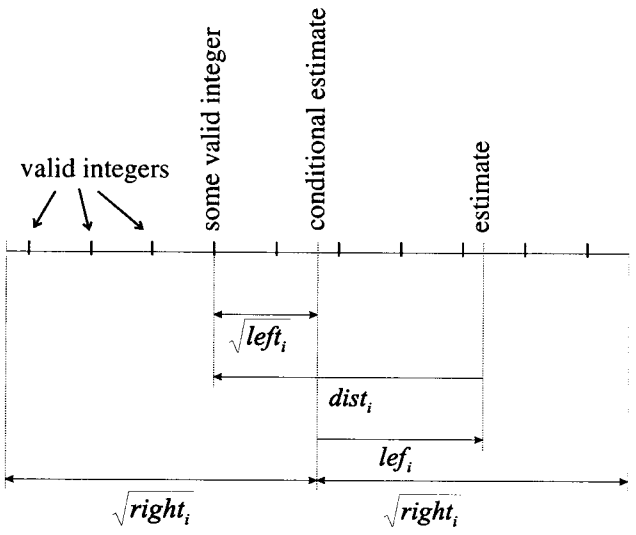

Figure 5.5: The relation between some variables used in this chapter. An arrow pointing to the right indicates a positive number, an arrow pointing to the left a negative number, and a two-sided arrow indicates that the number is intrinsically positive.

where Γ is the gamma function, defined as

$$\Gamma(x) = \int_0^\infty e^{-t} t^{x-1} dt \text{ for } x > 0 \tag{5.82}$$

The volume function can be computed recursively for $n \geq 3$ by

$$V_n = \frac{2\pi}{n} V_{n-2} \tag{5.83}$$

with

$$V_1 = 2 \text{ and } V_2 = \pi \tag{5.84}$$

For the determinant of the variance covariance matrix we have the following relations

$$|Q_{\hat{a}}| = \prod_{i=1}^{n} \lambda_i = \prod_{i=1}^{n} \sigma^2_{\hat{a}_i|i+1,\ldots,n} \tag{5.85}$$

where λ_i is the i-th eigenvalue of matrix $Q_{\hat{a}}$. The volume E_n can thus easily be computed, as the conditional variances are available from matrix D, see Eq. (5.20).

5.6.2 Setting χ^2, I

The volume E_n turns out to be a good indicator for the number of candidates (grid points) contained in the ellipsoid. A volume of E_n cycles^n corresponds to approximately $k = nint(E_n)$ candidates. The mismatch is caused by the discrete nature of the grid points. Centering the

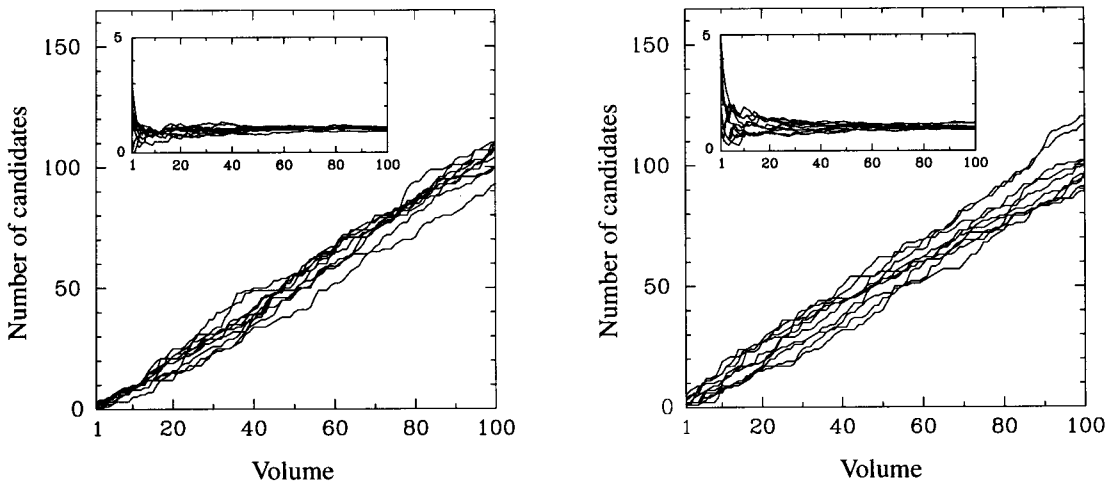

Figure 5.6: Number of candidates inside ellipsoid versus volume; left: single frequency phase data, right: dual frequency phase data.

same ellipsoid at a different location, may result in a different number of candidates, $k \in \mathbf{Z}$, while the volume $E_n \in \mathbf{R}$, remains unchanged.

The value χ^2 can be taken such that a certain number of candidates will be inside the ellipsoidal region. A straightforward search can then be performed to obtain the requested number of candidates. A list with the best k candidates, possibly ordered after their norms, can be set up and updated during the sequential adjustment. In this way the size of the ellipsoid is controlled prior to the search. To some extent one can already infer the quality of the integer estimator in advance.

Figure 5.6 concerns 10 experiments each with two epochs (sampling rate 1 second) of single frequency data (left) and dual frequency phase data (right) to seven satellites on a 2.2 km baseline (with dual frequency this gives 12 ambiguities). The actual number of candidates contained in the ambiguity search ellipsoid is given as function of the volume of the ellipsoid [cycles^{12}]. The volume ranges from 1 to 100. The volume turns out to be a good indicator for the actual number of candidates in the ambiguity search ellipsoid. The inset shows the quotient of the number of candidates and the volume, i.e. the relative error of the volume as a predictor for the number of candidates.

5.6.3 Setting χ^2, II

Another method to set the value for χ^2 such that at least two candidates are contained in the ellipsoidal search space, was proposed in Teunissen et al. (1997), see also Teunissen et al. (1996). Since the decorrelated ambiguities have such a high precision (typically some tenths of a cycle), rounding to the nearest integer will produce a candidate with a norm close to the minimum. So setting χ^2 equal to the squared norm of this candidate will guarantee at least one and most likely not more than a few candidates. Other candidates with small norms can be found through rounding all ambiguities but one to their nearest integer, and one ambiguity to the next-nearest integer. If we have n ambiguities, this will give us n more candidates with likely small norms. Setting χ^2 to the next-smallest squared norm, will guarantee now

at least two candidates, and most likely not more than a few.

These $n+1$ squared norms can be computed in an efficient way using again the LDL^T decomposition of $Q_{\hat{a}}^{-1}$. Re-arranging the first part of Eq. (5.78) gives

$$t(a) = \sum_{i=1}^{n} d_i \left[\sum_{j=i}^{n} l_{ji} \left(a_j - \hat{a}_j \right) \right]^2 \tag{5.86}$$

$$= \sum_{i=1}^{n} d_i e_i^2 \tag{5.87}$$

(Note that e_i^2 equals $left_i$.) Eq. (5.79) showed an efficient way for computing the squared norm $t(a')$ for a candidate which differs ∇ in the last ambiguity a_1 from a candidate with known squared norm $t(a)$. We will now generalize this for the case that an arbitrary ambiguity k differs ∇:

$$a_{,k} = a + c_k \nabla \tag{5.88}$$

with c_k a vector with zeros on all positions with exception of position k which has the value one:

$$c_k = (\underbrace{0, 0, \ldots,}_{k-1} 1, \underbrace{0, 0, \ldots, 0}_{n-k})^T \tag{5.89}$$

The squared norm for the vector $a_{,k}$ can be written as

$$\begin{aligned} t(a_{,k}) &= \sum_{i=1}^{k} d_i (e_i + l_{ki} \nabla)^2 + \sum_{i=k+1}^{n} d_i e_i^2 \\ &= \sum_{i=1}^{k} d_i (e_i^2 + 2 e_i l_{ki} \nabla + l_{ki}^2 \nabla^2) + \sum_{i=k+1}^{n} d_i e_i^2 \\ &= t(a) + \sum_{i=1}^{k} d_i (2 e_i l_{ki} \nabla + l_{ki}^2 \nabla^2) \end{aligned} \tag{5.90}$$

Compare this result with that of Eq. (5.79). There we used $(dist_1 + lef_1)$ instead of e_1 since these are available during the search process. The form shown here is more efficient when we have only the LDL^T decomposition of $Q_{\hat{a}}^{-1}$, as is the case prior to the search.

We start by taking for a

$$a = (nint(\hat{a}_1), nint(\hat{a}_2), \ldots, nint(\hat{a}_n)) \tag{5.91}$$

and once we have computed its squared norm $t(a)$, we can compute very efficiently other n likely small norms $t(a_{,k})$ with (5.90) by taking for ∇

$$\nabla = \begin{cases} 1 & \text{if } nint(\hat{a}_k) - \hat{a}_k < 0 \\ -1 & \text{if } nint(\hat{a}_k) - \hat{a}_k > 0 \end{cases}$$

with k from 1 to n. During the computation of the $n+1$ norms we keep track of the smallest and next-smallest value. χ^2 is set to the next-smallest value for the norm. The ellipsoid will contain at least two candidates.

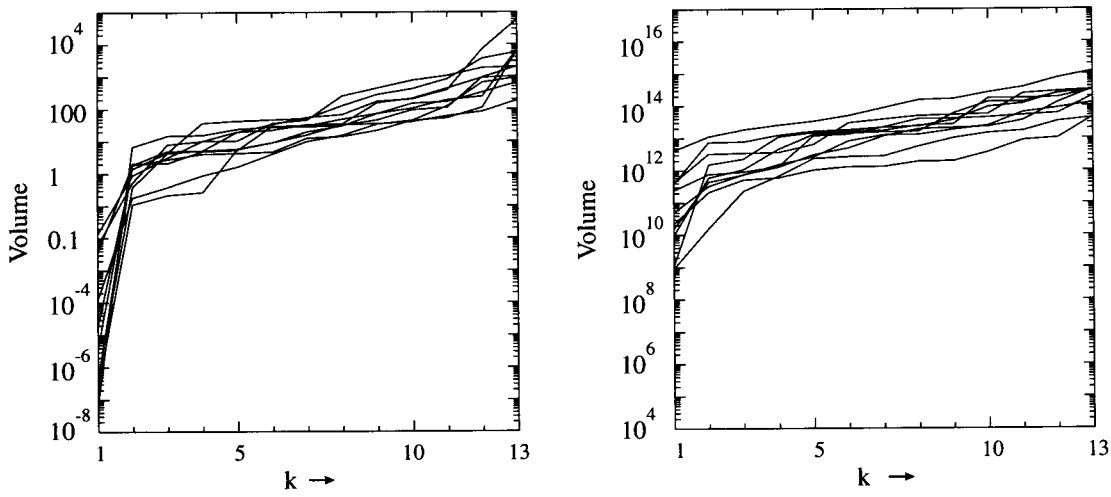

Figure 5.7: Volume of the ambiguity search space containing at least k 'near' candidates; left: transformed ellipsoid, right: original ellipsoid.

To illustrate this strategy, the following experiment was done: we computed the squared norm belonging to the vector one gets when rounding all ambiguities to their nearest integer. We also computed the n squared norms one gets when rounding all ambiguities but one to the nearest integer: the remaining one is rounded to the next-nearest integer. With χ^2 set to these norms, the volume of the ambiguity search ellipsoid was computed.

This was done for the same 10 dual frequency experiments for which the relation between volume and number of candidates was demonstrated (see Figure 5.6). Per experiment the volumes were sorted after increasing order, and plotted in Figure 5.7, i.e. the smallest volume is plotted at $k = 1$, the second smallest at 2, etc. At left we plotted the results for the transformed problem, at right those for the original problem. Looking at the experiments with the transformed ambiguities, one can see that the next-smallest volume (which guarantees at least two candidates) never exceeds the value of 10. This translates into a maximum number of candidates of approximately 10 (see Figure 5.6).

For the original ambiguities the volumes are of the order 10^{10}–10^{12}, which shows that no acceptable volumes are obtained if the ambiguities are not decorrelated. Searching ellipsoids with such large volumes would mean that we have to cope with an enormous number of candidates.

For the case of the transformed ambiguities, we actually set χ^2 to the next-smallest squared norm. In Table 5.1 one can find the epoch numbers for the 10 experiments, the resulting volume and the number of candidates inside the ellipsoid. This number is below 10 for all experiments.

The same was done for a 10.4 km baseline (measured simultaneously with the 2.2 km baseline, observing the same 7 satellites; the baselines have one station in common). Although here we find in some experiments up to 14 candidates, the procedure is still capable to determine the two minimum candidates in an efficient way due to the almost lack of correlation between the ambiguities.

Epochs	2.2 km Volume	Number of candidates	10.4 km Volume	Number of candidates
1 – 2	0.38	2	8.76	14
31 – 32	0.11	2	1.36	2
61 – 62	1.41	2	13.95	14
91 – 92	6.76	4	5.58	9
121 – 122	1.89	2	1.59	3
151 – 152	1.85	4	2.89	2
181 – 182	2.07	2	0.67	2
211 – 212	0.53	2	0.90	3
241 – 242	0.89	2	9.50	7
271 – 272	0.18	2	1.83	3

Table 5.1: Volume and number of candidates inside the ambiguity search ellipsoid, by setting χ^2 to the next-smallest squared norm.

5.6.4 Setting χ^2, III

Although the method described in the previous section performs quite well, an even more tight value for a χ^2 such that at least k candidates are contained in the ellipsoidal search space can be obtained.

This is done by setting χ^2 to the norm of a candidate obtained by rounding the *conditional* estimates to their nearest integer. Since the conditional estimates are more precise than their unconditional counterparts, it is more likely that a candidate will be obtained with a norm close to its minimum.

To obtain other n small norms we proceed as in the previous section: all but one conditional estimates are rounded to the nearest integer, and one is rounded to the next-nearest integer.

The computational load is slightly higher than for the case where we round the estimates, but still modest. Again best results are obtained when applying the procedure to the decorrelated ambiguities.

The norm of a candidate can be computed as, see Eq. (5.78)

$$t(a) = \chi^2 - d_1 right_1 left_1 \tag{5.92}$$

The definition for $left_i$ reads, see Eq. (5.70)

$$\begin{aligned} left_i &= \left[a_i - \hat{a}_i + \sum_{j=i+1}^{n} l_{ji}(a_j - \hat{a}_j) \right]^2 \\ &= \left[a_i - \hat{a}_{i|i+1,\ldots,n} \right]^2 \end{aligned} \tag{5.93}$$

In our case we take for a_i the nearest integer to $\hat{a}_{i|i+1,\ldots,n}$ which gives

$$\begin{aligned} left_i &= \left[nint(\hat{a}_{i|i+1,\ldots,n}) - \hat{a}_i + \sum_{j=i+1}^{n} l_{ji}(a_j - \hat{a}_j) \right]^2 \\ &= \left[nint\left(\hat{a}_i - \sum_{j=i+1}^{n} l_{ji}(a_j - \hat{a}_j) \right) - \hat{a}_i + \sum_{j=i+1}^{n} l_{ji}(a_j - \hat{a}_j) \right]^2 \end{aligned} \tag{5.94}$$

The definition for $right_i$ reads

$$right_i = \frac{d_{i+1}}{d_i}(right_{i+1} - left_{i+1}) \tag{5.95}$$

and can be computed recursively. The recursion starts with

$$right_n = \frac{\chi^2}{d_n} \tag{5.96}$$

and proceeds until the first level is reached. The norm is then computed using Eq. (5.92). For χ^2 an arbitrary value can be chosen.

The other n small norms where one of the conditional estimates is rounded to the next-nearest integer, are computed analogously. We start with computing the norm $t_1(a)$ where $\hat{a}_{1|2,\ldots,n}$ (the last ambiguity, conditioned at all other ambiguities) is rounded to the next-nearest integer, and end with the norm $t_n(a)$ where $\hat{a}_n$ (the first ambiguity, which is not yet conditioned at any ambiguity) is rounded to the next-nearest integer. We proceed in this order since then for $t_j(a)$ we only have to compute $left_i$ and $right_i$ for $i = j-1$ to 1, since $left_i$ and $right_i$ for $i = n$ to j are not affected by the constraining of $\hat{a}_{j|j+1,\ldots,n}$ to the new value.

5.7 Example ambiguity search

The search in the ambiguity ellipsoid will be illustrated using the original ambiguities a of the three-dimensional example of Section 5.4. Next, in order to show what is gained by the decorrelating transformation, also the search with the transformed ambiguities z will be demonstrated. This section is concluded by comparing a search with original and transformed ambiguities for a GPS baseline.

The (real valued) estimates for the ambiguities a are:

$$\begin{aligned} \hat{a}_1 &= 5.45 \\ \hat{a}_2 &= 3.10 \\ \hat{a}_3 &= 2.97 \end{aligned} \tag{5.97}$$

The so-called search tree is depicted in Figure 5.8 at left, and should be read from left to right. Per level, i.e. per ambiguity, the candidates encountered are represented by a node. A full candidate vector, i.e. a grid point inside the ellipsoid, is found when a node on level a_1 is connected with a node on level a_2, which in turn is connected with a node on level a_3.

The search starts with ambiguity a_3. The interval is centered at $\hat{a}_3 = 2.97$ and ranges from 0.462 to 5.478. Valid integers for a_3 are thus [1,2,3,4,5]. This interval is scanned from left to right. Ambiguity a_3 is conditioned at $a_3 = 1$. Equation (5.75) applied to ambiguity

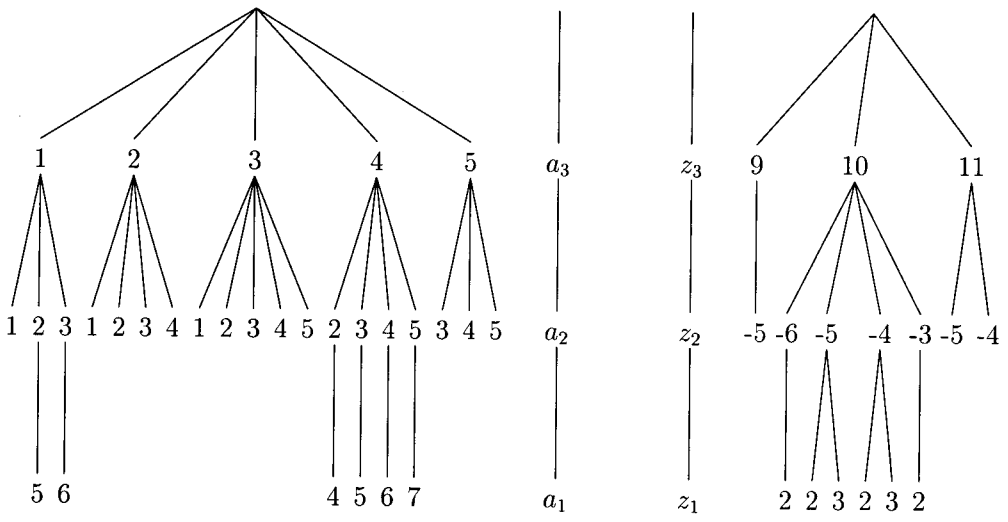

Figure 5.8: The search tree for the original problem (left) and for the transformed problem (right).

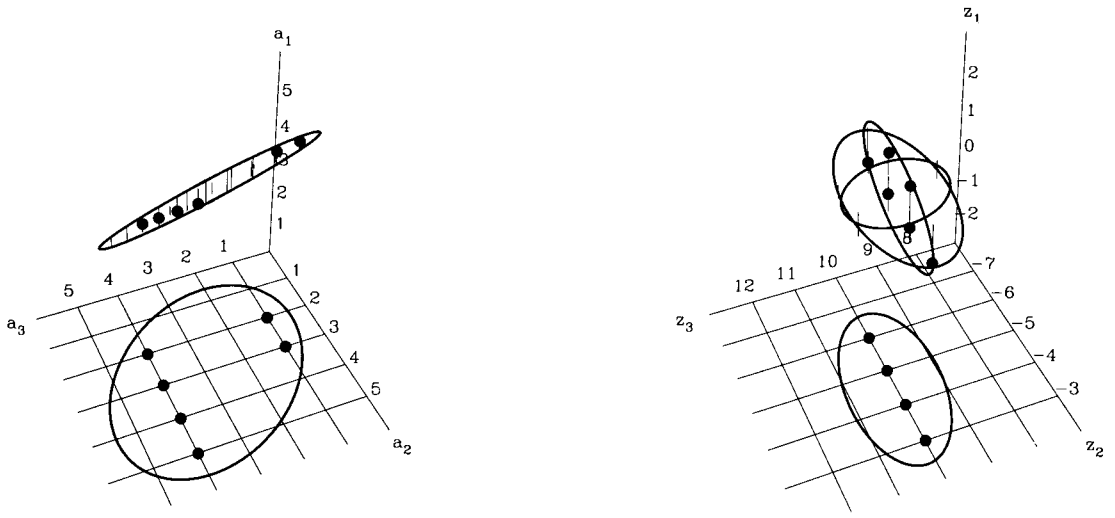

Figure 5.9: The ellipsoid in 3-D and its perpendicular projection onto the 2-3 plane for the original problem (left) and for the transformed problem (right).

a_2, gives the integers [1,2,3]. After conditioning ambiguity $a_2 = 1$, it is not possible with (5.75) applied to ambiguity a_1, to find valid integers for ambiguity a_1. Conditioning a_1 to an integer will result in a grid point that is outside the ambiguity search ellipsoid, no matter which integer is taken. We proceed with the second candidate for ambiguity $a_2 = 2$. For this candidate we find the integer $a_1 = 5$. As we have reached level 1, we have found a full integer vector, that satisfies (5.62), i.e. a grid point that is inside the ambiguity search ellipsoid. The vector is $(a_1 = 5, a_2 = 2, a_3 = 1)$, see also Figure 5.9. The process is continued until no integers are left on any level. The search is terminated and six candidate vectors have been found. The volume of this ambiguity search ellipsoid is $E_3 = 7.3$ cycles^3.

The (real valued) estimates for the ambiguities z are:

$$\begin{aligned} \hat{z}_1 &= 2.35 \\ \hat{z}_2 &= -4.57 \\ \hat{z}_3 &= 10.02 \end{aligned} \tag{5.98}$$

The search tree for the transformed problem is depicted in Figure 5.8 (right), the ambiguity search ellipsoid in Figure 5.9 (right). In comparing the tree on the left with the tree on the right in Figure 5.8, it can be seen that the search in the transformed problem can be performed much more efficiently. In the tree at left, there are 13 so-called 'dead ends', in the tree at right only 3. For a dead end, computations have to be carried out (the bounds), that do not result in a full candidate vector. The discontinuity in the signature of conditional variances causes the so-called 'halting' of the search.

The solution, the integer least-squares estimate, is $\check{a} = (5, 3, 4)$. In the transformed problem we obtain $\check{z} = (2, -5, 10)$. This solution has to be transformed by Z^{-T} and results in exactly the same solution. The squared norm is $t(\check{a}) = 0.218$.

The differences between original and transformed ambiguities are even much larger for real GPS examples. In Figure 5.10 we give the number of valid integers per ambiguity, encountered during the full search. They are given for both the original and transformed ambiguities. The data are from a 2.2 km baseline with dual frequency data to seven satellites. Two epochs of data were taken, separated by one second.

For this baseline (three coordinate unknowns), observed for a short time span, three conditional variances of the original ambiguities are very large and the remaining nine ones are very small. From Figure 5.10 we see that at level $i = 10$ (the third ambiguity in the search) there are over 3.10^8 candidates. After having proceeded to ambiguity a_1 there are only 2 full candidate vectors left, which implies that there are very many dead ends. The volume of the ambiguity search ellipsoid is $E_{12} = 2.8$ cycles^{12}. By the transformation, the signature of conditional variances is flattened, and so is the graph of the number of candidates per level: the search on the transformed ambiguities can be performed very efficiently, there are only a few dead ends left.

5.8 Alternative search procedures

5.8.1 Alternating search around the conditional estimate

In this and the following section, we will describe two other implementations, that are alternatives to the straightforward search.

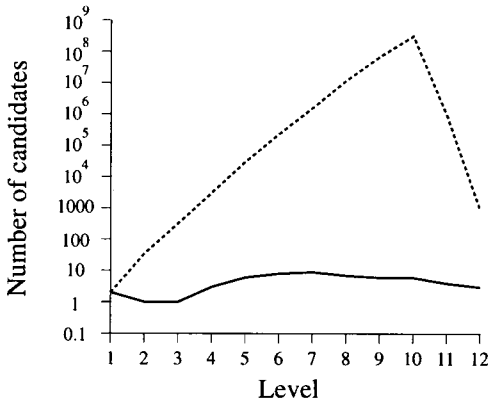

Figure 5.10: Number of candidates per level; dashed line: before transformation, solid line: after transformation.

Instead of scanning the interval per ambiguity (5.75) from left to right for integers, one can search in an alternating way around the conditional estimate. In the conditional estimation we will start by conditioning ambiguity a_i to integer $nint(\hat{a}_{i|i+1,\ldots,n})$. Next, the second nearest, third nearest, etc are tried. The candidates for a_i are chosen in a sequence, that starts with the one closest to the center of the interval (5.76) and goes alternatingly towards the bounds, see Section 2.4 in Teunissen (1995b).

With this strategy one tries, in each step of the sequential conditioning, to stay as far as possible from the borders of the ellipsoidal region (5.62).

When all candidates contained in the ellipsoid are required, this strategy has no benefit over the straightforward search in which the candidates per interval are taken from 'left to right'. When used in connection with a shrinking strategy (see next section), and when only one of a great number of candidates within the ellipsoid is required, the strategy of searching alternatingly around the conditional estimate will have benefit.

5.8.2 Shrinking the ellipsoidal region

The best candidate, the grid point nearest to $\hat{a}$, is the integer least-squares estimate for the vector of ambiguities. As we are in principle interested in only this candidate, the search can be designed to find it as quickly as possible. The sequential conditional estimation aims in the first place at constructing a complete n-dimensional vector with integers that fulfills (5.64), or in other words aims at finding a grid point that is inside the ellipsoid.

As soon as such a vector $\bar{a}$ is found, the corresponding squared norm $\|\hat{a} - \bar{a}\|^2_{Q_{\hat{a}}^{-1}}$ is taken as a new value for χ^2. We shrink the ellipsoidal region. The sequential conditional estimation is then continued (not started over!) in this shrunken ellipsoid, see Section 5 of Teunissen (1993). If one, possibly after repeated shrinking, fails to find a candidate in the ellipsoid, the last found integer vector is the sought for integer least-squares estimate, $\check{a} = \bar{a}$, see Teunissen (1995b).

5.9 Efficient computation schemes for the three step procedure

Methods for computing the fixed solution can be divided in two groups: (i) those that need explicit computation of the integer least-squares estimates $\check{a}$, and (ii) methods that do not. This influences the way the decorrelating Z-transformation is computed. It is either computed explicitly as Z or Z^{-T} to be used for (5.104) or in (5.111), or implicitly, viz. as $Q_{\hat{b}\hat{z}}$ (or N_{bz}), see (5.108) or (5.109).

Both methods start with the inversion of the $(n_b + n)$ Cholesky factor C of Eq. (5.17):

$$C^{-1} = \begin{bmatrix} C_b^{-1} & \\ -C_a^{-1}C_{ab}C_b^{-1} & C_a^{-1} \end{bmatrix} \tag{5.99}$$

The part for the ambiguities, C_a^{-1}, is then used in the decorrelation step, which is carried out, prior to the actual integer estimation.

The variance-covariance matrix of the fixed baseline coordinates $\hat{b}|\check{a}$ can easily be obtained in-place with the lower triangular matrix C_b^{-1} of dimension n_b, see Eq. (5.17). For the ambiguities absent case, we have:

$$E\{y - A_a\check{a}\} = B_b b \tag{5.100}$$

with $\check{a}$ the integer least-squares estimate for the vector of ambiguities, and consequently $Q_{\check{b}}$ equals $C_b^{-T}C_b^{-1}$.

The variance-covariance matrix of the float solution can also be efficiently computed using the sub-matrices of C^{-1}. As $Q_{\hat{x}_1}$ equals $C^{-T}C^{-1}$:

$$\begin{bmatrix} Q_{\hat{b}} & Q_{\hat{b}\hat{a}} \\ Q_{\hat{a}\hat{b}} & Q_{\hat{a}} \end{bmatrix} = \begin{bmatrix} C_b^{-T}C_b^{-1} + C_b^{-T}C_{ba}C_a^{-T}C_a^{-1}C_{ab}C_b^{-1} & -C_b^{-T}C_{ba}C_a^{-T}C_a^{-1} \\ -C_a^{-T}C_a^{-1}C_{ab}C_b^{-1} & C_a^{-T}C_a^{-1} \end{bmatrix} \tag{5.101}$$

matrix $Q_{\hat{b}\hat{a}}$ can be written as

$$Q_{\hat{b}\hat{a}} = -C_b^{-T}C_{ba}C_a^{-T}C_a^{-1} \tag{5.102}$$

This matrix will be needed for the implicit computation schemes (see Section 5.9.2). Its transpose, $Q_{\hat{a}\hat{b}}$, can be computed in-place using the sub-matrices of C^{-1}; in this way $-C_a^{-1}C_{ab}C_b^{-1}$ is replaced row-by-row by $Q_{\hat{a}\hat{b}}$.

5.9.1 Explicit computation of $\check{a}$

The most efficient way, if one wants to have available the values of $\check{a}$ explicitly, is to compute directly Z^{-T}. The original integer ambiguities are then computed from the decorrelated ambiguities as

$$\check{a} = Z^{-T}\check{z} \tag{5.103}$$

Starting from here, two routes are possible to obtain the fixed solution. First there is the explicit computation by constraining the, now considered known, integer ambiguities:

$$\check{b} = \hat{b} - Q_{\hat{b}\hat{a}}Q_{\hat{a}}^{-1}(\hat{a} - \check{a}) \tag{5.104}$$

The second method starts from the normal matrix system of (5.4) in which the ambiguities are no longer unknown parameters. Substituting $\check{a}$ into the first n equations of (5.4), we get

$$N_b \check{b} = h_b - N_{ba}\check{a} \tag{5.105}$$

Note that in the first scheme $Q_{\hat{b}\hat{a}}$ needs to be stored, and $Q_{\hat{a}}^{-1}$ has to be computed. In the second scheme N_{ba} (part of the normal matrix for the float solution) has to be stored (before computing the float solution), and furthermore either C_b (baseline part of the Cholesky factor of the normal matrix), or $Q_{\hat{b}}$ has to be stored. The scheme depicted in Figure 5.11 is based on (5.105).

5.9.2 Implicit computation of $\check{a}$

If we look at the complete system, i.e. the baseline coordinates and the ambiguities, the following transformation is applied to the parameters by the Z-transformation:

$$\begin{bmatrix} b \\ z \end{bmatrix} = \begin{bmatrix} I & \\ & Z^T \end{bmatrix} \begin{bmatrix} b \\ a \end{bmatrix} \tag{5.106}$$

Applying this transformation to the variance-covariance matrix of (5.5) gives:

$$\begin{bmatrix} Q_{\hat{b}} & Q_{\hat{b}\hat{a}}Z \\ Z^T Q_{\hat{a}\hat{b}} & Z^T Q_{\hat{a}} Z \end{bmatrix} = \begin{bmatrix} Q_{\hat{b}} & Q_{\hat{b}\hat{z}} \\ Q_{\hat{z}\hat{b}} & Q_{\hat{z}} \end{bmatrix} \tag{5.107}$$

Using (5.103), Eq. (5.104) can now be rewritten as

$$\begin{aligned} \check{b} &= \hat{b} - Q_{\hat{b}\hat{a}} Q_{\hat{a}}^{-1}(\hat{a} - \check{a}) \\ &= \hat{b} - Q_{\hat{b}\hat{a}} Z Z^{-1} Q_{\hat{a}}^{-1} Z^{-T} Z^T (\hat{a} - \check{a}) \\ &= \hat{b} - Q_{\hat{b}\hat{z}} Q_{\hat{z}}^{-1}(\hat{z} - \check{z}) \end{aligned} \tag{5.108}$$

This shows that it is not necessary to explicitly compute matrix Z or its inverse. The fixed solution is computed with the transformed ambiguities. The computation scheme based on (5.108) is shown in Figure 5.12.

Intermezzo
As an alternative, one can operate upon N_{ba} instead of on $Q_{\hat{b}\hat{a}}$. With (5.105) we obtain:

$$\begin{aligned} N_b \check{b} &= h_b - N_{ba}\check{a} \\ &= h_b - N_{ba} Z^{-T} Z^T \check{a} \\ &= h_b - N_{bz}\check{z} \end{aligned} \tag{5.109}$$

End of intermezzo

Starting from Eq. (5.108) we can make a distinction between the following two cases:

1. $n_b < n$
In the normal case the number of ambiguity parameters is larger than the number of baseline coordinates. Then, instead of transforming a matrix of unity to Z, it is more efficient to transform $Q_{\hat{b}\hat{a}}$ directly to $Q_{\hat{b}\hat{z}}$. This saves memory since Z becomes now superfluous. It also

saves CPU time, since the column dimension of $Q_{\hat{b}\hat{a}}$ equals the number of baseline coordinates n_b, whereas the column dimension of Z equals the number of ambiguities n. The row dimension of both matrices is equal. Since the construction of Z, (or $Q_{\hat{b}\hat{z}}$) is essentially a sequence of column manipulations, less operations are needed and CPU time will be saved. CPU time is also saved because the matrix product $Q_{\hat{b}\hat{a}}Z$ does not need to be evaluated explicitly anymore. In this way, the decorrelating transformation is computed implicitly.

$$\begin{aligned}\check{b} &= \hat{b} - Q_{\hat{b}\hat{z}}Q_{\hat{z}}^{-1}(\hat{z} - \check{z}) \\ &= \hat{b} - Q_{\hat{b}\hat{z}}(\tilde{L}\tilde{D}\tilde{L}^T)(\hat{z} - \check{z})\end{aligned} \tag{5.110}$$

2. $n_b > n$
If the number of non-ambiguity parameters is larger than the number of ambiguity parameters, it is more efficient to compute Z explicitly and use it to transform $Q_{\hat{b}\hat{a}}$ into $Q_{\hat{b}\hat{z}}$. The fixed baseline coordinates are then computed as

$$\begin{aligned}\check{b} &= \hat{b} - Q_{\hat{b}\hat{z}}Q_{\hat{z}}^{-1}(\hat{z} - \check{z}) \\ &= \hat{b} - (Q_{\hat{b}\hat{a}}Z)(\tilde{L}\tilde{D}\tilde{L}^T)(\hat{z} - \check{z})\end{aligned} \tag{5.111}$$

Again we need to have stored $Q_{\hat{b}\hat{a}}$.

5.10 Timing results

To show the performance of the alternatives proposed in the previous section, we applied them to a number of different measurement scenarios. The following comparisons are made

1. Single baseline versus a 4-station Network
2. Dual frequency versus Single frequency
3. Phase-only versus Phase-and-code
4. Static versus Kinematic

In all experiments we used two epochs of data, while varying the observation time span (from instantaneous to 300 seconds). As shown in Teunissen (1994) it is the time span that largely influences the amount of correlation between the ambiguities, and therefore the CPU time needed for their decorrelation. Enlarging the sampling rate has a much smaller effect. The ambiguity search ellipsoid is characterized by its elongation and the ambiguity decorrelation number, (ibid.).

The same 7 satellites, all with elevation above 10 degrees, were tracked in all experiments. The weights for the phase observables were chosen to be equal (in meters) for both the L1 and the L2 frequency. When code observables were included, their weight relative to that of the phase observable was set to 1/10000.

The measurements were made at Ypenburg in the Netherlands ($\phi = 52^o$ N, $\lambda = 4^o24'$ E), on May 5, 1994, between 20:00 and 20:05 (GPS time) using Trimble 4000 SSE receivers. The length of the baseline used for the single baseline experiments (YP01-BR01) is approximately 10.4 km, while the inter-station distances for the network experiments vary between 2.3 and 10.4 km.

Timing was done on a 486-66 MHz-PC under MS-DOS. The implementation was in Fortran 77 using the Microsoft Power station compiler with maximum optimization applied.

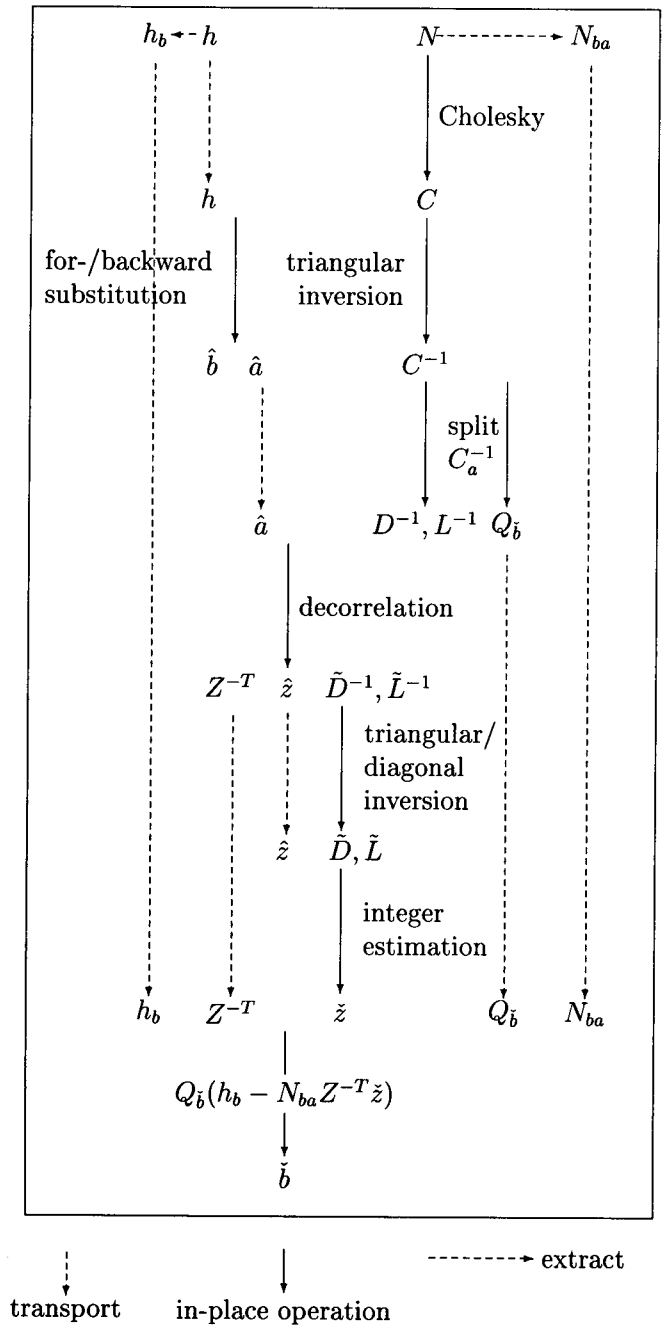

Figure 5.11: Explicit computation scheme for the GPS relative positioning float/fixed solution, via Eq. (5.105).

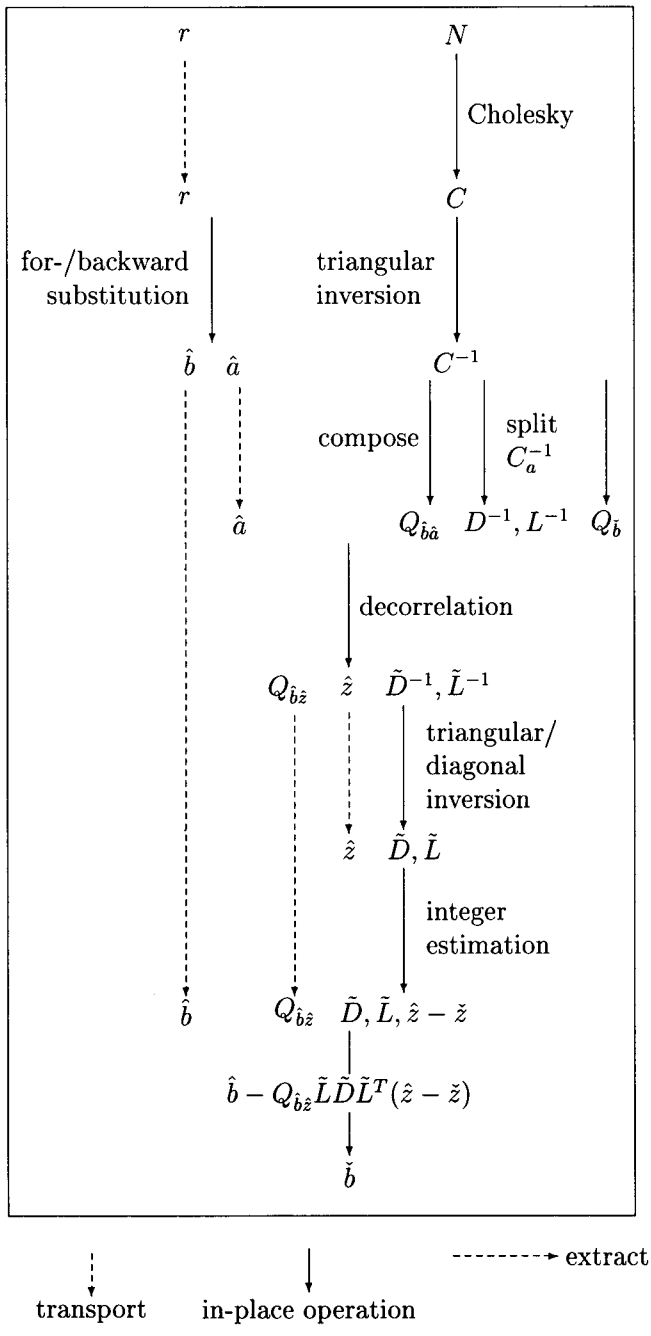

Figure 5.12: Implicit computation scheme for the GPS relative positioning float/fixed solution, via Eq. (5.108).

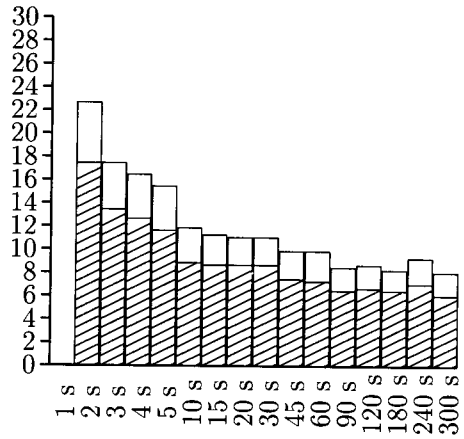

Figure 5.13: CPU time in milliseconds for decorrelation, for a varying time span and two epochs of data. Dual frequency, phase-only, static baseline.

5.10.1 Single baseline, dual frequency

In Figure 5.13 the two main schemes for computing the decorrelating transformation are compared for the single static baseline using dual frequency phase measurements. The white bars show the time for computing the Z^{-T}-matrix, the superimposed hatched bars, the time for directly transforming $Q_{\hat{b}\hat{a}}$. In this figure and in the ones that follow, CPU time is only shown if indeed the correct integer ambiguities were found; so in this figure the one second time span is left blank. The correctness of the integer estimation was checked using a validated ground truth obtained with a time span of 15 minutes. The figure shows that by enlarging the time span, the time needed for decorrelation of the ambiguities decreases. The larger the time span, the more the receiver-satellite geometry changes. The original double difference ambiguities are then less correlated. The figure also demonstrates that working directly upon the, in this case 3-by-12 $Q_{\hat{b}\hat{a}}$ matrix, takes less time than computing the full 12-by-12 Z^{-T}-matrix. The time is approximately 20-25% less.

Figure 5.14 at left shows the results for the same experiments as in Figure 5.13, but now for a roving receiver. Allowing one of the stations to be moving from epoch to epoch increases the correlation between the ambiguities and therefore the CPU time needed for decorrelation. Again we see the beneficial effect on the correlation of an enlarged time span. As we have now a roving receiver, matrix $Q_{\hat{b}\hat{a}}$ has dimension 6-by-12, (there are 2 times 3 coordinates). The reduction in CPU time as compared with computing Z^{-T} explicitly, is therefore less than for the static case (now about 15%).

In Figure 5.14 (right) the results of the same experiments are plotted, but now using also code observations. The inclusion of the code observables has two effects on the correlation. Firstly it lowers the absolute level, and secondly it removes to a large extent the effect of enlarging the observation time span. As a consequence the CPU time for decorrelation is almost equal for all experiments; enlarging the time span, only slightly decreases the CPU time. The reduction of the CPU time when operating on $Q_{\hat{b}\hat{a}}$ instead of constructing Z^{-T} explicitly, is of the same order as without code, since the dimensions of $Q_{\hat{b}\hat{a}}$ did not change. There is one exception, viz. for the instantaneous case (0 s). Then the dimension of $Q_{\hat{b}\hat{a}}$ is 3-by-12. Here we see a reduction of the same order as we saw for the static scenario.

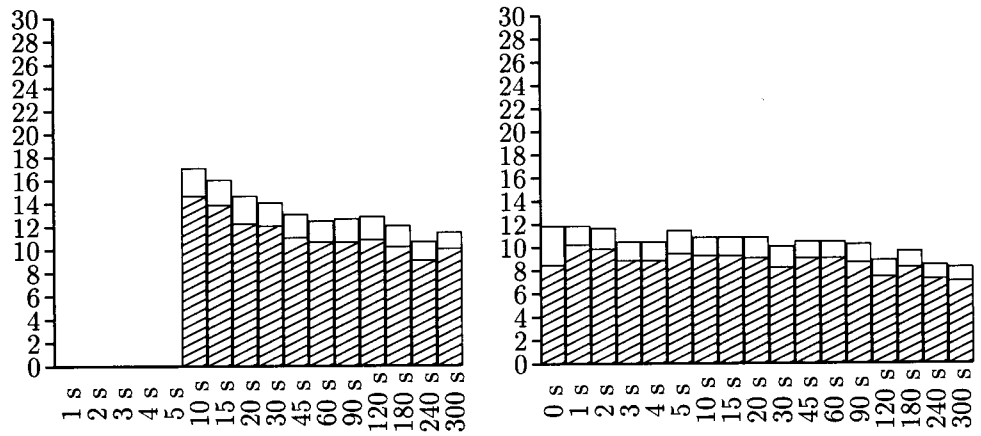

Figure 5.14: CPU time in milliseconds for decorrelation, for a varying time span and two epochs of data. Dual frequency, phase-only, kinematic baseline (left). Dual frequency, phase-and-code, kinematic baseline (right).

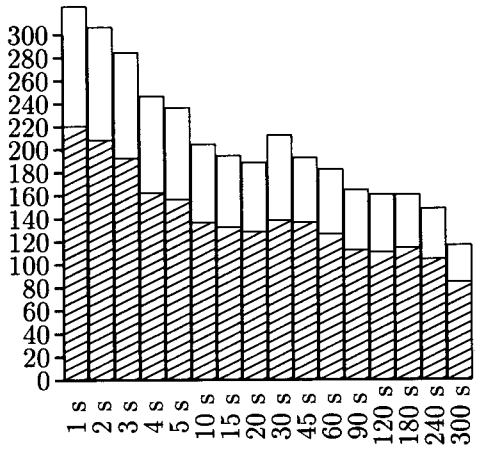

Figure 5.15: CPU time in milliseconds for decorrelation, for a varying time span and two epochs of data. Dual frequency, phase-only, static network of 4 stations.

5.10.2 Network, dual frequency

Now we will show the results obtained for a small network of 4 stations. Experiments were done in static as well as in kinematic mode. In the kinematic mode, 3 of the 4 stations were allowed to be roving.

In Figure 5.15 the results for the static case are shown. With the 7 satellites tracked on two frequencies, we have a total of 36 ambiguities, i.e. 3 times as much as for the single baseline case. The time needed for decorrelation is roughly 15 times the time needed for one baseline. The gain when using $Q_{\hat{b}\hat{a}}$ is larger than for the single baseline case (about 30%).

The network counterpart of the kinematic baseline, Figure 5.14, is given in Figure 5.16 (left). A gain of approximately 20% is observed. Figure 5.16 (right), the dual frequency phase and code case with roving receivers, can be compared to Figure 5.14. The average gain using $Q_{\hat{b}\hat{a}}$ is equal to the one we saw in Figure 5.16 (left). Again the instantaneous case forms an exception, for the same reason as given for the baseline case. The CPU time needed for

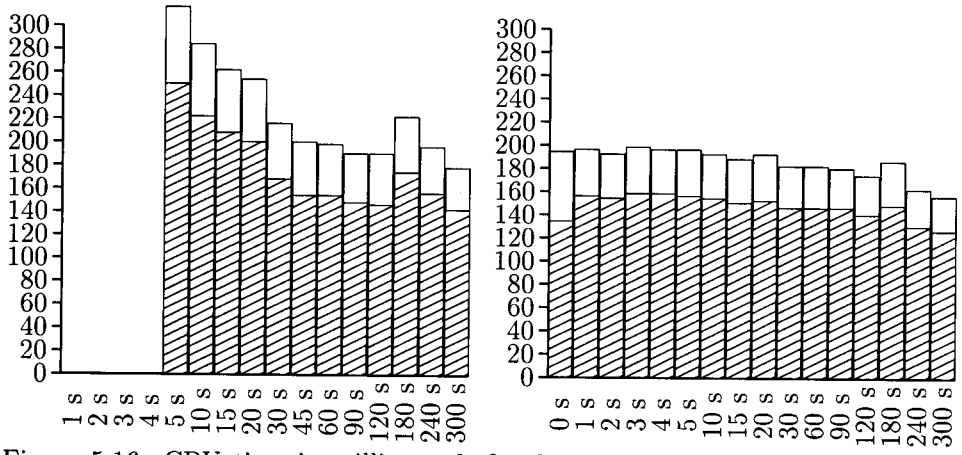

Figure 5.16: CPU time in milliseconds for decorrelation, for a varying time span and two epochs of data. Dual frequency, phase-only, kinematic network of 4 stations (left). Dual frequency, phase-and-code, kinematic network of 4 stations (right).

decorrelation is almost equal for all experiments.

5.10.3 Single baseline, single frequency

In Figure 5.17 only observation time spans larger than or equal to 45 seconds are considered. With single frequency phase observations on a 10.4 km baseline, it was not possible to obtain the correct integer vector for shorter time spans. Comparison with Figure 5.13, the dual frequency case, directly reveals that the CPU times are very little. In the single frequency case there are only 6 ambiguities, whereas there are 12 in the dual frequency case. Furthermore, the ambiguities, on the input, are less correlated in the single frequency than in the dual frequency case, see Teunissen (1994). The average gain when using $Q_{\hat{b}\hat{a}}$ is about 15%.

Figure 5.17 (right) shows the case with single frequency phase and code for the kinematic baseline. Here we see almost no gain since Z^{-T} and $Q_{\hat{b}\hat{a}}$ have the same dimension of 6-by-6. The little improvement that can be seen stems from the fact that no initialization is needed for the Z^{-T}-matrix when working with $Q_{\hat{b}\hat{a}}$. Note again that for the instantaneous case where $Q_{\hat{b}\hat{a}}$ has dimension 3-by-6 there is on improvement of about 15%.

5.10.4 Overall procedure

To place the timing results in perspective, we will consider for all cases, the time needed for the full procedure of parameter estimation for the implicit scheme, see Table 5.2. We give the experiment with the shortest and with the longest observation time span. The latter is limited to 300 seconds.

The normal equations were taken as a point of departure. The column 'Total CPU time' is the time needed for computing the float solution, performing the decorrelation plus the integer estimation, and computing the fixed solution. The two constituents of the second step are also specified on an individual basis. For the dual frequency cases, the decorrelation takes between 60% and 80% of the total time.

		Time span (s)	CPU time for Decorrelation (ms)	CPU time for Integer estimation (ms)	Total CPU time (ms)	Time span (s)	CPU time for Decorrelation (ms)	CPU time for Integer estimation (ms)	Total CPU time (ms)	Reduction of CPU time operating on $Q_{\hat{b}\hat{a}}$(%)
					Baseline, Dual frequency					
L1L2	static	2	17.5	0.4	20.7	300	6.2	0.2	9.2	21-23
L1L2	kinematic	10	14.7	0.2	18.6	300	10.0	0.2	13.9	13-16
L1L2P1P2	static	0	8.7	0.2	11.7	300	5.3	0.2	8.3	
L1L2P1P2	kinematic	0	8.7	0.2	11.7	300	7.1	0.2	11.1	13-16
					4-station Network, Dual frequency					
L1L2	static	1	221.3	16.4	271.0	300	85.8	3.1	124.5	27-35
L1L2	kinematic	5	253.4	8.9	315.5	300	144.7	0.9	201.8	20-23
L1L2P1P2	static	0	134.4	1.8	170.6	300	84.7	1.7	122.1	
L1L2P1P2	kinematic	0	134.4	1.8	170.6	300	127.4	1.9	185.8	19-21
					Baseline, Single frequency					
L1	static	45	1.2	0.1	1.9	300	0.7	0.1	2.4	11-17
L1	kinematic					300	1.2	0.1	2.9	
L1P1	static	0	1.0	0.1	2.3	300	0.7	0.1	1.9	7-15
L1P1	kinematic	0	1.0	0.1	2.3	300	0.8	0.1	2.6	0-5

Table 5.2: CPU times in milliseconds for decorrelation of the ambiguities, integer estimation and overall procedure. Reduction in CPU time when operating on $Q_{\hat{b}\hat{a}}$ instead of working on Z^{-T}.

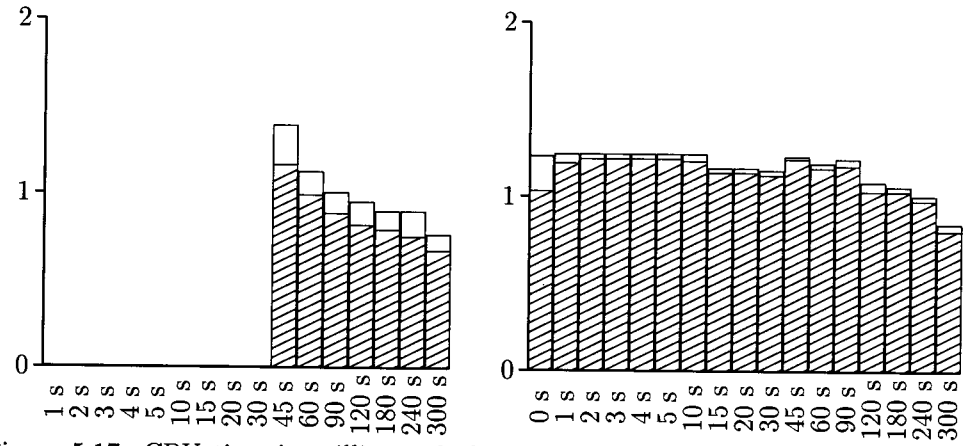

Figure 5.17: CPU time in milliseconds for decorrelation, for a varying time span and two epochs of data. Single frequency, phase-only, 7 satellites tracked, static baseline (left). Single frequency, phase-and-code, 7 satellites tracked, kinematic baseline (right).

5.10.5 Summary

The computation of the decorrelating transformation is by far the most time consuming task in the computation of the float and fixed solution. This is however no drawback for the LAMBDA method, since the CPU time gained in the integer estimation by decorrelating the ambiguities, exceeds the time needed to compute it by orders of magnitude. For a dual frequency phase and code kinematic baseline, the CPU time for the overall procedure is at the 10 ms level, and thus very fast anyway. Approximately 70% is taken by the decorrelation. The time needed for the decorrelation of the ambiguities, depends on 1. the number of ambiguities n, i.e. the dimension of the problem, and 2. the amount of correlation of the original double difference ambiguities. Important factors that influence the amount of correlation are whether or not code observations are included, whether we have a kinematic or a static setup, and the observation time span.

When the number of ambiguity parameters is larger than the number of non-ambiguity parameters, the 'implicit' scheme is more efficient; both in terms of CPU time as in terms of the use of core memory. The latter seems trivial in a time where computer memory is becoming abundant, but it will prove its usefulness when treating large networks, where the number of ambiguities reach from hundreds to thousands. Using the implicit scheme, the whole process of decorrelation, integer estimation and constraining the ambiguities can be done in-place. For single baseline cases, the difference between the explicit and the implicit computation is small.

For a dual frequency phase and code 4-station kinematic network (i.e. 3 roving receivers) a fixed solution is computed in less than 0.2 seconds.

References

Apostol, T. M. (1969). *Multi-variate calculus and linear algebra, with applications to differential equations and probability*, Volume 2 of *Calculus*. Wiley, New York. Second edition.

Blewitt, G. (1989). Carrier phase ambiguity resolution for the Global Positioning System applied to geodetic baselines up to 2000 km. *Journal of Geophysical Research 94*(B8), 10187–10203.

Counselman, C. C. and S. A. Gourevitch (1981). Miniature interferometer terminals for earth surveying: ambiguity and multipath with Global Positioning System. *IEEE Trans. on Geoscience and Remote Sensing 19*(4), 244–252.

de Jonge, P. and C. Tiberius (1996). The LAMBDA method for integer ambiguity estimation: implementation aspects. LGR-Series 12, Delft Geodetic Computing Centre, Delft University of Technology.

de Jonge, P. J. and C. C. J. M. Tiberius (1994). A new GPS ambiguity estimation method based on integer least squares. In *Proceedings 3th International Symposium on Differential Satellite Navigation Systems (DSNS'94)*, London, UK. The Royal Institute of Navigation. London, UK, April 18–22, Paper no. 73, 9pp.

Dong, D.-N. and Y. Bock (1989). Global Positioning System network analysis with phase ambiguity resolution applied to crustal deformation studies in California. *Journal of Geophysical Research 94*(B4), 3949–3966.

Dongarra, J. J., J. R. Bunch, C. B. Moler, and G. W. Stewart (1979). *LINPACK user's guide*. SIAM Publications, Philadelphia, USA.

Euler, H. J. and H. Landau (1992). Fast GPS ambiguity resolution on-the-fly for real-time applications. In *Proceedings of the Sixth International Geodetic Symposium on Satellite Positioning*, pp. 650–659. Columbus, Ohio, March 17–20, 1992.

Frei, E. (1991). *Rapid differential positioning with the Global Positioning System*. Ph. D. thesis, Astronomisches Institut Universität Bern. 177 pp.

Golub, G. H. and C. F. Van Loan (1989). *Matrix Computations, second edition*. Johns Hopkins Series in the Mathematical Sciences. The Johns Hopkins University Press.

Han, S. (1995). Ambiguity resolution techniques using integer least-squares estimation for rapid static or kinematic positioning. In *Proceedings Satellite Navigation Technology: 1995 and beyond*, Brisbane, Australia, June 26–28. 10 pp.

Han, S. and C. Rizos (1995). A new method of constructing multi-satellite ambiguity combinations for improved ambiguity resolution. In *Proceedings of ION GPS-95, 8th International Technical Meeting of the Satellite Division of the Institute of Navigation*, Palm Springs, CA, pp. 1145–1153. The Institute of Navigation.

Hatch, R. (1990). Instantaneous ambiguity resolution. In *Proceedings of IAG Symposium No. 107 'Kinematic Systems in Geodesy, Surveying, and Remote Sensing (KIS'90)*, Banff, Canada, September 10–13, pp. 299–308. Springer Verlag.

Li, Z. and Y. Gao (1997). Construction of high dimensional ambiguity transformation for the LAMBDA method. In *Proceedings of International Symposium on Kinematic Systems in Geodesy, Geomatics and Navigation KIS'97*, Banff, Canada, June 3–6, pp. 409–416.

Mervart, L. (1995). *Ambiguity Resolution Techniques in Geodetic and Geodynamic Applications of the Global Positioning System*. Ph. D. thesis, Astronomisches Institut Universität Bern.

Rothacher, M. and L. Mervart (1996). Bernese GPS software version 4.0. Technical report, Astronomical Institute University of Berne.

Teunissen, P. J. G. (1993). Least-squares estimation of the integer GPS ambiguities. LGR-Series 6, Delft Geodetic Computing Centre, Delft University of Technology. Invited lecture, Section IV Theory and Methodology, IAG General Meeting, Beijing, China, August 1993.

Teunissen, P. J. G. (1994). A new method for fast carrier phase ambiguity estimation. In *Proceedings IEEE Position, Location and Navigation Symposium PLANS'94*, pp. 562–573. Las Vegas, NV, April 11–15.

Teunissen, P. J. G. (1995a). The invertible GPS ambiguity transformations. *manuscripta geodaetica 20*(6), 489–497.

Teunissen, P. J. G. (1995b). The least-squares ambiguity decorrelation adjustment: A method for fast GPS integer ambiguity estimation. *Journal of Geodesy 70*(1–2), 65–82.

Teunissen, P. J. G. (1995c). On the GPS double difference ambiguities and their partial search spaces. In *Proceedings IAG Symposium No. 114, Geodetic Theory Today*, pp. 39–48. Springer Verlag. III Hotine-Marussi symposium on Mathematical Geodesy, L'Aquila, Italy, May 29–June 3, 1994.

Teunissen, P. J. G. (1996). GPS carrier phase ambiguity fixing concepts. In A. Kleusberg and P. J. G. Teunissen (Eds.), *GPS for Geodesy*, Volume 60 of *Lecture Notes in Earth Sciences*, Chapter 8, pp. 263–335. Springer Verlag.

Teunissen, P. J. G., P. J. de Jonge, and C. C. J. M. Tiberius (1994). On the spectrum of the GPS DD-ambiguities. In *Proceedings of ION GPS-94, 7th International Technical Meeting of the Satellite Division of the Institute of Navigation*, pp. 115–124. The Institute of Navigation. Salt Lake City, UT, September 20–23.

Teunissen, P. J. G., P. J. de Jonge, and C. C. J. M. Tiberius (1995). A new way to fix carrier-phase ambiguities. *GPS World 6*(4), 58–61.

Teunissen, P. J. G., P. J. de Jonge, and C. C. J. M. Tiberius (1996). The volume of the GPS ambiguity search space and its relevance for integer ambiguity resolution. In *Proceedings of ION GPS-96, 9th International Technical Meeting of the Satellite Division of the Institute of Navigation, Kansas City, Missouri, September 17–20*, pp. 889–898. The Institute of Navigation. Kansas City, Missouri, September 17–20.

Teunissen, P. J. G., P. J. de Jonge, and C. C. J. M. Tiberius (1997). The least-squares ambiguity decorrelation adjustment: its performance on short GPS baselines and short observation spans. *Journal of Geodesy 71*(10), 589–602.

Teunissen, P. J. G. and C. C. J. M. Tiberius (1994). Integer least-squares estimation of the GPS phase ambiguities. In *Proceedings of International Symposium on Kinematic Systems in Geodesy, Geomatics and Navigation KIS'94*, Banff, Canada, August 30–September 2, pp. 221–231.

Tiberius, C. C. J. M. and P. J. de Jonge (1995). Fast positioning using the LAMBDA-method. In *Proceedings 4th International Symposium on Differential Satellite Navigation Systems (DSNS'95)*, Bergen, Norway, April 24–28. The Nordic Institute of Navigation. Paper no. 30, 8 pp.

Chapter 6

Ambiguity resolution at medium distances

6.1 Introduction

As a definition for medium distance we will use here the one given by Bock (1996). It can be summarized as being the distance for which it is necessary to model the ionospheric and tropospheric delays, and for which the broadcast ephemerides are not of sufficient quality anymore. On the other hand, dual frequency ambiguity resolution with the ionosphere in some way constrained, is still feasible, and reference frame errors are not yet dominant. This definition limits the medium distance to somewhere between 10^1 and 10^3 km. For the lower bound of the distance, with the good quality of the broadcast ephemerides nowadays, use of precise ephemerides, or modeling of orbit parameters is not necessary. Ambiguity resolution in medium distance networks is treated in e.g. Blewitt (1989), Dong and Bock (1989), Mervart et al. (1994), Mervart (1995), Mervart et al. (1996).

The delays caused by the ionosphere play a key role. If one models the ionosphere as slant delays, or equivalently uses the ionosphere-free combination, a function of ambiguities is estimated, that is a rational number rather than an integer number. As pointed out in Section 4.2.3 it can be converted to an integer valued function, but that would produce an observable with a synthetic wavelength that is too small for successful integer resolution.

Constraining the ionospheric slant delays in some fashion, renders again integer estimable L1 and L2 ambiguities (see Section 4.2.4).

In this chapter we will show results using two types of models for constraining the ionospheric delay. In the first model the delays are (hard) constrained to zero by simply omitting them from the model (short baseline model). In Section 6.2 some results from the application of this model will be given.

In the second model the ionospheric slant delays are stochastically constrained both in an absolute and in a relative station sense.

As the software developed in the framework of this thesis is neither equipped for the estimation of orbital parameters nor for estimation of constrained ionosphere parameters, the LAMBDA method has been implemented in the GAMIT software of the Massachusetts Institute of Technology/Scripps Institution of Oceanography. In Section 6.3 and 6.4 a short description of the GAMIT software, and the current ambiguity resolution strategy employed by it, will be given. In Section 6.5 the implementation of the LAMBDA method in GAMIT will be treated, and in Section 6.6 some results will be shown of both the original and the LAMBDA aided ambiguity resolution strategy for a network in California.

6.2 The short baseline model

The simplest form of constraining the ionosphere is to omit the ionospheric delays from the model, i.e., the constraints are that the ionospheric delays are zero. This is generally referred to as the short baseline model, which is in widespread use for so-called 'rapid static' positioning. The generally accepted maximum distance for this type of application during daytime, is 10 km or less for time spans up to 1 minute.

For distances longer than this, for some parts of the day, the ionospheric delays, and, more important, the between-station differences of ionospheric delays, may still be small enough to allow successful ambiguity resolution. However, the delays may be already of a size that they bias the fixed solution.

As an example, we computed for a baseline of approximately 12.7 km in the Netherlands, fixed solutions using dual frequency phase and code data of only one epoch. Using 50 minutes worth of data, starting at 17:35:00 GPS time (18:35:11 local time) December 22, 1996, 3000 solutions were obtained. Trimble 4000 SSI receivers were used; the standard deviation for the phase observables was set to 3 mm and the standard deviation for the code observables to 30 cm. No attempt was made to estimate tropospheric zenith delays (due to the zero length time span), but the hydrostatic delays were modeled using the mapping function of Niell (1996) and the model for the hydrostatic zenith delay of Davis et al. (1985) with a standard model for the atmosphere.

For all of the 3000 experiments, with an elevation cut-off of 10 degrees, 8 satellites were observed, and the correct integer ambiguities were estimated. In Figure 6.1 at left, for North, East, and Height, the relative frequency of the estimates for the increments to the a priori coordinate values is given.

The histograms show a peculiar behaviour, which leads to the suspicion that the modeling was not adequate. To remedy this, we computed the fixed solution using the same integer ambiguities as estimated before, but now we included the ionospheric slant delays in the model. Two types of models were used, one using dual frequency phase and code, and one using dual frequency phase only (since the ambiguities are resolved, one epoch of data suffices also for the latter model). In Figure 6.1 at right we plotted the histograms for the increments using the extended models. The histograms in black are for the model with code included, the histograms in grey are for the model without code. Comparing the histograms at left with those at right, we see that the inclusion of the ionospheric slant delays in the model, renders estimates that are approximately normal distributed (as they should be). In addition it can be observed that the code observables do not contribute much to the fixed solution.

The a priori coordinates come from a solution that has an accuracy of few centimeters, hence no conclusions should be drawn about the bias in the estimates. Furthermore, to show most clearly the difference between the models, the width of the bins is equal for the increments referring to one coordinate for the different models, but they differ among coordinates.

In Figure 6.2 for the model with dual frequency phase and modeling of the ionosphere, histograms for the increments for the three coordinates using an equal bin width are given. The empirical standard deviations for the baseline coordinates are $\sigma_N = 5.0$ mm, $\sigma_E = 2.8$ mm, and $\sigma_H = 7.6$ mm.

About the distance and the circumstances for which ambiguity resolution using a zero constraint for the ionosphere is still feasible, remarkably little is known (SSG 1.157 1997). The maximum distance will however inevitably depend on the ionospheric conditions, and

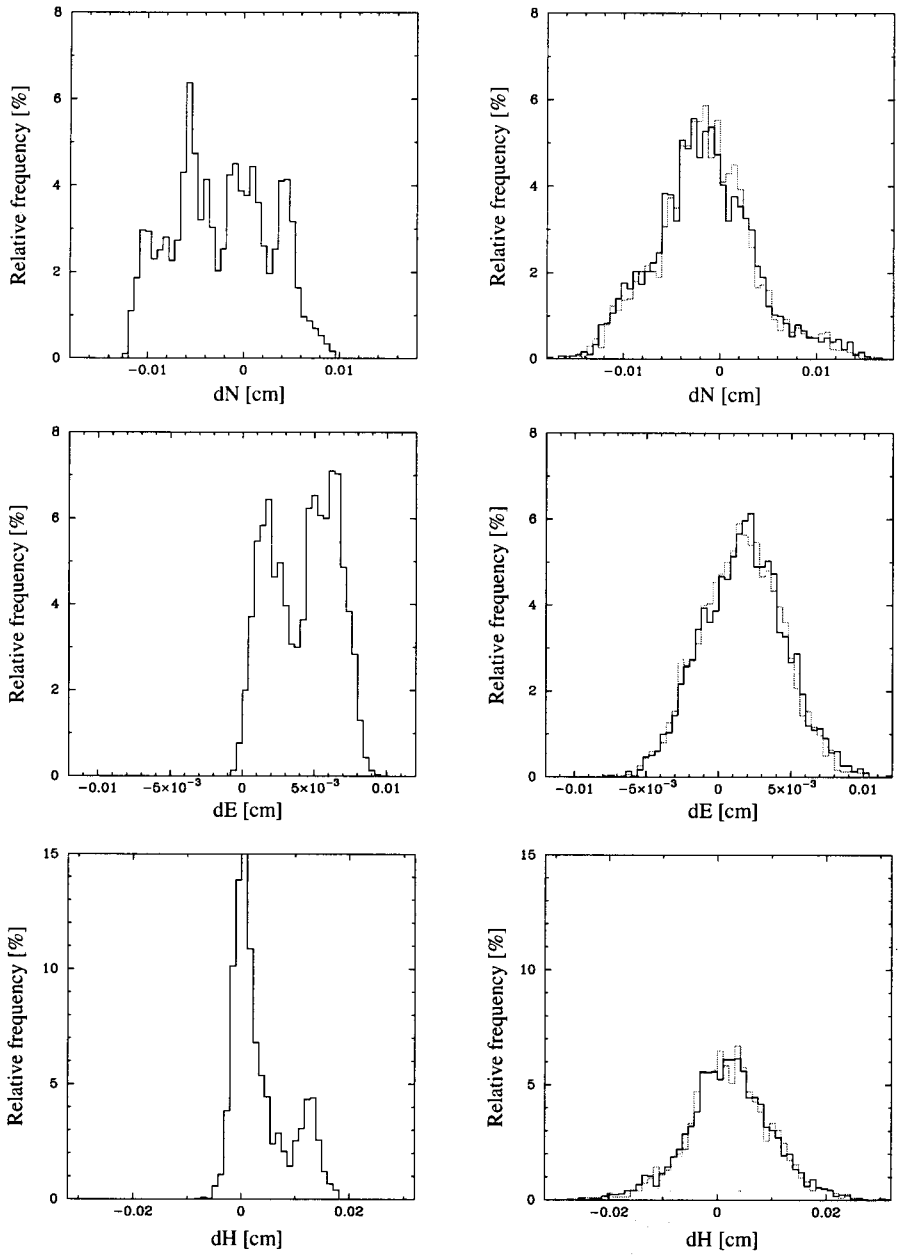

Figure 6.1: Histograms (relative frequency) for the increments in North, East and Height for the fixed solution of a 12.7 km baseline (3000 experiments). At left for the model without ionospheric slant delays modeled, at right for the models with ionospheric slant delays.

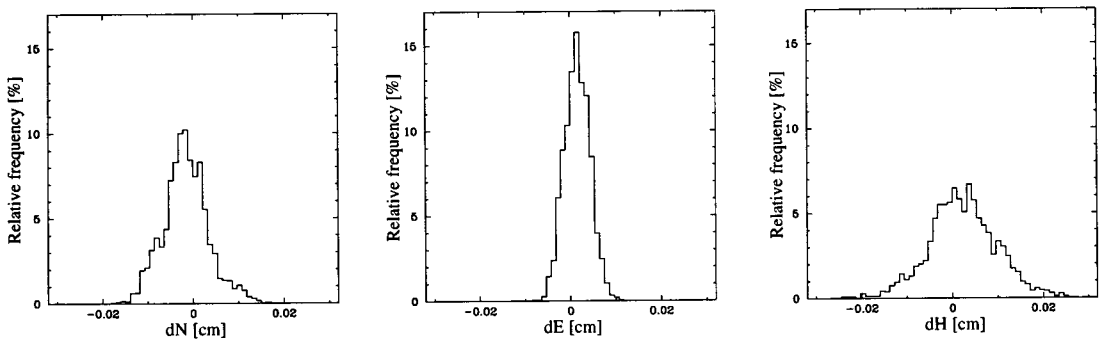

Figure 6.2: Histograms (relative frequency) for the increments in North, East and Height for the fixed solution of a 12.7 km baseline (3000 experiments).

particularly on the between-station difference of the ionospheric delay. At night these differences are considerably smaller than during daytime.

To show how well during the nighttime ambiguities can be resolved, we computed every 30 seconds during one day (April 5 1998), the fixed solution for a baseline of approximately 56.5 km in Southern California between Pinyon (PIN1) and Temecula (BILL). We used only one epoch of dual frequency code and phase data from two Ashtech Z-XII3 receivers, with the observables weighted as above. There is a considerable difference in height between the two stations, the (WGS-84) ellipsoidal height for Pinyon is approximately 1256 meter, and for Temecula 470 meter so that the meteorological circumstances and thus also the tropospheric delays vary considerably for both stations. The hydrostatic tropospheric delays were corrected a priori using Niell's mapping function combined with Davis' model for the zenith delay. With an elevation cut-off of 7 degrees, between 5 and 10 satellites were observed, viz. 5 satellites for 0.4% of the experiments, 6 (18.7%), 7 (29.9%), 8 (19.7%), 9 (25.9%), 10 (5.4%). The a priori coordinates came from a one day network solution computed with the GAMIT software (see the next sections).

In Figure 6.3 the slant ionospheric delays at Pinyon, computed using dual frequency code data with a common clock are depicted. The epochs refer to GPS time, local time is GPS time minus 8 hours. The diurnal cycle can clearly be observed.

At each epoch between epoch 510 and 1466 (20:14:30 - 04:12:30 local time) ambiguity resolution was successful. Outside this interval, except for some isolated epochs, the ambiguity resolution failed. The interval of successful ambiguity resolution nicely corresponds with the period at night with low ionospheric activity.

In Figure 6.4 the time series for the increments in North, East and Height are plotted for the fixed solution. The dotted line represents the model of dual frequency phase and code, without estimation of ionospheric slant delays, the solid line the model of dual frequency phase only, with estimation of slant delays. The signatures of the time series for both models show a different behaviour. Those originating from the model without ionospheric slant delays show a stronger long term variation due to the unmodeled ionosphere, those originating from the model with ionospheric slant delays show a short term variation, which is probably due to phase multipath (Genrich and Bock 1992). In the height, a long term variation is visible, caused by the unmodeled water vapor tropospheric delay.

In Figure 6.5 the increments for the model with ionospheric slant delays are grouped into

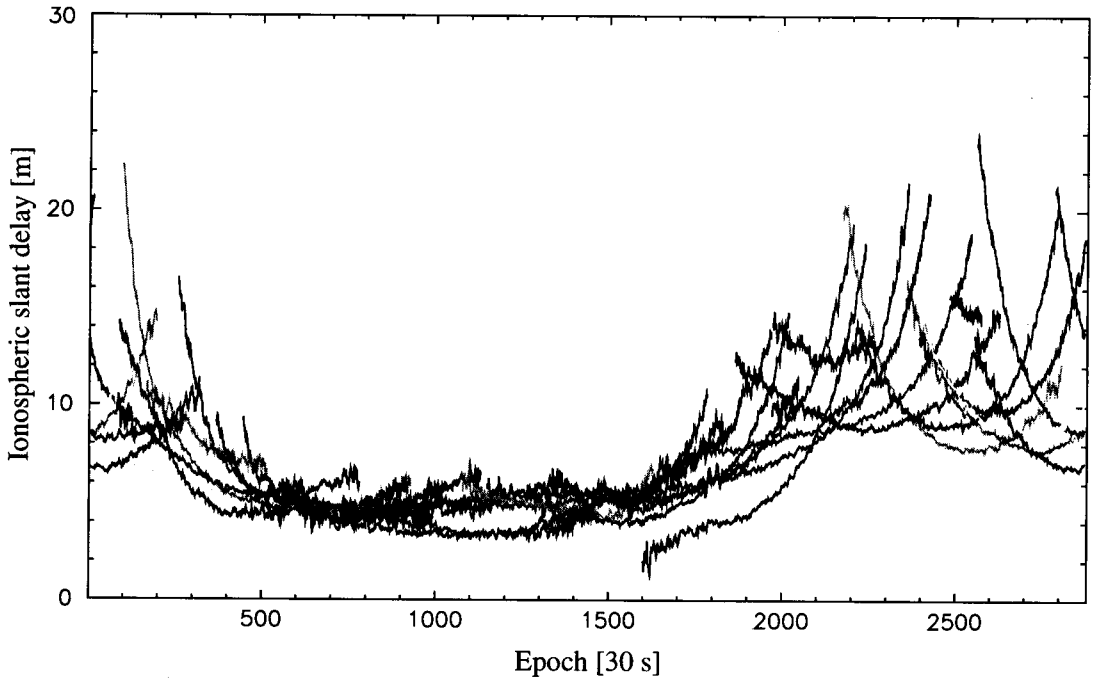

Figure 6.3: Slant ionospheric delays at Pinyon, at April 5, 1998. First epoch is 0:00 GPS time (16:00 local time).

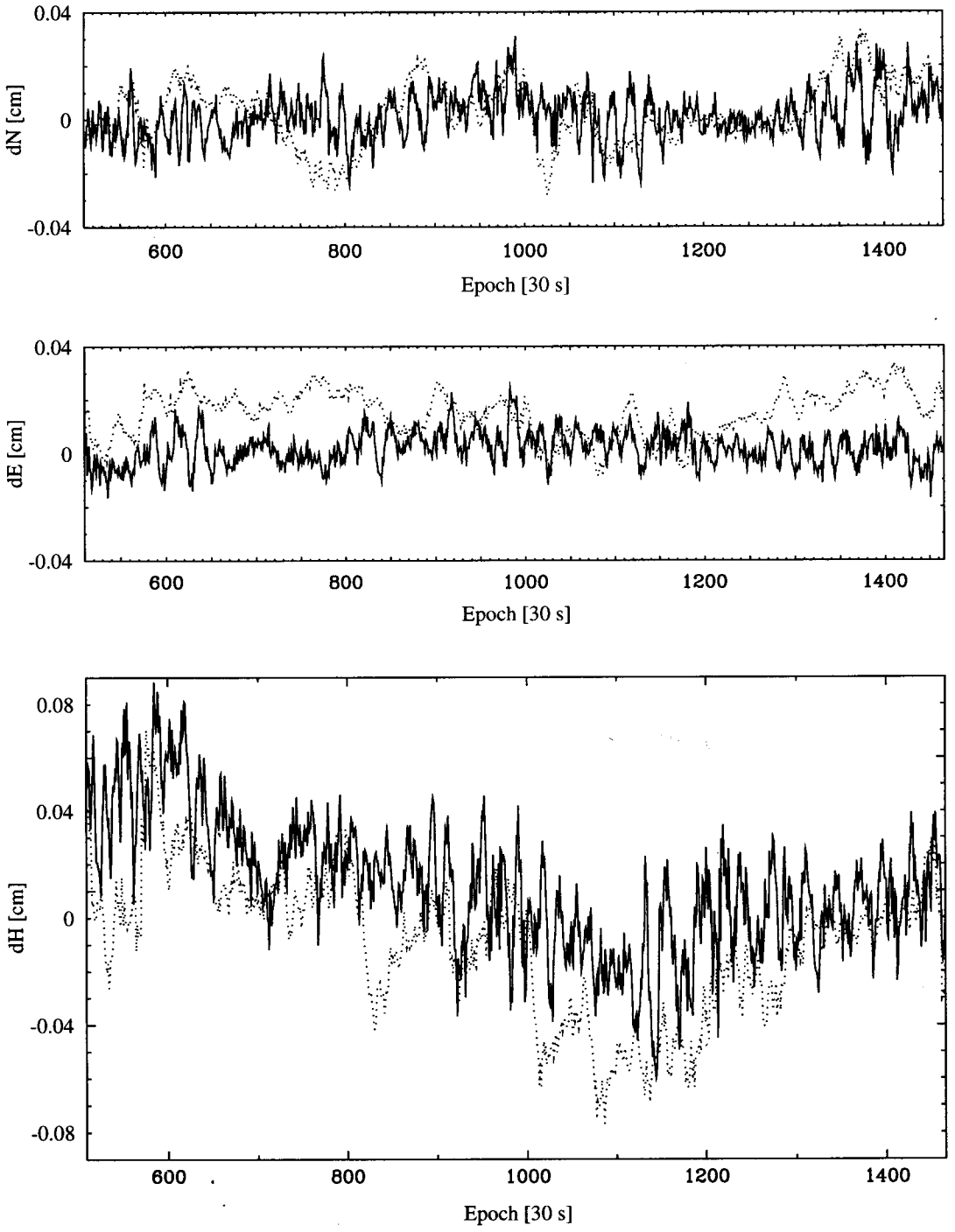

Figure 6.4: Time series for the increments in North, East and Height for the fixed solution of a 56.5 km baseline (957 experiments). Dotted line: dual frequency phase and code, no ionospheric slant delays modeled, solid line: dual frequency phase, ionospheric delays modeled.

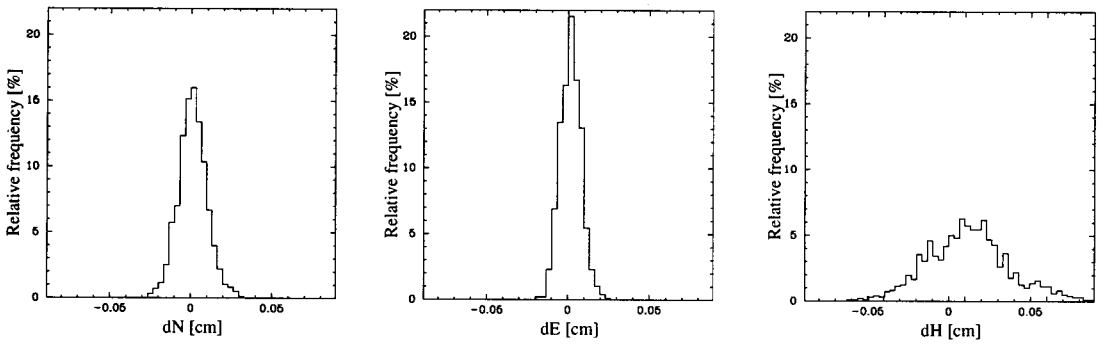

Figure 6.5: Histograms (relative frequency) for the increments in North, East and Height for the fixed solution of a 56.5 km baseline (957 experiments).

histograms. The empirical standard deviation and mean for the coordinates are: $\sigma_N = 8.8$ mm, $\text{mean}_N = 1.2$ mm, $\sigma_E = 6.3$ mm, $\text{mean}_E = 1.7$ mm, $\sigma_H = 25.0$ mm, $\text{mean}_H = 12$ mm. Taking into account the distance of the baseline, the North and East components are remarkably well estimated, coupling high precision to a very small bias. The height is considerably less well established, which is mainly due to remaining tropospheric delays. One has to bear in mind however that the difference in height between the two station is almost 800 meter.

6.3 The four-step bootstrapping procedure of GAMIT

The estimation process within GAMIT is based on the use of DD carrier phase and ionospheric pseudo observables. To keep the size of the system of normal equations within bounds, as soon as a new ambiguity parameter needs to be introduced for a certain receiver-satellite combination, the present ambiguity parameter is eliminated (implicitly solved for). For time spans of one day this will typically happen when a satellite rises again after it had set at an earlier epoch. For the float solution this has no consequences, since eliminating a parameter is equivalent to solve for it explicitly. For the fixed solution, however, it means that even if one fixes all 'explicit' ambiguities, in the fixed solution still the 'implicit' ambiguities are present. For a time span of a day the number of implicit ambiguities equals approximately the number of explicit ambiguities.

Not all ambiguities are resolved together in GAMIT. First the wide lane ($N_{L2} - N_{L1}$) ambiguities are resolved, and then the narrow lane (N_{L1}) ambiguities. The procedure is described in Dong and Bock (1989), Feigl et al. (1993), and Bock (1996):

Step 1:
Using the ionosphere-free linear combination of carrier phase (LC), the geometric parameters b, viz. baseline coordinates, tropospheric zenith delay parameters and orbital parameters are estimated together with the LC ambiguities a_{LC}. To impose a reference frame, tight

constraints are applied to the station coordinates and orbits r. The model reads

$$\begin{aligned} E\{y^{(1)}\} &= \begin{bmatrix} A_b & A_{a_{\mathrm{LC}}} \end{bmatrix} \begin{bmatrix} b \\ a_{\mathrm{LC}} \end{bmatrix} \; ; \; D\{y^{(1)}\} = Q_y^{(1)} \\ E\{y_2\} &= r \qquad\qquad\qquad ; \quad D\{y_2\} = Q_{y_2} \end{aligned} \tag{6.1}$$

and results in

$$\begin{bmatrix} \hat{b}^{(1)} \\ \hat{a}_{\mathrm{LC}}^{(1)} \end{bmatrix} \tag{6.2}$$

Step 2:
With all geometric parameters constrained to the values from step 1, the wide lane ambiguities are resolved in a sequential way. This is done using the so-called ionospheric constraint formulation, see Section 4.3. The inclusion of constraints for the ionospheric delays, by introducing pseudo observables ensures the integer nature of the ambiguities.

For the pseudo observables a distance dependent variance-covariance matrix is chosen, which constrains the ionosphere in both absolute and relative between-station sense (Schaffrin and Bock 1988).

For the pseudo observables of a single baseline l_1^j, l_1^k, l_2^j and l_2^k constituting a single DD observable, the variance-covariance matrix reads

$$D\{\begin{bmatrix} l_1^j \\ l_1^k \\ l_2^j \\ l_2^k \end{bmatrix}\} = \beta^2 \begin{bmatrix} 1 & 0 & \frac{1}{\cosh\delta} & 0 \\ 0 & 1 & 0 & \frac{1}{\cosh\delta} \\ \frac{1}{\cosh\delta} & 0 & 1 & 0 \\ 0 & \frac{1}{\cosh\delta} & 0 & 1 \end{bmatrix} \tag{6.3}$$

where β is a user defined constant, depending on the ionospheric activity, and δ the arc length between stations scaled such, that for baseline lengths up to 10,000 km it will never exceed the value of $\ln(1+\sqrt{2}) \approx 0.88$ radians:

$$\delta = \ln(1+\sqrt{2})\,\frac{R}{10^7}\,\frac{\|r_1 - r_2\|}{R} \approx 0.56\,\frac{\|r_1 - r_2\|}{R} \tag{6.4}$$

with R the Earth's radius in meters. The scaling is necessary since $1/\cosh$ has a point of inflection at $\ln(1+\sqrt{2})$ which has no physical meaning for this application.

The variance of the DD ionospheric pseudo observable follows then as

$$D\{l_{12}^{jk}\} = 4\beta^2(1 - \frac{1}{\cosh\delta}) \tag{6.5}$$

i.e. the variance increases with increasing baseline length.

The two orthogonal linear combinations due to the transformation of Section 4.3, Eq. (4.63) read

$$\begin{aligned} &\frac{\eta_2}{\eta_2 - \eta_1}\Phi_{\mathrm{L1}} - \frac{\eta_1}{\eta_2 - \eta_1}\Phi_{\mathrm{L2}} \\ &-\frac{\eta_1^2 + \eta_2^2}{\eta_0(\eta_1 + \eta_2)}l + \frac{\eta_1}{\eta_1 + \eta_2}\Phi_{\mathrm{L1}} + \frac{\eta_2}{\eta_1 + \eta_2}\Phi_{\mathrm{L2}} \end{aligned} \tag{6.6}$$

The precision of the second linear combination is governed by the precision of the ionospheric constraints, which is for the baseline lengths involved in the regional networks at least one order less precise than the phase observables.

They result in the following functions of ambiguities

$$\begin{aligned} &\frac{\eta_2}{\eta_2-\eta_1}\lambda_1 N_{\mathrm{L1}} - \frac{\eta_1}{\eta_2-\eta_1}\lambda_2 N_{\mathrm{L2}} \\ &\frac{\eta_1}{\eta_1+\eta_2}\lambda_1 N_{\mathrm{L1}} + \frac{\eta_2}{\eta_1+\eta_2}\lambda_2 N_{\mathrm{L2}} \end{aligned} \tag{6.7}$$

which for the purpose of ambiguity resolution are rewritten as

$$\begin{aligned} &\frac{\eta_2\lambda_1-\eta_1\lambda_2}{\eta_2-\eta_1}N_{\mathrm{L1}} - \frac{\eta_1}{\eta_2-\eta_1}\lambda_2(N_{\mathrm{L2}}-N_{\mathrm{L1}}) \\ &\frac{\eta_1\lambda_1+\eta_2\lambda_2}{\eta_1+\eta_2}N_{\mathrm{L1}} + \frac{\eta_2}{\eta_1+\eta_2}\lambda_2(N_{\mathrm{L2}}-N_{\mathrm{L1}}) \end{aligned} \tag{6.8}$$

to obtain wide lane type ambiguities.

One has to bear in mind however, that there is a difference with the case when one applies the classic wide lane transformation of Section 4.3.2:

$$T = \begin{bmatrix} 1 & \\ \frac{f_1}{f_1-f_2} & -\frac{f_2}{f_1-f_2} \end{bmatrix} \otimes I \tag{6.9}$$

If we look at the synthetic wavelengths of the ambiguities in (6.8), we have

$$\begin{aligned} &\frac{c}{f_1+f_2}N_{\mathrm{L1}} - \frac{cf_2}{f_1^2-f_2^2}(N_{\mathrm{L2}}-N_{\mathrm{L1}}) \\ &\frac{c(f_1^3+f_2^3)}{f_1f_2(f_1^2+f_2^2)}N_{\mathrm{L1}} + \frac{cf_1^2}{f_2(f_1^2+f_2^2)}(N_{\mathrm{L2}}-N_{\mathrm{L1}}) \end{aligned} \tag{6.10}$$

with

$$\frac{c}{f_1+f_2} \approx 10.7 \text{ cm} \qquad \frac{cf_2}{f_1^2-f_2^2} \approx 37.7 \text{ cm} \tag{6.11}$$

$$\frac{c(f_1^3+f_2^3)}{f_1f_2(f_1^2+f_2^2)} \approx 22.4 \text{ cm} \qquad \frac{cf_1^2}{f_2(f_1^2+f_2^2)} \approx 15.2 \text{ cm} \tag{6.12}$$

In fact we have a mixture of wavelengths. The only thing that can be said about it (if we want to hold on to the concept of wavelengths), is that the $(N_{\mathrm{L2}}-N_{\mathrm{L1}})$ ambiguity in the first linear combination (which is more precise than the second combination, since the precision of the latter is governed by the less precise ionospheric pseudo observables) possesses a longer wavelength than the N_{L1} ambiguity.

With $a_w = N_{\mathrm{L2}} - N_{\mathrm{L1}}$ and $a_n = N_{\mathrm{L1}}$, the model reads

$$E\{y^{(2)} - A_b\hat{b}^{(1)}\} = \begin{bmatrix} A_{a_w} & A_{a_n} \end{bmatrix} \begin{bmatrix} a_w \\ a_n \end{bmatrix} \; ; \; D\{y^{(2)}\} = Q_y^{(2)} \tag{6.13}$$

which results in the float solution

$$\begin{bmatrix} \hat{a}_w^{(2)} \\ \hat{a}_n^{(2)} \end{bmatrix} \; ; \; \begin{bmatrix} Q_{\hat{a}_w^{(2)}} & Q_{\hat{a}_w\hat{a}_n^{(2)}} \\ Q_{\hat{a}_n\hat{a}_w^{(2)}} & Q_{\hat{a}_n^{(2)}} \end{bmatrix} \tag{6.14}$$

The subsequent integer estimation step reads

$$\hat{a}_w^{(2)} \; ; \; Q_{\hat{a}_w^{(2)}} \Rightarrow \check{a}_w \tag{6.15}$$

Step 3:
With the wide lane ambiguities constrained to the integer values from step 2, the narrow lane ambiguities are estimated together with all geometric parameters from the ionosphere-free linear combination. The station coordinates are constrained as in step 1. This solution is followed by integer estimation of the narrow lane ambiguities.

Only the narrow lane ambiguities that have a successfully resolved wide lane counterpart, are candidates to be resolved here. The remainder of the narrow lane ambiguities form together with their unresolved wide lane counterparts again LC type of ambiguities.

With the LC linear combination as in Eq. (4.43) we have for the resulting ambiguity

$$N_{\mathrm{LC}} = \frac{-\eta_1}{\eta_2 - \eta_1}(\lambda_2 N_{\mathrm{L2}} - \frac{\eta_2}{\eta_1}\lambda_1 N_{\mathrm{L1}}) \tag{6.16}$$

For the receiver-satellite combination for which we have a successful resolved wide lane ambiguity it is rewritten as

$$N_{\mathrm{LC}} = \frac{-\eta_1}{\eta_2 - \eta_1}\lambda_2(N_{\mathrm{L2}} - N_{\mathrm{L1}}) + \frac{-\eta_1}{\eta_2 - \eta_1}(\lambda_2 - \frac{\eta_2}{\eta_1}\lambda_1)N_{\mathrm{L1}} \tag{6.17}$$

$$= c\frac{f_2}{f_2^2 - f_1^2}(N_{\mathrm{L2}} - N_{\mathrm{L1}}) + \frac{c}{f_1 + f_2}N_{\mathrm{L1}} \tag{6.18}$$

The integer estimate for the wide lane ambiguity is inserted in Eq. (6.18), which results in ambiguities with a wavelength of ≈ 10.7 cm.

The model reads

$$\begin{aligned} E\{y^{(1)} - A_{a_w}\check{a}_w\} &= \begin{bmatrix} A_b & A_{a_n} \end{bmatrix} \begin{bmatrix} b \\ a_n \end{bmatrix} \; ; \; D\{y^{(1)}\} = Q_y^{(1)} \\ E\{y_2\} &= r \qquad\qquad ; \; D\{y_2\} = Q_{y_2} \end{aligned} \tag{6.19}$$

which results in the float solution

$$\begin{bmatrix} \hat{b}^{(3)} \\ \hat{a}_n^{(3)} \end{bmatrix} \; ; \; \begin{bmatrix} Q_{\hat{b}^{(3)}} & Q_{\hat{b}\hat{a}_n^{(3)}} \\ Q_{\hat{a}_n\hat{b}^{(3)}} & Q_{\hat{a}_n^{(3)}} \end{bmatrix} \tag{6.20}$$

The subsequent integer estimation step reads

$$\hat{a}_n^{(3)} \; ; \; Q_{\hat{a}_n^{(3)}} \Rightarrow \check{a}_n \tag{6.21}$$

Step 4:
With the wide and narrow lane ambiguities fixed to the integer values from step 2 and 3, the geometric parameters are estimated using the ionosphere-free linear combination. The model reads

$$E\{y^{(1)} - A_{a_w}\check{a}_w - A_{a_n}\check{a}_n\} = A_b b \; ; \; D\{y^{(1)}\} = Q_y^{(1)} \tag{6.22}$$

which results in the eventual fixed solution

$$\check{b}^{(4)} \; ; \; Q_{\check{b}} \tag{6.23}$$

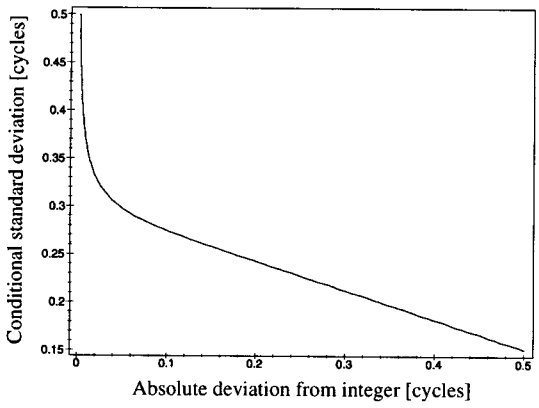

Figure 6.6: In the area below the curve, the probability of making a type 1 error is less than 0.001 while the probability of making a type 2 error is minimized.

6.4 Ambiguity resolution in GAMIT

The strategy applied in the GAMIT software to resolve the ambiguities is described in Dong and Bock (1989). It is primarily based on a sequence of roundings to the nearest integer. The criterion for rounding is based on the Neyman-Pearson criterion. It yields

$$\kappa \leq \alpha \tag{6.24}$$

with

$$\kappa = \sum_{n=1}^{\infty} \left[\operatorname{erfc}\left(\frac{n - (\hat{a}_i - nint(\hat{a}_i))}{\sqrt{2}\sigma_{\hat{a}_i}} \right) - \operatorname{erfc}\left(\frac{n + (\hat{a}_i - nint(\hat{a}_i))}{\sqrt{2}\sigma_{\hat{a}_i}} \right) \right] \tag{6.25}$$

and α the level of significance. The complementary error function $\operatorname{erfc}(x)$ is defined for all complex x by

$$\operatorname{erfc}(x) = 1 - \frac{2}{\sqrt{\pi}} \int_0^x e^{-t^2} dt \tag{6.26}$$

This criterion differs from the one in Dong and Bock (1989) by the use of the single sigma value instead of the $\bar{\sigma}_{\hat{a}_i} = 3\sigma_{\hat{a}_i}$ value.

In Figure 6.6 the region is depicted where the probability of making a type 1 error (i.e. rounding an ambiguity to the wrong integer value) is less than $\alpha = 0.001$ (level of significance, see Section 3.9), and the probability of making a type 2 error (decision not to round to the nearest integer, while in fact it is the correct integer value $(1 - \gamma)$, see Section 3.9) is minimized. The probability of ambiguities being rounded that are close to an integer but have a large standard deviation, as well of those far from an integer value, but with a small standard deviation, is decreased by the use of a so-called 'taper' function T. The taper function currently used, differs from the one described in Dong and Bock (1989):

$$T = \begin{cases} 0 & \text{if } \|\hat{a}_i - nint(\hat{a}_i)\| \geq 0.15 \text{ or } \sigma_{\hat{a}_i} \geq 0.15, \\ 3\left(1 - \frac{\|\hat{a}_i - nint(\hat{a}_i)\|}{0.15}\right)^2 (0.15 - \sigma_{\hat{a}_i}) & \text{otherwise} \end{cases} \tag{6.27}$$

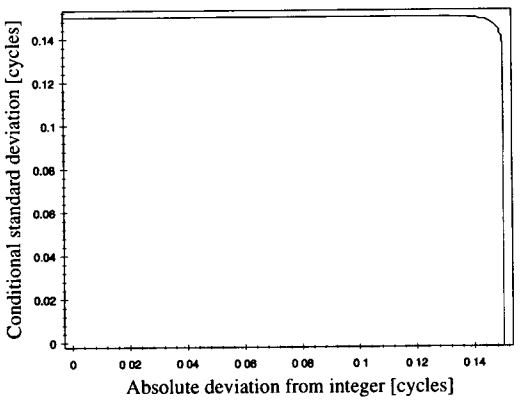

Figure 6.7: Area (below the curve), where the ambiguities are rounded to their nearest integer value.

The resulting decision function d is then

$$d(\hat{a}_i - nint(\hat{a}_i), \sigma_{\hat{a}_i}) = T/\kappa \tag{6.28}$$

The ambiguity resolution takes place sequentially: for all ambiguities that have not been resolved so far, the decision function (6.28) is computed. The ambiguity with the highest value exceeding 1000 will be constrained to its rounded integer value. In Figure 6.7 the area is depicted where the decision function is larger than 1000, and consequently rounding of the real valued ambiguity is performed. As the figure shows, the decision function is hardly anymore based on the Neyman-Pearson principle. The heuristic taper function dominates the resolution criterion.

To constrain the value of the selected ambiguity, the vector of ambiguities and the variance-covariance matrix generally have to be permuted such that this ambiguity is at the last position. By constraining an ambiguity to the integer value found for it, the remainder of the ambiguities and their variance-covariance matrix are updated. Instead of the estimates of the ambiguities, we get then the conditional estimates of the ambiguities. The vector of conditional estimates, and its variance-covariance matrix, after $n - i$ ambiguities have been constrained, are denoted as

$$\hat{a}_{|i+1,\ldots,n} \quad ; \quad Q_{\hat{a}_{|i+1,\ldots,n}} \tag{6.29}$$

After that, the decision function is again computed with now the conditional estimates and their conditional standard deviation as input for it.

Despite its shortcomings, the procedure sketched here, has proved to work very satisfactory, and ambiguities for a number of regional networks are resolved operationally at a daily basis.

If no more ambiguities can be found that satisfy the criterion set for the decision function, two other methods are tried. The first method is to use the Melbourne-Wübbena (MW) combination. It is only used in the case of wide lane ambiguities (step 2), and needs precise pseudorange data to be successful. It is computed for one ambiguity only at a time, and hence we are dealing here with the unconditional estimates. As in general not all ambiguities

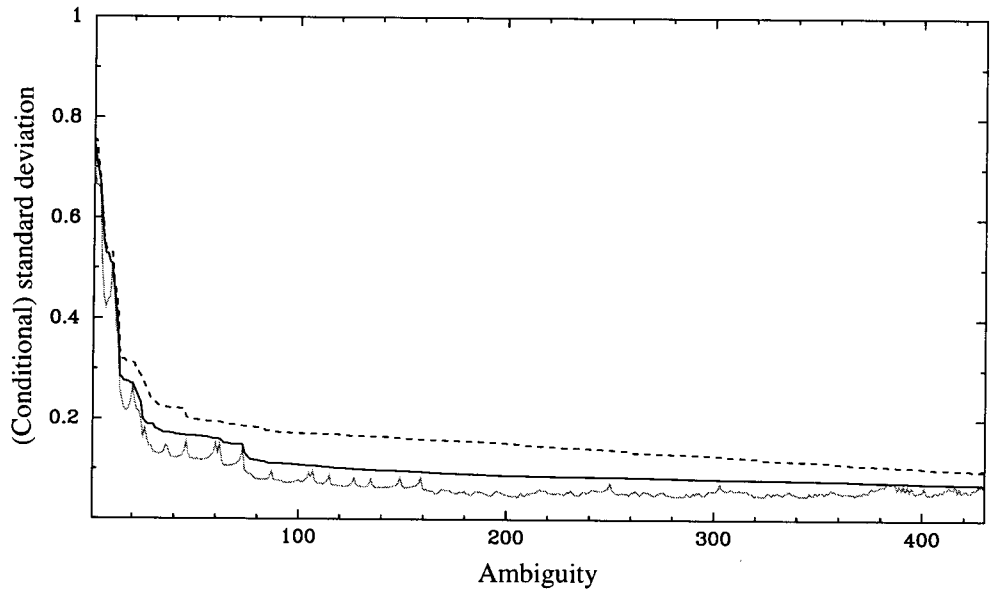

Figure 6.8: Conditional standard deviation of decorrelated MW wide lane ambiguities (solid grey curve), and standard deviation (sorted in increasing order) of the original (dashed black curve) and decorrelated (solid black curve) MW wide lane ambiguities.

are observed for the same time span, and some of them have been observed for only a very short time span, estimation of the MW combination for all ambiguities together, followed by a constraining of resolved ambiguities, might help the resolution of the ambiguities that were observed for only a small time span.

In Figure 6.8 for the Californian network of Figure 4.6 plus one extra station, the standard deviation of the original MW wide lane ambiguities as well as the standard deviation and conditional standard deviation of the decorrelated wide lane ambiguities are plotted. Since they come from a simulation study they are scaled by an unknown scale factor. The standard deviations are sorted in increasing order.

The solution is for a period of 24 hours and hence the time spans that ambiguities are observed, show a large variation. The plot shows that for this type of network the Z-transformation also improves the standard deviation of the MW ambiguities, and that conditioning the ambiguities in a sequential way gives an extra improvement. Although the improvement is not as large as in the case where the modeling is done in terms of coordinates instead of ranges, it still might be of help to resolve these ambiguities.

In the second strategy, a search is performed analogously to the one employed by the LAMBDA method. For a small set of ambiguities (typically 5–10) the following minimization problem is solved

$$\min(\hat{a}-a)^T Q_{\hat{a}}^{-1}(\hat{a}-a) \quad a \in \mathbf{Z} \tag{6.30}$$

6.5 LAMBDA implementation in GAMIT

The LAMBDA method was implemented in the four-step procedure. Besides the normal bootstrapping strategy an alternative strategy was devised:

Standard Bootstrapping.
Instead of using the decision function, the MW combination, and search, the ambiguities are resolved using the LAMBDA method. Since it was impossible to interfere too much in the existing software, it was not possible to fix only a subset of the ambiguities. The LAMBDA method is used to resolve both the wide lane (in step 2), and the narrow lane (in step 3) ambiguities. This will be referred to as standard bootstrapping.

Alternative Bootstrapping.
All ambiguities (both wide and narrow lane) are resolved in step 2 using the LAMBDA method. It will be referred to as alternative bootstrapping. Step 2 is replaced by:

$$E\{y^{(2)} - A_b\hat{b}^{(1)}\} = \begin{bmatrix} A_{a_w} & A_{a_n} \end{bmatrix} \begin{bmatrix} a_w \\ a_n \end{bmatrix} \; ; \; D\{y^{(2)}\} = Q_y^{(2)} \tag{6.31}$$

which results in the float solution

$$\begin{bmatrix} \hat{a}_w^{(2)} \\ \hat{a}_n^{(2)} \end{bmatrix} \; ; \; \begin{bmatrix} Q_{\hat{a}_w^{(2)}} & Q_{\hat{a}_w\hat{a}_n^{(2)}} \\ Q_{\hat{a}_n\hat{a}_w^{(2)}} & Q_{\hat{a}_n^{(2)}} \end{bmatrix} \tag{6.32}$$

The subsequent integer estimation step reads

$$\begin{bmatrix} \hat{a}_w^{(2)} \\ \hat{a}_n^{(2)} \end{bmatrix} \; ; \; \begin{bmatrix} Q_{\hat{a}_w^{(2)}} & Q_{\hat{a}_w\hat{a}_n^{(2)}} \\ Q_{\hat{a}_n\hat{a}_w^{(2)}} & Q_{\hat{a}_n^{(2)}} \end{bmatrix} \Rightarrow \begin{bmatrix} \check{a}_w \\ \check{a}_n \end{bmatrix} \tag{6.33}$$

And step 3 is omitted.

6.6 Results for a regional network

The use of the LAMBDA method within GAMIT has been tested on a one day data set (day 260 of 1996) of a network in California, see Figure 6.9. The network consists of 21 permanent stations from the permanent GPS arrays SCIGN (Southern Californian Integrated GPS Network), CORS (Continuously Operating Reference Stations) and BARD (Bay Area Deformation Array), and occupies an area of roughly 250 by 800 km. It is tied to 4 stations outside the Californian region to enable estimation of orbital parameters, and provide a reference frame.

The ambiguities related to the baselines `FARB-KOKB`, `ALGO-DRAO`, `ALGO-RCM5`, and `BRIB-DRAO` were kept floating.

Before we will analyze the performance of LAMBDA we will have a look at rounding the ambiguities using the decision function strategy. In Figure 6.10 the conditional standard deviation is plotted as function of the distance of the conditional estimate to the nearest integer at time of fixing. The ambiguities that were allowed to be fixed according to the decision function are marked by stars; at left the wide lane ambiguities are plotted, at right the narrow lane ambiguities.

Site ID (IGS)	Name	Site ID (IGS)	Name
ALGO	Algonquin, Canada	BLYT	Blythe
BRIB	Briones	CARR	Carr Hill
CASA	Mammoth Lakes	CICE	Ensenada
COSO	China Lake	CRFP	Yucaipa
DHLG	Durmid Hill	DRAO	Penticton, Canada
FARB	Farallon	GOL2	Goldstone 2
HARV	Harvest Platform	KOKB	Kokee Park, Hawaii
MATH	Lake Mathews	MONP	Monument Peak
PBL1	Pt. Blunt	PIN1	Pinyon Flat 1
PLO1	Pt. Loma	PVEP	Palos Verdes
RCM5	Richmond, Florida	SIO3	Scripps 3
TIBB	Tiburon	TRAK	Bommer Canyon
VNDP	Vandenberg		

Table 6.1: Names and site ID's of the stations in the network used in the experiments, a grey box indicates that the station is not in the California area.

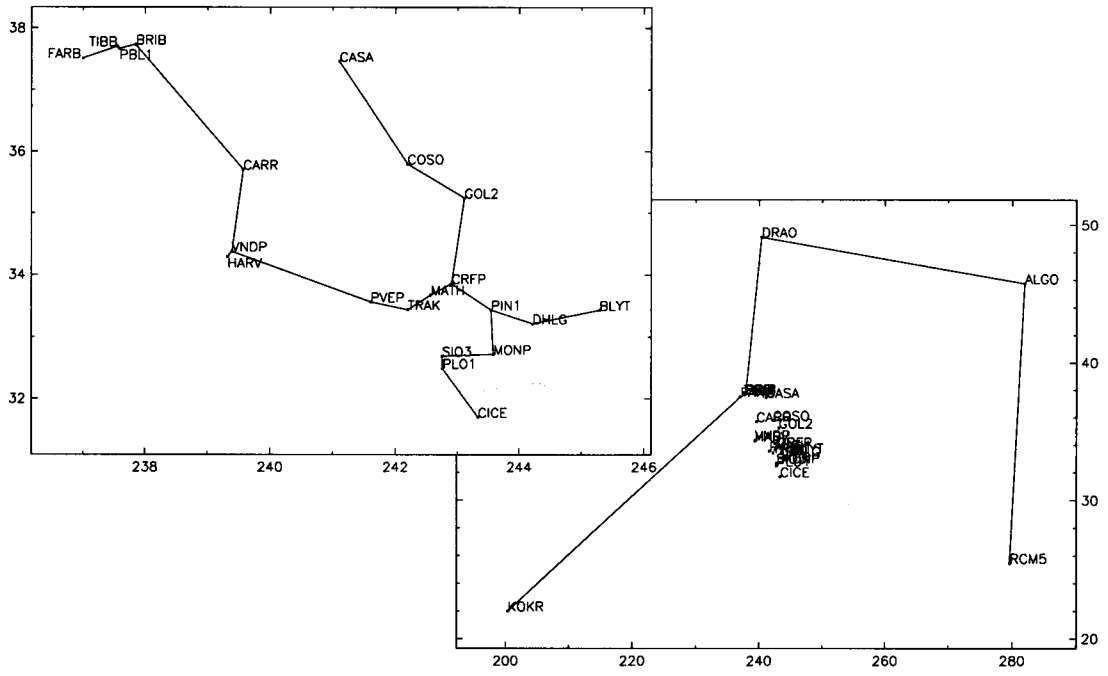

Figure 6.9: Map of the network used in the experiments, at right the whole network is depicted, at left in detail the California part is shown.

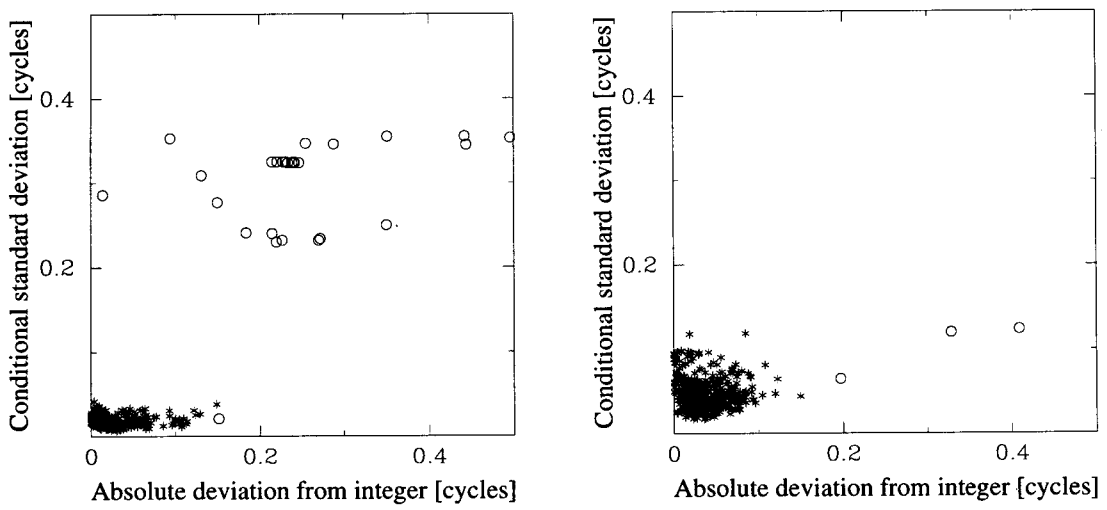

Figure 6.10: Conditional standard deviation as function of the distance of the conditional estimates to the nearest integer at time of fixing by the decision function (stars). The circles refer to the ambiguities that could not be fixed (i.e. after 443 wide lane ambiguities and 440 narrow lane ambiguities, respectively were fixed). Left: wide lane ambiguities, right: narrow lane ambiguities.

By definition, all data points marked by a star are inside the region plotted in Figure 6.7. Of the 470 wide lane ambiguities 443 were allowed to be fixed; of the 443 narrow lane ambiguities 440 could be fixed (27 narrow lane ambiguities were kept floating, since the wide lane counterpart could not be fixed). The circles refer to the ambiguities that could not be fixed, and hence they are conditioned on the 443 wide lane and 440 narrow lane ambiguities, respectively that could be fixed.

Similar plots were made for the ambiguities that were resolved using the LAMBDA method with the standard bootstrapping method. Recall that with the current implementation we can only resolve the whole set of ambiguities. In Figure 6.11 at left the conditional standard deviation versus the distance of the conditional estimate to the estimated integer value for it, (which was in all cases also the nearest integer) for the decorrelated wide lane ambiguities is plotted. At first sight the results seem worse than those obtained by the decision function approach (Figure 6.10), but we have to keep in mind that here all 470 ambiguities were fixed.

We see that there are five apparent outliers with a large conditional standard deviation. A total of 460 ambiguities satisfy the criterion of having a decision function value greater than 1000. So with the current criterion (which is a heuristic one that may or may not be applied on the decorrelated ambiguities) 17 more functions of ambiguities could have been fixed. This is of course only true if the ambiguities outside the 'decision region' were the last ones to be fixed, which is not the case here. If the decision region were a little bit enlarged however, i.e. if it would allow ambiguities to be fixed with a deviation from the nearest integer of up to 0.17 cycles, all but five ambiguities (the ones related to the outliers in conditional standard deviation) could be fixed, since these were the last ambiguities to be fixed.

Figure 6.11 at right shows the conditional standard deviation versus the conditional es-

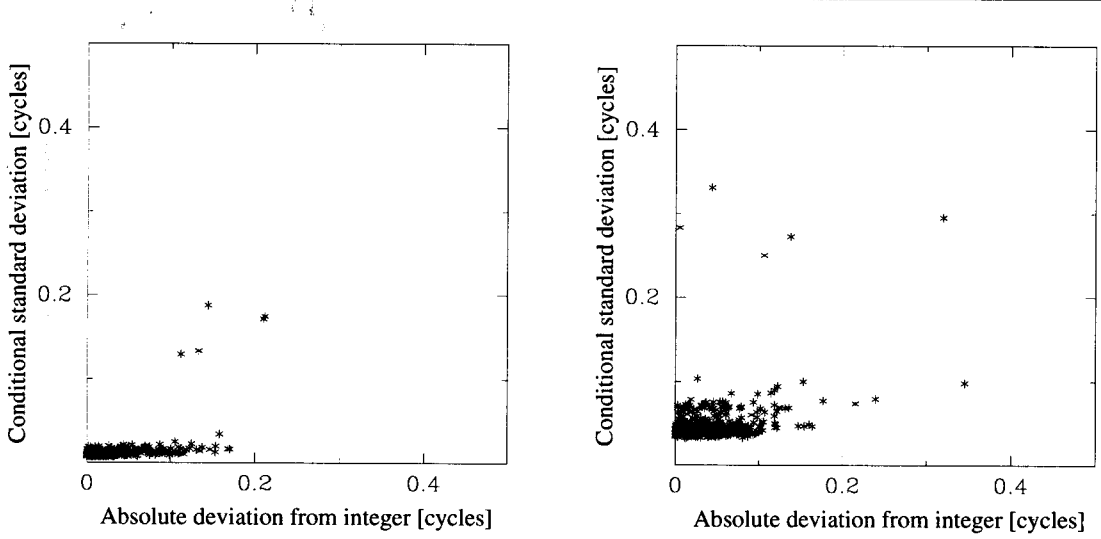

Figure 6.11: Conditional standard deviation as function of the distance of the conditional estimate to the nearest integer at time of fixing for the decorrelated ambiguities. Left: wide lane ambiguities, right: narrow lane ambiguities.

timate of the decorrelated narrow lane ambiguities. The plot is somewhat more erratic than the one for the wide lanes, but again five apparent outliers are visible. If we again would allow ambiguities to be fixed with a deviation to the nearest integer of up to 0.17 cycles, the 450 first resolved ambiguities would fall inside the region of the decision function. (Again we have to be a little careful here, since in the preceding wide lane ambiguity resolution all 470 ambiguities were fixed, the results for the narrow lanes might change if only the 465 wide lane ambiguities with a conditional standard deviation less than or equal to 0.17 cycles were fixed.)

The size of the fractional parts of the (conditional) estimates and the size of the (conditional) variance is decreased by two processes: 1. the decorrelating Z-transformation, and 2. the conditioning forced by the sequential least-squares estimation.

Effect of the decorrelation on the unconditional estimates.
To show that the decorrelating Z-transformation also has an advantageous effect on the *unconditional* estimates, we made histograms of the fractional parts (i.e. the float value minus its nearest integer value) of the estimates. Figure 6.12 shows the fractional parts for the original ambiguities for both the wide lanes and the narrow lanes. In Figure 6.13 the fractional parts of the decorrelated ambiguities for the wide and narrow lanes are shown.

For the decorrelated ambiguities, the nearest integer always turned out to be the integer estimate. This demonstrates that instead of the search process a simple rounding scheme could have been applied to the decorrelated ambiguities.

For the original ambiguities, the distance between the unconditional float estimate and the integer estimate sometimes exceeds $\frac{1}{2}$ cycle, see Figure 6.14.

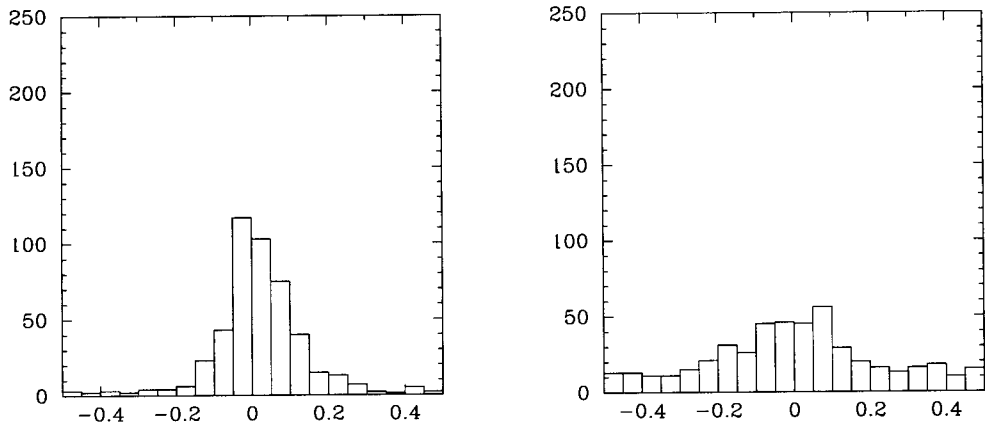

Figure 6.12: Histogram of the fractional parts of the unconditional estimates for the original ambiguities. Left: wide lane ambiguities, right: narrow lane ambiguities.

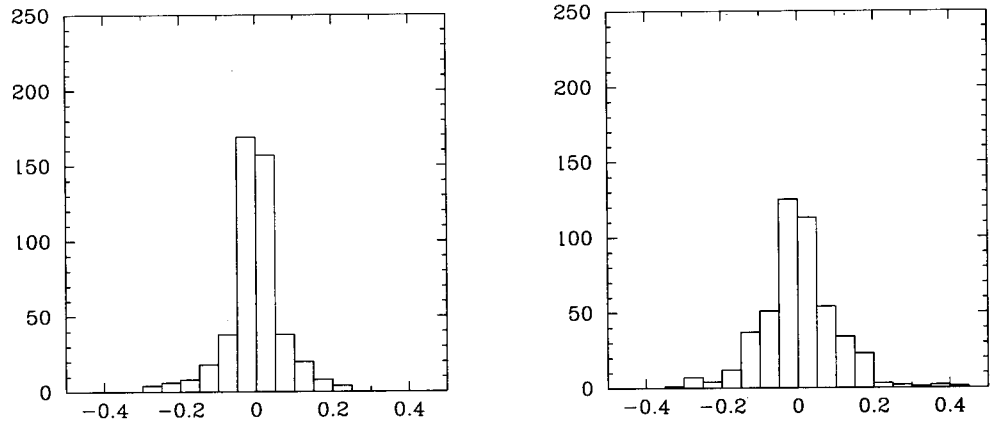

Figure 6.13: Histogram of the fractional parts of the unconditional estimates for the decorrelated ambiguities. Left: wide lane ambiguities, right: narrow lane ambiguities.

Effect of the conditioning on the estimates.
In Figure 6.15 histograms of the fractional parts of the conditional estimates of the decorrelated wide and the narrow lanes as estimated by the LAMBDA method are given.

If we compare the histograms of the fractional parts of the conditional estimates of the decorrelated ambiguities in Figure 6.15 with the histograms of the fractional parts of the unconditional estimates in Figure 6.13, an overall decrease in distance to the nearest integer can be observed, due to the sequential conditioning.

Effect of the decorrelation on the conditional variances.
In Figure 6.16 the conditional variances for both the original and the decorrelated wide lane ambiguities are plotted. The original ambiguities are ordered according to the order in which they were fixed by the GAMIT decision function, the decorrelated ambiguities are ordered according to order in which they were fixed using the LAMBDA method. Since only

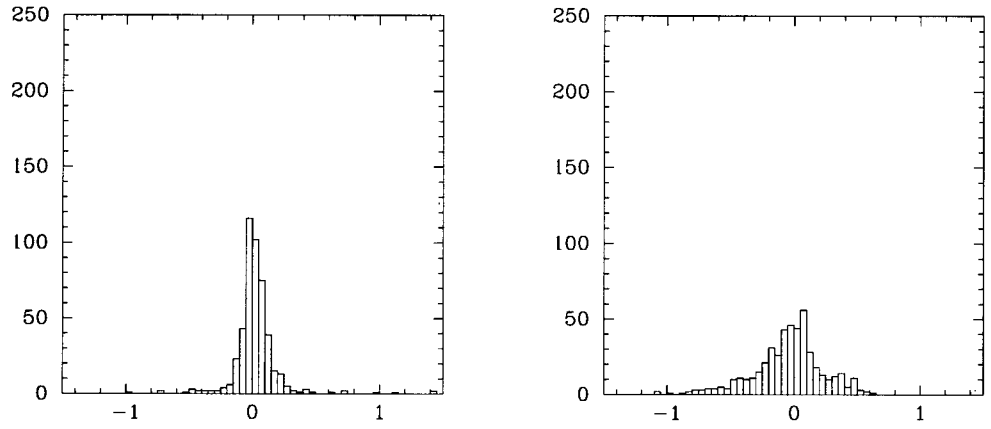

Figure 6.14: Histogram of the differences between the unconditional estimates and the integer estimates for the original ambiguities. Left: wide lane ambiguities, right: narrow lane ambiguities.

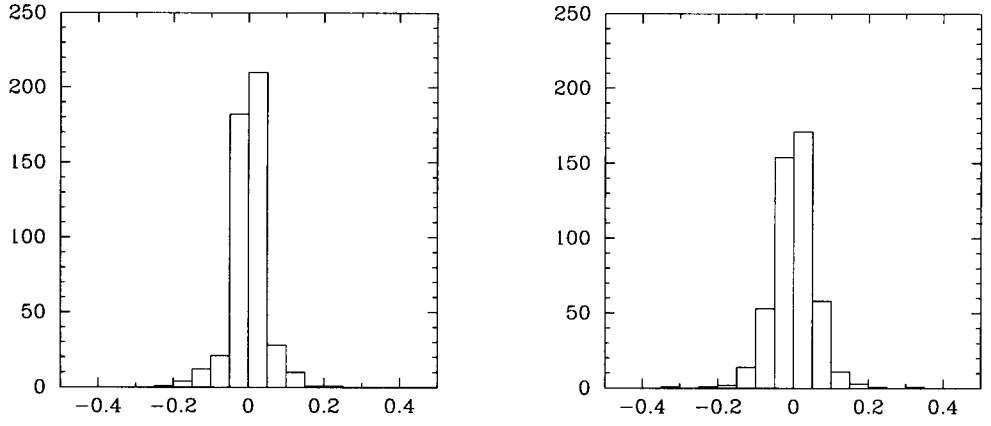

Figure 6.15: Histogram of the fractional parts of the conditional estimates for the decorrelated ambiguities as determined by the LAMBDA method. Left: wide lane ambiguities (470), right: narrow lane ambiguities (470).

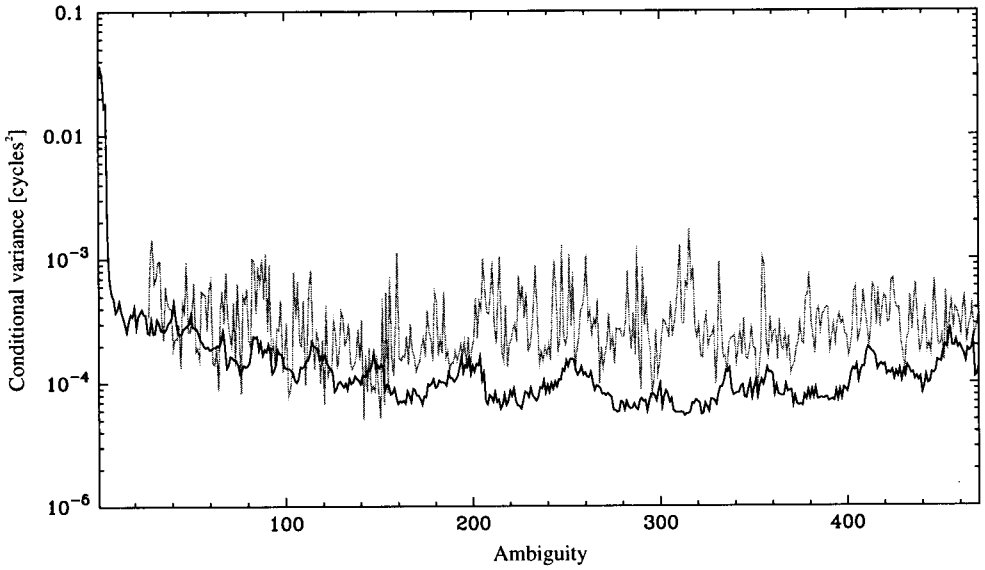

Figure 6.16: Conditional variances of the wide lane ambiguities. Black curve: decorrelated ambiguities in the order in which they were fixed by the LAMBDA method, grey curve: original ambiguities in the order in which they were fixed by the GAMIT decision function (443 ambiguities).

443 of the 470 ambiguities were fixed by the decision function, the curve for the original ambiguities ends with ambiguity 27. The plot clearly shows that over all the decorrelation renders ambiguities with smaller conditional variances than those of the original ambiguities.

Effect of the conditioning on the variances.
Figure 6.17 shows the effect the conditioning has on the variances. In the figure both the variances and the conditional variances of the decorrelated wide lane ambiguities are plotted. By definition, for ambiguity 470, the first ambiguity that is fixed, the variance equals the conditional variance. Since it is the first ambiguity that is fixed, it cannot profit from the conditioning of previous ambiguities. For the whole range of ambiguities that follow, the conditional variances are smaller than their unconditional counterparts.

6.6.1 Comparison of the bootstrapping strategies

As we mentioned before, an alternative bootstrapping scheme was implemented. It aims at performing the integer estimation for the whole set of ambiguities.

This alternative was not successful; the correlation between the decorrelated ambiguities remains still rather high. This causes an enormous amount of incomplete integer vectors to be generated, rendering the strategy extremely inefficient.

An indication for the correlation that is still present after the Z-transformation is the size of the ambiguity decorrelation number $r_{\hat{z}}$. In Table 6.2 these numbers are given for both strategies, for the original as well as the decorrelated ambiguities. The ambiguity decorrelation number ranges between 0 (full correlation causing singularity) and 1 (no correlation);

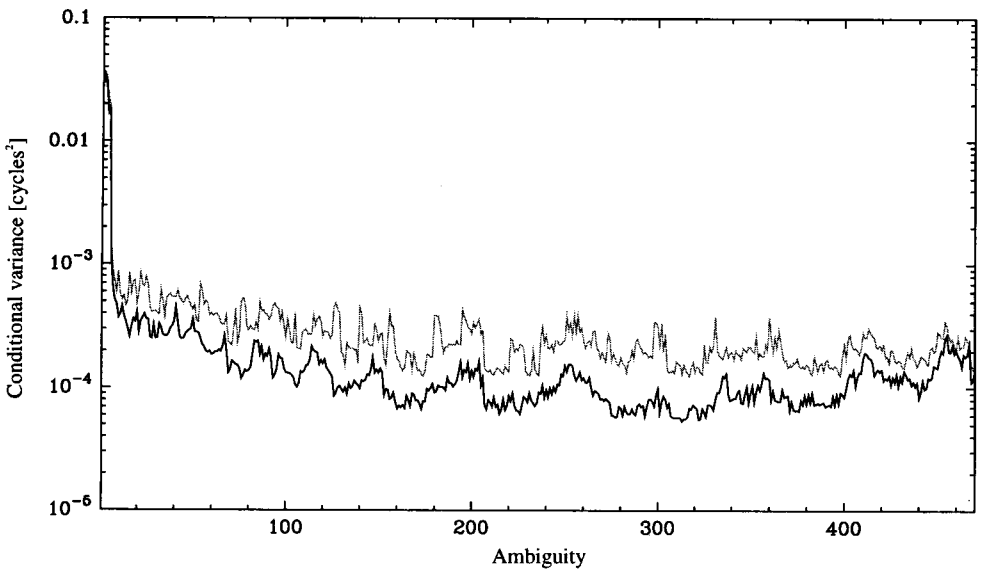

Figure 6.17: Variances and conditional variances of the decorrelated wide lane ambiguities. Black curve: conditional variances, grey curve: variances.

we strive for low correlation.

We see that the Z-transformation succeeds in decreasing the correlation, but that the remaining correlation for the alternative strategy is still quite high. We have to be a little bit careful with comparing the decorrelation numbers, since they depend also on the number of ambiguities n. Looking at the definition of the ambiguity decorrelation number (Eqs. (5.54–5.55)), we can define the average logarithmic ratio of the conditional and the unconditional standard deviation as

$$\frac{1}{n}\sum_{i=1}^{n}\log_{10}\left(\frac{\sigma_{\hat{a}_i|i+1,\ldots,n}}{\sigma_{\hat{a}_i}}\right) = \log_{10}\left(\sqrt[n]{r_{\hat{a}}}\right) \tag{6.34}$$

which is independent of the number of ambiguities. As can be seen in Table 6.2, for all ambiguities together this measure is larger than for the wide lane or narrow lanes.

The signature of conditional variances is also an indication for the efficiency of the search process. This signature should preferably be flat, without large discontinuities; if not flat, the values of the conditional variances should be increasing when going through the search process from n to 1. In Figure 6.18 we have plotted the conditional variances of the decorrelated wide lanes using the standard bootstrapping strategy, together with the conditional variances for all decorrelated ambiguities using the alternative strategy. Although not entirely without discontinuities, the values of the conditional variances for the decorrelated wide lanes are reasonably constant at the beginning, and increase at the end. This increase is probably due to the fact that some of the ambiguities are only observed for a very small time span.

The signature of conditional variances for the alternative strategy on the other hand, has a larger variation at start, and makes a rather large jump to a minimum at approximately ambiguity 440. This seems to cause that 'halting' starts to occur approximately at this level. Inspection of some intermediate results confirms this. In fact, even after hours (!) of CPU

	Normal bootstrapping		Alternative bootstrapping
	Wide lane	Narrow lane	Wide and narrow lane
$\log_{10}(r_a)$	-176.2	-235.0	-507.9
$\log_{10}(r_z)^{(*)}$	-72.8	-82.4	-232.4
$\log_{10}(r_z)^{(**)}$	n/a	n/a	-211.5
$\log_{10}(\sqrt[n]{r_a})$	-0.375	-0.500	-0.540
$\log_{10}(\sqrt[n]{r_z})^{(*)}$	-0.155	-0.175	-0.247
$\log_{10}(\sqrt[n]{r_z})^{(**)}$	n/a	n/a	-0.225

Table 6.2: Some diagnostic quantities from the ambiguity resolution for the three alternative bootstrapping strategies. $^{(*)}$: no a priori ordering of the original ambiguities, $^{(**)}$: original ambiguities a priori ordered according to decreasing value of variance.

time, still not one complete integer vector was found. For the wide lanes only case, the search rendered two complete integer vectors in less than 1 second CPU time (HP-UX 9000/735).

The reason that the decorrelated ambiguities are still so much correlated must lie in the fact that the ionospheric constraints are rather loose. In the limiting case, with constraints with an infinitesimal small weight, there is full correlation between the wide lane and the narrow lane ambiguities.

We also investigated whether the a priori order of the ambiguities has an influence on the ability to decorrelate the ambiguities. Much to our surprise, since it was never observed for the short baseline model where we usually have some tens of ambiguities, this was the case. A priori ordering the original ambiguities according to decreasing value of variance, resulted in a less correlated set of ambiguities after decorrelation. The ambiguity decorrelation number for the decorrelated ambiguities decreased from 232.4 to 211.5. In Figure 6.19 the signatures of the conditional variances resulting from a decorrelation upon the ambiguities in the original order, and those resulting from a decorrelation upon the sorted ambiguities is depicted. Since the decorrelating process consists of a repeatedly treating of two ambiguities at a time, a global optimization with respect to decorrelation is not guaranteed. At least for this example, the a priori ordering of the ambiguities, helped to lower the decorrelation.

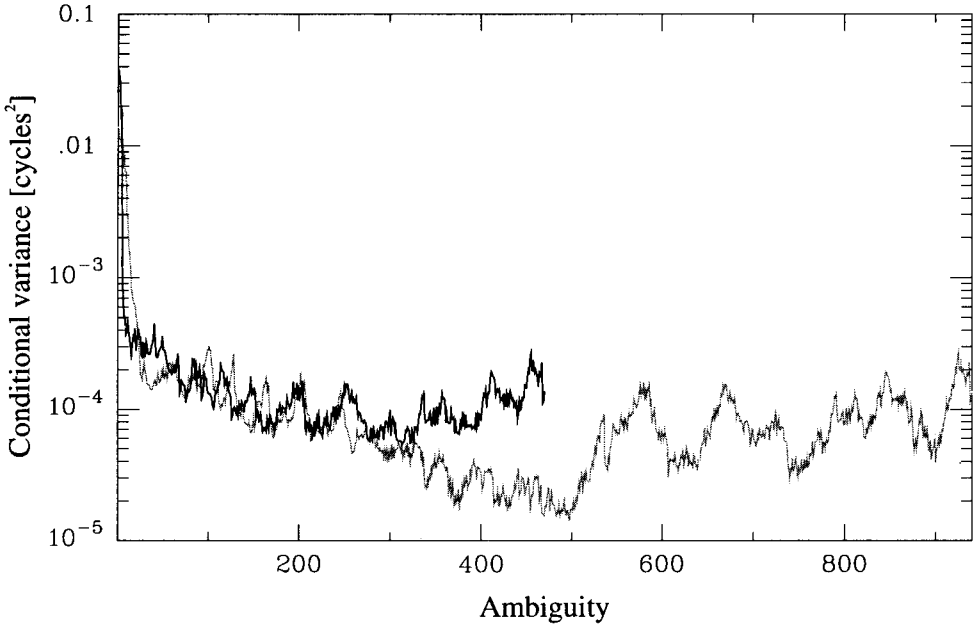

Figure 6.18: Conditional variances of the decorrelated wide lane ambiguities (black curve), and of the decorrelated wide and narrow lane ambiguities together (alternative bootstrapping, grey curve).

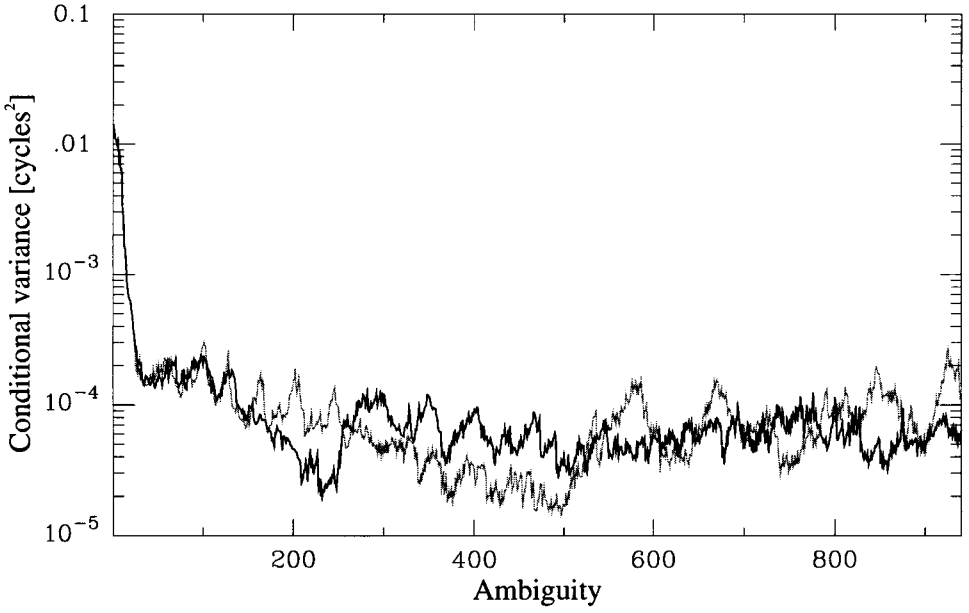

Figure 6.19: Conditional variances of the decorrelated wide and narrow lane ambiguities together (alternative bootstrapping). Black curve: original ambiguities a priori ordered according to decreasing value of variance, grey curve: original ordering.

6.7 Concluding remarks

Although the ambiguities are most correlated when the observation time span is very short, even for a time span of one day applied for the daily solution of permanent GPS arrays, a decorrelation of the ambiguities has a significant effect. The decorrelation makes it possible to apply techniques developed in the context of rapid static surveying to these networks, thereby effectively removing the artificial border between both applications.

On the other hand, rapid static surveying applications could benefit from techniques developed for the regional networks. Especially methods to constrain the ionospheric delays might enable the enlargement of the distance for which using a very short time span, ambiguity resolution is successful.

Due to the hybrid character of the regional networks with ambiguities observed for time spans that may differ considerably, there is clearly a need to enable the determination of a subset of the ambiguities which can be fixed with sufficient reliability. Validation techniques for the integer estimates (which we did not treat in this thesis) that are developed for the rapid static applications might also be applied to the network case.

Thus, for the rapid static application, the challenge lies in extending the distance while maintaining the short time spans. For the regional networks the challenge lies in reducing the time span while maintaining the large distances involved in it. Eventually then the rapid static surveying and the regional network application may be merged into one general method for ambiguity resolution based on the same theory and techniques.

References

Blewitt, G. (1989). Carrier phase ambiguity resolution for the Global Positioning System applied to geodetic baselines up to 2000 km. *Journal of Geophysical Research 94*(B8), 10187–10203.

Bock, Y. (1996). Medium distance GPS measurements. In A. Kleusberg and P. J. G. Teunissen (Eds.), *GPS for Geodesy*, Volume 60 of *Lecture Notes in Earth Sciences*, Chapter 9, pp. 337–377. Springer Verlag.

Davis, J. L., T. A. Herring, I. I. Shapiro, A. E. E. Rogers, and G. Elgered (1985). Geodesy by radio interferometry: effects of atmospheric modeling errors on estimates of baseline length. *Radio Science 20*(6), 1593–1607.

Dong, D.-N. and Y. Bock (1989). Global Positioning System network analysis with phase ambiguity resolution applied to crustal deformation studies in California. *Journal of Geophysical Research 94*(B4), 3949–3966.

Feigl, K. L., D. C. Agnew, Y. Bock, D. Dong, A. Donnellan, B. H. Hager, T. A. Herring, D. D. Jackson, T. H. Jordan, R. W. King, S. Larsen, K. M. Larson, M. H. Murray, Z. Shen, and F. H. Webb (1993). Space geodetic measurement of crustal deformation in central and Southern California, 1984–1992. *Journal of Geophysical Research 98*(B12), 21677–21712.

Genrich, J. F. and Y. Bock (1992). Rapid resolution of crustal motion at short ranges with the Global Positioning System. *Journal of Geophysical Research 97*(B3), 3261–3269.

Mervart, L. (1995). *Ambiguity Resolution Techniques in Geodetic and Geodynamic Applications of the Global Positioning System.* Ph. D. thesis, Astronomisches Institut Universität Bern.

Mervart, L., G. Beutler, M. Rothacher, and S. Schaer (1996). The impact of ambiguity resolution on GPS orbit determination and on global geodynamics studies. In G. Beutler, G. W. Hein, W. G. Melbourne, and G. Seeber (Eds.), *GPS Trends in Precise Terrestrial Airborne and Spaceborne Applications*, Volume 115 of *International Association of Geodetic Symposia*, pp. 285–289. Springer Verlag.

Mervart, L., G. Beutler, M. Rothacher, and U. Wild (1994). Ambiguity resolution strategies using the results of the International GPS Geodynamics Service (IGS). *Bulletin Géodésique 68*, 29–38.

Niell, A. E. (1996). Global mapping functions for the atmospheric delay at radio wavelengths. *Journal of Geophysical Research 101*(B2), 3227–3246.

Schaffrin, B. and Y. Bock (1988). A unified scheme for processing GPS dual-band phase observations. *Bulletin Géodésique 62*, 144–160.

SSG 1.157 (1997). Personal communication. Inquiry conducted among the members of the IAG Special Study Group 1.157, 'GPS ambiguity resolution and validation'.

Appendix A

GPSVEQ

Most of the ideas and concept in this thesis have been implemented in the GPS network processing software GPSVEQ. It is based on using the original GPS phase and code observable types, instead of forming differences between observables and forming linear combinations of observable types. It has been in use as a research tool since 1994, and the results in the majority of the papers on the LAMBDA method for ambiguity resolution were computed using it. In principle any set of observable types may be used as long as the chosen model allows its use.

Parameters that may be estimated are 1. station coordinates, 2. hydrostatic and/or wet tropospheric zenith delays, 3. ambiguities, 4. receiver and satellite clocks, 5. ionospheric slant delays.

Station coordinates, tropospheric zenith delays and ambiguities may be defined for a part of the total time span. In practice this means that one or more of the stations may be moving, that zenith delays may be estimated that are valid for only a part of the total time span, and that cycle slips are neutralized by introducing a new ambiguity parameter. Since all these global parameters are estimated in one batch the amount of memory available at a particular computer limits the number of parameters. The program is at the first place developed with static applications in mind, but for research purposes small kinematic networks have been computed with it.

Again for research purposes the data may be divided in multiple time spans, where for each of these time spans a separate adjustment may be performed. The solution may be iterated for non-linearity. For static solutions this is usually not needed, but for kinematic solutions using only phase data and a small time span, it was found to be necessary.

When by testing an outlier or cycle slip is found, the model may be adapted (i.e. removing an observation, or inserting an extra ambiguity parameter), after which a new adjustment may be performed. In this way the removal of outliers and cycle slips is automated.

After the float solution ambiguities may be resolved. The fixed solution may be computed using the same model as for the float solution (but with the ambiguities constrained to integers), or an extended model may be used (e.g. one where ionospheric slant delays are estimated). In that case, another do-while loop is inserted after the fixed solution for an adjustment using the extended model (see Figure A.1 where the main structure of GPSveQ in stylized MATLAB notation can be found).

```
for i = 1 : number of time spans
    do
        for j = 1 : number of iterations
            for k = 1 : number epochs
                eliminate the local parameters
                update system of normal equations
            end
            compute the global parameters
            for k = 1 : number of epochs
                compute the local parameters
                if j=number of iterations then
                    compute the one-dimensional test statistics
                    update ê^T Q_y^{-1} ê
                end
            end
        end
        Do the testing, and if necessary adapt the model
    while OMT is rejected
    ambiguity resolution
    fixed solution
end
```

Figure A.1: Main structure of GPSVEQ.

Appendix B

$r^S(t)$, $\dot{r}^S(t)$, and $\ddot{r}^S(t)$ in ECEF WGS-84

Corrected mean motion, Time from epoch, and Mean anomaly:

$$\begin{aligned} n &= \sqrt{\frac{\mu}{A^3}} + \Delta n \\ t_k &= t - t_{oe} \\ M_k &= M_0 + n t_k \end{aligned} \tag{B.1}$$

Eccentric anomaly:

$$\begin{aligned} E_k &= M_k + e \sin E_k \text{ (solved by iteration)} \\ \dot{E}_k &= \frac{n}{1 - e \cos E_k} \end{aligned} \tag{B.2}$$

True anomaly:

$$\begin{aligned} \nu_k &= \arctan \frac{\sqrt{1-e^2} \sin E_k}{\cos E_k - e} \\ \dot{\nu}_k &= \frac{\sqrt{1-e^2}\dot{E}_k}{1 - e \cos E_k} \\ \ddot{\nu}_k &= \frac{-2e\sqrt{1-e^2} \sin E_k}{(1 - e \cos E_k)^2} \dot{E}_k^2 \end{aligned} \tag{B.3}$$

Argument of latitude:

$$\phi_k = \nu_k + \omega \tag{B.4}$$

Argument of latitude correction:

$$\begin{aligned} \delta u_k &= C_{us} \sin 2\phi_k + C_{uc} \cos 2\phi_k \\ \dot{\delta} u_k &= 2\,\dot{\nu}_k (C_{us} \cos 2\phi_k - C_{uc} \sin 2\phi_k) \\ \ddot{\delta} u_k &= -4\dot{\nu}_k^2 (C_{us} \sin 2\phi_k + C_{uc} \cos 2\phi_k) + 2\ddot{\nu}_k (C_{us} \cos 2\phi_k - C_{uc} \sin 2\phi_k) \end{aligned} \tag{B.5}$$

Radius correction:

$$\begin{aligned} \delta r_k &= C_{rs} \sin 2\phi_k + C_{rc} \cos 2\phi_k \\ \dot{\delta} r_k &= 2\,\dot{\nu}_k (C_{rs} \cos 2\phi_k - C_{rc} \sin 2\phi_k) \\ \ddot{\delta} r_k &= -4\dot{\nu}_k^2 (C_{rs} \sin 2\phi_k + C_{rc} \cos 2\phi_k) + 2\ddot{\nu}_k (C_{rs} \cos 2\phi_k - C_{rc} \sin 2\phi_k) \end{aligned} \tag{B.6}$$

Inclination correction:

$$\begin{aligned}
\delta i_k &= C_{is} \sin 2\phi_k + C_{ic} \cos 2\phi_k \\
\dot{\delta} i_k &= 2\,\dot{\nu}_k (C_{is} \cos 2\phi_k - C_{ic} \sin 2\phi_k) \\
\ddot{\delta} i_k &= -4\dot{\nu}_k^2 (C_{is} \sin 2\phi_k + C_{ic} \cos 2\phi_k) + 2\ddot{\nu}_k (C_{is} \cos 2\phi_k - C_{ic} \sin 2\phi_k)
\end{aligned} \tag{B.7}$$

Corrected argument of latitude:

$$\begin{aligned}
u_k &= \phi_k + \delta u_k \\
\dot{u}_k &= \dot{\nu}_k + \dot{\delta} u_k \\
\ddot{u}_k &= \ddot{\nu}_k + \ddot{\delta} u_k
\end{aligned} \tag{B.8}$$

Corrected radius:

$$\begin{aligned}
r_k &= A(1 - e \cos E_k) + \delta r_k \\
\dot{r}_k &= Ae\,\dot{E}_k \sin E_k + \dot{\delta} r_k \\
\ddot{r}_k &= \frac{Ae(\cos E_k - e)}{(1 - e \cos E_k)} \dot{E}_k^2 + \ddot{\delta} r_k
\end{aligned} \tag{B.9}$$

Corrected inclination:

$$\begin{aligned}
i_k &= i_0 + i_{dot} t_k + \delta i_k \\
\dot{i}_k &= i_{dot} + \dot{\delta} i_k \\
\ddot{i}_k &= \ddot{\delta} i_k
\end{aligned} \tag{B.10}$$

Satellite position in orbital plane:

$$\begin{aligned}
\begin{bmatrix} x'_k \\ y'_k \end{bmatrix} &= r_k \begin{bmatrix} \cos u_k \\ \sin u_k \end{bmatrix} \\
\begin{bmatrix} \dot{x}'_k \\ \dot{y}'_k \end{bmatrix} &= \dot{r}_k \begin{bmatrix} \cos u_k \\ \sin u_k \end{bmatrix} + r_k \dot{u}_k \begin{bmatrix} -\sin u_k \\ \cos u_k \end{bmatrix} \\
\begin{bmatrix} \ddot{x}'_k \\ \ddot{y}'_k \end{bmatrix} &= (\ddot{r}_k - r_k \dot{u}_k^2) \begin{bmatrix} \cos u_k \\ \sin u_k \end{bmatrix} + (2\dot{r}_k \dot{u}_k + r_k \ddot{u}_k) \begin{bmatrix} -\sin u_k \\ \cos u_k \end{bmatrix}
\end{aligned} \tag{B.11}$$

Corrected longitude of ascending node:

$$\begin{aligned}
\Omega_k &= \Omega_0 + (\dot{\Omega} - \dot{\Omega}_e) t_k - \dot{\Omega}_e t_{oe} \\
\dot{\Omega}_k &= \dot{\Omega} - \dot{\Omega}_e
\end{aligned} \tag{B.12}$$

Rotation matrix from orbital plane to ECEF:

$$
\begin{aligned}
R_k &= \begin{bmatrix} \cos\Omega_k & -\cos i_k \sin\Omega_k \\ \sin\Omega_k & \cos i_k \cos\Omega_k \\ 0 & \sin i_k \end{bmatrix} \\
\dot{R}_k &= \begin{bmatrix} -\dot{\Omega}\sin\Omega_k & -\dot{\Omega}_k \cos i_k \cos\Omega_k + \dot{i}_k \sin i_k \sin\Omega_k \\ \dot{\Omega}\cos\Omega_k & -\dot{\Omega}_k \cos i_k \sin\Omega_k - \dot{i}_k \sin i_k \cos\Omega_k \\ 0 & \dot{i}_k \cos i_k \end{bmatrix} \\
\ddot{R}_k &= \begin{bmatrix} -\dot{\Omega}^2\cos\Omega_k & (\dot{\Omega}^2 + \dot{i}_k^2)\cos i_k \sin\Omega_k + 2\dot{i}_k\dot{\Omega}\sin i_k \cos\Omega_k + \ddot{i}_k \sin i_k \sin\Omega_k \\ -\dot{\Omega}^2\sin\Omega_k & -(\dot{\Omega}^2 + \dot{i}_k^2)\cos i_k \cos\Omega_k + 2\dot{i}_k\dot{\Omega}\sin i_k \sin\Omega_k - \ddot{i}_k \sin i_k \cos\Omega_k \\ 0 & -\dot{i}_k^2 \sin i_k + \ddot{i}_k \cos i_k \end{bmatrix}
\end{aligned}
\tag{B.13}
$$

Satellite position in ECEF coordinates:

$$
\begin{aligned}
r^s(t) &= \begin{bmatrix} x_k \\ y_k \\ z_k \end{bmatrix} = R_k \begin{bmatrix} x'_k \\ y'_k \end{bmatrix} \\
\dot{r}^s(t) &= \begin{bmatrix} \dot{x}_k \\ \dot{y}_k \\ \dot{z}_k \end{bmatrix} \dot{R}_k \begin{bmatrix} x'_k \\ y'_k \end{bmatrix} + R_k \begin{bmatrix} \dot{x}'_k \\ \dot{y}'_k \end{bmatrix} \\
\ddot{r}^s(t) &= \begin{bmatrix} \ddot{x}_k \\ \ddot{y}_k \\ \ddot{z}_k \end{bmatrix} = \ddot{R}_k \begin{bmatrix} x'_k \\ y'_k \end{bmatrix} + 2\dot{R}_k \begin{bmatrix} \dot{x}'_k \\ \dot{y}'_k \end{bmatrix} + R_k \begin{bmatrix} \ddot{x}'_k \\ \ddot{y}'_k \end{bmatrix}
\end{aligned}
\tag{B.14}
$$

To obtain the satellite position in ECI coordinates, the corrected longitude of the ascending node and its derivative (Eq. (B.12)) are replaced by

$$
\begin{aligned}
\Omega_k &= \Omega_0 + \dot{\Omega} t_k \\
\dot{\Omega}_k &= \dot{\Omega}
\end{aligned}
\tag{B.15}
$$

Appendix C

Inverting $\bar{d}^T\bar{d}$

For the inverse of matrix

$$N = \begin{bmatrix} n_{11} & n_{12} \\ n_{21} & n_{22} \end{bmatrix} \tag{C.1}$$

yields

$$N^{-1} = \begin{bmatrix} \left(n_{11} - n_{21}^T n_{22}^{-1} n_{21}\right)^{-1} & -n_{11}^{-1} n_{21}^T \left(n_{22} - n_{21} n_{11}^{-1} n_{21}^T\right)^{-1} \\ -n_{22}^{-1} n_{21} \left(n_{11} - n_{21}^T n_{22}^{-1} n_{21}\right)^{-1} & \left(n_{22} - n_{21} n_{11}^{-1} n_{21}^T\right)^{-1} \end{bmatrix} \tag{C.2}$$

where

$$\left[-n_{11}^{-1} n_{21}^T (n_{22} - n_{21} n_{11}^{-1} n_{21}^T)^{-1}\right]^T = -n_{22}^{-1} n_{21} (n_{11} - n_{21}^T n_{22}^{-1} n_{21})^{-1} \tag{C.3}$$

With

$$N = \begin{bmatrix} mI_{r-1} & -E_{r-1,m} \\ -E_{m,r-1} & rI_m \end{bmatrix} \tag{C.4}$$

where $E_{p,q}$ stands for a p by q matrix filled with 1's, and I_p for the matrix of unity of dimension p, we evaluate

$$(n_{11} - n_{21}^T n_{22}^{-1} n_{21})^{-1} \tag{C.5}$$

as

$$(mI_{r-1} - \frac{1}{r} E_{r-1,m} I_m E_{m,r-1})^{-1} \tag{C.6}$$

which using $E_{m,s}E_{m,r} = mE_r$ transforms into:

$$(mI_{r-1} - \frac{m}{r} E_{r-1})^{-1} = \frac{1}{m}(I_{r-1} - \frac{1}{r} E_{r-1})^{-1} \tag{C.7}$$

Using the matrix lemma 2.3.3 from Golub and Van Loan (1989) at page 59

$$(I - A)^{-1} = I + \sum_{k=1}^{\infty} A^k \text{ if } \|A\| < 1 \tag{C.8}$$

where $\|.\|$ is a norm satisfying the sub-multiplicative property like e.g. the Frobenius norm:

$$\|A\|_F = \sqrt{\sum_{i=1}^{m} \sum_{j=1}^{n} |a_{ij}|^2} \tag{C.9}$$

and

$$(E_q)^k = q^{k-1}E_q \quad ; \quad \|\frac{1}{p}E_q\|_F = \frac{q}{p} \tag{C.10}$$

we find

$$\begin{aligned}(mI_{r-1} - \frac{1}{r}E_{r-1,m}I_mE_{m,r-1})^{-1} &= \frac{1}{m}\left(I_{r-1} + \sum_{k=1}^{\infty}\frac{1}{r^k}(r-1)^{k-1}E_{r-1}\right)\\ &= \frac{1}{m}\left(I_{r-1} + \frac{1}{r-1}\sum_{k=1}^{\infty}\left(\frac{r-1}{r}\right)^k E_{r-1}\right)\\ &= \frac{1}{m}\left(I_{r-1} + \frac{1}{r-1}\left(\sum_{k=0}^{\infty}\left(\frac{r-1}{r}\right)^k - 1\right)E_{r-1}\right)\end{aligned} \tag{C.11}$$

With

$$\sum_{k=0}^{\infty}x^k = \frac{1}{1-x} \qquad -1 < x < 1 \tag{C.12}$$

we eventually obtain

$$\begin{aligned}(mI_{r-1} - \frac{1}{r}E_{r-1,m}I_mE_{m,r-1})^{-1} &= \frac{1}{m}\left(I_{r-1} + \frac{1}{r-1}(r-1)E_{r-1}\right)\\ &= \frac{1}{m}(I_{r-1} + E_{r-1})\end{aligned} \tag{C.13}$$

Another way to obtain this result is to recognize that this is a so-called combinatorial matrix (Knuth 1973), page 36. Such a $p \times p$ matrix is defined as

$$a_{ij} = y + \delta_{ij}x \tag{C.14}$$

and its inverse is given by

$$b_{ij} = \frac{-y + \delta_{ij}(x+py)}{x(x+py)} \tag{C.15}$$

Analogously we find for

$$\begin{aligned}(n_{22} - n_{21}n_{11}^{-1}n_{21}^T)^{-1} &= (rI_m - \frac{1}{m}E_{m,r-1}I_{r-1}E_{r-1,m})^{-1}\\ &= \frac{1}{r}\left(I_m - \frac{r-1}{rm}E_m\right)^{-1}\\ &= \frac{1}{r}\left(I_m + \frac{r-1}{m}E_m\right)\end{aligned} \tag{C.16}$$

Now we can easily determine

$$\begin{aligned}-n_{22}^{-1}n_{21}(n_{11} - n_{21}^Tn_{22}^{-1}n_{21})^{-1} &= \frac{1}{rm}I_mE_{m,r-1}(I_{r-1} + E_{r-1})\\ &= \frac{1}{m}E_{m,r-1}\end{aligned} \tag{C.17}$$

and

$$-n_{11}^{-1}n_{21}^{T}(n_{22}-n_{21}n_{11}^{-1}n_{21}^{T})^{-1}=\frac{1}{m}E_{r-1,m} \tag{C.18}$$

Putting everything together eventually leads to

$$\begin{bmatrix} mI_{r-1} & -E_{r-1,m} \\ -E_{m,r-1} & rI_m \end{bmatrix}^{-1}=\begin{bmatrix} \frac{1}{m}\left(I_{r-1}+E_{r-1}\right) & \frac{1}{m}E_{r-1,m} \\ \frac{1}{m}E_{m,r-1} & \frac{1}{r}\left(I_m+\frac{r-1}{m}E_m\right) \end{bmatrix} \tag{C.19}$$

References

Golub, G. H. and C. F. Van Loan (1989). *Matrix Computations, second edition.* Johns Hopkins Series in the Mathematical Sciences. The Johns Hopkins University Press.

Knuth, D. E. (1973). *Fundamental Algorithms, second edition*, Volume 1 of *The Art of Computing Programming.* Addison-Wesley Publishing Company.

Appendix D

Computation of $H_{\bar{A}_2}$ and $Q^{-1}P^{\perp}_{\bar{A}_2}$

D.1 No estimation of ionosphere, distinct clocks for each observable type

$$\bar{A}_2 = \begin{bmatrix} \bar{d}_1 & & & \\ & \bar{d}_2 & & \\ & & \ddots & \\ & & & \bar{d}_q \end{bmatrix} ; Q^{-1} = \begin{bmatrix} Q_{y_1}^{-1} & & & \\ & Q_{y_2}^{-1} & & \\ & & \ddots & \\ & & & Q_{y_q}^{-1} \end{bmatrix} \tag{D.1}$$

$$\bar{A}_2^T Q^{-1} \bar{A}_2 = \begin{bmatrix} \bar{d}_1^T Q_{y_1}^{-1} \bar{d}_1 & & & \\ & \bar{d}_2^T Q_{y_2}^{-1} \bar{d}_2 & & \\ & & \ddots & \\ & & & \bar{d}_q^T Q_{y_q}^{-1} \bar{d}_q \end{bmatrix} \tag{D.2}$$

$$\left(\bar{A}_2^T Q^{-1} \bar{A}_2\right)^{-1} = \begin{bmatrix} \left(\bar{d}_1^T Q_{y_1}^{-1} \bar{d}_1\right)^{-1} & & & \\ & \left(\bar{d}_2^T Q_{y_2}^{-1} \bar{d}_2\right)^{-1} & & \\ & & \ddots & \\ & & & \left(\bar{d}_q^T Q_{y_q}^{-1} \bar{d}_q\right)^{-1} \end{bmatrix} \tag{D.3}$$

$$H_{\bar{A}_2} = \begin{bmatrix} H_{\bar{d}_1} & & & \\ & H_{\bar{d}_2} & & \\ & & \ddots & \\ & & & H_{\bar{d}_q} \end{bmatrix} \tag{D.4}$$

$$P_{\bar{A}_2} = \begin{bmatrix} P_{\bar{d}_1} & & & \\ & P_{\bar{d}_2} & & \\ & & \ddots & \\ & & & P_{\bar{d}_q} \end{bmatrix} \tag{D.5}$$

$$P^{\perp}_{\bar{A}_2} = \begin{bmatrix} P^{\perp}_{\bar{d}_1} & & & \\ & P^{\perp}_{\bar{d}_1} & & \\ & & \ddots & \\ & & & P^{\perp}_{\bar{d}_q} \end{bmatrix} \tag{D.6}$$

$$Q^{-1}P_{\bar{A}_2}^{\perp} = \begin{bmatrix} Q_{y_1}^{-1}P_{\bar{d}_1}^{\perp} & & & \\ & Q_{y_2}^{-1}P_{\bar{d}_2}^{\perp} & & \\ & & \ddots & \\ & & & Q_{y_q}^{-1}P_{\bar{d}_q}^{\perp} \end{bmatrix} \tag{D.7}$$

D.2 No estimation of ionosphere, common clocks

$$\bar{A}_2 = \begin{bmatrix} \bar{d} \\ \bar{d} \\ \vdots \\ \bar{d} \end{bmatrix} \; ; Q^{-1} = \begin{bmatrix} w_1 & & & \\ & w_2 & & \\ & & \ddots & \\ & & & w_q \end{bmatrix} \otimes Q_y^{-1} \tag{D.8}$$

$$\bar{A}_2^T Q^{-1} \bar{A}_2 = \mu_1 \bar{d}^T Q_y^{-1} \bar{d} \tag{D.9}$$

$$\left(\bar{A}_2^T Q^{-1} \bar{A}_2\right)^{-1} = \frac{1}{\mu_1} \left(\bar{d}^T Q_y^{-1} \bar{d}\right)^{-1} \tag{D.10}$$

$$H_{\bar{A}_2} = \frac{1}{\mu_1} \begin{bmatrix} w_1 H_{\bar{d}} & w_2 H_{\bar{d}} & \cdots & w_q H_{\bar{d}} \end{bmatrix} \tag{D.11}$$

$$P_{\bar{A}_2} = \frac{1}{\mu_1} \begin{bmatrix} w_1 & w_2 & \cdots & w_q \\ w_1 & w_2 & \cdots & w_q \\ \vdots & \vdots & \ddots & \vdots \\ w_1 & w_2 & \cdots & w_q \end{bmatrix} \otimes P_{\bar{d}} \tag{D.12}$$

$$P_{\bar{A}_2}^{\perp} = \frac{1}{\mu_1} \left(\begin{bmatrix} w_1 & w_2 & \cdots & w_q \\ w_1 & w_2 & \cdots & w_q \\ \vdots & \vdots & \ddots & \vdots \\ w_1 & w_2 & \cdots & w_q \end{bmatrix} \otimes P_{\bar{d}}^{\perp} + \begin{bmatrix} \mu_1 - w_1 & -w_2 & \cdots & -w_q \\ -w_1 & \mu_1 - w_2 & \cdots & -w_q \\ \vdots & \vdots & \ddots & \vdots \\ -w_1 & -w_2 & \cdots & \mu_1 - w_q \end{bmatrix} \otimes I \right) \tag{D.13}$$

$$Q^{-1} P_{\bar{A}_2}^{\perp} = \frac{1}{\mu_1} \left(\begin{bmatrix} w_1^2 & w_1 w_2 & \cdots & w_1 w_q \\ w_2 w_1 & w_2^2 & \cdots & w_2 w_q \\ \vdots & \vdots & \ddots & \vdots \\ w_q w_1 & w_q w_2 & \cdots & w_q^2 \end{bmatrix} \otimes Q_y^{-1} P_{\bar{d}}^{\perp} + \right.$$
$$\left. \begin{bmatrix} w_1(\mu_1 - w_1) & -w_1 w_2 & \cdots & -w_1 w_q \\ -w_2 w_1 & w_2(\mu_1 - w_2) & \cdots & -w_2 w_q \\ \vdots & \vdots & \ddots & \vdots \\ -w_q w_1 & -w_q w_2 & \cdots & w_q(\mu_1 - w_q) \end{bmatrix} \otimes Q_y^{-1} \right) \tag{D.14}$$

D.3 Estimation of ionosphere, distinct clocks for each observable type

$$\bar{A}_2 = \begin{bmatrix} \bar{d} & & \eta_1 I \\ & \ddots & \eta_2 I \\ & & \vdots \\ & & \bar{d} \quad \eta_q I \end{bmatrix} ; Q^{-1} = \begin{bmatrix} w_1 & & & \\ & w_2 & & \\ & & \ddots & \\ & & & w_q \end{bmatrix} \otimes Q_y^{-1} \tag{D.15}$$

$$\bar{A}_2^T Q^{-1} \bar{A}_2 = \begin{bmatrix} w_2 \bar{d}^T Q_y^{-1} \bar{d} & & & w_2\eta_2 \bar{d}^T Q_y^{-1} \\ & \ddots & & \vdots \\ & & w_q \bar{d}^T Q_y^{-1} \bar{d} & w_q \eta_q \bar{d}^T Q_y^{-1} \\ w_2\eta_2 Q_y^{-1}\bar{d} & \cdots & w_q\eta_q Q_y^{-1}\bar{d} & \mu_3 Q_y^{-1} \end{bmatrix} \tag{D.16}$$

$$\left(\bar{A}_2^T Q^{-1} \bar{A}_2\right)^{-1} = \frac{1}{w_1\eta_1^2} \begin{bmatrix} k_2(\bar{d}^T Q_y^{-1}\bar{d})^{-1} & \eta_2\eta_3(\bar{d}^T Q_y^{-1}\bar{d})^{-1} & \cdots & \eta_2\eta_q(\bar{d}^T Q_y^{-1}\bar{d})^{-1} & -\eta_2 H_{\bar{d}} Q_y \\ \eta_3\eta_2(\bar{d}^T Q_y^{-1}\bar{d})^{-1} & k_3(\bar{d}^T Q_y^{-1}\bar{d})^{-1} & & \eta_3\eta_q(\bar{d}^T Q_y^{-1}\bar{d})^{-1} & -\eta_3 H_{\bar{d}} Q_y \\ \vdots & & \ddots & & \vdots \\ \eta_q\eta_2(\bar{d}^T Q_y^{-1}\bar{d})^{-1} & \eta_q\eta_3(\bar{d}^T Q_y^{-1}\bar{d})^{-1} & & k_q(\bar{d}^T Q_y^{-1}\bar{d})^{-1} & -\eta_q H_{\bar{d}} Q_y \\ -\eta_2 Q_y H_{\bar{d}}^T & -\eta_3 Q_y H_{\bar{d}}^T & \cdots & -\eta_q Q_y H_{\bar{d}}^T & M \end{bmatrix} \tag{D.17}$$

where

$$k_i = \frac{w_1\eta_1^2 + w_i\eta_i^2}{w_i} \tag{D.18}$$

$$\begin{aligned} M &= \frac{1}{\mu_3}\left(w_1\eta_1^2 I + \left(\mu_3 - w_1\eta_1^2\right) P_{\bar{d}}\right) Q_y \\ &= \frac{1}{\mu_3}\left(\mu_3 I - \left(\mu_3 - w_1\eta_1^2\right) P_{\bar{d}}^{\perp}\right) Q_y \\ &= \left(I - \frac{\mu_3 - w_1\eta_1^2}{\mu_3} P_{\bar{d}}^{\perp}\right) Q_y \end{aligned} \tag{D.19}$$

$$H_{\bar{A}_2} = \begin{bmatrix} -\frac{\eta_2}{\eta_1} H_{\bar{d}} & & H_{\bar{d}} & \\ \vdots & & & \ddots \\ -\frac{\eta_q}{\eta_1} H_{\bar{d}} & & & H_{\bar{d}} \\ \frac{1}{\eta_1}(I - \frac{\mu_3 - w_1\eta_1^2}{\mu_3} P_{\bar{d}}^{\perp}) & \frac{w_2\eta_2}{\mu_3} P_{\bar{d}}^{\perp} & \cdots & \frac{w_q\eta_q}{\mu_3} P_{\bar{d}}^{\perp} \end{bmatrix} \tag{D.20}$$

$$P_{\bar{A}_2} = \begin{bmatrix} (I - \frac{\mu_3 - w_1\eta_1^2}{\mu_3} P_{\bar{d}}^{\perp}) & \frac{w_2\eta_1\eta_2}{\mu_3} P_{\bar{d}}^{\perp} & \cdots & \frac{w_q\eta_1\eta_q}{\mu_3} P_{\bar{d}}^{\perp} \\ \frac{w_1\eta_1\eta_2}{\mu_3} P_{\bar{d}}^{\perp} & (I - \frac{\mu_3 - w_2\eta_2^2}{\mu_3} P_{\bar{d}}^{\perp}) & & \frac{w_q\eta_2\eta_q}{\mu_3} P_{\bar{d}}^{\perp} \\ \vdots & & \ddots & \\ \frac{w_1\eta_q\eta_1}{\mu_3} P_{\bar{d}}^{\perp} & \frac{w_2\eta_q\eta_2}{\mu_3} P_{\bar{d}}^{\perp} & & (I - \frac{\mu_3 - w_q\eta_q^2}{\mu_3} P_{\bar{d}}^{\perp}) \end{bmatrix} \tag{D.21}$$

$$P_{\bar{A}_2}^{\perp} = \frac{1}{\mu_3} \begin{bmatrix} \mu_3 - w_1\eta_1^2 & -\eta_1 w_2 \eta_2 & \cdots & -\eta_1 w_q \eta_q \\ -\eta_2 w_1 \eta_1 & \mu_3 - w_2\eta_2^2 & & -\eta_2 w_q \eta_q \\ \vdots & & \ddots & \\ -\eta_q w_1 \eta_1 & -\eta_q w_2 \eta_2 & & \mu_3 - w_q\eta_q^2 \end{bmatrix} \otimes P_{\bar{d}}^{\perp} \tag{D.22}$$

$$Q^{-1}P_{\bar{A}_2}^{\perp} = \frac{1}{\mu_3} \begin{bmatrix} w_1(\mu_3 - w_1\eta_1^2) & -w_1\eta_1 w_2\eta_2 & \cdots & -w_1\eta_1 w_q\eta_q \\ -w_2\eta_2 w_1\eta_1 & w_2(\mu_3 - w_2\eta_2^2) & & -w_2\eta_2 w_q\eta_q \\ \vdots & & \ddots & \\ -w_q\eta_q w_1\eta_1 & -w_q\eta_q w_2\eta_2 & & w_q(\mu_3 - w_q\eta_q^2) \end{bmatrix} \otimes Q_y^{-1}P_{\bar{d}}^{\perp} \tag{D.23}$$

D.4 Estimation of ionosphere, common clocks

$$\bar{A}_2 = \begin{bmatrix} \bar{d} & \eta_1 I \\ \bar{d} & \eta_2 I \\ \vdots & \vdots \\ \bar{d} & \eta_q I \end{bmatrix} \; ; Q^{-1} = \begin{bmatrix} w_1 & & & \\ & w_2 & & \\ & & \ddots & \\ & & & w_q \end{bmatrix} \otimes Q_y^{-1} \tag{D.24}$$

$$\bar{A}_2^T Q^{-1} \bar{A}_2 = \begin{bmatrix} \mu_1 \bar{d}^T Q_y^{-1} \bar{d} & \mu_2 \bar{d}^T Q_y^{-1} \\ \mu_2 Q_y^{-1} \bar{d} & \mu_3 Q_y^{-1} \end{bmatrix} \tag{D.25}$$

$$\left(\bar{A}_2^T Q^{-1} \bar{A}_2\right)^{-1} = \frac{1}{\mu_4} \begin{bmatrix} \mu_3 (\bar{d}^T Q_y^{-1} \bar{d})^{-1} & -\mu_2 H_{\bar{d}} Q_y \\ -\mu_2 Q_y H_{\bar{d}}^T & M \end{bmatrix} \tag{D.26}$$

where

$$M = \frac{1}{\mu_3} \left(\mu_4 I + \mu_2^2 P_{\bar{d}}\right) Q_y \tag{D.27}$$

$$H_{\bar{A}_2} = \begin{bmatrix} H_{1,1} & H_{1,2} & \cdots & H_{1,q} \\ H_{2,1} & H_{2,2} & \cdots & H_{2,q} \end{bmatrix} \tag{D.28}$$

where

$$H_{1,j} = -\frac{w_j}{\mu_4} (\eta_j \mu_2 - \mu_3) H_{\bar{d}} \tag{D.29}$$

$$H_{2,j} = \frac{w_j \eta_j}{\mu_3} I + \frac{w_j \mu_2 (\eta_j \mu_2 - \mu_3)}{\mu_4 \mu_3} P_{\bar{d}} \tag{D.30}$$

$$\begin{aligned} P_{\bar{A}_2} &= \begin{bmatrix} h_{1,1} & h_{1,2} & \cdots & h_{1,q} \\ h_{2,1} & h_{2,2} & \cdots & h_{2,q} \\ \vdots & \vdots & \ddots & \vdots \\ h_{q,1} & h_{q,2} & \cdots & h_{q,q} \end{bmatrix} \otimes P_{\bar{d}} + \frac{1}{\mu_3} \begin{bmatrix} w_1 \eta_1^2 & w_2 \eta_1 \eta_2 & \cdots & w_q \eta_1 \eta_q \\ w_1 \eta_2 \eta_1 & w_2 \eta_2^2 & \cdots & w_q \eta_2 \eta_q \\ \vdots & \vdots & \ddots & \vdots \\ w_1 \eta_q \eta_1 & w_2 \eta_q \eta_2 & \cdots & w_q \eta_q^2 \end{bmatrix} \otimes I \\ &= \begin{bmatrix} -h_{1,1} & -h_{1,2} & \cdots & -h_{1,q} \\ -h_{2,1} & -h_{2,2} & \cdots & -h_{2,q} \\ \vdots & \vdots & \ddots & \vdots \\ -h_{q,1} & -h_{q,2} & \cdots & -h_{q,q} \end{bmatrix} \otimes P_{\bar{d}}^{\perp} + \begin{bmatrix} k_{1,1} & k_{1,2} & \cdots & k_{1,q} \\ k_{2,1} & k_{2,2} & \cdots & k_{2,q} \\ \vdots & \vdots & \ddots & \vdots \\ k_{q,1} & k_{q,2} & \cdots & k_{q,q} \end{bmatrix} \otimes I \end{aligned} \tag{D.31}$$

where

$$h_{i,j} = \frac{w_j}{\mu_3 \mu_4} (\mu_3 - \mu_2 \eta_i)(\mu_3 - \mu_2 \eta_j) \tag{D.32}$$

$$\begin{aligned} k_{i,j} &= w_j \eta_i \eta_j + h_{i,j} \\ &= \frac{w_j}{\mu_4} \sum_{k=1}^{q} w_k (\eta_i - \eta_k)(\eta_j - \eta_k) \end{aligned} \tag{D.33}$$

$$P_{\bar{A}_2}^{\perp} = \begin{bmatrix} h_{1,1} & h_{1,2} & \cdots & h_{1,q} \\ h_{2,1} & h_{2,2} & \cdots & h_{2,q} \\ \vdots & \vdots & \ddots & \vdots \\ h_{q,1} & h_{q,2} & \cdots & h_{q,q} \end{bmatrix} \otimes P_{\bar{d}}^{\perp} + \begin{bmatrix} 1-k_{1,1} & -k_{1,2} & \cdots & -k_{1,q} \\ -k_{2,1} & 1-k_{2,2} & & -k_{2,q} \\ \vdots & & \ddots & \\ -k_{q,1} & -k_{q,2} & & 1-k_{q,q} \end{bmatrix} \otimes I \qquad \text{(D.34)}$$

$$Q^{-1}P_{\bar{A}_2}^{\perp} = \begin{bmatrix} w_1h_{1,1} & w_1h_{1,2} & \cdots & w_1h_{1,q} \\ w_2h_{2,1} & w_2h_{2,2} & \cdots & w_2h_{2,q} \\ \vdots & \vdots & \ddots & \vdots \\ w_qh_{q,1} & w_qh_{q,2} & \cdots & w_qh_{q,q} \end{bmatrix} \otimes Q_y^{-1}P_{\bar{d}}^{\perp} + \begin{bmatrix} w_1-w_1k_{1,1} & -w_1k_{1,2} & \cdots & -w_1k_{1,q} \\ -w_2k_{2,1} & w_2-w_2k_{2,2} & & -w_2k_{2,q} \\ \vdots & & \ddots & \\ -w_qk_{q,1} & -w_qk_{q,2} & & w_q-w_qk_{q,q} \end{bmatrix} \otimes Q_y^{-1} \qquad \text{(D.35)}$$